2014-9

The Role of Tight and Adherens Junctions in Cervical Neoplasia

Ciaran Cunniffe
Technological University Dublin, ciaran.cunniffe@mydit.ie

The role of tight and adherens junctions in cervical neoplasia

A thesis submitted for the degree of Doctor of Philosophy

by

Ciarán Cunniffe B.Sc. (Medical and Molecular Cytology)

Supervisors: Dr. Brenda Brankin, Dr. Fergus Ryan

School of Biological Sciences,

Dublin Institute of Technology

September 2014

Abstract

Cervical cancer is the second most common cancer in women and is caused by a persistent infection of the cervical epithelium by the Human Papilloma Virus (HPV). Adherens (AJ) and tight junctions (TJ) play a key role in maintaining the apical-basolateral polarity and cohesive structure of epithelial cells. These junctions are maintained by the interaction of several key proteins including, claudins, catenins, cadherins and SNAIL. This study aims to identify the expression profile of several AJ and TJ proteins and to identify and genotype HPV DNA in several cases of cervical neoplasia. This study also aims to investigate the pathogenesis of aberrant AJ and TJ expression using cell based models.

This study utilised a PCR based method to detect and genotype HPV DNA in 126 formalin-fixed paraffin embedded tissue samples. In tandem, tissue microarrays were produced from cervical biopsy samples and utilised to immunohistochemically examine the expression of several AJ and TJ proteins. The HeLa cervical cancer cell line was transfected with plasmids containing claudin-1 and claudin-7 genes to generate cell lines stably expressing claudin-1 claudin-7 respectively. Knockdown of SNAIL expression was performed in the SiHa cervical cancer cell line.

An aberrant expression profile of AJ and TJ proteins was observed in cases of cervical neoplasia with increased expression of claudin-1, claudin-7, N-cadherin p120-catenin, SNAIL and decreased expression of E-cadherin compared to normal cervical epithelium. HPV DNA was detected and genotyped in 60 cervical tissue samples. HPV-16 was the most prevalent subtype,

and was the subtype most associated with aberrant AJ and TJ expression. Knockdown of SNAIL expression had no effect on E-cadherin expression in SiHa cells while overexpression of claudin-1 and claudin-7 suppressed cellular motility in vitro, and decreased permeability in HeLa cells.

This study identified aberrant expression of several AJ and TJ proteins which may be of potential use as biomarkers in the identification of pre-invasive cervical lesions. This study also identified that claudin-1 and claudin-7 overexpression in HeLa cells reduced cell migration and increased TEER values. This indicates the acquisition of invasive and metastatic properties in malignant cells is likely reliant on the synergistic interaction of several AJ and TJ proteins.

.

Declaration

I certify that this thesis which I now submit for examination for the award of Doctor of Philosophy, is entirely my own work and has not been taken from the work of others, save and to the extent that such work has been cited and acknowledged within the text of my work.

This thesis was prepared according to the regulations for postgraduate study by research of the Dublin Institute of Technology and has not been submitted in whole or in part for award in any other Institute.

The work reported on in this thesis conforms to the principles and requirements of the Institute's guidelines for ethics in research.

The Institute has permission to keep, lend or copy this thesis in whole or in part, on condition that any such use of the material of this thesis be duly acknowledged.

Ciarán Cunniffe

Signature: _____ Date: _____

Acknowledgements

Many people have contributed to the completion of this thesis and I offer my sincere gratitude and appreciation to all who have helped along the way.

Firstly, many thanks to my supervisors, Dr. Brenda Brankin and Dr Fergus Ryan, for their effort, insight and patience during the course of my work in DIT.

To Dr. Eibhlis O'Donovan and Colma Barnes at the Rotunda Maternity Hospital for facilitating this study.

To all of the academic staff in the school of Biological Science, particularly Helen Lambkin, Greg Byrne, Stephan Schwartz, Gwilym Williams, Brid Ann Ryan, Louis Armstrong and Mary Hunt for their input and advice at various stages of my time in DIT.

To the technical staff, particularly Daireen and Kathleen, for their patience, generosity, and for letting me 'borrow' so many reagents over the years.

To the other post-grad students, Beatrice, Rali, Paul, Patrice and Dave, who always made the lab a friendly and enjoyable place to work in.

And lastly thanks to all my friends and family, particularly my parents John and Anne.

Abbreviations

AAs	amino acids
AJ	adherens junction
AP	alkaline phosphatase
ATP	adenosine 5’-triphosphate
BPV	bovine papillomavirus
CDK	cyclin-dependent kinase
CIN	cervical intraepithelial neoplasia
CIS	carcinoma *in situ*
CISH	chromatic *in situ* hybridisation
CK	cytokeratin
CMV	cytomegalovirus
CRPV	cotton-tail rabbit papillomavirus
DNA	deoxyribonucleic acid
E2F	eukaryotic transcription factor 2
EDTA	ethylene-diamine-tetra-acetic acid
FISH	fluorescent *In situ* hybrisidation
FFPE	formalin fixed paraffin embedded
HDAC	histone deacetylases
HPV	human papillomavirus
HR	high risk
HRP	horse radish peroxidase
HSIL	high grade squamous intraepithelial lesion

IHC	immunohistochemistry
ISH	*in situ* hybridisation
kDa	kilodalton
LCR	long coding region
LLETZ	long loop excision of the transformation zone
LR	low risk
LSIL	low grade squamous intraepithelial lesion
ORF	open reading frame
pAE	early polyadenylation signal
pAL	late polyadenylation signal
PCR	polymerase chain reaction
PAP	papanicolaou stain
PBS	phosphate buffered saline
PolyA	polyadenalation
pRB	phosphorylated retinoblastoma protein
PV	papillomavirus
SIL	squamous intraepithelial lesion
SCC	squamous cell carcinoma
Rb	retinoblastoma protein
RNA	ribonucleic acid
RT	room temperature
TEER	trans-epithelial electrical resistance
TJ	tight junction
TGFβ	transforming growth factor beta

TMA	tissue microarray
TZ	transformation zone
VLP	virus like particle

Table of Contents

List of figures

List of tables

1. General Introduction

1.1 Cervical cancer overview

Cervical cancer is a malignancy that develops in the epithelium lining the cervix. This epithelium consists of two major subtypes, a simple columnar type in the endocervix, and the stratified squamous epithelium in the ectocervix. Squamous cell carcinoma arising from the stratified squamous epithelium is the most common cervical malignancy, accounting for approximately 85% of cervical malignancies. Adenocarcinoma, derived from the simple columnar epithelium, constitutes around 10% of cervical malignancies with the remaining 5% consisting of adenosquamous and other rare tumour types [1]. Cervical cancer develops from precursor lesions called cervical intraepithelial neoplasia (CIN), also termed squamous intraepithelial lesions (SIL), which may progress to invasive carcinomas or may also regress to normal epithelium. The introduction of cervical screening programmes, to detect these premalignant lesions before they develop into invasive carcinomas, has greatly reduced the incidence of cervical cancer. Indeed, it has been shown that in countries with established systematic screening programmes, the number of cervical cancer deaths has been reduced by around 70% [2]

One of the most important discoveries in the aetiological investigation of cervical cancer over the last 25 years has been the demonstration that cervical cancer is caused by the persistent infection by certain genotypes of the Human Papillomavirus (HPV). The important role of HPV in the development of cervical cancer is highlighted by the fact that HPV DNA is

present in 99% of cervical tumours [3]. Based on their association with cervical cancer and precursor lesions, HPVs can also be grouped to high-risk and low-risk HPV types. Low-risk HPV types include types 6, 11, 42, 43, and 44. High-risk HPV types include types 16, 18, 31, 33, 34, 35, 39, 45, 51, 52, 56, 58, 59, 66, 68, and 70. Of these high risk types, four are most often found within the malignant cells of cervical cancers, with type 16 accounting for about half of the cases in the United States and Europe and types 18, 31, and 45 accounting for an additional 25 to 30% of cases [4].

1.2 The Cervix

The cylindrical lower part of the uterus, the cervix, has a constricted opening at each end; the os. The internal os is located at the upper end of the cervix and is the opening of the cervix inside the uterine cavity (Figure 1.1). The external os is located at the lower end of the cervix and opens into the vagina [5] .The passageway linking the external and internal os is termed the endocervical canal. The lining of the endocervical canal differs completely from the rest of the uterine endometrium as it contains large branched glands. The endocervix is lined with a single layer of columnar, mucin-secreting simple columnar epithelium.

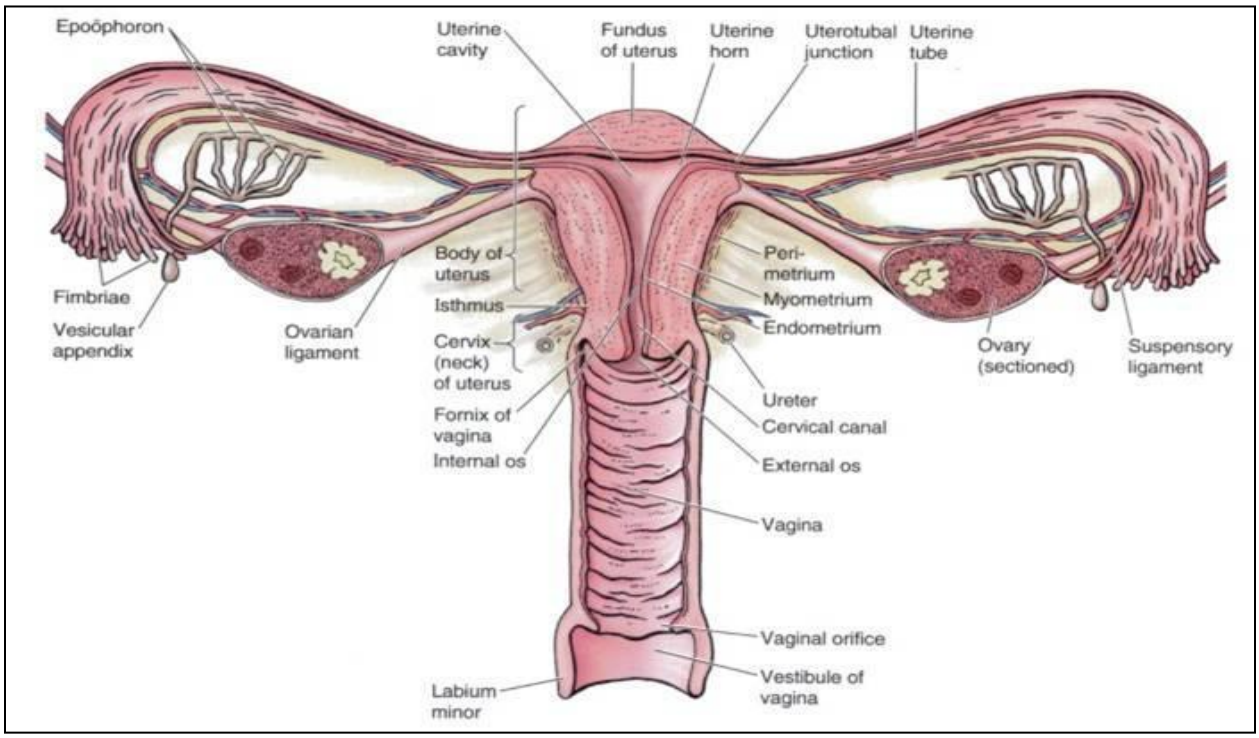

Figure 1.1 Diagram of the uterus, including the location of the cervix, the internal and external os and the cervical canal [6]**.**

Towards the external os the columnar epithelium is gradually replaced by stratified squamous epithelium, in an area known as the transformation zone (TZ) or the squamo-columnar junction. The TZ is the area of the cervical epithelium most likely to be affected by disease [6]. The ectocervix is the portion of the cervix that projects into the vagina and has a convex surface with an epithelial lining. The epithelium of the ectocervix is non-keratinised stratified squamous epithelium which is continuous with the squamous epithelium lining the vagina [6]. The epithelium of the ectocervix consists of several distinct layers of cells (Figure 1.2). Along the basement membrane are the basal cells which are immature, actively dividing cells with relatively large nuclei [7]. The layer of cells above this are termed the parabasal and intermediate layers; with cells in this part of the epithelium showing a recognisable chromatin pattern and often being vacuolated. In fully mature epithelium, a superficial layer lies above the intermediate layer, with superficial cells containing small pyknotic nuclei [7].

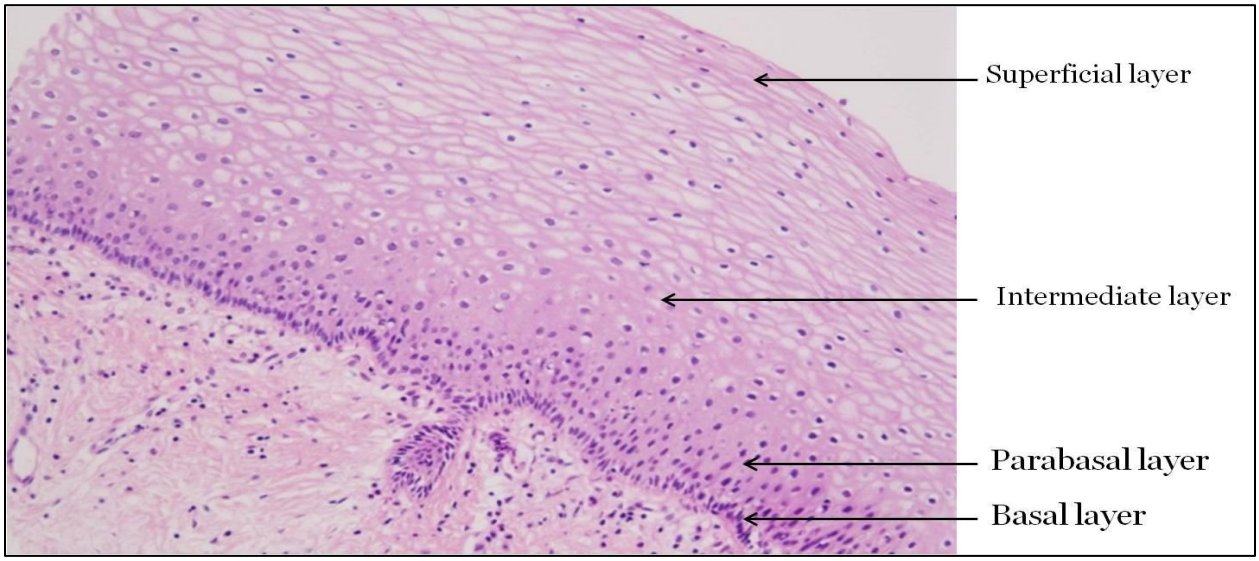

Figure 1.2 Outline of different cell layers found in the stratified squamous epithelium of the ectocervix. Arrows indicate the position of basal, parabasal, intermediate and superficial cell layers within the epithelium.

1.3 Cervical cancer epidemiology

Cervical cancer is the second most common cancer in women worldwide, with an estimated 528,000 new cases annually, and being responsible for approximately 266,000 deaths in 2012 (WHO 2012). A large majority, around 85%, of the global burden occurs in the less developed regions, where it accounts for almost 12% of all female cancers, most likely as a result of the lack of systemic cervical screening programmes in many developing countries [8] [2]. Eastern Africa has some of the highest incidences in the world, with an age standarised rate (ASR) of 42.7 per 100,000, meaning in these countries it is the most common cancer in women, overtaking even breast cancer (WHO 2012). Mortality rates are also highest in developing countries with 87% of world cervical deaths occurring in these countries. Mortality varies 18-fold between the different regions of the world, with rates ranging from less than 2 per 100,000 in Western Asia, Western Europe and Australia/New Zealand to more than 20 per 100,000 in Melanesia (20.6), Middle (22.2) and Eastern (27.6) Africa (WHO 2012).

In Ireland, cervical cancer incidence has an ASR of 15.1 per 100,000 which is above the EU average of 11.3 and also above the UK (7.9) German (9.8) and Swedish (8.6) average. Cervical cancer incidences in are Ireland are similar to Poland (15.3), Denmark (12.1), and Croatia (12.1) (WHO 2012) (Figure 1.3). The highest incidences in Europe are found mostly in eastern European countries such as Romania, Bulgaria and Serbia which all have an ASR above 20.6 (Figure 1.3). The mortality rate in Ireland at an ASR of 4.3 per 100,000 people is above the EU average of 3.7 and the same as both the Czech Republic and Croatia (WHO 2012). In Europe the lowest mortality rates are found in the UK, Germany, Iceland and Finland, with rates in

these countries all below 2.5 per 100,000 (Figure 1.3). The highest mortality rates in Europe are found mostly in the east, with Russia, Ukraine and Romania all having mortality rates above 7.5 per 100,000 (Figure 1.3).

The recent introduction of vaccines against HPV should help significantly reduced the incidence of cervical cancer in countries with properly implemented vaccination programmes. Early studies show that HPV vaccination, recommended for both women and men between 9-26 years old who have not previously been exposed to HPV, has the potential to significantly reduce the rate of cervical cancer worldwide [9]. Two main vaccines are currently available, Gardasil and Cervarix. The Gardasil vaccine is produced by Merck & Co., Inc. and protects against two low risk (6 and 11) and two high risk (16 and 18) HPV subtypes. The Cervarix vaccine is produced by GlaxoSmithKline and offers protection against high risk HPV types 16 and 18. The vaccines have been shown to provide protection against persistent cervical HPV 16/18 infections for up to 8 years, which is the maximum time of research follow-up thus far [10]. Both vaccines are based on virus like particles (VLPs) that are composed of the viral L1 proteins, which is the main capsid protein of the virus, and elicits a strong immunogenic response in the host immune system [11].

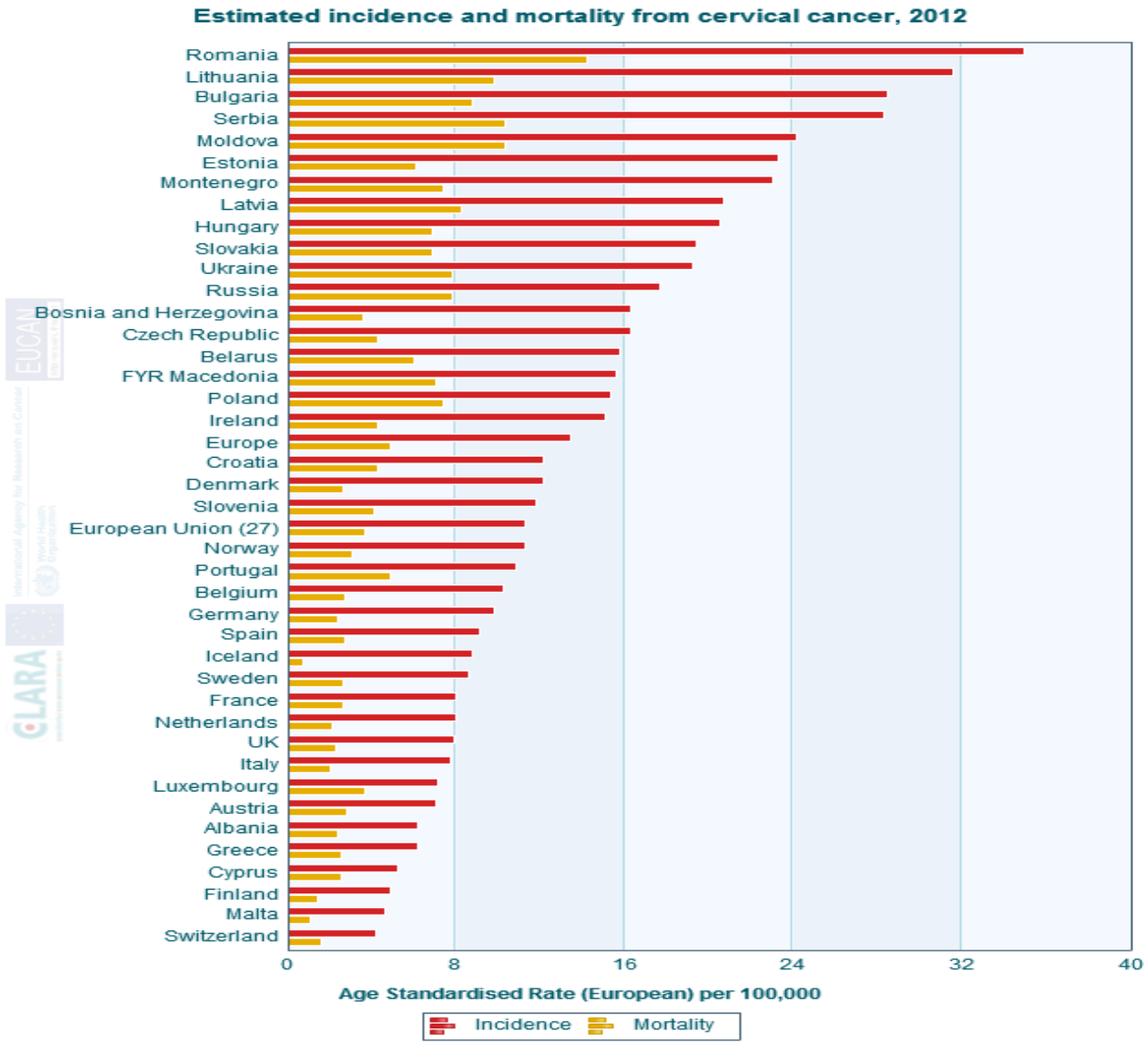

Figure 1.3 Comparison of European estimated cervical cancer incidence and mortality for 2012 (WHO 2012).

The highest incidence and mortality rates in Europe are mostly found in eastern European countries such as Romania, Lithuania and Bulgaria. Ireland has higher rates of incidence and mortality than the EU average and of other western european countries such as the UK, France and Germany.

1.4 Papillomavirus background

Papillomaviruses are members of the Papillomaviridae family, which consist of a vast group of DNA viruses that infect a wide array of animals, in a species specific manner [12]. Papillomaviruses nomenclature divides the family into genus, species, types, subtypes and variants [12]. There are 16 genera in the Papillomavirus family, each genus is designated a letter from the Greek alphabet e.g alpha-papillomaviruses, beta-papillomviruses etc. [13] The most clinically important HPV types are contained within the alpha-papillomavirus genera (Figure 1.5). Different genera share less that 60% nucleotide homology in the Late gene 1 (L1) and less than 43% sequence homology in the full length genome [13]. Contained within the 16 genera there are 44 species. Species within genera have between 60 and 70% sequence homology in the L1 gene. Each species is identified by a number, with each genus containing a varying number of species. Within a species there may be several types which not only have a large degree of genetic similarity, but also usually share biological and pathological properties. Specific types are usually named after the host species they infect, such as Bovine Papillomavirus or Canine Oral Papillomavirus [12]. When more than one distinct isolate of papillomavirus occurs in a single host, each isolate is assigned a number, e.g. Human Papillomavirus type 1, Human Papillomavirus type 2 etc. In order for a papillomavirus to be defined as a specific type, it must have less than 90% L1 sequence homology with any other papillomavirus type [13]. Subtypes are defined as being between 2-10% divergent in the L1 gene from a known PV type. An example of this is HPV-55 genome which is 95% homogenous to the HPV-44 genome and therefore is classified as a sub-type of HPV-44. Lastly, variants differ in their genomic sequence by less than 2% from another papillomavirus type [13] [14].

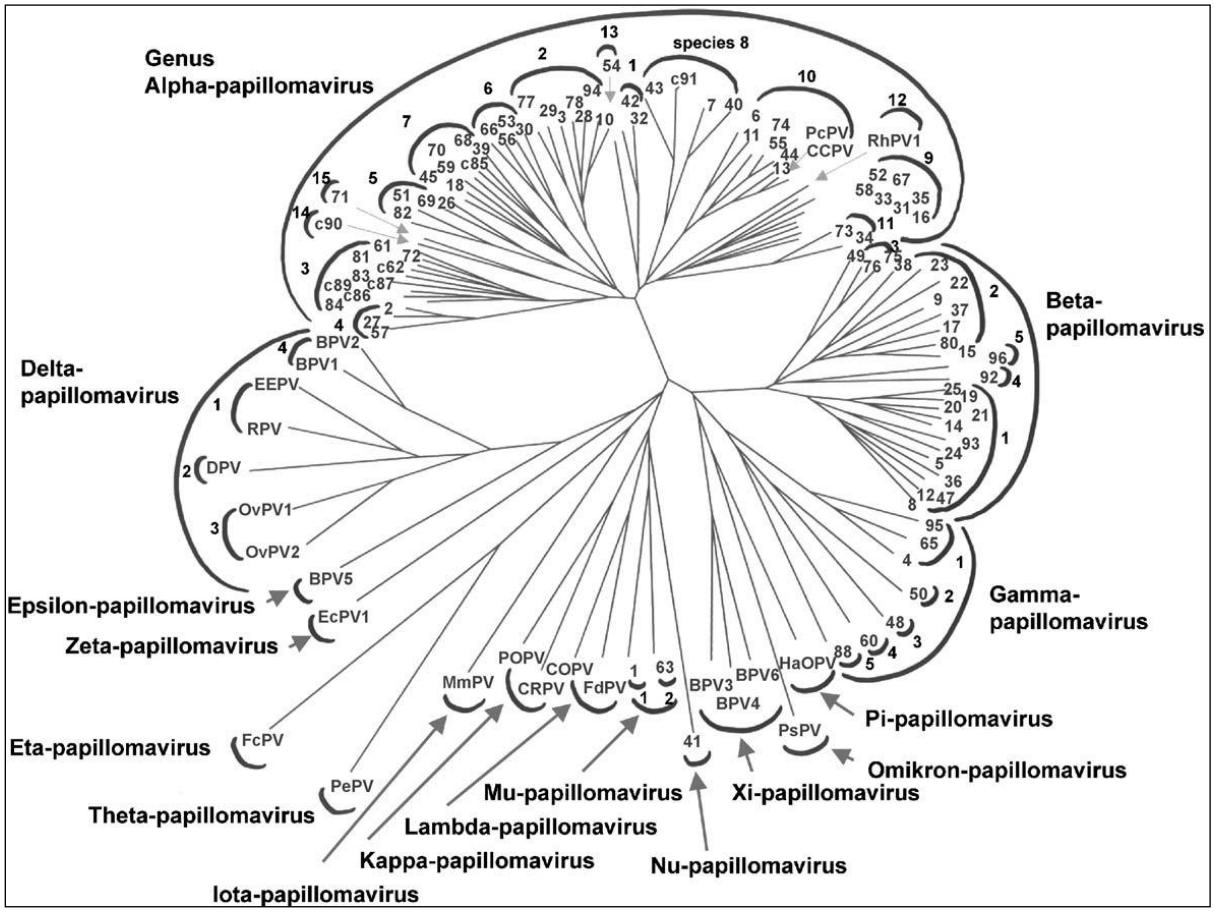

Figure 1.4 Phylogenic papillomaviridae tree outlining the 16 different papillomavirus genera [13]

1.5 Papillomavirus life cycle

Initial infection requires access of the virion to cells in the basal layer of the cervical epithelium usually through a micro-abrasion in the epithelium (Figure 1.5). Following infection and uncoating, it is thought that the virus maintains its genome as a low copy number episome in the basal cells of the epithelium [15]. In uninfected epithelium, basal cells exit the cell cycle soon after migrating into the suprabasal cell layers and undergo a process of terminal differentiation. During papillomavirus infection the restraint on cell cycle progression is abolished and normal terminal differentiation is retarded [16]. For the production of infectious virions, HPV must amplify its viral genome and package them into infectious particles. For most HPV types this occurs in the mid or upper epithelial layers following an increase in activity of the late promoter [17]. The late promoter is tightly regulated so as to limit the exposure of the highly immunogenic viral capsids to the host immune system. After the viral genome is packed into the capsid protein the newly formed viruses are not released from the cell until it reaches the surface of the epithelium and the cells are sloughed off [15].

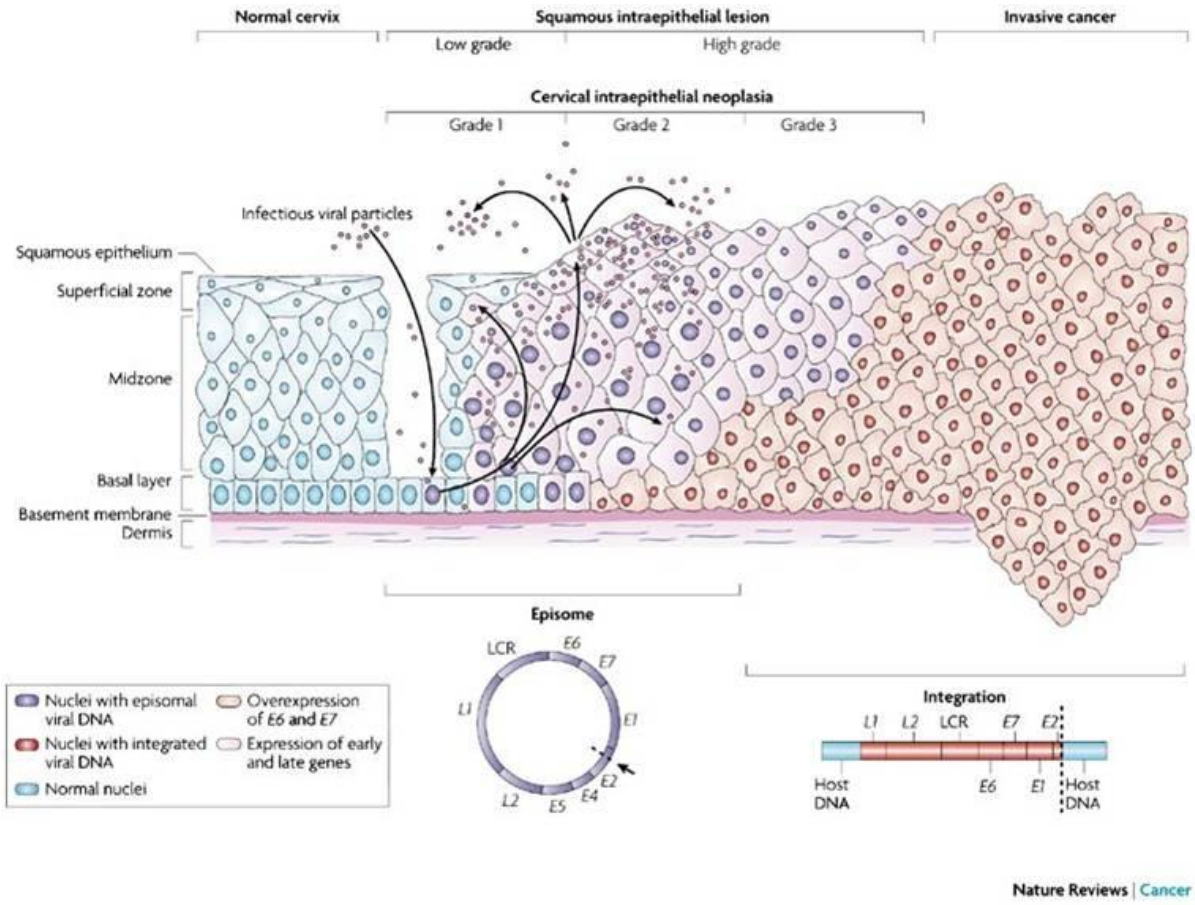

Figure 1.5 HPV mediated progression from normal cervical epithelium to invasive cancer [18]

The disease begins with infection of the basal cells of the epithelium by viral particles. Viral genes become expressed in infected cells which may lead to the proliferation of dysplastic cells within the epithelium. When dysplastic cells make up to one third of the depth of the epithelium the disease is classified as a low grade squamous epithelial lesion (LSIL). When dysplastic cells make up more than one third and up to the entire depth of the epithelium the disease is classified as a high grade squamous epithelial lesion (HSIL). Over time, with persistent expression of viral genes, dysplastic cells may penetrate the basement membrane leading to the development of an invasive cancer.

1.6 HPV induced cervical abnormalities

Infection of cervix with HPV most commonly results in genital warts. These lesions occur as a result on non-oncogenic HPV-6 and HPV-11 infection [19]. Infection with a high-risk HPV type can lead to abnormalities in cells of cervical epithelium giving rise to initially non-invasive neoplastic lesions, termed cervical intraepithelial neoplasia (CIN), which can in turn lead to the development of invasive tumours [12] . Neoplastic cells are characterised by a number of features including hyperchromasia, increase in mitotic figures and a high nuclear to cytoplasmic ratio [20]. CIN is subdivided in three grades, with CIN 1 the lowest and CIN 3 the highest. In CIN 1 lesions abnormal cells are confined to no more than a third of the basal side of the epithelium. In CIN 2 lesions abnormal cells are present in up to two thirds of the epithelium with maturation only occurring in the superficial third of the epithelium, while in CIN 3 lesions more than two thirds of the epithelium contains abnormal cells (Figure 1.5 & 1.6) [21]. More recently a two tier system, termed the Bethesda system, for grading neoplastic lesions of the cervix has been developed with CIN 1 now termed low grade squamous intraepithelial lesion (LSIL) and CIN 2 and 3 being combined to form a new classification termed high grade squamous intraepithelial lesion (HSIL) (Figure 1.5 & Figure 1.6) [22]. All grades of lesions may either progress to a higher grade or regress over time. CIN 1 or LSIL lesions have a 60% likelihood of regression, a 30% risk of becoming a persistent lesion, a 10% risk of progression to a CIN3 lesion and a 1% chance of becoming an invasive carcinoma [22]. CIN 2 has 40% likelihood of regression, 40% chance of persistence, 20% risk of progression to CIN3 and a 5 %

risk of becoming an invasive carcinoma. CIN 3 has a 33% likelihood of regressing, a 56% chance of persistence and a less than 12% risk of progressing to an invasive carcinoma [21] [22].

1.7 CIN Treatment

Several methods may be utilised to remove or destroy pre malignant lesions of the cervix, including laser ablation, cold coagulation, and long loop excision of the transformation zone (LLETZ), also referred to as loop electrosurgical excision procedure (LEEP) [23]. LLETZ is one of the most frequently used treatments for CIN as it can be performed without general anesthetic and generally has very few complications [24] [25]. After examination of the cervix during colposcopy, the transformation zone and any additional dysplasia is identified using a dilute acetic acidic solution that temporarily stains densely nucleated areas. CIN lesions contain a larger amount of immature, proliferating cells and therefore these areas stain stronger than normal fully mature epithelium that is more sparsely nucleated [23]. After identification of the lesion, a physician uses a wire loop with an electrical current passing through it to excise and caurterise the area identified [24]. One of the benefits of LEETZ compared to other techniques is that the lesion is not destroyed and can be subsequently histologically analysed to assess the severity and extent of dysplasia. The effect of LEETZ on fertility is still debated with previous studies finding that it had no effect on fertility [26], whereas a more recent study found that those with a time interval from LEEP to pregnancy of less than 12 months compared with 12 months or more were at significantly increased risk for spontaneous abortion, with risk of 18% compared with 4.6%, respectively [27].

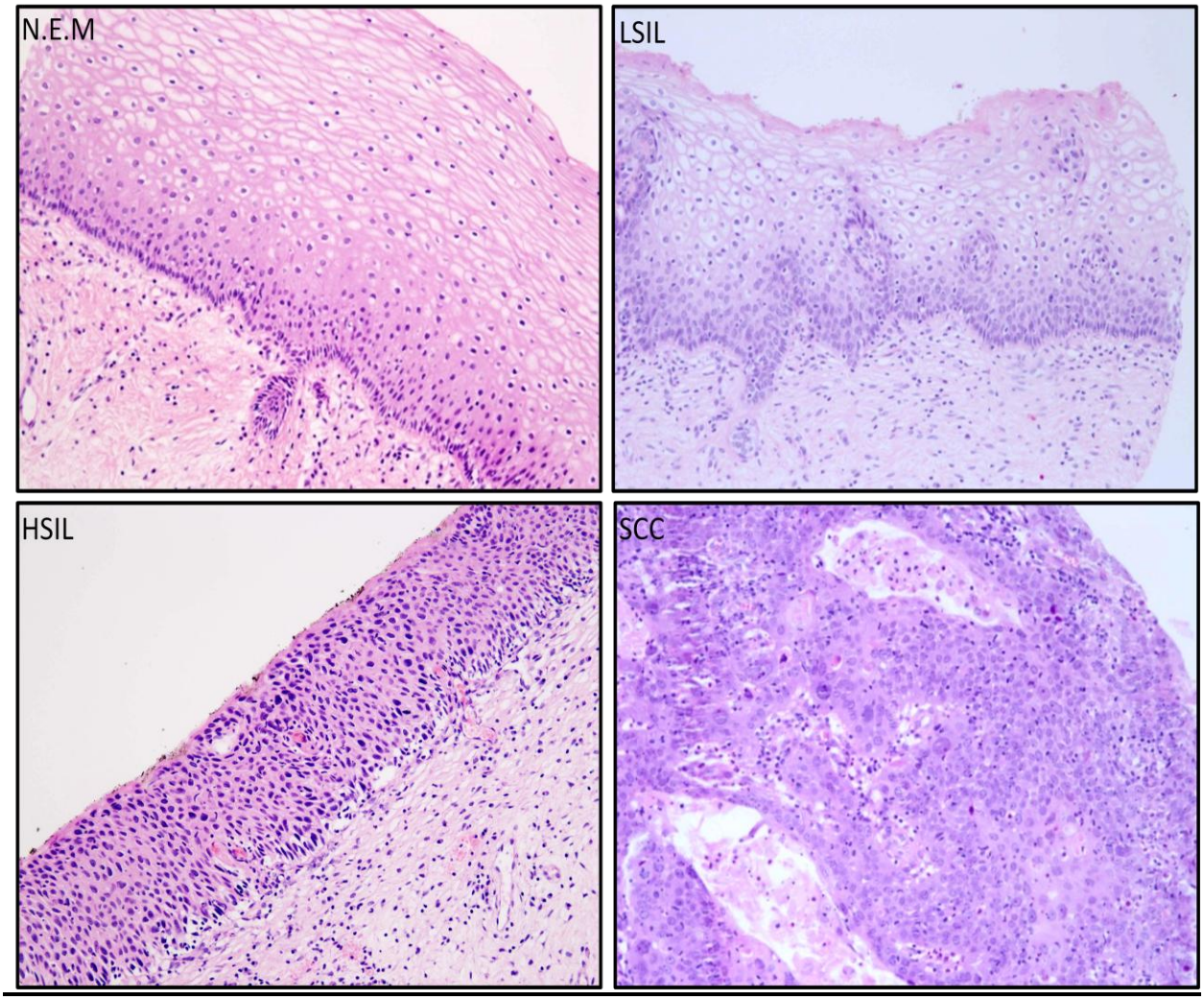

Figure 1.6 Images from cervical samples used in this study showing different grades of squamous intra-epithelial lesion in the uterine cervix. N.E.M = No evidence of malignancy. LSIL = Low grade squamous intra-epitthelial lesion, with abnormal immature cells in the basal third of the epithelium. HSIL = High grade squamous intra-epitthelial lesion, with diffuse atypia and immature cells occupying the entire depth of the epithelium. SCC = Squamous cell carcinoma, malignant cells invaded though basement membrane with complete loss of epithelial structure and large number of proliferating cells. Stained with hematoxylin and eosin, x100 magnification

1.8 HPV Proteins

The HPV genome is divided into early and late genes, depending on the stage the viral life cycle they are expressed, transcribed into 6 early proteins (E1, E2, E4, E5, E6, E7) and two late proteins (L1 and L2) (Figure 1.8) [28]. The transcription of the open reading frames (ORFs) into functional proteins is regulated by promoters within the viral genome. The HPV-16 genome contains two major promoters. The P97 promoter lies upstream of the E6 ORF and is responsible for almost all early gene expression (Figure 1.7). The P670 promoter lies within the E7 ORF region and is responsible for late gene expression [28] [29]. The HPV-16 P97 promoter, equivalent to P99 in HPV-31 and P105 in HPV-18, is very potent and tightly controlled, primarily by upstream cis-elements in the LCR [17]. Induction of the late P670 promoter in HPV-16, and equivalent promoters in other HPV types, only occurs in differentiated keratinocytes [30]

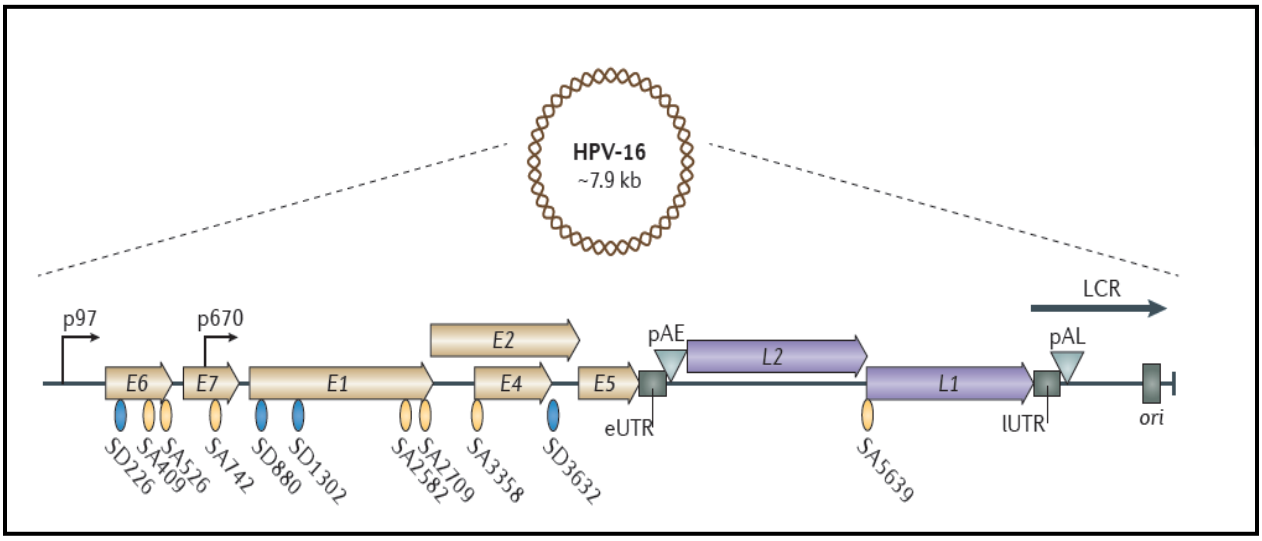

Figure 1.7 Linear representation of the HPV-16 genome [28]

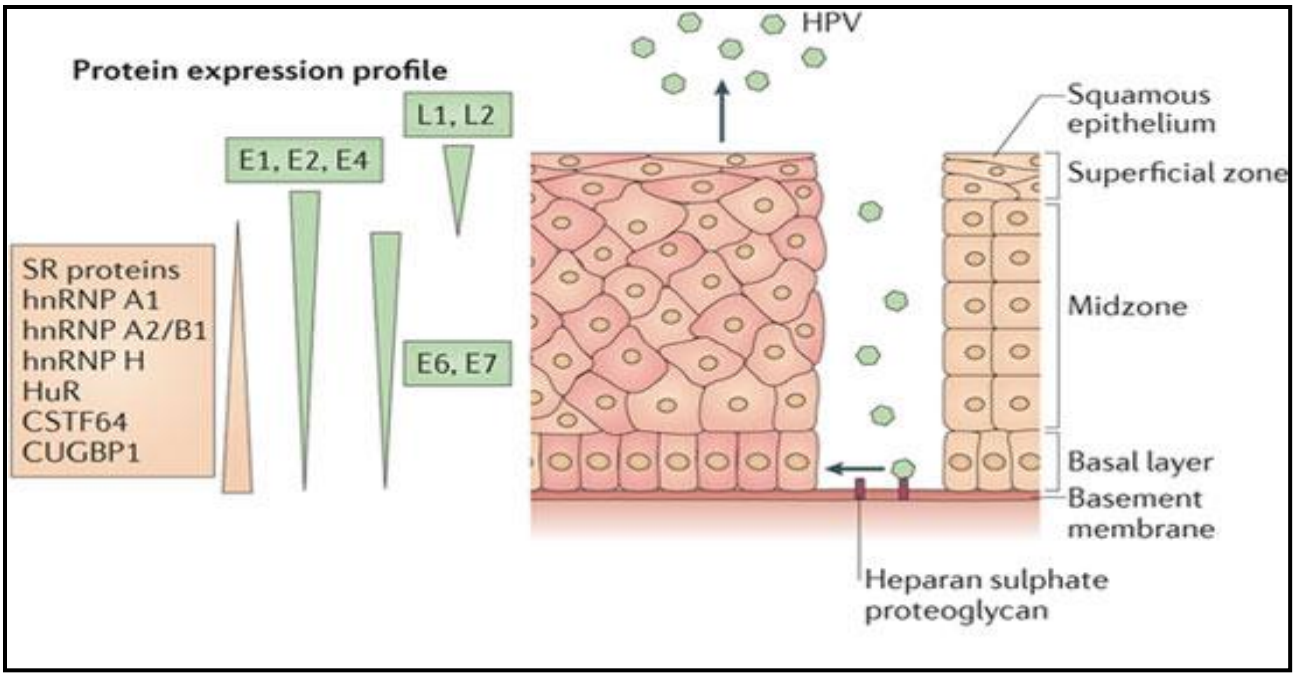

Figure 1.8 Diagram showing the HPV protein expression profile in the cervical epithelium, displaying the relative expression levels of the different HPV proteins at different stages of the viral life cycle. [28]

1.8.1 E1 Protein

The E1 ORF is the largest ORF in the HPV genome and encodes one the most conserved proteins in the HPV genome [12]. E1 proteins are approximately 68 kDa in size and are expressed at low levels in HPV-positive cells [29]. E1 is the only viral protein shown to have enzymatic activity; it can function as an ATPase and as an ATP dependent helicase. This enzymatic activity allows the E1 protein to play a key role in viral replication by catalysing the unwinding of the DNA at the origin of replication [31]. E1 has been shown to bind the alpha subunit of DNA polymerase, recruiting the replication machinery to the viral origin of replication. Replication is initiated by

the E1 protein through binding to AT-rich regions in the LCR. Binding is stabilised and strengthened through cobinding with E2 protein [29].

1.8.2 E2 Protein

The E2 protein is required for both the replication of viral DNA and transcriptional regulation[32]. E2 proteins are approximately 50 kDa in size and function as dimers. The C terminus encodes a DNA binding domain that has been crystallized and shown to consist of a dimeric β-barrel structure that binds to LCR region of HPV DNA [29]. The LCR of high-risk HPV types contain 4 E2 binding sites, 3 of which are adjacent to the E1 binding sites and increase E1 binding affinity [16]. E2 can have a dual function depending on its concentration. At low concentration it acts as a promoter of early gene expression, whereas while at high concentrations it represses early gene expression by interfering with the binding of transcription factors such as TFIID and Sp1 [33].

1.8.3 E4 Protein

The E4 ORF completely overlaps with the E2 ORF (Figure 1.8). However it is transcribed in a different reading frame. The E4 protein is heterogenous, forming a fusion product with a 5 amino acid sequence from the N-terminus of E1. For this reason it is referred to as E1^E4 [29]. Despite its position in the genome and its 'E' name it is primarily expressed in the later stages of the viral life cycle. E1^E4 proteins from high-risk types associate with keratin networks in cells

and, when overexpressed in transient-transfection assays, can induce their collapse [34]. This suggests a role for E1^E4 in facilitating the release of virions from the cell, but in natural infections of high-risk types only a limited amount of collapse has been observed [16]

1.8.4 E5 Protein

The HPV E5 proteins are small hydrophobic proteins whose exact functions remain unresolved. These proteins are localized to endosomal membranes and the Golgi but on occasion are found in the cellular membranes. E5 has weak oncogenic properties which occur through increasing epidermal growth factor receptor (EGFR) expression, and inhibiting the expression of major histocompatibility complex (MHC)-I and MHC-II on the plasma membrane [35]. E5 expression alone is not sufficient to initiate cell transformation, however it can act to increase the potency of E6 and E7 when co-expressed with them [36]. E5 has recently been shown to initiate cell fusion, producing genetically unstable tetraploid cells which may be more susceptible to oncogenic transformation [37]

1.8.5 E6 Protein

The E6 protein contains approximately 160 amino acids and is one of the earliest expressed proteins in the viral life cycle (Figure 1.8). In conjunction with other viral proteins, E6 serves to drive the cell into an actively dividing and undifferentiated state that is more favourable for the production and replication of new virions [31]. It is the promotion of a pro-replicative state

within the cell that leads to the malignant transformation of infected cells and ultimately, tumour development. The influence of E6 protein over the cell cycle is illustrated by the ability of E6 protein from highrisk HPV being sufficient for the induction and maintenance of cellular transformation in-vitro [38]. One of the primary methods by which E6 interferes with the cell cycle is through its interaction with the pro-apotosis protein p53 (Figure 1.9) [31]. The p53 protein responds to DNA damage by transcriptionally activating a number of cell cycle regulatory pathways, including the p21 and GADD 45 pathways that can arrest the cell cycle or trigger apoptosis [29]. The degradation of p53 occurs through a trimeric complex containing E6, E6-associated protein (E6AP) and p53. E6AP recruits a complex of enzymes called the ubiquitin complex, which then target p53 for proteosomal degradation [39]. Low-risk HPV E6 proteins can also bind to p53, but with very low affinity and do not degrade p53 [31]. In addition to its effects on p53, HPV also targets a number of other pro-apoptosis proteins including Bak, Fas-associated death domain containing protein (FADD) and procaspase 8, which is degraded by E6/E6AP furthering reducing the ability of the cell to enter apoptosis [40]

E6 in conjunction with the transcription factor Myc, can up regulate the transcription of TERT (Telomerase reverse transcriptase) from its promoter, allowing the cell to repair the telomere after each division and maintain telomere length [41]. Human telomerase is a ribonucleoprotein complex composed of at least the reverse catalytic transcriptase (hTERT) and an RNA component (hTR) [42]. hTERT is expressed only in specific germ-line cells, proliferative stem cells of renewal tissues, and cancer cells. Because telomerase activity is hardly detected in most somatic tissues, telomeres shorten with each cell division, eventually leading to senescence [42]

1.8.6 E7 Protein

E7 is a small nuclear phosphoprotein made up of approximately 100 amino acids. E7 is known to bind to the retinoblastoma tumor suppressor gene product, pRb, and its family members, p107 and p130 (Figure 1.10), via a binding motif conserved in its CR2 region [31]. In the hypophosphorylated state, pRb family proteins can bind to transcription factors such as E2F family members and repress the transcription of particular genes involved in DNA synthesis and cell-cycle progression [31]. Phosphorylation of pRb by G1 cyclin-dependent kinases releases E2F (Figure 1.10) leading to cell cycle progression into the S phase. As E7 is able to bind to unphosphorylated pRb, it may prematurely induce cells to enter the S phase by disrupting pRb–E2F complex [43]

E7 interacts with inhibitors of cyclin-dependent kinases including p21 and p27 [44] [45]. p21 is an important mediator of cell cycle arrest via its inhibition of cyclin dependent kinases [46]. This process occurs during keratinocyte differentiation ultimately leading to cell senescence; therefore the sequestering of p21 by E7 may be critical in allowing continued replication of the viral genome in differentiated squamous cells where otherwise replication of DNA has ceased [31]. In addition to the inactivation of pRb family members, other oncogenic functions of E7 have been reported. Histone deacetylases have been shown to play an important role in cell cycle regulation. HPV16-E7 targets chromatin remodelling histone deacetylase complexes through its C-terminal zinc finger. This interaction potentially enables E7 to alter expression of cellular genes by modulating their chromatin structure [47].

E7 may play a role in helping the virus to evade the host immune system though it's influence on E-cadherin expression. Langerhans cells are one of the major immune cells present in the cervical epithelium and play a role in activation of the adaptive immune response by detecting, processing and presenting foreign antigens to other leucocytes [48]. It has previously been observed that dysplastic cervical lesions contain fewer langerhans cells than normal cervical epithelium [49], likely creating an environment favorable for HPV persistence. The expression of E-cadherin on the cell membranes of keratinocytes is required for langerhans cell migration into the epithelium [50], thus any reduction in E-cadherin expression likely contributes to a concurrent reduction in the number of langerhans cells in the epithelium. The role of E7 in regulating E-cadherin expression is demonstrated by experiments showing silencing of E7 in HPV 16-transformed keratinocytes restores functional E-cadherin expression [51]. A study by Laurson et al., 2010 [52] observed that E7 mediated repression of E-cadherin expression occurs at the epigenetic level, through augmentation of cellular DNA methyltransferase I (Dnmt1) activity. Interestingly Laurson et al. 2010 observed that Dmnt1 does not methylate the E-cadherin promoter directly, suggesting that E7-augmented Dnmt1 activity is directed to a cellular gene/genes whose protein acts on the E-cadherin promoter. In this study the role of the SNAIL protein, which can bind to the E-cadherin promoter, in repressing E-cadherin expression is examined in cervical cell lines (Chapter 5).

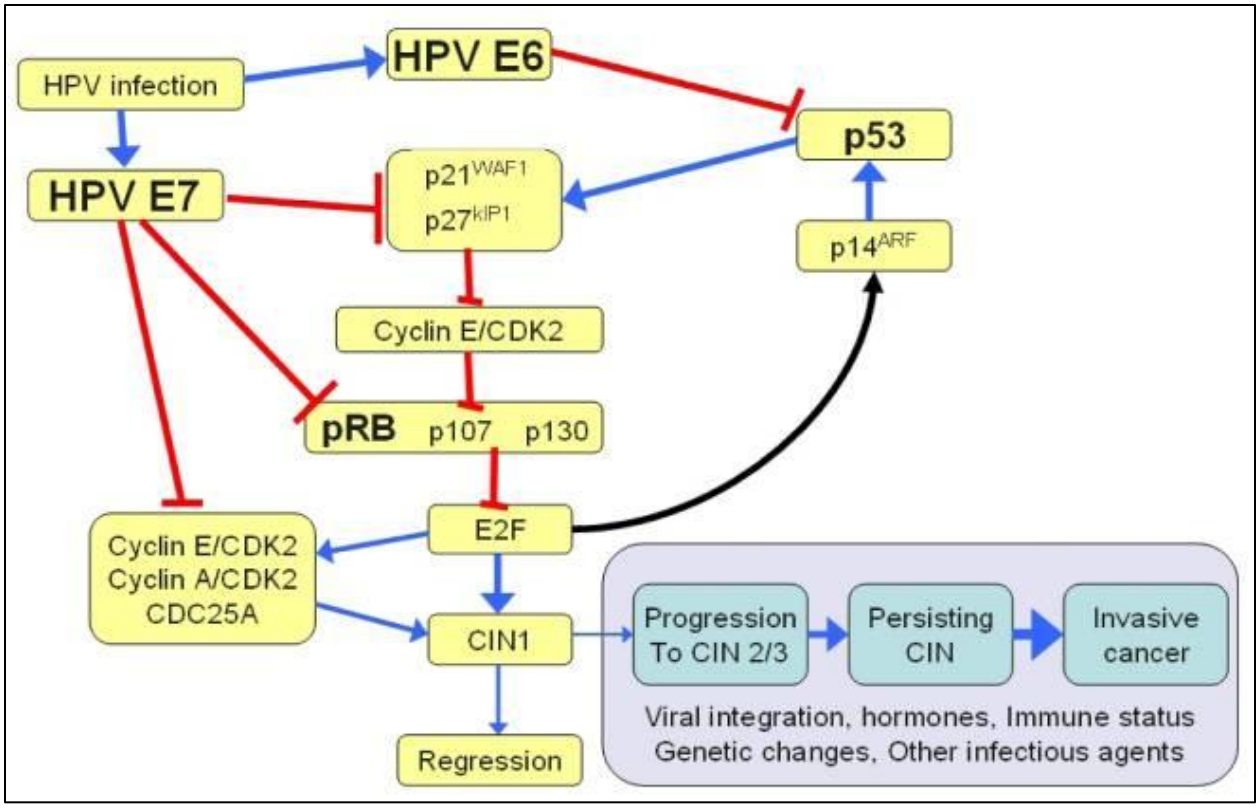

Figure 1.9 Schematic presentation of the HPV viral oncoproteins E6/E7 and their interaction with cell-cycle regulatory proteins in cervical carcinogenesis [53]

1.8.7 L1 Protein

The L1 protein is the major capsid protein and is the principal viral protein responsible for generating an immunogenic response in the host. It is one of the most conserved proteins in the HPV genome and is expressed late in the viral life cycle (Figure 1.9). Due to its highly conserved structure, the L1 sequence is used as a basis for classifying Papillomaviridae into their separate genus, type and subtypes [13]. Papillomavirus capsids contain two virally encoded proteins L1 and L2, synthesised late in the infection cycle, which encapsulate the histone-associated, closed circular double-stranded DNA minichromosome [16]. The viral capsid

is primarily composed of 72 pentamers (capsomeres) of the L1 protein, in association with 12 or more copies of the L2 protein [12] .The major late protein L1 pentamers have the intrinsic property of self-assembly into empty capsids, referred to as virus like particles (VLPs) [54]. VLPs are structurally and immunologically similar to infectious viruses, as determined by electron microscopy and their ability to bind conformation-dependent monoclonal antibodies. L1 can bind to cell surface hepran sulphates, which are thought to be site of viral attachment to the host cell [55].

1.8.8 L2 Protein

The L2 protein is the minor capsid protein and is approximately 50 kDa in size. As well as playing a structural role in the viral capsid it has also been suggested to play a number of other roles. VLPs made up of L1 and L2 proteins combined show a different pattern of distribution once taken into a cell compared to VLPs made up of L1 alone [56]. L1 VLPs remain widely and diffusely distributed throughout the cytoplasm, whereas L1/L2 VLPs exhibit a radial distribution across the cytoplasm and accumulate in the perinuclear region, suggesting that L2 may be involved in the transport of the virions across the cytoplasm [57].

1.9 Detection of HPV

Nearly all HPV detection assays currently in use rely on the assessment of viral nucleic acids, mostly DNA. Originally, Southern blot and Northern blot hybridizations were the methods of choice for HPV DNA and RNA detection, respectively. These methods, however, require large amounts of input material are time consuming and in principle can only detect one HPV type at a time. In addition, they are not applicable to routine formalin-fixed tissue specimens that typically contain crosslinked, severely degraded nucleic acids. The HPV detection methods that are currently in use can broadly be subdivided into target amplification methods and signal amplification methods. Target amplification methods utilize nucleic acid polymerases, target-specific oligonucleotides('primers'), and a mixture of deoxyribonucleotides to amplify a specific nucleic acid sequence up to a level at which it can be easily detected [58].

Signal amplification methods are based on an initial hybridization step of nucleic acids in the specimen with target-specific probes in liquid phase or in situ on cells or tissue slides, after which the signal (i.e. the hybridization event) is amplified and ultimately visualized with one of the various available methodologies. The most common of these tests, and the one that has been approved by the Federal Drug Administration, is the Hybrid Capture 2 (HC2) test. This is a solution based hybridisation method that uses two RNA probe cocktails, one that contains probes for 5 low-risk HPV types, and one that contains probes for 13 high-risk types, to detect the presence of HPV [59]. The HPV DNA-RNA hybrid is immobilised on the wall of a microtiter plate before a luminescent product is generated through a series of reactions. As the intensity

of the signal is proportional to the amount of target that was present in the sample this is a semi-quantative method for HPV detection [59]

PCR is widely used tool capable of amplifying very limited amounts of DNA, generating thousands to millions of copies of a particular DNA sequence, to a level which is more easily detectable. Since its initial development 1980s by Kary Mullis [60] it has become a widely used tool in medical and biological labs in both research and diagnostic settings. Today PCR is one of the most widely used tools for the detection of HPV DNA due to its ability to test samples with low levels of tissue or cells or poor quality DNA. Given the fact that many different HPV types exist, two different primer designs were developed to identify both the broad presence of HPV and specific subtypes of the virus. Type-specific PCR uses a set of primers that is specific for only one distinct type of HPV, where as consensus primers can detect a broad-spectrum of HPV types with only one primer set. Most type-specific and consensus primers are directed against highly conserved sequences of the HPV genome, almost exclusively within the L1 or E1 open reading frames [61]. Some of the first consensus PCR assays designed were the MY09⁄ 11 and GP5⁄6-PCR systems. From the latter two, which target 450 base pair and 150 base pair regions within L1, respectively, second-generation, modified versions (i.e. PGMY from MY09⁄ 11 and GP5+⁄6+- PCR from GP5⁄ 6-PCR, respectively) were developed. Today, these assays still belong to the most commonly used HPV detection assays. By utilizing the conserved L1 sequences targeted by MY09 and GP5+ primers, a short-fragment PCR assay, the SPF_{10}, was subsequently developed that amplifies a 65 base pair region [62]. Despite overall sequence conservation in the viral L1 and E1 regions, these assays still had to deal with some degree of inter-type heterogeneity at the nucleotide level, which precluded the selection of single primer pairs that

fully match corresponding sequences of a broad spectrum of HPVs. Therefore, to ensure broad-spectrum HPV detection, consensus primer assays either use low-stringency PCR conditions to allow some degree of mismatch acceptance between primers and target sequence (as used in GP5⁄6-PCR and GP5+⁄6+-PCR), degenerate primers with nucleotide variations at ambiguous base positions (as used in MY09⁄ 11), or combinations of the two (as used in SPF_{10}) [61] [63].

1.10 Structure and function of adherens and tight junctions

Adherens juctions and tight junctions comprise two modes of cell-cell adhesion that provide different but complimentary functions. The presence of adherens junctions is a defining feature of all epithelial sheets [64] with adherens junctions performing multiple vital functions including initiation and stabilization of cell-cell adhesion, regulation of the actin cytoskeleton, intracellular signaling and transcriptional regulation [65]. The core of the adherens junction includes interactions among transmembrane glycoproteins of the classical cadherin superfamily, such as E-cadherin, and the catenin family members including p120-catenin, β-catenin, and α-catenin (Figure 1.10 & Figure 1.11) [65]. Together, these proteins control the formation, maintenance and function of adherens junctions [65]. Junctional E-cadherin–catenin complexes exhibit several important characteristics that are critical for the proper functioning of epithelia. Homophilic interactions between the extracellular portions of E-cadherin molecules help to provide mechanically strong adhesive links between cells in the tissue (Figure 1.10) [66]. In addition, AJs help to define an epithelial cell's apical–basal axis in many systems and, in doing so, act as a reference point for the coordination of cell polarity across the epithelial sheet [66]. The process of AJ formation is dependent on the local activation of the Rho family GTPase Rac following contact between neighbouring cells [67] . Rac drives the formation of actin-based protrusions in the cell that carry E-cadherin to site of cell-cell contact and initiate junction formation [68] [69]. This collaboration between Rho GTPases and AJ components continues during AJ maturation, as tight junctions and apical–basal polarity are established through the action of both Rac and Cdc42. Interaction between these activated Rho family GTPases and Par6 leads to the activation of atypical PKC (aPKC), which has been shown

to be required for the maturation of AJs from simple cell–cell adhesions to junctional complexes [66] [70].

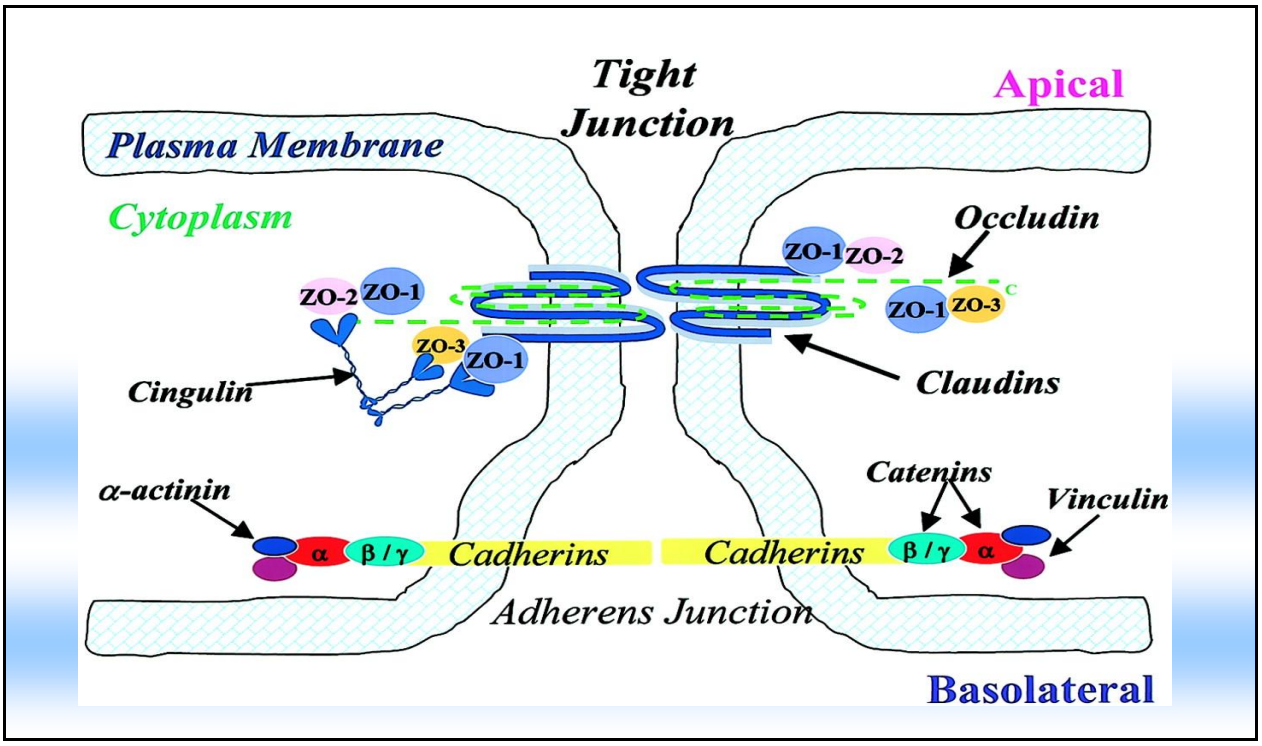

Figure 1.10 Structure and components of adherens and tight junctions [71]

Adherens and tight junctions are maintained by the interaction of a number of key proteins. Claudins and occludin are the main intercellular proteins of the tight junction that form cell-cell contacts between neighbouring cells, with cadherins performing a similar role in adherens junctions. Intra-cellular domains of claudin and occludin bind to several additional proteins, such as ZO-1, that link the junctions to the actin cytoskeleton of the cell.

Tight junctions have been proposed to have two mutually exclusive functions: a fence function which prevents the mixing of membrane proteins between the apical and basaolateral membanes; and a gate function which controls the paracellular passage of ions and solutes in-

between cells [72]. Tight junctions contain two types of transmembrane proteins, occludins and claudins, which confer these functions, and associated cytoplasmic proteins that link tight junctions to the actin-cytoskeleton (Figure 1.11) [73]. In epithelial cells, tight junctions are the most apical component of the junctional complexes, whereas their localisation is more variable in endothelia [73]. The two major types of integral membrane proteins are classified according to the number of transmembrane domains they contain: four-pass transmembrane proteins such as claudins, occludin and tricellulin, and single-span transmembrane proteins including the junctional adhesion molecule (JAM) and the Coxsackie and adenovirus-associated receptor (CAR) [74]. Lateral association between claudin molecules within the plasma membrane, combined with homotypic adhesive interactions between claudin molecules on adjacent cells, is thought to underlie the characteristic structure of tight junction strands [75]. The association of other integral membrane proteins to the claudin-based strands provides additional complexity to tight junction structure. Occludin, the first transmembrane component of tight junctions to be identified also localises to the tight junction strands and has been implicated in regulating the permeability properties of tight junctions and, in particular, has been linked to the regulation of size-selective diffusion [76]. JAMs and related proteins function as adhesion proteins, homotypically as well as heterotypically, and regulate various processes such as leukocyte transmigration [77]. Underlying the membrane domain is the cytoplasmic plaque, a network of densely packed peripheral proteins that connect the integral membrane proteins to the underlying actin cytoskeleton as well as to different types of signaling proteins. Prominent examples are the zona occludens proteins ZO-1, -2 and -3: each contains multiple protein-interaction domains, including three PDZ domains and an SH3 domain, through which they

demonstrate affinity for a number of cytoskeletal proteins, signalling molecules and membrane proteins [78].

Tight junctions are dynamic structures and thus a wide array of growth factors, cytokines, drugs, and hormones regulate tight junctions and barrier function. For example, the glucocorticoid hydrocortisone, prolactin, and unsaturated fatty acids all enhance the tight junction barrier partially by increasing the expression of occludin in endothelial and epithelial cells [79] [80] [81]. Cytokines and growth factors, such as tumor necrosis factor-α, interferon-γ, interleukin-1β, transforming growth factor-α also play a role in influencing TJ permeability and many cases lead to development of disease [81]. Cytokine mediated changes in paracellular permeability are linked to a multitude of pathologic conditions including inflammatory bowel disease (IBD), airway inflammation in asthma and cystic fibrosis, and diseases that perturb the blood-brain barrier (BBB) [82] [83] [84].

1.10.1 Epithelial Cadherin (E-cadherin)

E-cadherin is a transmembrane glycoprotein that is one of the primary constituents of adherens junctions in epithelial tissues with the protein being encoded in humans by the CDH1 gene which maps to chromosome 16q22.1. [85]. It is a member of the cadherin superfamily of calcium dependent proteins, which each contain five extracellular repeat domains, termed extracelluar cadherin (EC) domains. These domains are the primary areas of trans-cadherin interactions between neighbouring cells and initiate cell-cell adhesion and formation of the adherens junction (Figure 1.11) [86]. The intracellular portion of E-cadherin binds to several additional proteins that play a diverse set of roles, from binding to the actin cytoskeleton of the cell to intracellular signaling and gene regulation. On the cytoplasmic side of the membrane, a bundle of actin filaments is linked to the E-cadherin molecules via a protein complex (Figure 1.11). Alpha-catenin and either beta- or gamma-catenins are included in this complex [87]. Beta- and gamma-catenins share significant homology and bind to a specific domain at the E-cadherin C-terminus. Alpha-catenin links the bound beta- or gamma-catenin to the actin cytoskeleton [87]. The structure of the extracellular domain of classical E-cadherin contains five tandem repeats of a 100-residue-amino-acid-motif, and the biggest part of the N-terminal of these repeats contains the sites with adhesive activity [86]. This part of the molecule also has binding sites for calcium ions situated in the pockets between the repeats. The amino acid sequences that form the Ca2+ binding pockets are highly conserved between different members of the cadherin family and between different species [86]. Cell-cell adhesion is mediated through homotypic interactions of E-cadherin extracellular domains in a process of

lateral dimerisation. Parallel dimers are able to interdigitate with dimers from neighbouring cells forming the points of adhesion [86].

Malignant carcinoma cells are characterised in general by poor intercellular adhesion, loss of the differentiated epithelial morphology and increased cellular motility. Downregulation of E-cadherin expression, mutation of the E-cadherin gene, or other mechanisms that interfere with the integrity of the adherens junctions, are often observed in carcinoma cells [88]. In human tumours, the loss of E-cadherin mediated cell adhesion correlates with the loss of the epithelial morphology and with the acquisition of metastatic potential by the carcinoma cells [88]. Thus, a tumour invasion-suppressor role has been assigned to this gene [88].

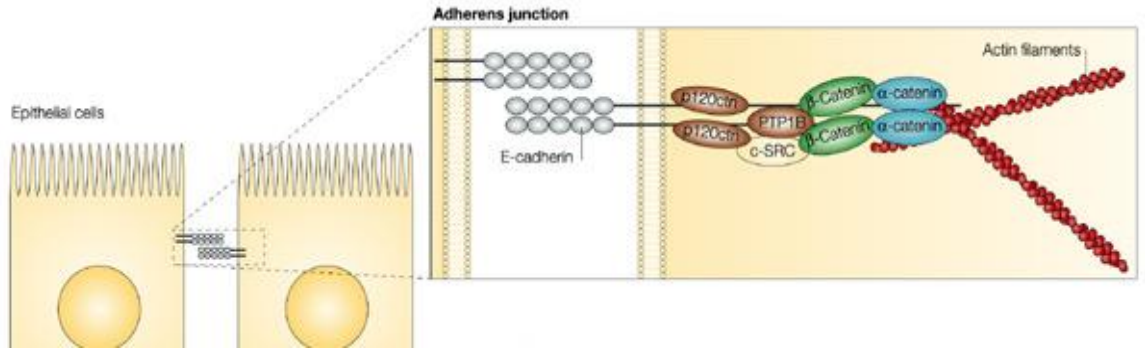

Figure 1.11 Outline of the structure and components of an adherens junction between two neighbouring epithelial cells. [89]

Adherens junctions are initiated by homotypic binding of E-cadherin between neighbouring cells. A number of intra-cellular components, such as p-120 catenin and β-catenin, bind to intra-cellular domains of E-cadherin and link the junction to the actin cytoskeleton of the cell.

1.10.2 p120-Catenin

p120 catenin (p120) is an armadillo (ARM) repeat-containing protein (Figure 1.12) that, along with the classical cadherins, β-catenin and α-catenin, plays a crucial role in the regulation of cell-cell adhesion at adherens junctions (AJs) [90]. p120 plays a pivotal role in both promoting E-cadherin stability and a sessile cellular phenotype or inducing cell migration and invasiveness of E-cadherin–deficient cells through its effects on Rho GTPase activities [91]. p120 family members share a conserved central domain composed of 9 ARM repeats and flanking N- and C-terminal regions. p120 plays a role in stabilising E-cadherin by interacting with the juxtamembrane domain of E-cadherin, which consists of 40 amino acids at the N-terminal end. It is believed that the binding of p120 to the juxtamembrane domain of cadherin blocks factors such as the ubiquitin ligase Hakai and components of the endocytic machinery, which tag and target cadherin for destruction and internalisation [92]. Both loss of expression and mislocalised expression of p120 have been observed in tumours [93] [94] . The role of p120 in regulating tumours growth, likely occurs as a result of the protein's interaction with E-cadherin [91]. In the mammary epithelial cell line MDA-MB-231, p120 induces the transformed growth of E-cadherin–deficient cells by activating a Rac1–MAPK signaling pathway normally activated by the adhesion of cells to the ECM. When E-cadherin is re-expressed in this cell line, it is stabilised by p120 association and selectively and potently inhibits the growth of epithelial cells [91].

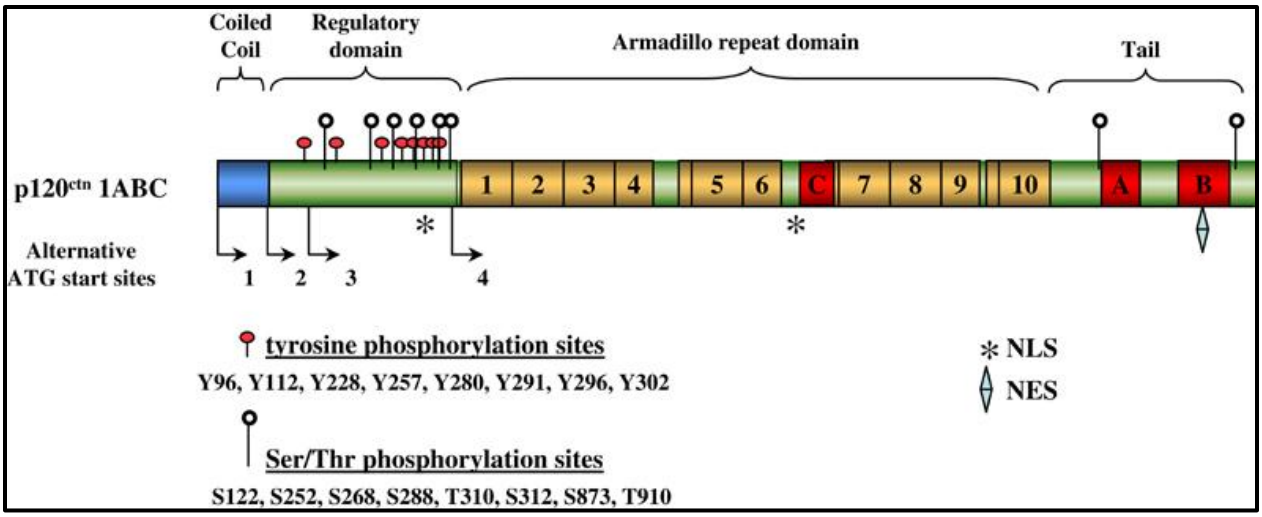

Figure 1.12 Structure and functional elements of p120-catenin [90]

p120 contains 10 central Armadillo repeat domains (orange) that are essential for cadherin binding. The carboxy-terminal tail contains at least two serine/threonine phosphorylation sites (open lollipops), and alternatively spliced exons A and B (red). The amino-terminal end contains two distinct regions, the coiled-coil domain (blue), and the regulatory domain (green). The regulatory domain contains the vast majority of tyrosine (red lollipops) and serine/threonine (open lollipops). Exact amino-acid locations of the known sites are listed. Their individual roles are unknown, but collectively, they participate in the dynamic regulation of p120 adhesive function.

1.10.3 Claudin family of proteins

The tight junction is an intercellular junctional structure that mediates adhesion between epithelial cells and is required for proper epithelial cell function [95]. Tight junctions control paracellular permeability across epithelial cell sheets and also serve as a barrier to intramembrane diffusion of components between cells apical and basolateral membrane domains [96]. Claudins are tetraspan transmembrane proteins of tight junctions. They determine the barrier properties of this type of cell–cell contact existing between the plasma membranes of two neighbouring cells. Claudins can completely tighten the paracellular cleft for

solutes, and they can form paracellular ion pores [97]. The claudin family consists of at least 24 members (Figure 1.13), with each showing a specific organ and tissue distribution [95]. A large degree of sequence homology is found between claudins 1–10, 14, 15, 17 and 19. Combined with functional findings, these claudins are therefore grouped together as the classical claudins (Figure 1.13) [98]. All other claudins are termed non-classical claudins (Figure 1.13).

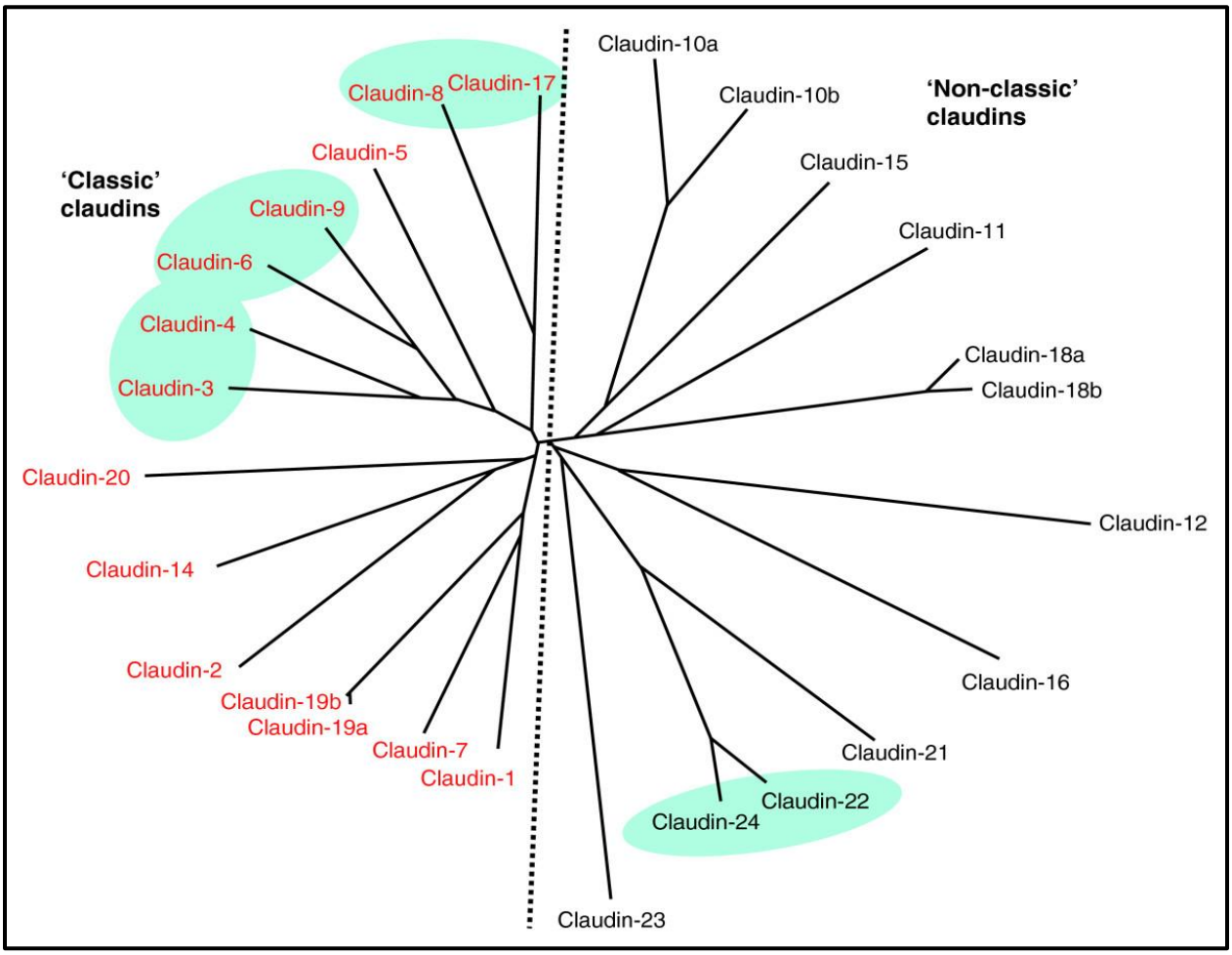

Figure 1.13 Phylogenic tree of the claudin family of proteins showing levels of similarity between different different proteins. In red are the classical claudins and in black are the non-classic claudins. Highly similar claudins encoded by genes located in close proximity in the human genome are highlighted in green. [95]

Claudins are tetraspan proteins with relatively short cytoplasmic amino and carboxy termini flanking a first extracellular loop of approximately 53 amino acids and a second shorter loop of approximately 24 amino acids in length (Figure 1.14) [95]. The cytoplasmic C-terminus sequence varies considerably in length (from 21–63 residues) and sequence between isoforms [98]. All claudins have C-terminal PDZ binding motifs that enables direct interaction with tight junction cytoplasmic proteins such as ZO-1,-2, and -3, multi-PDZ domain protein (MUPP)-1 and PALS-1 associated TJ protein (PATJ) (Figure 1.14) [97]. In particular, interactions with the cytoplasmic scaffolding proteins ZO-1 and ZO-2 indirectly link claudins to the actin cytoskeleton which stabilises the tight junction and is required to maintain their permeability characteristics. The function of the short N-terminal domain is yet to be fully elucidated [99]. Just as different tissue types tend to have their own unique pattern of claudin expression; different tumours have been shown to have distinct patterns of abnormal claudin expression. Claudin 3 and claudin 4 have been shown to be overexpressed in certain types of ovarian cancer [100], whereas Claudin-1 is overexpressed in colon tumours [101] but loss of expression is observed in some breast tumours [102]. A small number of studies have also observed changes in claudin expression in both pre-invasive and invasive cervical lesions. Lee et al., 2005 observed a gradual increase in claudin-1 and claudin-7 expression in accordance with the progression from LSIL to HSIL and invasive cancer. Sobel et al., 2005 observed an increase in claudin-2 and claudin-4 expression as well as claudin-1 and -7, in pre-invasive and invasive cervical lesions.

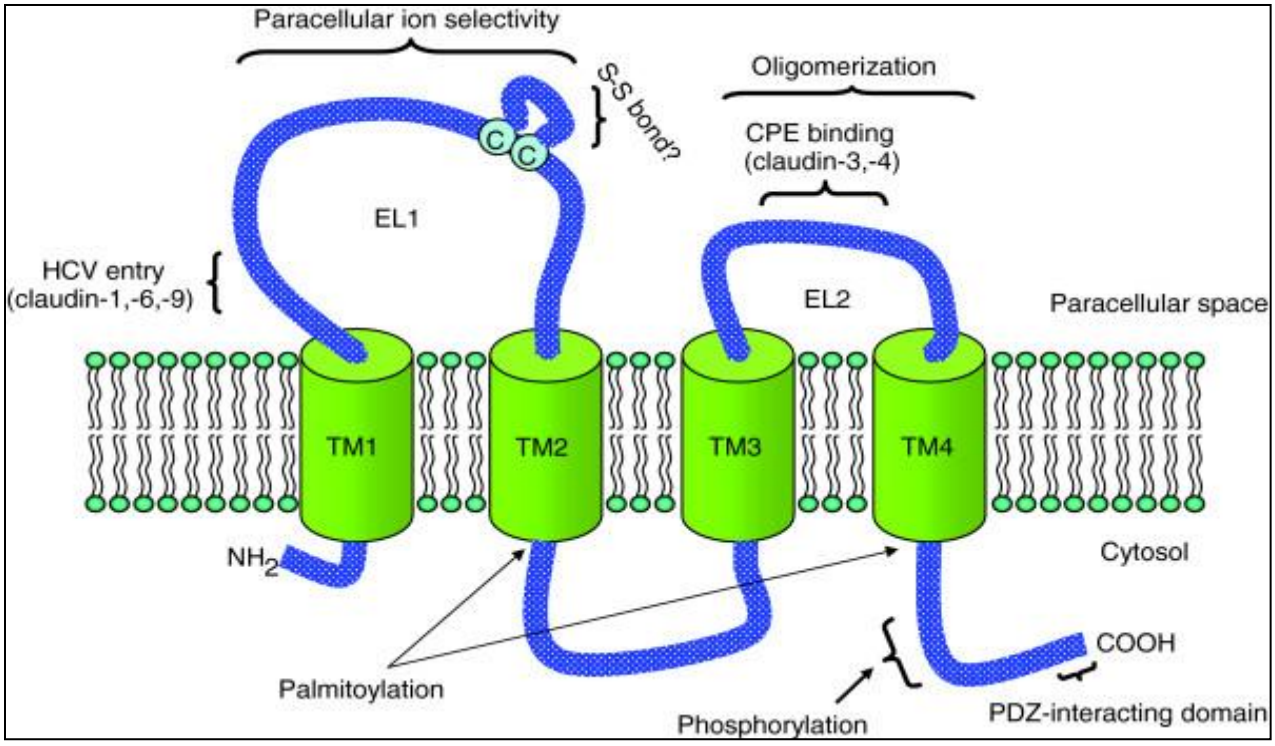

Figure 1.14 Schematic representation of the claudin monomer. The model depicts the conserved structural features of claudins and some of the known interactions and modifications. EL1 and EL2 denote the extracellular loops 1 and 2, respectively. The transmembrane domains 1 to 4 (TM1 to TM4) and the regions important for hepatitis C virus (HCV) entry and Clostridium perfringens enterotoxin (CPE) binding are shown [95]

1.10.4 Claudin-1

Claudin-1 protein is made up of 211 amino acids and has a molecular weight of 22,744 Da. The gene encoding the protein is located on chromosome 3q28-q29. Claudin-1 has quite a wide distribution in normal human tissue being found in the epidermis of skin [103], distal nephron [104] and ovarian epithelium [105], as well as several other tissues [106]. Experiments in claudin-1 knockout nude mice have shown that Claudin-1 plays a key role in maintaining the epidermal barrier, with claudin-1 deficient mice dying at 1 day post birth from transepidermal water loss [107]. Claudin-1 had been observed to bind homophillically with claudin-1 proteins on neighbouring cells and can also form heterotypic interactions with Claudin-3 proteins in co-transfected fibroblast cells [75] [108]. The role of claudin-1 controlling paracellular permeability is further highlight by experiments that show Claudin-1 transfected epithlial cell lines display an increase in transepithilal electric resistance [109], most likely by decreasing cation permeability [110].

In terms of pathology, Claudin-1 has been observed to have many roles. Claudin-1 is a co-receptor for HCV infection of human hepatoma cell lines and is the first factor to confer susceptibility to HCV when ectopically expressed in non-hepatic cells. Discrete residues within the first extracellular loop (EL1) of CLDN1, but not protein interaction motifs in intracellular domains, are critical for HCV entry [111]. Dysregulation of claudin-1 expression itself has been associated with pathogenesis in many different tumours. Studies have identified that Claudin-1 overexpression is associated with an increased invasiveness in oral carcinoma cells through upregulation of several matrix metalloproteases [112] [113]. Claudin-1 expressing colon

carcinoma cells that underwent siRNA mediated knockdown of Claudin-1 displayed significantly decreased anchorage-independent growth and invasion with a significant decrease in MMP-9 activity [114]. Conversely, claudin-1 overexpression suppresses metastasis and invasion in lung cancer cell lines [115].

1.10.5 Claudin-7

Claudin-7 is a member of the classical claudin family and is a protein made up of 211 amino acids with a molecular weight of 22,390 Da [116]. Like other claudins, claudin-7 expression is tissue specific with expression observed in the nephron, breast and corniel epithelium [106]. Claudin-7 is essential for NaCl homeostasis in distal nephrons, and the paracellular ion transport pathway plays an indispensable role in keeping ionic balance in kidneys. In claudin-7 knockout mice severe salt wasting, chronic dehydration, and growth retardation was observed; with knockout mice surviving no longer than 12 days [117]. The role of claudin-7 in regulating cellular paracellular permeability is further highlighted by experiments showing that claudin-7 transfected epithelial cells display increased TEER values [109] and also experiments in LLC-PK1 cells that show claudin-7 overexpression decreases paracellular permeability to Cl- and increases paracellular permeability to Na+ [118].

The role of claudin-7 in disease and tumourigenesis is becoming clearer, with aberrant expression observed in several different tumour types. Increased expression of claudin-7 has been observed in gastric [119] and ovarian tumours [120]. In contrast, reduced expression has been observed in prostate [121] and oesophageal tumours [122]. In vitro studies using cell lines

have helped shed further light on how claudin-7 drives tumourigenesis. Knockdown of claudin-7 expression in oesophageal squamous cell carcinoma cells induces loss of E-cadherin, along with increased cell growth and enhanced cell invasion [123]. Similarly, claudin-7 inhibits the migration and invasion of lung cancer cells through a mechanism involving the ERK/MAPK signalling pathway [124]. In contrast claudin-7 may have tumour promoting properties in other cell lines, with overexpression of claudin-7 promoting invasion in ovarian cell lines [125] and also in colon carcinoma cell lines [126].

1.10.6 Neural-cadherin (N-cadherin)

N-cadherin is encoded in humans by the CDH2 gene and is similar to other members of the classical cadherin super-family in that it is a calcium dependent cell-cell adhesion glycoprotein comprising five extracellular cadherin repeats, a transmembrane region and a highly conserved cytoplasmic tail [127]. In embryogenesis, N-cadherin is a key molecule during gastrulation and neural crest development, where N-cadherin mediated contacts activate several pathways like Rho GTPases and function in tyrosine kinase signalling [128]. N-cadherin is expressed by a group of cells in the developing embryo known as the neural crest which are a pluripotent population of cells that arise from the dorsal part of the neural tube during or just before closure. After an epithelial-mesenchymal transition (EMT), they migrate over long distances along distinct pathways to many different regions of the embryo and contribute to a diverse array of tissues and cell types, such as the peripheral nervous system, melanocytes, some endocrine cells, craniofacial cartilage and bone [128]. In adult tissues N-cadherin expression is restricted to

neural tissue, retina, endothelial cells, fibroblasts, osteoblasts, mesothelium, myocytes [128]. In neural tissue it is involved in a number of key events that range from the control of axonal growth and guidance to synapse formation to synaptic plasticity [129].

N-cadherin has also been implicated in the tumorigenesis of several epithelial and other malignancies [130]. One of the methods by which this process is driven is through a downregulation of E-cadherin and upregulation of N-cadherin; termed a 'cadherin switch' [131]. The effect of E-cadherin downregulation is that cells can lose their cohesive structure and can more easily detach and disseminate from their original site. N-cadherin up-regulation is thought to promote tumourigenesis in a number of ways. Epithelial cell lines with overexpressed N-cadherin have been shown to have increased motility and have a greater invasive and metastatic potential [132] [133]. The increased invasiveness and metastatic behaviour of N-cadherin over-expressing cells may in part be due to N-cadherins ability to interact with the Fibroblast growth factor receptor and enhance its downstream signalling [132] [134]. In addition to modulating the invasive characteristics of tumour cells, expression of N-cadherin might also promote metastasis by facilitating interactions with the endothelium. Endothelial cells express two cadherins: VE-cadherin, which is localised in junctions and serves to organise the junctional complex in these cells, and N-cadherin, which is extrajunctional and has an unclear role [131]. Endothelial cells may use N-cadherin to interact with other N-cadherin-expressing cells such as vascular smooth muscle cells and/or pericytes [135]. It is equally likely that tumour cells that express N-cadherin have an increased ability to interact with endothelial cells and that this interaction may enable metastasis by allowing the tumour cells access to the vasculature [131].

N-cadherin has now been identified as potential novel target for cancer therapy. A peptidic N-cadherin antagonist (ADH-1) has been developed and has entered clinical testing as a potential novel cancer therapy [136]. ADH-1 has been shown to inhibit cell growth and motility in vitro, and tumour growth and invasion in vivo [136]. In addition, Erez et al. 2004 [137] have shown that treatment of endothelial cells, which express both N-cadherin and VE-cadherin, with ADH-1 induces apoptosis in a cell-density-dependent manner and suggest that ADH-1 might be effective at preventing tumour angiogenesis.

1.10.7 Snai1 (Snail)

Snail is a part of a family of zinc fingered proteins that play an important role in the regulation of development via its ability to downregulate the expression of ectodermal genes within the mesoderm of the embryo [138]. The protein is encoded in humans by the SNAI1 gene localised on the chromosome 20q13.2, and encodes a protein with 264 amino acids and 29.1kDa [138] While the protein undoubtedly is necessary for successful embryonic development, highlighted by the fact that Snail null mice die during embryogenesis [139], the protein may promote tumourigenesis in a process termed epithelial to mesenchymal transition (EMT) [140]. EMT is a hypothesised process that describes how epithelial cells can lose their normal cohesive structure and adopt a more motile and invasive phenotype that is commonly observed in malignant cells. Snail can drive this process by repressing the expression of proteins normally associated with the epithelial phenotype such as E-cadherin and Claudin-1. Snail is able to repress the expression of E-cadherin by binding to certain E-box motifs in the proximal E-

cadherin promoter and negatively regulating the expression of the gene [141]. Snail has been shown to repress Claudin-1 expression by a similar mechanism in MDCK (Madin–Darby canine kidney) cells, with cells overexpressing Snail showing a dramatic down-regulation of Claudin-1 protein levels and a significant reduction of Claudin-1 mRNA [142]. Additionally Snail has been recently proposed to act as a cell survival factor and inhibitor of cellular senescence in some prostate carcinoma cells lines, with long-term siRNA mediated knockdown of Snail inducing a severe decline in cell numbers of transfected cells [143]. Currently there is very little known about the role SNAIL may play in cervical neoplasia, or about it's expression in pre-invasive and invasive cervical lesions. An IHC based study of 144 cervical tissue samples, 28 normal tissue 116 SCC, by Zhao et al 2013., found an increase in SNAIL expression in SCC samples compared to normal cervical tissue, but there are very few other studies published to corroborate these findings.

1.11 Epithelial to Mesenchymal Transition (EMT)

Epithelial tissues line the cavities and surfaces of structures throughout the body. The cells that make up the epithelium are typically closely packed together in continuous cohesive sheets that are attached to a basement membrane, which acts as a scaffold for the epithelial cells to grow [144]. Epithelial cells are normally polarised, or have distinct domains at apical and basolateral portions of their plasma membranes. Each plasma membrane domain has a distinct protein composition, giving them distinct properties and allowing directional transport of molecules across the epithelial sheet [144]. Mesenchymal tissue is a form of connective tissue usually found in the mesoderm germ layer of the developing embryo. It consists of undifferentiated, motile, non-polarised, loosely associated cells surrounded by a ground substance ECM (Extra Cellular Matrix), containing reticular fibers [145]

Epithelial to mesenchymal transition (EMT) is a process by which an epithelial cell loses the cohesiveness and apical-basolateral polarity normally associated with it, and adopts characteristics usually associated with a mesenchymal phentotype, such as enhanced migratory capacity, invasiveness, and greatly increased production of ECM components [146]. EMT is a process that occurs normally during several phases of embryogenesis, including implantation and placenta formation [147] and neural crest formation [148]. EMT also occurs is tissues that have been damaged or injured and are undergoing fibrosis. In mouse models this type of EMT is mediated by inflammatory cells and fibroblasts through secretion of pro-inflammatory cytokines, growth factors and matrixmetaloproteases (MMPs) [149]. Epithelial cells come under the influence of these signalling molecules and, acting together with the inflammatory cells,

induce basement membrane damage and focal degradation of type IV collagen and laminin [149] [150]. Although the concept of EMT was originally devised to explain various processes that occur during embryogenesis, the concept has since been applied as a model for cancer progression and metastasis [151]. It was observed that a number of processes that occur during EMT in embryogenesis such as, loss of epithelial markers, loss of cell polarity, cytoskeleton reorganisation and activation of MMPs, closely resembled those that occurred during tumourigenesis in epithelial malignancies (Figure1.15) [151]. It is therefore possible that the understanding of comparisons of EMT signaling pathways in embryological development and cancer progression may make it possible to identify novel pathways specific to cancer progression and to suggest new therapeutic strategies in cancer therapy [152] [153].

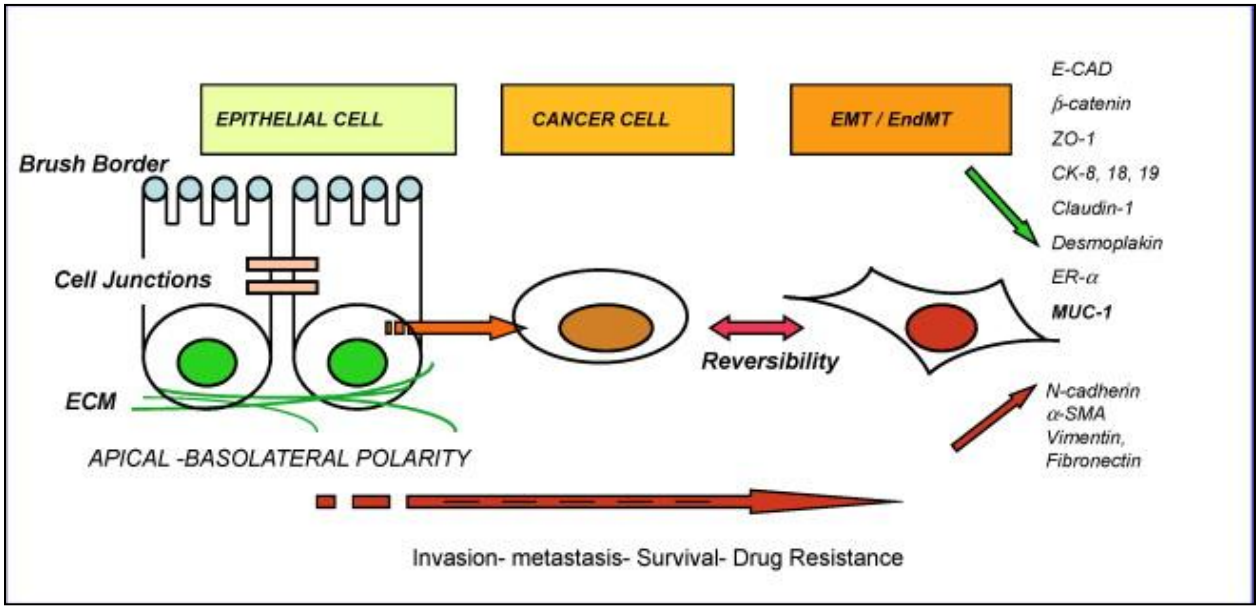

Figure 1.15 Alterations of the apical–basal and planar cell polarity pathways in epithelial–mesenchymal transitions. The EMT signature is characterised by the convergent loss and relocalisation of epithelial markers (e.g. E-cadherin, β-catenin), and gain of mesenchymal markers (e.g. N-cadherin, α-SMA, vimentin and fibronectin) [154].

Multiple complex signaling systems are required for induction of EMT because epithelial cells undergoing EMT must undergo both functional and morphologic changes. In the case of many carcinomas, EMT-inducing signals emanating from the tumour-associated stroma, notably HGF, EGF, PDGF, and TGF-β, appear to be responsible for the induction or functional activation in cancer cells of a series of EMT-inducing transcription factors [150]. Transforming growth factor beta (TGF-β) in particular is thought to play a key role in EMT promotion [150] and was first identified as an inducer of EMT in experiments on mammary epithelial cells by Miettinen et al. 1994 [155]. TGF- β induces EMT through multiple signalling pathways including direct phosphorylation of Smad 2 and Smad 3 (Figure 1.16) [153]. SMAD are small signal transduction proteins that activate several signaling pathways in the nucleus. TGF-β also activates other EMT-related signal pathways including the Wnt, Integrin and Notch pathways (Figure 1.16) [153] . TGF-β and other growth factors also serve to activate a number of transcription factors such as Snail, Slug, zinc finger E-box binding homeobox 1 (ZEB1), Twist, and FOXC2 [153]. Loss of E-cadherin expression is a considered a key step in EMT and several of these transcriptional factors are able suppress expression of E-cadherin. Snail and Zeb bind directly to E-box motifs in the E-cadherin promoter [156], whereas Twist and Goosecoid, repress E-cadherin expression indirectly [152] [157].

Loss of cell polarity is also a crucial step in EMT. In epithelial cells, three protein complexes partake in establishing and maintaining apicobasal polarity Par, Crumbs and Scribble [158]. SNAIL alters epithelial cell polarity by repressing the transcription of Crumbs3 and abolishing the localisation of both Par and Crumbs complexes at tight junctions [159]. Similarly, Zeb1 directly represses the transcription of cell polarity genes, including Crumbs3, Pals1-

associated tight junction proteins (PATJ), and the member of the Scribble complex Lethal giant larvae (Lgl2) [160]. TGF-β contributes to the loss of cell polarity during EMT in two ways, through the canonical pathway by inducing Snail and Zeb genes expression and through a noncanonical pathway that involves the downregulation of Par3 expression and the Par6-mediated degradation of RhoA and local alteration of the actin cytoskeleton [157] [161] [162].

An additional component to the regulation of EMT is the effect of small micro RNAs (miRNAs) that can play a role in inhibition or promotion of EMT inducers (Figure 1.16). Micro RNAs are small non-coding RNA molecules which primarily influence post-transcriptional regulation of gene expression. For example, microRNA 200 (miR200) and miR205 inhibit the repressors of E-cadherin expression, ZEB1 and ZEB2, and thereby help in maintaining the epithelial cell phenotype (Figure 1.16) [163]. Another miRNA, miR-148a, promotes the expression of E-cadherin and reduces the levels of mesenchymal markers (N-cadherin, fibronectin or vimentin) in hepatoma cells by inhibiting SNAIL expression [164]. In contrast, miR-9, a MYC/MYCN-induced miRNA, directly targets the E-cadherin-encoding mRNA leading to increased cell motility/invasiveness in breast tumour cells [165].

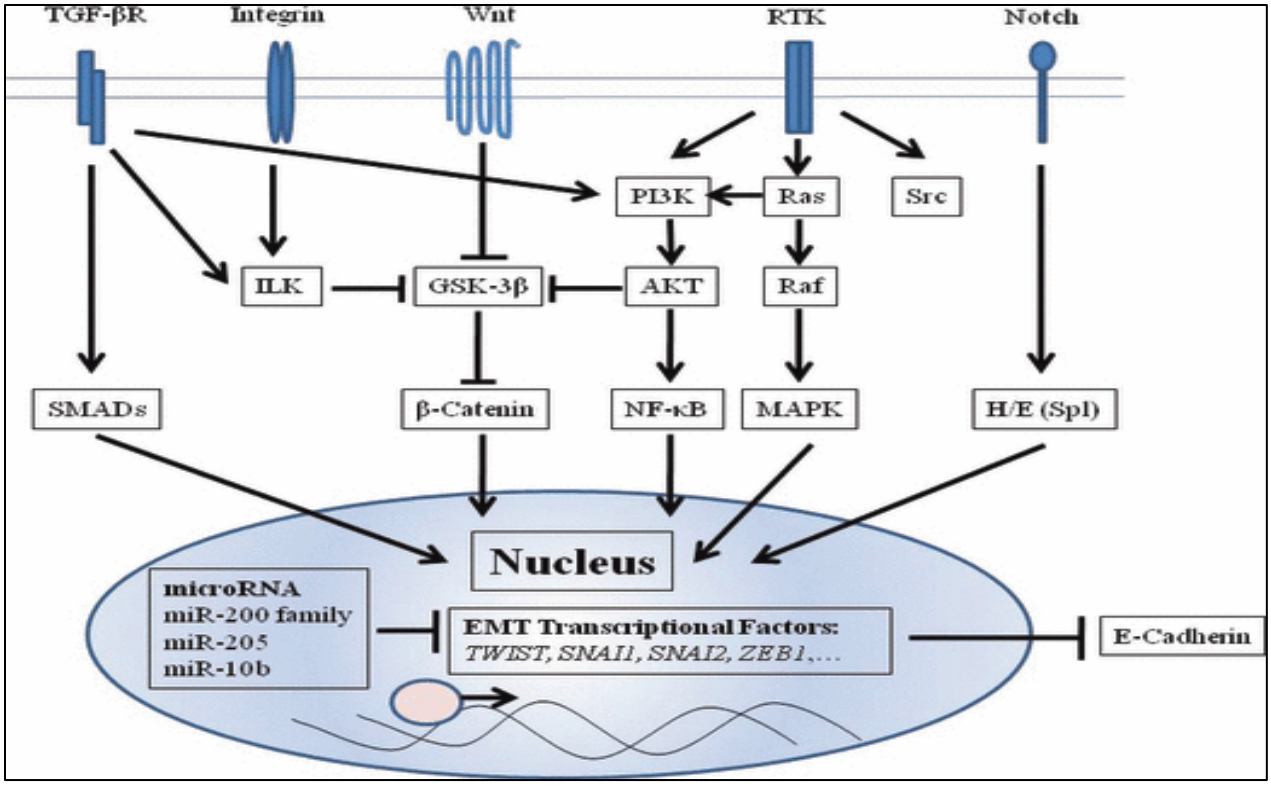

Figure 1.16 Depiction of signal pathways regulating the epithelial–mesenchymal transition (EMT) [153]

Transforming growth factor (TGF)-β signals toward the SMAD pathway or the PI3K/AKT axis. Wnt ligands block β-catenin degradation leading to excess β-catenin entering the nucleus and upregulating SLUG and SNAIL transcription. In integrin signaling, overexpression of ILK leads to nuclear translocation of β-catenin. Signals via RTK lead to EMT through the Ras-Raf-MAPK pathway or the PI3K/AKT pathway.

1.12 Hypothesis and aims of this study

The hypothesis of this study is that the expression of a number of tight and adherens junction proteins are altered in HPV induced cervical lesions. Altered protein expression within adherens and tight junctions leads to disruption of their normal structure and function leading to a loss of cell polarity and cohesion. Loss of cell cohesion and polarity allows dysplastic cells to adopt invasive and motile characteristics that may allow dissemination of cells from their site of origin.

- **Overarching aim**
    - To elucidate mechanisms by which HPV induced neoplastic cervical cells invade surrounding tissue and form distant metastases
        - Discover novel biomarkers indicative of disease progression
        - Discover novel tumourigenic pathways that may be of use as targets for new cervical cancer treatments.

- **Specific aims**
    - To construct tissue microarrays containing normal and neoplastic cervical tissue and examine the expression profile of several integral tight and adherens junction proteins

    - To detect and genotype HPV DNA in cervical samples and to look for an association between specific HPV genotypes and aberrant expression of adherens and tight junction proteins

    - To analyse the pathogenesis of aberrant tight and adherens junctions protein expression in cervical cancer cell models

2 Materials and Methods

2.1 Introduction

2.1.1 Tissue Microarrays (TMAs)

Tissue microarrays are conventional paraffin blocks containing several different tissue samples that have been transferred from other donor tissue blocks. They are produced by using a needle to biopsy a standard histological section and placing the core into an array on a recipient paraffin block (Figure 2.1) [166]. The idea of studying a large number of formalin fixed and paraffin wax embedded tissues simultaneously in a single histological section was proposed as far back a 1986 by Battifora et al., [167], although this so called 'sausage' technique described could only include a limited number of samples. The microarray technique, described by Kononen et al. 1998 [168], elegantly eliminated this drawback by the introduction of a high precision punching instrument, which enabled the exact and reproducible placement and relocalisation of distinct tissue samples. Tissue microarray cores are typically between 0.6 and 2.0mm in diameter while arrays may consist of anywhere from 40 to 1000 cores, depending on core size. Arrays can be utilised for a wide range of techniques including histochemical stains, immunologic stains with either chromogenic or fluorescent visualisation, in situ hybridisation (including both mRNA ISH and FISH), and even tissue micro-dissection techniques [166].

There are a number of advantages to using TMAs as compared to normal histological tissue blocks. The technique allows a large number of samples to be examined on one slide and a result of this it greatly reduces the amount of reagents and other materials that need to be

used in any assay. It also reduces the variability that may be associated with an assay examining a large number of samples, as all samples are treated in an identical manner and processed in a single batch. This method also preserves the original tissue block should any further examination of the tissue be necessary in the future.

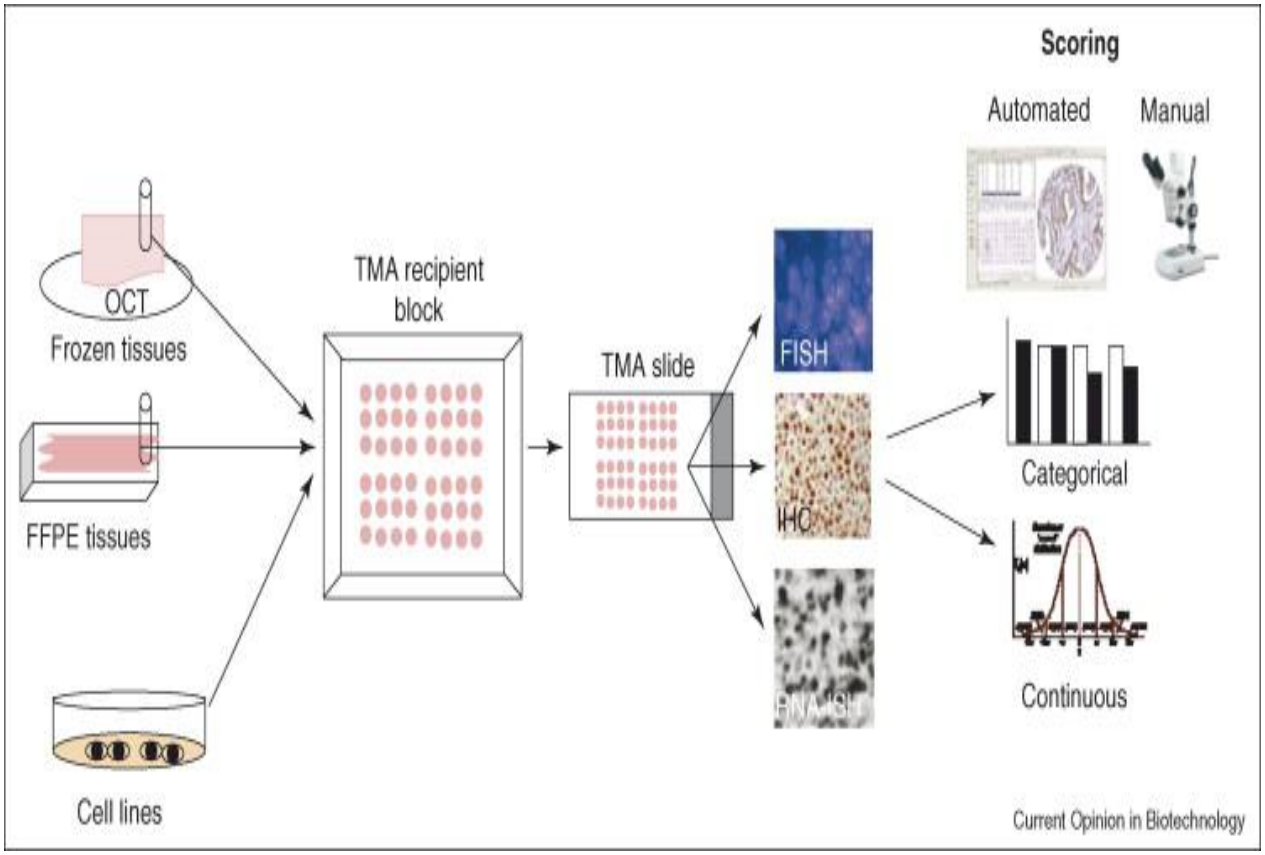

Figure 2.1 Schematic diagram of tissue microarray construction [169].

A large number of individual samples from either frozen tissue, formalin fixed paraffin embedded tissue or cell line are embedded into a single recipient tissue block. The recipient tissue block can then be sectioned and examined using standard histological techniques.

2.1.2 Immunohistochemistry

The publication of a paper by Coons et al. 1941 [170] describing a technique for detecting cellular antigens in tissue sections using fluorescently labeled antibodies marked the beginning of immunohistochemistry (IHC). Since then, IHC has become a valuable tool in both diagnosis and research of infectious and neoplastic diseases. The basis of IHC is very simple and bridges three scientific disciplines: immunology, histology, and chemistry. The fundamental concept behind IHC is the demonstration of antigens (Ag) within tissue sections by means of specific antibodies (Abs). Once antigen–antibody (Ag-Ab) binding occurs, it is demonstrated with a coloured histochemical reaction visible by light microscopy or using fluorochromes visualised under fluorescence microscopy [171]. There are a number of conditions that are essential for the detection of an antigen using immunohistochemistry, the antigen must be preserved in the tissue in the same context as it was during sampling, antibody-antigen binding must be specific and sensitive and there must be efficient labelling and detection of the antibody [172]. Various processes that occur during tissue processing, such as fixation and embedding can cause antigen to be masked, depleted or lost entirely. One of the most common forms of fixation, formalin fixation, causes inter and intra molecular protein cross linking, which can mask the antigen present in the tissue [172]. In order to overcome this, methods of antigen-retrieval were developed. Protease-induced epitope retrieval (PIER) was introduced by Huang et al., 1976 [173]. Many enzymes have been used for this purpose, including trypsin, proteinase K, and pepsin. Heat induced epitope retrieval (HIER) was introduced by Shi et al. In 1991 [174], their method involved heating the sections in a boiling solution of a heavy metal salt. Buffer

using heavy metals were gradually phased out in favour of less toxic alternatives such as citrate and EDTA buffers.

2.1.3 Avidin-Biotin Conjugate Method (ABC) Method

This immunhistochemical method was developed by Hsu et al. 1981 [175] to give much greater sensitivity than the standard avidin-biotin method. This method can be direct or indirect depending on whether biotin is bound to the primary antibody (direct) or to a secondary antibody (indirect). With the indirect method the primary antibody first binds to the antigen, secondly the biotinylated secondary antibody binds to the primary. Then complexs of avidin and biotin horseradish peroxidase conjugate bind to the biotinylated secondary. As the avidin contains more than one biotin-horse radish peroxidase it serves to bring multiple labels to the site of the antigen [176]. Once the enzyme label has been localised to site of the antigen the substrate of the enzyme is added. This results in a product being formed that can be visualised using light microscopy. An example of this process is the reaction between the enzyme horse-radish peroxidase, it substrate hydrogen peroxidase and the chromogen diaminobenzadine (Figure 2.2).

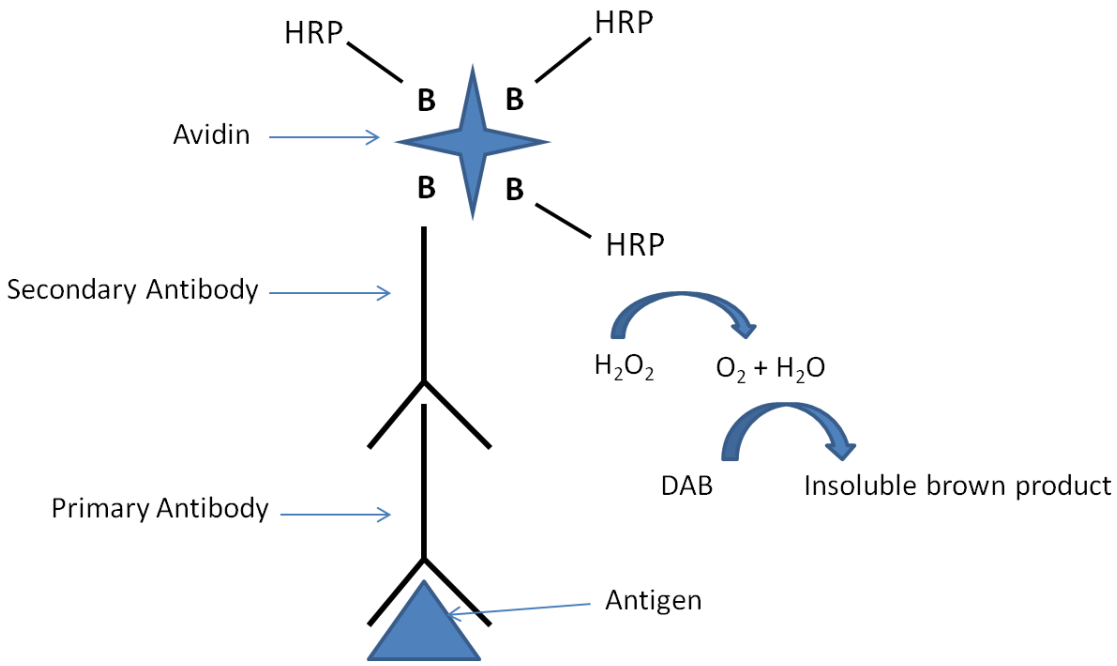

Figure 2.2 Detection of antigen using the Avidin-biotin complex method in conjuction with DAB

Primary antibody binds to antigen followed by a biotinylated secondary binding to the primary antibody. Avidin-biotin-HRP complex then binds to the biotinylated antibody localising the label to the site of the antigen. DAB and H_2O_2 are added leading to the development of an insoluble brown product.

2.1.4 Stable and transient transfection

Transfection is a procedure that involves the introduction of foreign nucleic acids into cells to produce genetically modified cells. The process was first described in 1965 by Vaheri and Pagano and has since become a widely used and valuable tool in biomedical research. By selectively enhancing or inhibiting the expression of a certain gene in cells, the technique allows the study of gene function and offers insights into the role of certain genes in many different biological processes and diseases.

Transfection methods are broadly classified into three groups based on the nature of the technique used to deliver foreign nucleic acids into the target cell, with the ideal method having high transfection efficiency, low cell toxicity, minimal effects on normal physiology, and being easy to use and reproducible [177]. Biological methods typically use a viral vector, most commonly based on adenoviruses, to deliver nucleic acid into a target cell. Biological methods usually have high transfection efficiency but can suffer from high cytotoxicity [178]. Chemical methods allow entry of foreign DNA into the target cell by forming positively charged complexes with the foreign DNA that is attracted to the negatively charged cell membrane. Various different chemical transfection techniques are utilised including calcium phosphate [179] and cationic lipid [180] and newer methods such as Genejuice, which uses a novel polyamine based on a non-toxic cellular protein. Chemical methods are generally cheap and easy to use but can suffer variable transfection efficiency based on cell type and condition and some of the chemicals used can be cytotoxic [177]. Physical transfection methods offer several different approaches to transfecting DNA including electroporation, biolistic particle delivery

and direct injection [181]. Electroporation is one of the most commonly used methods of physical transfection. First described by Neumann et al. 1982 [182] this method uses an electric field to create small temporary destabilisations in the cell membrane that causes it to become highly permeable to exogenous molecules, such as DNA, in the surrounding medium [181]. Optimisation of electroporation can be laborious and the equipment is expensive compared to some chemical methods, however once optimised it offers fast and efficient method of transfection.

Transfected nucleic acids can be expressed stably or transiently. In a transient transfection the introduced nucleic acids are not integrated into the chromosomal DNA and thus persist only for a limited time, usually up to 72 hrs, as the transfected nucleic acid is not copied during cell division and becomes diluted after repeated cell division. To achieve a stable transfection, cells which integrate the exogenous nucleic acid into the chromosomal DNA are selected, using a selection marker present in the expression vector, ensuring long term gene expression and inheritance in cell progeny (Figure 2.3). Foreign DNA integrates in the chromosomal DNA randomly at one or very few sites [183] and site integration influences the transcription rate of the gene of interest [184]. Cellular DNA in the nucleus is combined with proteins to help protect the DNA from damage, to control gene expression and DNA replication and to ensure its fits properly within the nucleus. This compact structure is called chromatin and is found in two varieties: euchromatin and heterochromatin [185]. Euchromatin consists of DNA complexed to several nucleosomes which in turn are made up of proteins called histones. Histones have small sequences of DNA wrapped around them loosely allowing RNA polymerase and gene regulatory proteins to bind to DNA sequences and allow gene transcription [185]. In

heterochromatin the DNA is tightly wound and packed thus preventing any transcription of genes present in the chromatin. The site at which transfected DNA becomes integrated is thus of critical importance. If the transfected DNA becomes integrated into the heterochromatin, it is unlikely that any expression of the target gene will occur, whereas if it becomes integrated into cellular euchromatin, expression of the target gene is much more likely. If transfected DNA successfully integrates into to cellular euchromatin, a number of factors can still influence whether the gene becomes properly expressed. Integration of the DNA can cause a deleterious rearrangement of the endogenous DNA at the site of integration potentially leading to deletions, duplications and translocations which can interfere with coding sequences [186] [187] [188] [189]. The endogenous genome does seem to have specific areas however, in which DNA integration is likely to occur termed "integrational hotspots"[189].

The development of genome manipulation and the establishment of stable cell lines is a pivotal achievement in molecular biology, allowing large scale recombinant protein production, analysis of gene function and regulation and giving rise to potential new treatment for several diseases.

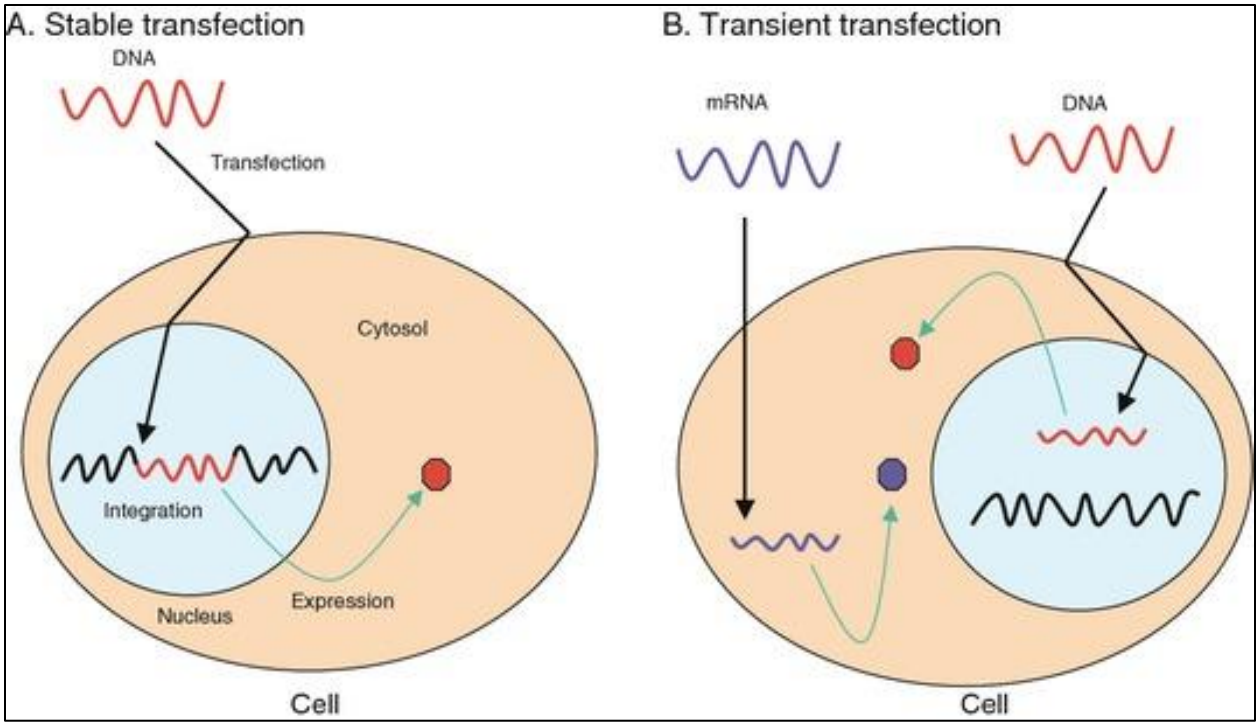

Figure 2.3 Outline of stable and transient transfection principals

Diagram showing a stable transfection (A) with foreign DNA (red wave) passing through the cell membrane and into the cell nucleus where it becomes integrated into the host genomic DNA (black wave) and expressed sustainably. In a transient transfection foreign DNA in introduced to the nucleus and translated, but not integrated into the host genome. Foreign mRNA may also be transfected and transcribed in a transient transfection. Hexagons represent expressed proteins from transfected nucleic acids. [177]

2.1.5 RNA interference (RNAi)

RNA-mediated interference (RNAi), also referred to as post transcriptional gene silencing (PTGS), is a simple and rapid method of silencing gene expression. The silencing of a gene is a consequence of degradation of RNA into short RNAs that activate ribonucleases to target homologous mRNA. The first observations of the RNAi pathway was in the 1980s by Ecker *et al* 1986, who observed the transcription of antisense RNA was found to effectively block the expression of target genes in transgenic plants. Fire and Mello were the first to identify the process by which gene silencing occurred and to identify double stranded RNA as being the causative agent in gene silencing [190]. The experiments of Baulcombe and Hamilton [191] offered further understanding of the process by identifying that small 21-25 nueclotide RNA fragments cleaved from the larger double stranded RNA, later named siRNA, were responsible for gene silencing. While initial studies utilised introduction of exogenous dsRNA, it is now clear that higher eukaryotes contain a large number of genes that encode small RNAs referred to as micro-RNAs (miRNAs) [192]. Both miRNAs and exogenous dsRNAs mediate their effects at the RNA level, miRNAs by inhibiting translation and exogenous dsRNAs through degradation of target RNAs [192] [193]. Today RNAi is a commonly used tool in many areas of molecular biology, medical research and biotechnology.

The process of RNAi begins with activation of a ribonuclease called Dicer that initiates the cleavage of dsRNA to siRNA (Figure 2.4) [194]. These si-RNA molecules are double-stranded fragments of 20–25 base pairs with a 2-nucleotide overhang at the 3' end [195]. After processing by Dicer, mature siRNAs associate with argonaut and other proteins to create an

RNA-induced silencing complex (RISC) [196]. RISC possess endonuclease activity that degrade mRNA complementary to the attached siRNA, with argonaut proteins being primarily responsible for the endonuclease activity of RISC [196]. RNA molecules produced by the dicer are double stranded and thus the RISC must bind preferentially to only one of the strands to prevent degradation of two separate mRNA targets. To prevent this occurring argonaut protein unwinds the siRNA and binds preferentially to only one strand of the RNA, termed the guide strand, and the other strand is degraded during RISC activation [197]. The guide strand is thought to be selected based on the differences on the thermodynamic stability of the 5' end, with the more stable 5' end forming the guide strand and the strand with the less stable 5' end being degraded [198].

Because of its specificity and efficiency, RNAi is considered as an important tool not only for functional genomics, but also for gene-specific therapeutic activities that target the mRNAs of disease-related genes [199].

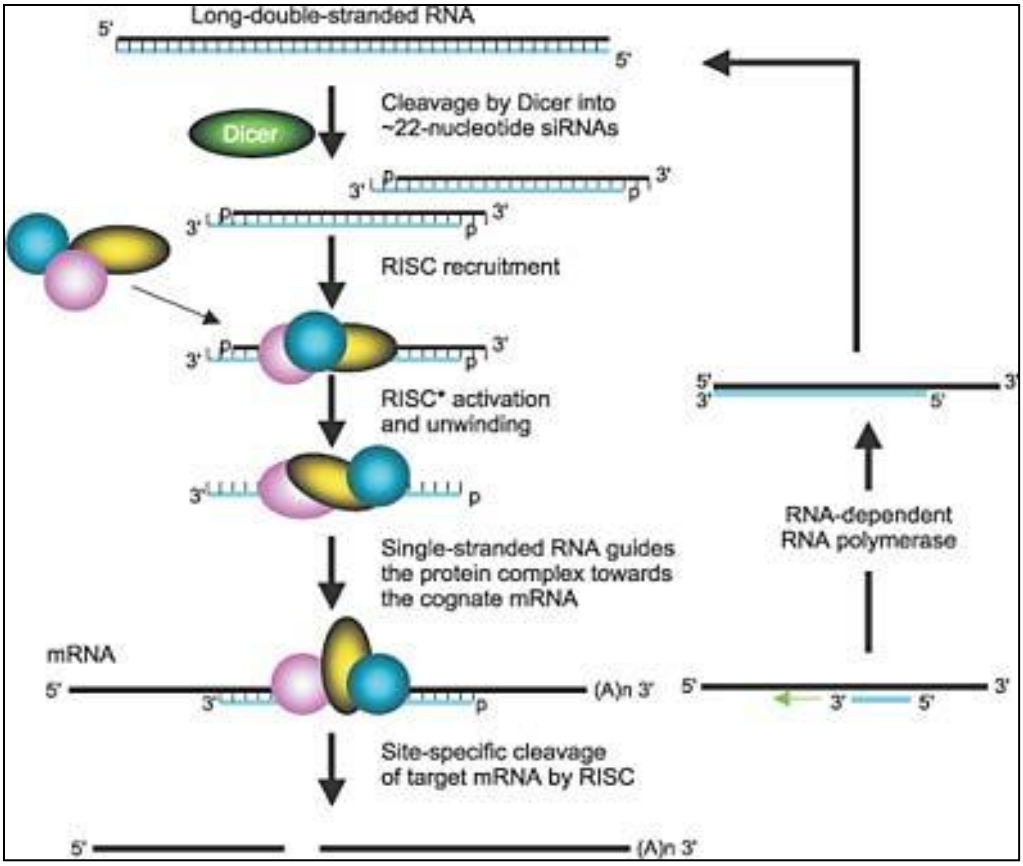

Figure 2.4 Schematic diagram of RNAi pathway, detailing siRNA cleavage by Dicer, RISC recruitment and site-specific cleavage of target mRNA. [200]

The process of RNA interference begins with cleavage of long double stranded RNA into small siRNA strands by Dicer. A number of enzymes then associate with the siRNAs to form RNA-induced silencing complex (RISC). RISC unwinds the siRNA into a single stranded RNA molecule and guides it to its specific mRNA target, resulting in cleavage of the target mRNA.

2.2 Sample collection and evaluation, selection of cohort

2.2.1 Sample collection

Ethical approval was received from the Rotunda Hospital to collect patient information and formalin fixed paraffin embedded (FFPE) cervical tissue samples. Ethical approval was also obtained from Dublin Institute of Technology ethics committee for this program of research to proceed. Under the terms of the ethical approval, access only the patient number and disease state of the sample were granted and no follow up or patient outcome information was provided. Before collection of any tissue blocks, haemotoxylin and eosin (H&E) stained sections cut by the pathology laboratory Rotunda Hospital, from retrospective cervical biopsy samples (sent between 2005 and 2007), were examined in order to identify tissue blocks that contained normal cervical tissue, pre-cancerous and invasive lesions and had large enough lesions to allow for tissue microarray production. Following microscopic examination of the H&Es, samples with at least two blocks that contained sufficient lesions were identified (one block for tissue microarray production, one for evaluation of HPV status) and their corresponding patient and block numbers recorded. The appropriate tissue blocks were then retrieved from the hospitals archival storage area. As patient information is confidential, all patient samples were assigned an arbitrary number for the duration of this study.

2.2.2 Haematoxylin and Eosin staining and lesion identification

The tissue blocks collected from the hospital had previously been sectioned by the pathology laboratory, Rotunda Hospital, and in order to ensure that the area containing the lesion was still present in the tissue blocks, it was necessary to cut a new section and perform a haemotoxylin and eosin stain from each block. 5µm tissue sections were cut, floated onto a glass slide and melted for 2 hours in an oven at 60˚C. The sections were then de-waxed for 5 minutes each in two separate xylene baths, two separate absolute alcohol baths and a spirit bath before being placed in water. Sections were placed in Mayer's haematoxylin for 1 minute before being washed in warm water for 1 minute. Sections were placed in an acid-alcohol solution for 2 seconds before being immediately washed in water for 1 minute. Sections were then placed in a 1% eosin solution for 5 minutes before being washed in water for 1 minute. Following this, the sections were dehydrated by placing sections for 5 minutes each in spirit, absolute alcohol (two baths) and xylene (two baths). Sections were mounted with DPX and left to dry on a flat surface. Upon examination of the sections, 188 cases were deemed to have adequate lesions present of which 160 with the greatest amount of lesion present were selected for TMA production and evaluation of HPV status, as each TMA required 40 cases and 4 TMAs were produced.

2.3 Construction of tissue microarrays and immunohistochemical staining

2.3.1 Tissue microarray instrument/design

The instrument used in the production of the tissue micro-arrays was a Beecher Instruments Manual Tissue Array MTA-1 (Beecher Instruments, Wisconsin, USA). The needles used to produce the cores were model number MP10, 1.0mm Manual Tissue Array Needles, produced by Beecher Instruments. Each tissue micro-array was designed to have: 12 cases of cervical carcinoma, 12 cases of high-grade squamous intraepithelial lesion, 12 cases of low-grade squamous intra-epithelial lesion and 4 cases of non-neoplastic cervical epithelium, giving a total of 40 cases per TMA. In turn, each case was sampled in triplicate giving a total of 120 cores per TMA.

2.3.2 Identification of lesion and tissue block orientation

Sampling the correct area is of critical importance during tissue-microarray production. To ensure the correct area is sampled, H&Es from every donor tissue block were examined and the area of interest was clearly circled on the glass slide. During construction of tissue microarrays the slide was overlaid on the tissue block to ensure proper orientation, and to ensure the area of the tissue block was correctly sampled.

2.3.3 Tissue microarray (TMA) production

A blank recipient paraffin block was placed in the receptacle of the array machine (figure 2.1), before then being secured by tightening of the clamp screws. A core was removed from the recipient paraffin block and the tissue extraction needle was selected. Next the donor block bridge (figure 2.1) was placed above recipient block clamp before the desired tissue block with appropriate overlying H&E slide was placed on the bridge. The punch was aligned to the area of interest on the tissue block using the overlying H&E template. When correctly aligned, the punch was pushed down steadily to remove the area of interest from the donor block. The bridge holding the donor block was then removed before the needle was slowly lowered to just above the previously punched hole in the recipient block. Once aligned, the stylus of the needle was pushed down to force the core into the hole in the recipient block, leaving the core protruding approximately 1mm above the surface of the recipient paraffin block. The paraffin extraction needle was then selected before the horizontal axis of the micrometer (figure 2.1) was adjusted to a position 1.5mm beside the previous punch. This process was then repeated until all the required samples had been added to the recipient block. When all the samples had been added, the recipient block was placed in a 56˚C oven for 15-20 minutes until the wax had softened. A glass slide was then placed on the surface of the block and pushed down firmly and evenly to ensure all cores are embedded evenly and surface of the block was flat.

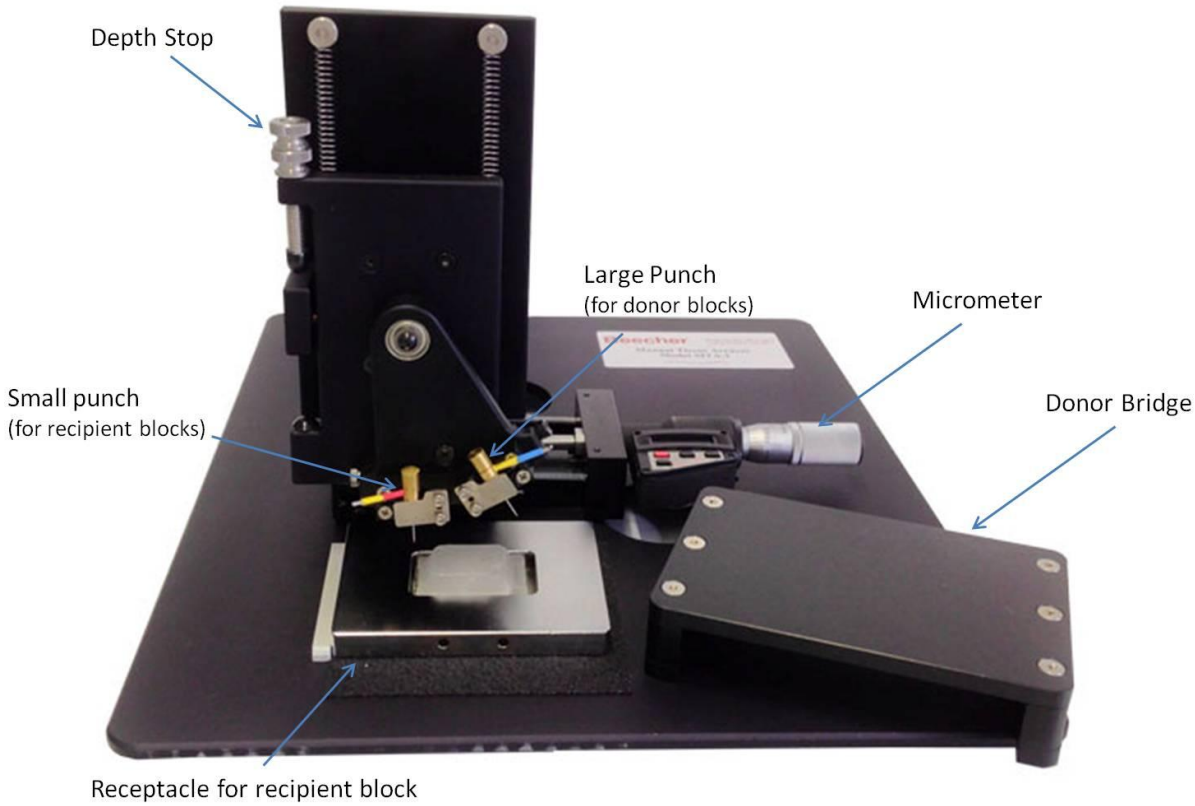

Figure 2.5 Schematic diagram of the Beecher Instruments MTA-1 tissue micro-array machine.

The instrument contains a receptacle into which the recipient paraffin block is placed and secured. The small punch needle is used to remove a core from the recipient block while the large punch removes a sample from the donor block, to a depth controlled by the depth stop. The micrometer is used to set the distance between each sample inserted into the recipient block.

2.3.4 Antibody Optimisation

Optimal staining conditions were determined for all antibodies listed in table 2.1. Various antibody dilutions (ranging from 1:25 up to 1:1000 depending on the antibody) were used with a number of different antigen retrieval methods to assess which dilution worked best with which antigen retrieval technique. A number of different antigen retrieval techniques were used, protease induced epitope retrieval (PIER), heat induced epitope retrieval (HIER) (using a microwave oven) and a combination of these two methods. The buffers used for HIER were 10mmol/l citrate buffer (pH6) and 1mmol/l EDTA buffer (pH8)

Table 2.1 Antibodies utilised in this study for IHC based detection of biomarkers.

Protein	Antibody Clone	Company	Raised In
E-cadherin	NCH-38	Dako	Mouse (Monoclonal)
Beta-Catenin	B-catenin-1	Dako	Mouse (Monoclonal)
p120-Catenin	EPR357(2)	Epitomics	Rabbit (Monoclonal)
N-cadherin	EPR1792Y	Epitomics	Rabbit (Monoclonal)
Snail	Ab63371	Abcam	Rabbit (Polyclonal)
Claudin-1	51-9000	Invitrogen	Rabbit (Polyclonal)
Claudin-7	34-9100	Invitrogen	Rabbit (Polyclonal)
Occludin	33-1500	Invitrogen	Mouse (Monoclonal)

Table displays the clone, manufacturer and the species the antibody was raised in for all of the antibodies used in this study.

Antigen Retrieval

(i) Protease Enzyme Treatment

After dewaxing, sections were covered with 0.1% protease (Sigma) in PBS that had been heated to 37˚C. Sections were incubated at 37˚C for 5 minutes. After incubation sections were washed in distilled water before continuing with ABC protocol

(ii) Microwave Oven Treatment

After dewaxing, sections were placed in 10mmol/l citrate buffer pH6 (appendix) or 1mmol/l EDTA buffer (appendix). Sections were then heated in a microwave for 12 minutes and left to cool for 20 minutes. Sections were washed in distilled water before continuing with the standard ABC protocol.

(iii) Microwave + Protease treatment

Sections were treated as per microwave oven protocol as described in 2.3.4 (ii). Following washing with distilled water, 0.1% protease in PBS (appendix) was applied to sections for 30 seconds. Sections were washed with PBS before continuing standard ABC protocol.

2.3.5 Avidin-biotin Complex Immuno-Peroxidase method

Using a standard histology microtome (Lecia), 5µm cervical sections were cut from formalin-fixed paraffin tissue blocks. Folds or creases were removed by placing the sections in a 42˚C water bath for 10 to 15 seconds before mounting sections on Superfrost Plus glass slides (Thermo-fisher). Sections were then placed in a 60^{o}C oven for one hour in order to melt the paraffin, before being dewaxed in two washes of xylene for 5 minutes each. Sections were then

rehydrated by placing slides in two washes of 100% ethanol, one wash of 95% ethanol and one wash of distilled water for five minutes each. Antigen retrieval, using the methods previously described, was then carried out. The optimum antigen retrieval method that was determined for each antibody can be seen in table 3.1. Following antigen retrieval, sections were washed in distilled water before blocking of endogenous peroxidases was carried out by treating sections with 3% hydrogen peroxide in methanol for 5 minutes. Sections were then washed in phosphate buffered saline (PBS) 3 times, before being treated with the Vectastain Elite ABC kit (Vector laboratories). Normal horse serum, diluted 1:200 in PBS, was applied to the sections for 5 minutes. Sections were drained and approximately 500µl of specific primary antibody was applied and incubated at room temperature for 1 hour. Following 3 washes with PBS, the biotinylated secondary antibody (diluted 1:100 in PBS) was applied for 15 minutes. Sections were washed in PBS 3 times before being treated with ABC reagent (diluted 1:100 in PBS) and then again washed in PBS 3 times. Peroxidase labeling was visualised using 0.06% 2,4-diaminobenzidine (Sigma) diluted in PBS and 0.03% hydrogen peroxide (BDH). Sections were lightly counterstained by application of Mayers haematoxylin for 40 seconds and then blued in distilled water. Sections were then dehydrated by way of 95% ethanol for 30 seconds, two washes of 100% ethanol for 5 minutes each and 2 washes of xylene for 5 minutes each. Finally, sections were coverslipped in DPX.

2.4 Detection and genotyping of HPV DNA in cervical tissue

2.4.1 Extraction of DNA

DNA was extracted from all samples using the Qiagen DNeasy Blood & Tissue Kit protocol. Included in this protocol was a xylene dewaxing pretreatment step for FFPE tissue that was recommended by the manufacturer. Five 10µm sections from each block were cut on a microtome and placed into a sterile 1.5ml eppendorf tube. To prevent contamination between blocks a different blade was used for each block, the microtome was cleaned with 70% alcohol (appendix) and finally DNAway solution (Sigma) was applied to the microtome between each sample. To remove the paraffin wax 1200µl of xylene (BDH) was added to the eppendorf tube and vortexed vigorously. The sample was centrifuged at 14,000rpm for 5 minutes before the supernatant was removed and 1200µl of 100% ethanol (Sigma) was added. The sample was vortexed vigorously before being centrifuged at 14,000rpm for 5 minutes. The supernatant was removed and another ethanol wash then performed. After removing the supernatant, being careful not to remove any pellet, the eppendorf tube was left open in a 37˚C oven until any residual ethanol was evaporated. The pellet was then re-suspended in 180µl of ATL buffer (Qiagen) and 20µl of Proteinase K. The sample was vortexed vigorously before being incubated overnight at 56˚C in an oven. Following overnight incubation the sample was briefly vortexed, 200µl of AL Buffer (Qiagen) was added, before being briefly vortexed again and adding 200µl of ethanol (Sigma). The sample was then vortexed vigorously for 30 seconds, before transferring the entire sample to the upper well of a QIAamp spin column (Qiagen). The sample was the centrifuged for 1 minute at 8000rpm. The spin column was placed in a new collection tube and

the tube containing the filtrate was discarded. 500µl of AW1 buffer (Qiagen) was added to the spin column and it was centrifuged at 8000rpm for 1 minute. The collection tube containing the filtrate was discarded and a new collection tube applied to the spin column. 500µl of AW2 buffer (Qiagen) was added to the spin column and it was centrifuged at 14000rpm for 3 minutes. The spin column was placed in a sterile 1.5ml eppendorf tube and 200µl of AE Buffer (Qiagen) was applied to the spin column. The spin column was left to incubate for 1 minute at room temperature before being centrifuged at 8000 rpm for 1 minute. Samples were then stored at -20˚C until required.

2.4.2 Controls for PCR

With each reaction a positive control was carried out using DNA extracted from the HPV 18 positive cell line HeLa. A negative control reaction with water in place of template DNA was also included with each batch. To ensure there was no carry over contamination between samples, skeletal muscle (HPV-) was sectioned on the microtome in between sectioning of cervical samples. The DNA from the skeletal muscle section was extracted and underwent GP5+/6+ PCR amplification, to confirm there was no contamination of samples.

2.4.3 PCR Amplification of Cervical DNA

In order to establish whether the DNA extracted from each sample was of sufficient quality for a PCR reaction, a β-globin PCR was carried out using the PC03/04 primer pair. HPV DNA was detected using the GP5+/6+ primer pairs. All PCR reactions were carried out in a final volume of 25µl containing 1x reaction buffer (200mmol/l Tris-HCl pH8.4, 500mmol/l KCl) (Invitrogen), 0.2mmol/l dNTPs (Invitrogen), 1U Platinum Taq polymerase (Invitrogen) and 3µl template DNA. $MgCl_2$ and primer concentration are detailed in table 2.2. The PCR protocol was as follows: an initial 5 minute denaturation step at 95˚C, followed by 40 cycles of 95˚C for 30 seconds, 48˚C (GP5+/6+) or 60˚C (PC03/04) for 30 seconds, 72˚C for 30 seconds before an final elongation step of 72˚C for 5 minutes. All PCR reactions were analysed on a 2% agarose gel (appendix) stained with 0.5µg/ml ethidium bromide (Fluka). Gels were run at 120V for 1 hour.

Table 2.2 Primers used for DNA quality assessment and HPV detection.

Primer	Primer Sequence 5'-3'	$MgCl_2$ Concentration	Primer Concentration	Product Size
PC03 PC04	ACACAACTGTGTTCACTAGC CAACTTCATCCACGTTCACC	1.5mmol/l	40nmol/µl	110bp
GP5+ GP6+	TTTGTTACTGTGGTAGATACTAC GAAAAATAAACTGTAAATCAT	2.5mmol/l	40nmol/µl	150bp
GP5+ M13	TGTAAAACGACGGCCAGTTTTG TTACTGTGGTAGATACTAC	2.5mmol/l	40nmol/µl	168bp

Primer sequences, magnesium concentrations, primer concentration and product size for primers used in this study

2.4.4 Purification of PCR amplimers

Purification of PCR products was performed using the High pure PCR purification Kit (Roche). This product removes excess dNTPs, primers and PCR buffers from PCR reaction solutions. After amplification, PCR reaction solution was made up to 100µl with distilled water, then mixed with 400µl of binding buffer. The solution was loaded into a provided spin column and centrifuged for 1 minute at 8000rpm. The eluate from the collection tube was discarded and 400µl of wash buffer was loaded into the spin column. The spin column was then centrifuged at 8000rpm for 1 minute. The eluate in the collection tube was discarded and 300µl of wash buffer was added to

the spin column. The spin column was centrifuged at 14000rpm for 1 minute and the collection tube was then discarded. A new collection tube was attached to the spin column and 20µl of elution buffer was applied. The spin column was then centrifuged at 8000rpm for 1 minute. The solution present in the spin column contained the purified DNA and was frozen at -20˚C until required.

2.4.5 Sequencing of PCR products and BLAST comparison of sequences

After purification of GP5+/6+ PCR amplimers generated from cervical DNA, samples were sent for sequencing to Eurofins Mwg Operon (Ebersberg, Germany). Samples that were successfully sequenced were returned to us in FASTA format, which is a text-based file format containing the complete nucleotide sequence. The sequences were compared to known HPV L1 sequences using the basic local alignment search tool (BLAST). Using this database, sequence homology in the PCR amplimers could be found with sequences in the L1 gene of various different HPV genotypes, thus allowing the identification of the HPV genotype present in cervical samples.

2.5 Establishment and assessment of stable cell lines

2.5.1 Cell lines and cell Culture

Three cervical cancer cell lines were used during this study. HeLa, a HPV-18 positive cervical cell line, and SiHa and CasKi both HPV-16 positive. Cell lines were grown in complete RPMI medium (Sigma), including 2mmol/l L-glutamine (Gibco) 10% foetal calf serum (Sigma) and 40 U penicillin/streptomycin (Sigma) at 37°C and 5% CO_2 in a humidified atmosphere. Cells were grown to confluence before being trypsinised with 2% trypsin diluted in 0.02% EDTA (Sigma) for 10 minutes at 37°C. 10ml complete RPMI medium was added to the culture dish to inactivate trypsin. 0.5 x 10^5 cells were added to a 6mm cell culture dish containing 2ml complete RPMI were cultured overnight at 37°C and 5% CO_2. In addition, 0.5 x 10^5 cells were added to a 25ml cell culture flask containing 10ml of complete RPMI medium and incubated at 37°C and 5% CO_2 to maintain the cell culture for future use.

2.5.2 Transformation of One Shot® TOP10 chemically competent *E. Coli*

Two separate expression vectors, one encoding claudin-1 and another encoding claudin-7, were purchased from Genecopedia (Rockville, MD, USA). An outline of the structure of these expression vectors can be seen in figure 2.2. 1µg of plasmid was diluted in 2.5µl of H_2O and was added to a 50µl vial of One Shot® TOP10 chemically competent *E. Coli* (Life Technologies) and mixed gently. After incubation on ice for 25 minutes the cells were heat-shocked for 30 seconds at 42°C and placed for 2 minutes on ice. 250µl of pre-warmed S.O.C medium was added and the tube and the tube was placed in a horizontal shaker at 225 rpm at 37°C for 1 hour. 200µl of the

transformation solution was spread on a LB agar plate containing 100µg/ml ampicillin and incubated at 37°C overnight.

2.5.3 Production and isolation of high quality plasmid

In order to prepare purified plasmid DNA in large quantities both plasmids were purified with the Genopure Plasmid Midi Kit (Roche). Bacterial colonies grown on ampicillin containing agar plates (from 2.5.2) were picked, inoculated and cultured overnight at 37°C in 100ml LB medium containing 100µl/ml ampicillin, with vigorous shaking. To pellet the bacteria, the culture medium was centrifuged for 10 minutes at 3000 x g at 4°C and the supernatant was discarded. The pellet was air-dryed and resuspended in 8ml suspension buffer. 8ml lysis buffer was added and mixed gently by inverting the tube and the mixture was then incubated at room temperature for 2-3 minutes. 8ml of chilled neutralisation buffer was added and mixed immediately by inverting the tube before being incubated on ice for 5 minutes. The bacterial lysate was filtered and then loaded into a column and allowed to flow though the column. The flowthrough was passed though the column again before being discarded. Three separate times 4ml of wash buffer was passed through the column and discarded after each wash. The column was then inserted into a collection tube capable of withstanding high speed centrifugation and 2.5ml of elution buffer pre-warmed to 50°C was added to the column and allowed to flow through. The flowthrough was passed though the column again before 3.6ml of isopropanol was added into the tube to precipitate the eluted plasmid. The plasmid DNA was centrifuged for 30min at 15000 x g at 4°C. The supernatant was then carefully discarded and the plasmid DNA was washed with 3ml of chilled 70% ethanol and centrifuged for an additional 10 minutes at 15000 x g at 4°C. The supernatant was removed and the tube was allowed to air-dry for 15

minutes. The DNA plasmid pellet was re-dissolved in 50µl nuclease free water buffer and stored at -20°C.

2.5.4 Transfection of expression vectors and stable clone selection

2 x 10^6 HeLa cells were plated per well into 35mm plates and incubated overnight at 37°C, 5% CO_2. 100µl of serum free RPMI-1640 media was added to a sterile 1.5ml eppendorf tube. 3µl of Genejuice (Novagen) per 1µg of DNA was added drop-wise to the media and was mixed thoroughly by vortexing. The mixture was incubated at room temperature for 5 minutes. For transient transfections a range of plasmid DNA amounts was used (0.1µg, 0.25µg, 0.5µg, 1µg and 2µg), for stable transfections 1µg of plasmid DNA was used. The appropriate amount of plasmid DNA was added to the serum free RPMI/Genejuice solution, mixed by gentle pipetting, and incubated at room temperature for 15 minutes. The entire volume was then added drop-wise to the well of the plate and the plate was rocked to distribute the transfection mixture. The cells were incubated at 37°C and 5% CO_2. For transient transfections, 24 hours post transfection the medium was removed and the cells were lysed and protein extracted as described in 2.4.5. For stable cell lines cells were transferred to a 100mm plates and 200µg/ml of G418 was added to allow genticin selection. Cells were then incubated for 3 weeks to allow clones of cells expressing the plasmid to grow. After 3 weeks isolated colonies were picked and subcultured in a 35mm plate.

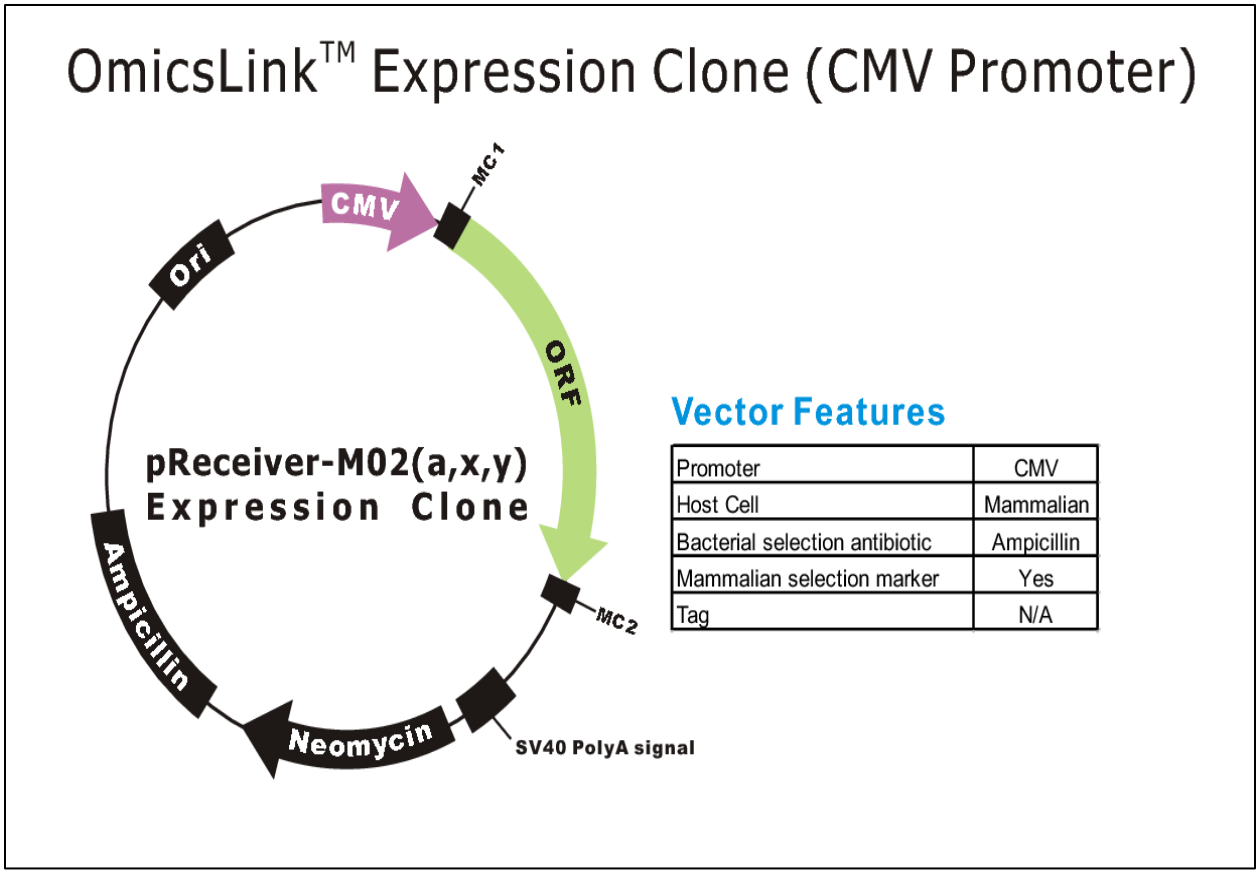

Figure 2.6 Outline of expression vector utilised to create C1-HeLa and C7-HeLa stable cell lines. Expression vector contains a CMV promoter region ahead of an open reading frame containing either the Claudin-1 or Claudin-7 gene. The expression vector contains an ampicillin bacterial selection marker for generation of large amounts of plasmid in bacterial cultures and a neomycin selection marker for selective isolation of mammalian cells expressing the vector.

2.5.5 DNA Extraction

DNA was extracted from stable cell colonies using the Qiagen DNeasy Blood & Tissue Kit according to the manufactures protocol. Cells were harvested by trypsinisation and then centrifuged at 1500 rpm for 5 minutes in a 1.5ml eppendorf tube. The supernatant was discarded and the pellet resuspended in 200µl PBS, 20µl Protinase K and 200µl buffer AL. The sample was vortexed vigorously before being incubated for 10 minutes at 56˚C. Following incubation the sample was briefly vortexed. The sample was then vortexed vigorously for 30 seconds, before transferring the entire sample to the upper well of a QIAamp spin column (Qiagen). The sample was then centrifuged for 1 minute at 8000rpm. The spin column was placed in a new collection tube and the tube containing the filtrate was discarded. 500µl of AW1 buffer (Qiagen) was added to the spin column and it was centrifuged at 8000rpm for 1 minute. The collection tube containing the filtrate was discarded and a new collection tube applied to the spin column. 500µl of AW2 buffer (Qiagen) was added to the spin column and it was centrifuged at 14000rpm for 3 minutes. The spin column was placed in a sterile 1.5ml eppendorf tube and 200µl of AE Buffer (Qiagen) was applied to the spin column. The spin column was left to incubate for 1 minute at room temperature before being centrifuged at 8000 rpm for 1 minute. The sample was then stored at -20˚C until required.

2.5.6 PCR verification of stable cell lines

To verify successful uptake of the expression vector in stable cell lines, DNA was extracted from each colony and a PCR reaction was performed using the primers listed in table 2.3. The forward primer was complementary to a sequence in the CMV promoter and the reverse primer was complementary to a sequence in either the CLDN1 or CLDN7 gene. PCR was carried out according to the method described in 2.3.2, using the primers listed in table 2.3 and according to the following cycling conditions: an initial 5 minute denaturation step at 95˚C, followed by 35 cycles of 95˚C for 30 seconds, 59°C for 30 seconds, 72˚C for 30 seconds before an final elongation step of 72˚C for 5 minutes. All PCR reactions were analysed on a 2% agarose gel (appendix) stained with 0.5µg/ml ethidium bromide (Fluka). Gels were run at 120V for 1 hour. PCR products were sequenced and matched to the human CLDN1 gene and CLDN7 gene respectively using BLAST to ensure specificity of primer sets.

Table 2.3 Table of primers sequences, $MgCl_2$ concentration, primer concentration and PCR product size used to verify the presence of expression vectors in stable cell lines.

Primer	Primer Sequence 5'-3'	$MgCl_2$ Concentration	Primer Concentration	Product Size
CLDN1 Fwd	CAGCCTCCGGACTCTAGC	1.5mmol/l	4ng/µl	200bp
CLDN1 Rev	GATGTTGTCGCCGGCATAG			
CLDN 7 Fwd	CAGCCTCCGGACTCTAGC	1.5mmol/l	4ng/µl	250bp
CLDN 7 Rev	GCAGTCCATCCACAGCCCC			

2.5.7 Protein extraction

Cells were harvested from 6-well plates by the addition of 200µl trypsin (Sigma) per well. After cells had detached 800µl of complete medium per well was added. After centrifugation of cells at 1500rpm for 5 minutes, the supernatant was removed and the pellet resuspended in 1ml of cold PBS. The cells were washed in PBS another two times and after centrifugation and removal of the PBS, the cells were lysed in 50µl of RIPA buffer containing 0.1% protease inhibitor (Calibiochem). The cell lysate was sonicated 5 times, for 10 seconds using a probe sonicator with the lysate kept on ice at all times. The cell lysate was centrifuged at 14000 rpm for 30 minutes at 4°C. The supernatant was transferred into a fresh eppendorf tube and the protein concentration was measured in triplicate with a Bradford assay using a BSA standard curve.

2.5.8 Western Blotting

30µg of sample protein was made up to a total volume of 15µl in distilled water and an additional 5µl of 4X Laemlli buffer was then added. Samples were heated to 95°C for 5 minutes and loaded onto a 12% polyacryamide gel (appendix) along with a molecular weight ladder. Gels were run at 100V for 3 hours. Proteins were then transferred onto a nitrocellulose membrane (0.45µm pore size) using pre-chilled pH 8.3 transfer buffer (appendix) in a wet tank apparatus. The tank was kept on ice to keep the buffer chilled and the gel was run at 100V for 70 minutes. After successful transfer of proteins, the membrane was blocked in 5% non-fat dry milk in TBS-0.1% tween. The appropriate antibody (Table 2.4) was diluted in 5% non-fat dry milk in TBS-0.1% tween and incubated with membrane for 16 hours at 4°C on a rotary shaker with gentle agitation. The membrane was washed 5 times in TBS-0.1% tween before being incubated with appropriate anti-mouse or anti-rabbit secondary HRP-linked secondary antibody (Sigma), diluted in 5% non-fat dry milk in TBS-0.1% tween for 1 hour at room temperature. The membrane was then washed in TBS-0.1% tween 5 times. Protein detection was carried out using the Enhanced Chemiluminescence Kit (Pierce Scientific). ECL solutions were mixed in a 1:1 ratio and applied to the membrane for 5 min. X-Omat film (Kodak) was then overlaid on the membrane for the appropriate amount of time and the film was developed.

Table 2.4 Antibodies used in this study for western blotting and the molecular weight of the proteins they detect.

Antibody	Manufacturer/Clone	Dilution	Molecular weight
Claudin-1	Invitrogen	1:250	23kDa
Claudin-7	Invitrogen	1:250	22kDa
Snail	Cell Signaling (L70G2)	1:1000	29kDa
E-cadherin	Invitrogen (4A2C7)	1:500	97kDa
Beta-Actin	Sigma	1:5000	42kDa

Table shows the manufacturer, clone, working dilution for each antibody and the molecular weight of the targeted protein.

2.5.9 Trans epithelial electrical resistance (TEER) Measurements

1.5ml of complete medium was added to each lower well of the plate before 0.5 x 10^5 cells were seeded in total volume of 0.5ml of complete medium and added to the insert of 12mm diameter transwell plate (Corning Costar, Cambridge, MA). An insert with no cells and only 0.5ml of complete medium was also used as blank to measure background resistance. Cells were then incubated at 37°C until fully confluent and a complete monolayer had formed. After reaching full confluence, the medium from each transwell insert was removed and replaced with fresh media. The plates were then incubated at room temperature to allow temperature equalisation. TEER values were measure using an STX2 electrode (World Precision Instruments) connected to an Epithlial Voltohmeter (EVOM) (World Precision Instruments) according to the manufacturer's instructions. Between each reading the STX2 probe was rinsed with complete medium. Experiments were carried out in triplicate and on three separate occasions.

Resistance per cm^2 was calculated according to the EVOM manual by subtracting the value of the blank insert from all values then multiplying by the formula for the area of a circle ($\pi d^2/4$).

2.5.10 Cell invasion assay

The Cytoselect 24-well cell invasion assay (Cell Biolabs) was used to evaluate the invasive properties of stable cell lines. Under sterile conditions the invasion chamber plate was allowed to incubate at room temperature for 10 minutes. The basement membrane layer of the cell culture insert was rehydrated by the addition of 300µl of warm, serum-free media to the inner compartment and incubated at room temperature for 1 hour. The rehydration medium was removed, taking care not to disturb the basement membrane. 500µl of media containing 10% fetal bovine serum was added to the lower well of the invasion plate. 300µl of serum free media containing 0.5 x 10^6 cells/ml was added to the upper insert and the plate was incubated at 37°C, 5% CO_2 for 48 hours. The media was then carefully aspirated from the upper insert and the surface of the insert was gently cleaned with cotton-tipped swabs to remove non-migratory cells. The insert was transferred to a clean well containing 400µl of cell stain solution (0.09% w/v crystal violet) and incubated for 10 minutes, before being washed several times with distilled water. Images were then captured of each well under a light microscope, with at least three individual fields per insert. Each insert was then transferred into an empty well containing 200µl of extraction solution and incubated for 10 minutes on an orbital shaker, before 100µl of solution was transferred to a 96-well microtiter plate and the absorbance @560nm was measured. Experiments were carried out three times on three separate occasions.

2.5.11 Gap closure/Wound healing assay

Cells were seeded at 0.5 x 10^6 cells per well in a 6 well plate and grown to full confluence. Cells were examined under an inverted microscope to ensure a continuous monolayer had formed. Gently and slowly the monolayer was scratched with a p200 pipette tip in a straight line across the center of the well, in a horizontal direction. While scratching across the surface of the well, the long-axial of the tip was kept perpendicular to the bottom of the well. Another line was then scratched though the center of the monolayer, this time in a vertical direction, to create a cross shaped gap in the monolayer. The cells were then washed twice with PBS before 2ml of complete medium was added to each well. Under a phase contrast microscope an appropriate area of the gap was identified and an image captured (0 hour timepoint). This coordinates of the area was noted for future orientation. The plate was placed in an incubator at 37°C, 5% CO_2 until the next timepoint. At 24 hour and 48 hour timepoints the plate was removed and another image was captured at the appropriate coordinates. The experiment was performed on three separate occasions.

2.5.12 MTT assay

Cells were seeded in 96 well plates ($1X10^4$ cells per well) and cultured at 37°C, 5% CO_2. At 24, 48 and 72 hour time points the assay was performed in triplicate and in three separate experiments according to the following protocol. A stock MTT solution was prepared at a concentration of 5mg/ml by dissolving 50mg MTT (Sigma Aldrich, St. Louis, MO, USA) in 10ml ddH20. A working solution of MTT reagent was prepared by diluting the stock solution 1:10 in RMPI-1640 media and filter sterilising the solution. At the appropriate time point the media was removed from each well and 100µl of working MTT solution added to the wells and the cells were incubated for 3 hours. After 3 hours, the cells were washed 3 times with sterile PBS and after the last wash all residual liquid was removed from the well. 100µl of DMSO was then added to each well and the plate was shaken on a rotary shaker for 10 minutes. The absorbance of each well at 595nm was then recorded using a spectrophotometer.

2.6 siRNA mediated knockdown of SNAIL in HeLa and SiHa cells

2.6.1 Transfection of siRNA plasmid

Predesigned Silencer® Select siRNAs (Life Technologies) were used in this study to examine knockdown of SNAIL expression in HeLa and SiHa cells. Two different siRNAs (s13185) and (s13187) were obtained (Life Technologies), both targeting the SNAIL mRNA, and co-transfected in to cells according to the following protocol. 0.5 x 10^6 HeLa cells were plated per well into 35mm plates and incubated overnight at 37°C, 5% CO_2. 100ul of serum free RPMI-1640 media was added to a sterile 1.5ml eppendorf tube. 3µl of Lipofectamine RNAiMAX (Life Technologies) per 10nM of siRNA was added drop-wise to the media and was mixed thoroughly by vortexing. The mixture was incubated at room temperature for 5 minutes. The appropriate amount of siRNA was added to the serum free RPMI/ Lipofectamine RNAiMAX solution, mixed by gentle pipetting, and incubated at room temperature for 15 minutes. The entire volume was then added drop-wise to the well of the plate and the plate was rocked to distribute the transfection mixture. The cells were incubated at 37°C and 5% CO_2 for 24 hours. Cells were transfected with a scrambled siRNA as a negative control. Scrambled siRNA contain sequences that are non-complementary to any known RNA sequences, and thus would not lead to the specific degradation of any cellular message.

2.6.2 RNA isolation

RNA was isolated from transfected cells using Trizol solution (Life Technologies). Cells were harvested by trypsinisation and then centrifuged at 1500 rpm for 5 minutes in a 1.5ml eppendorf tube. The supernatant was discarded, 1ml of Trizol solution was added and the solution was mixed thoroughly and incubated at room temperature for 5 minutes. 0.1ml of bromocholoropropane was added; the solution was mixed thoroughly and then incubated at room temperature for 5 minutes. The sample was then centrifuged at 12000 x g for 15 minutes at 4°C to allow phase separation. The upper aqueous phase of the sample was removed by angling the tube at 45° and pipetting the solution out, taking care to avoid drawing any of the interphase or organic layer into the pipette, and transferred to a new eppendorf tube. The interphase and organic phase were discarded. 0.5ml of 100% isopropanol was added to the aqueous phase and incubated on ice for 10 minutes, before being centrifuged at 12,000 × g for 10 minutes at 4°C. The supernatant was removed and discarded and the pellet resuspended in 1 ml of 75% ethanol. The sample was mixed briefly, then centrifuged at 7500 × g for 5 minutes at 4°C. The supernatant was removed and the sample allowed to air dry for 10 minutes before being resuspended in 50µl of RNase-free water. The sample was then heated to 55°C for 10 minutes, before being treated with DNase (Life Technologies) and stored at -80°C.

2.6.3 Reverse transcription of extracted RNA to cDNA

Creation of cDNA from RNA was achieved using the Enhanced Avian HS RT-PCR Kit (Sigma). In brief, 1µl of dNTP mix (500µm of each dNTP mix), 1µl of anchored oligo (dT)23 (3.5µM) and 2µg of template DNA were made up to 10ul with RNase free water and placed in a thermal cycler at 70°C for 10 minutes. The tube was removed from the thermal cycler and 2µl of 10X AMV-RT buffer, 1µl of enhanced AMV-RT (1U/µl), 1µl of RNase inhibitor and 6µl of RNase free water was added. The tube was incubated at 48°C for 50 minutes. The cDNA was then either utilised in a PCR reaction or stored at -20°C.

2.6.4 Real time PCR

Real-time PCR was carried out on reverse transcribed cDNA products using the GAPDH and SNAIL primers listed in table 2.5. All data on CT values (threshold cycle – the point at which fluorescence crosses the threshold) was normalised to an internal housekeeping gene, GAPDH, in order to control for differences in starting cDNA concentration. All PCRs were carried out using the Lightcycler Fast Start DNA Master SYBR Green Kit (Roche). 18µl of PCR reaction mix (without template cDNA) was prepared as detailed in table 2.6 and added to pre-cooled light cycler capillaries (Roche). 2µl of template cDNA was added to each capillary (blank containing 2µl of water) and the capillaries were sealed and centrifuged, before being transferred into the lightcycler machine. The real time PCR cycles were as follows: an initial denaturation step at 95°C for 10 minutes, 45 cycles of 95°C for 10 seconds, 59°C for 10 seconds, 72°C for 10 seconds.

A melt curve analysis was performed on all reactions, up to 95°C, with an increase in temperature of 0.1°C/sec. All real time PCRs were analysed for specificity by melt curve analysis to ensure only specific peaks for expected products were present. SNAIL primer sequences were retrieved from Medici et al., 2008 [201] and GAPDH sequences from Paulukat et al., 2001 [202].

Table 2.5 Primers used for real time PCR in this study

Primer	Primer Sequence 5'-3'	$MgCl_2$ Concentration	Primer Concentration	Product Size
GAPDH Fwd	ACCACAGTCCATGCCATCAC	1.5mmol/l	4ng/µl	453bp
GAPDH Rev	TCCACCACCCTGTTGCTGTA			
SNAIL Fwd	ACCACTATGCCGCGCTCTT	1.5mmol/l	4ng/µl	120bp
SNAIL Rev	GGTCGTAGGGCTGCTGGAA			

Forward and reverse primer sequences for GAPDH and SNAIL primers along with $MgCl_2$ and primer concentrations and the expected product size for each primer set.

Table 2.6 Reaction mix for real-time PCR.

Component	Volume	Final Conc.
Water	16.2µl	-
$MgCl_2$	0.8µl	2mM
PCR primer mix	1µl	50ng/µl
Lightcycler Faststart DNA master SYBR Green Mix	2µl	1X
Total	**18ul**	-

2.7 Data analysis and statistics

SPSS (Statistical Package for the Social Sciences) software was used to perform statistical analysis, including one way ANOVA tests to examine data for statistical significance and Fisher least standard difference for post-hoc testing. Microsoft Excel was used for constructing bar charts and all other graphs.

3. Examination of tight and adherens junction protein expression in cervical lesions

3.1 Introduction

Epithelial tissues are characterised by their cohesive structure and by their barrier and gate function in selectively regulating the flow of ions, cytokines, growth factors and other molecules through the epithelium and into the underlying tissue. The loss of cohesive structure and of the barrier and gate function associated with normal epithelium are two of the main features of epithelial malignancies such as cervical cancer [109]. Tight and adherens junctions are two distinct but complementary structures within epithelial tissues that play a key role in initiating and maintaining cell-cell contacts and cohesion [72]. As 90% of cancer deaths are caused by malignant cells losing their cohesive structure and disseminating away from their original site to form distant metastasis [203], understanding the mechanisms through which cells can lose their cohesive structure is of key importance. Identifying aberrant expression of tight and adherens junction proteins in cervical lesions may help identify some of the mechanisms by which junctional breakdown occurs, and may also help identify biomarkers that could indicate which pre-invasive cervical lesions are more likely to progress into invasive malignancies with the potential to metastasise.

3.2 Aims

- To select a cohort of cervical tissue samples, including all grades of cervical neoplasia and to utilise selected cervical samples to create tissue micro arrays (TMAs).
- To examine the expression of several integral adherens and tight junction proteins in cervical TMAs using immunohistochemistry.
- To analyse the expression profile of each protein and look for changes in expression between different grades of neoplasia that are statistically significant, possibly identifying biomarkers associated with the progression of neoplasia.

3.3 Antibody optimisation

In order to determine ideal staining conditions for formalin-fixed paraffin embedded tissue sections, IHC reactions were carried out using a range of different antibody dilutions for each antibody and under various different antigen unmasking methods. Antibody dilutions ranged from 1:20 up to 1:1000 (optimised dilutions can be seen in table 3.1) and unmasking techniques involved different levels of microwave heat treatment using citrate and EDTA buffers, and protease treatment. Cervical tissue samples were included in all optimisation steps, along with another tissue sample that had been reported to have high expression of the protein of interest. To ensure that any staining observed was due to specific binding of the primary antibody to the antigen, negative controls that replaced the primary antibody with PBS were performed simultaneously on the same tissue. All antibodies were successfully optimised on at least one tissue sample with the exception of occludin, with no staining observed on control tissues at any antibody dilution or using any antigen retrieval method. The manufacturer of this

antibody did not specify a recommended positive control tissue but stated the reactivity of the antibody had been verified on Madine Darby Canine Kidney cells. Human skin tissue was selected as a positive control tissue as other studies had previously identified occludin as being present in the stratum granulosum of human epidermis [204]. As the manufacturer of this antibody had only confirmed the reactivity of this antibody on a cell line it is possible that the process of formalin fixation may adversely affect the antigen that it is directed against. This antibody may therefore only be useful for immunohistochemistry using non-formalin fixed samples such as fresh frozen tissue (cryostat sections) or cell lines. A summary of the optimised conditions for each antibody can be seen in table 3.1. Images of the positive control and negative control tissues stained under their optimised conditions can be seen in figure 3.1.

Table 3.1 Outline of optimised antibody dilution, retrieval method, and positive control tissue for each antibody used in this study.

Protein	Optimised Antibody Diluton	Optimised Retrival Method	Optimised Positive control tissue
E-cadherin	1:100	12 min MW Citrate Buffer	Normal Cervix
N-cadherin	1:100	12 min MW Citrate Buffer	Liver
Claudin-1	1:50	12 min MW Citrate Buffer + 30 seconds protease	Skin
Claudin-7	1:50	12 min MW Citrate Buffer + 30 seconds protease	Cervix (HSIL lesion)
p120-catenin	1:125	12 min MW Citrate Buffer	Cervix (HSIL lesion)
SNAIL	1:1000	12 min MW Citrate Buffer	Cervix (HSIL lesion)/ Breast Carcinoma
Occludin	Unable to optimise	Unable to optimise	Skin/Normal Cervix

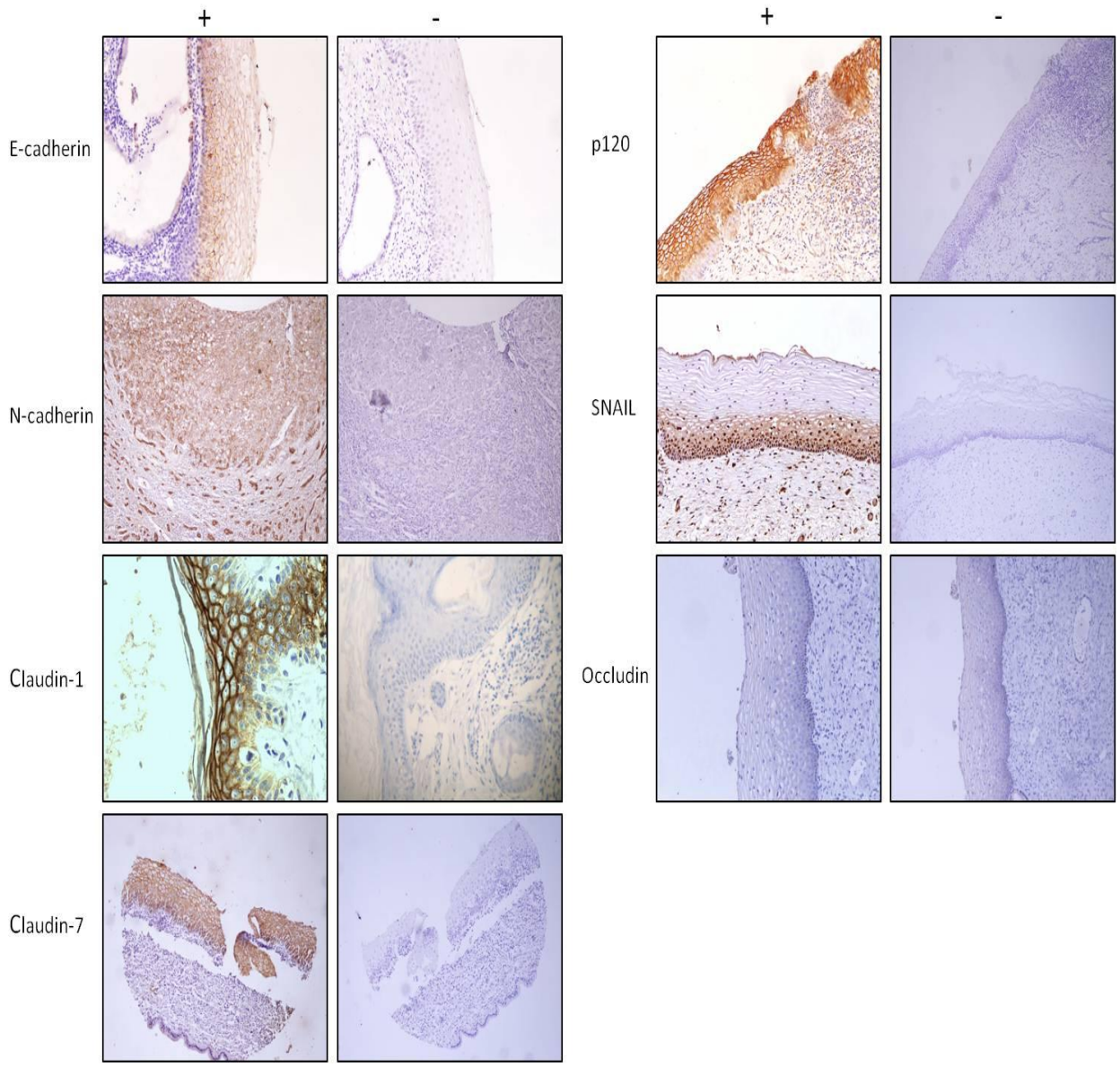

Figure 3.1 Images of positive and negative controls for each of the antibodies used in this study.

Optimised antibody dilutions, antigen retrieval methods and tissue type can be seen in table 3.1

3.4 Evaluation of tissue microarrays

In total 5 tissue microarray blocks were constructed, 4 arrays containing cervical tissue samples and 1 array containing control tissue samples for each antibody (Figure 3.3). Each cervical tissue microarray was designed to have a total of 40 samples each in triplicate, which would ultimately yield a total of 160 cervical samples. After the tissue microarrays were constructed a section was cut and a H&E stain was performed to analyse the morphology of each core (Figure 3.2). A pathologist at the Rotunda Hospital, Dr Eibhlis O'Donovan, analysed each core to decide if there was adequate epithelium present and, if so, to define what grade the lesion was.

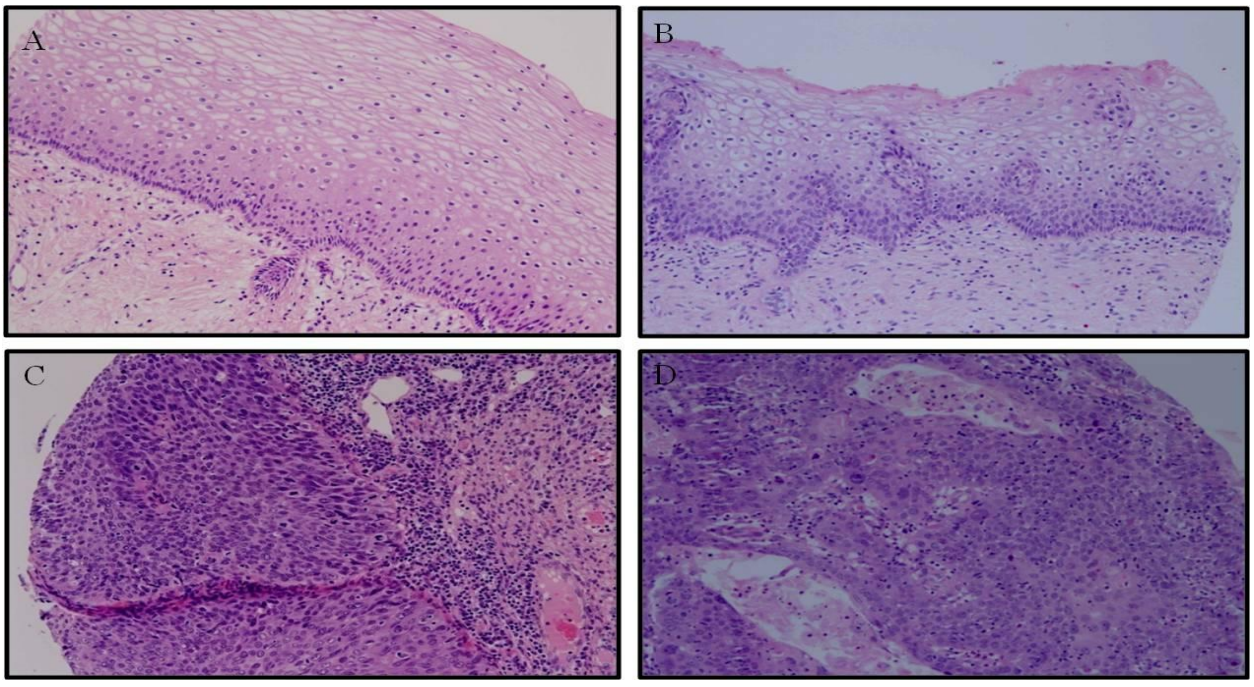

Figure 3.2 H&E stain of cervical tissue microarrays

A = No evidence of malignancy, B = Low grade squamous intra-epithelial lesion, C = High grade squamous intra-epithelial lesion, D = Squamous cell carcinoma

After analysis by the pathologist 126 cases were identified that had adequate lesion present, a summary of which can be seen in table 3.2. This amount was lower than the intended 160 samples but still included a large number of samples in all disease grades and was more than sufficient for subsequent experiments. The tissue blocks used for TMA productions had previously been used for diagnostic purposes in the Rotunda hospital, therefore a variable amount of tissue was present on each core sampled. As a result, when the TMAs were sectioned for use in this study, some cores were lost faster than others and thus all 126 samples were not always present for each biomarker. A greater number of N.E.M samples, 36, were present on the final TMAs than the intended 16. This was a result of inaccurate punch sampling of N.E.M tissue adjacent to the targeted lesion during TMA construction.

Figure 3.3 Image of the 4 cervical TMA blocks used in this study

Table 3.2 Number of cases selected for TMA construction and final number of cases on completed TMAs.

Lesion Grade	Number of cases selected for TMA construction	Final number of cases present on TMAs
N.E.M	16	36
LSIL	48	35
HSIL	48	45
SCC	48	10
Total	160	126

3.5 Evaluation of biomarker expression in cervical lesions

Following the optimisation of each antibody, the immunohistochemical expression of each protein was analysed on the cervical tissue microarrays. To evaluate the expression of all biomarkers except SNAIL, a 4-tier grading system validated for scoring HER-2 expression in gastric cancer was used [205]. No reactivity in any cell was graded as 0, faint or barely perceptible membranous reactivity was graded as 1+, weak to moderate basolateral or lateral membranous reactivity was graded as 2+, strong complete membranous reactivity was graded as 3+. For SNAIL a 4 tier grading system was used with no nuclear or cytoplasmic reactivity in any cell graded as 0, faint or barely perceptible nuclear or cytoplasmic reactivity was graded as 1+, weak to moderate nuclear or cytoplasmic reactivity was graded as 2+, strong complete nuclear or cytoplasmic reactivity was graded as 3+. In consultation with the pathologist it was decided for LSIL and HSIL cases only the dysplastic cells of the lesions would be graded, to avoid non dysplastic cells in the epithelium giving an erroneous grading score. Examples of staining patterns and grading scores for each antibody were presented to the pathologist to confirm samples were being accurately graded.

A one way ANOVA was performed to determine the statistical significance of the grading results for each protein across normal cervical tissue and all disease grades, with a p value of <0.05 deemed significant. For post hoc testing, a Fisher least standard difference (LSD) test was used to assess the significance of results between individual disease states (e.g NEM vs LSIL, NEM vs HSIL) etc. In all cases a p value <0.05 was deemed significant. As each sample was in triplicate staining scores presented were averages of the three scores.

3.5.1 E-cadherin

Normal cervical epithelium displayed moderate membranous staining of cells in the basal and intermediate layers of the epithelium. Low grade lesions showed little or no staining of dysplastic cells in the basal layer of the epithelium with some moderate staining in the intermediate and superficial layers of the epithelium. High grade lesions predominately had no staining or some infrequent weak staining of the dysplastic cells in the basal and intermediate layers with the superficial layer often showing some weak staining (Figure 3.5). In cases of squamous cell carcinomas a weak staining pattern or an absence of staining was most often observed (figure 3.5). The significance of any differences in E-cadherin expression in normal tissue compared to different disease grades were determined using a one way analysis of variance (ANOVA) test (table 3.4) and a fisher least standard difference (LSD) post-hoc test, with a p value <0.05 deemed significant (figure 3.5).

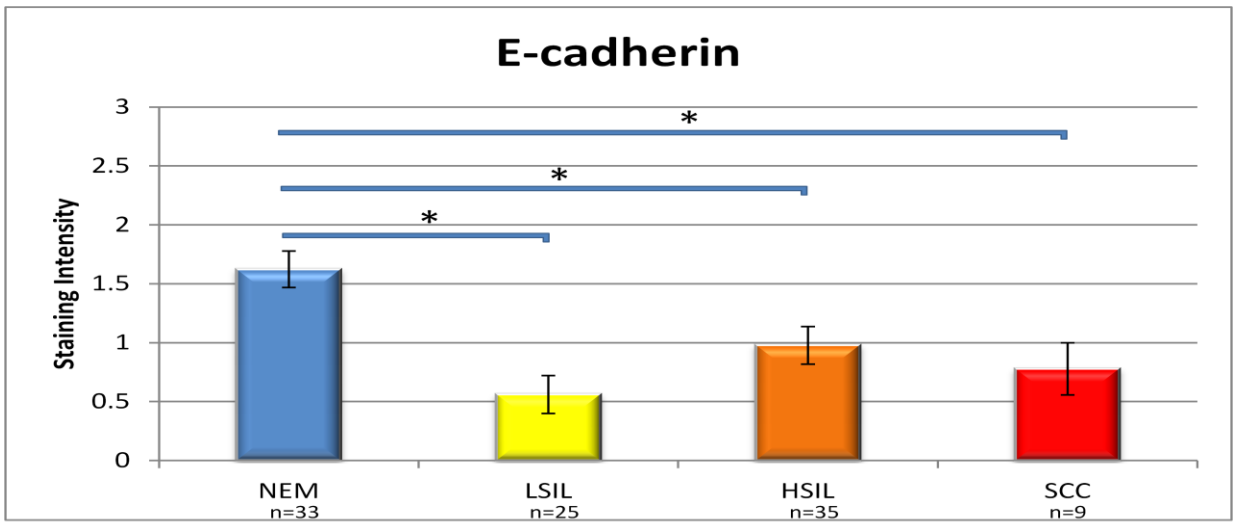

Figure 3.4 Bar chart showing the mean expression of E-cadherin according to pathological grade with error bars showing the standard error for each grade. Significant differences in expression between normal tissue and different disease grades ($p<0.05$) highlighted on chart using *. NEM = no evidence of malignancy, LSIL = low grade squamous intra-epithelial lesion, HSIL = high grade squamous intra-epithelial lesion, SCC = squamous cell carcinoma. n = number of samples

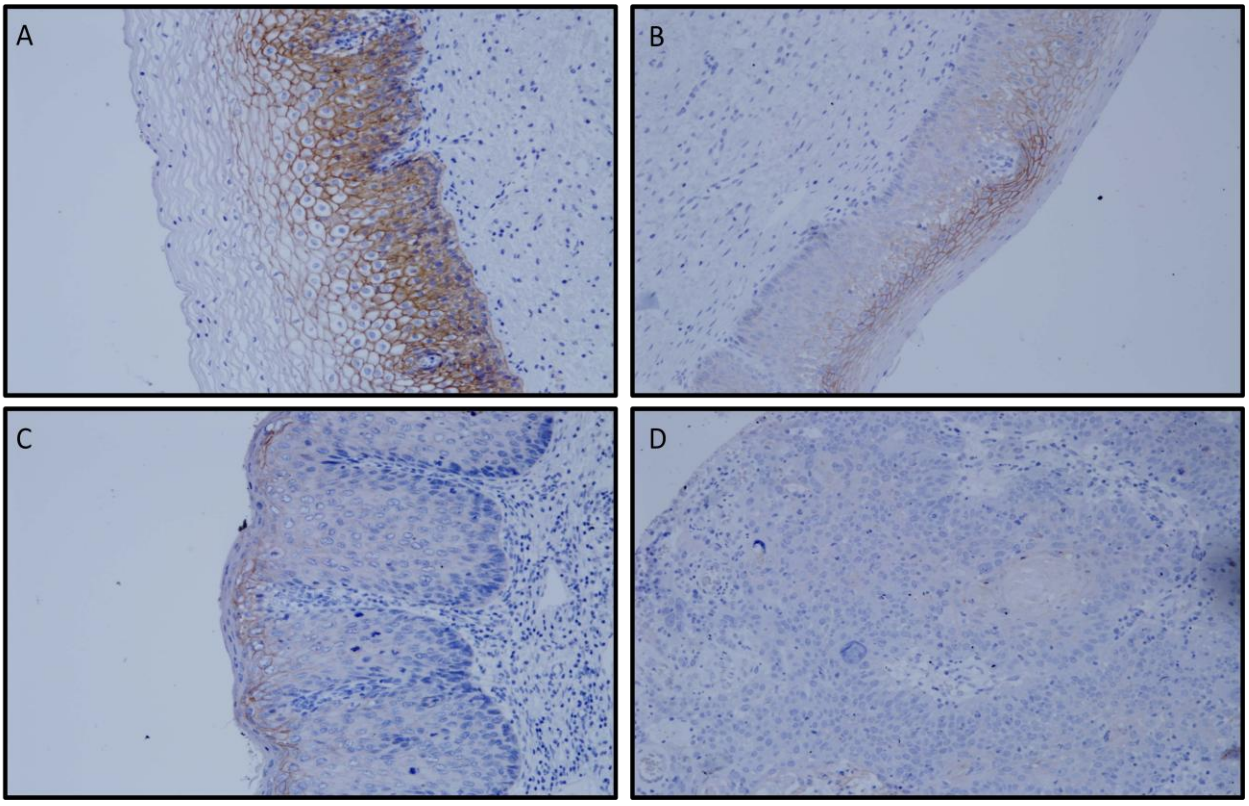

Figure 3.5 Expression of E-cadherin in cervical epithelium detected using immunohistochemistry

A = No evidence of malignancy (N.E.M), B = Low grade squamous epithelial lesion (LSIL), C = High grade squamous epithelial lesion (HSIL), D = Squamous cell carcinoma (SCC)

Table 3.3 Evaluation of E-cadherin IHC staining intensity in normal cervical epithelium and neoplasia

	Staining Intensity			
Grade (n=sample no.)	**0**	**1+**	**2+**	**3+**
N.E.M (n=33)	3 (9%)	10(30%)	14 (43%)	6 (18%)
LSIL (n=25)	14 (56%)	8 (32%)	2 (8%)	1 (4%)
HSIL (n=35)	15 (43%)	9 (26%)	7 (20%)	4 (34%)
SCC (n=9)	3 (33%)	5 (56%)	1 (11%)	0 (0%)

Table shows the scoring results for E-cadherin IHC staining of cervical TMAs. Staining intensity was assessed using a 0-3 scoring system as described in 3.5. As each cervical tissue specimen was sampled in triplicate, the results displayed in this table are the average of the three scores rounded to the nearest whole number.

Table 3.4 Statistical analysis of E-cadherin staining in normal cervical epithelium and neoplasia.

Statistical analysis of E-cadherin staining results						
Groups	***Count***	***Sum***	***Average***	***Variance***	***SD***	**SE**
NEM	33	54.332	1.646424	0.798182	0.8934	0.1555
LSIL	25	14	0.56	0.6525	0.8077	0.1615
HSIL	35	34.25	0.978571	1.089601	1.0438	0.1595
SCC	9	7	0.777778	0.444444	0.6666	0.2222
ANOVA	***SS***	***df***	***MS***	***F***	***P-value***	***F crit***
Between Groups	18.52644	3	6.175481	7.398154	<0.05	2.697423
Within Groups	81.8038	98	0.834733			
Total	100.3302	101				
SD = Standard Deviation, SE = Standard Error, SS = Sum of Squares, DF = Degrees of freedom, MS = Mean Square, F = F-Statistic, Fcrit = F-Critical value						

The IHC E-cadherin scoring data from table 3.3 was assessed using SPSS to determine the standard deviation and standard error within each group. A one way ANOVA analysis was performed to determine any statistically significant difference between the staining score of the different disease groups, with a p value of <0.05 considered significant.

3.5.2 N-cadherin

N-cadherin displayed weak membranous staining in normal cervical epithelium, predominantly in the basal and intermediate layers. Low grade lesions displayed moderate membranous staining in the dysplastic cells of the basal layers, with weaker staining in the differentiating cells of the intermediate and superficial layers. High grade lesions displayed moderate membranous staining throughout the epithelium. Squamous cell carcinoma cells showed predominantly moderate membranous staining with some weak cytoplasmic positivity (figure 3.7). The significance of changes in E-cadherin expression in normal tissue compared to different disease grades were determined using a one way analysis of variance (ANOVA) test (table 3.5) and a fisher least standard difference (LSD) post-hoc test, with a p value <0.05 deemed significant (figure 3.6).

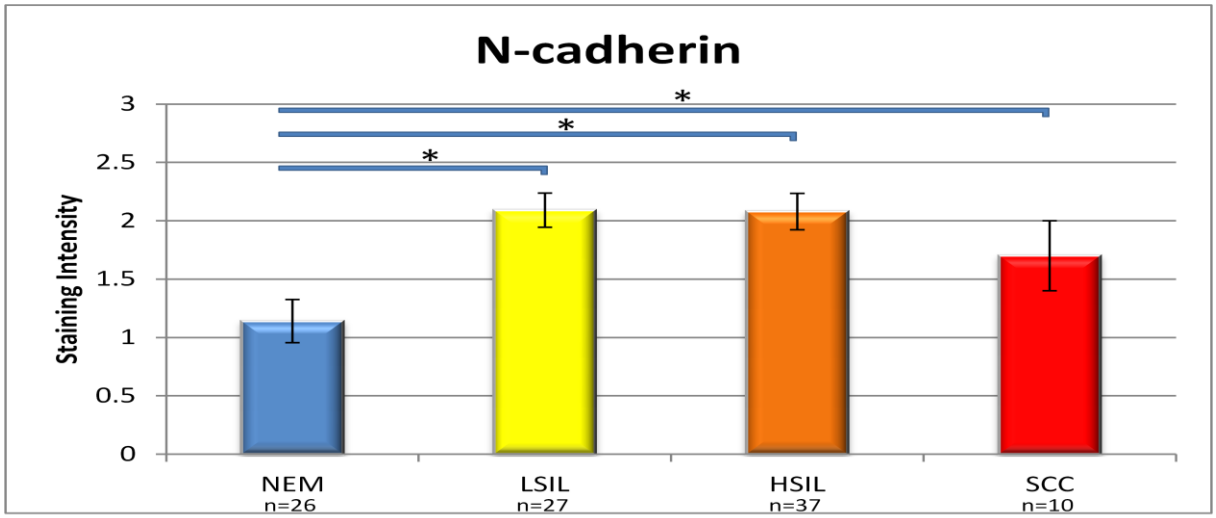

Figure 3.6 Bar chart showing the mean expression of N-cadherin according to pathological grade with error bars showing the standard error for each grade. Significant changes in expression between normal tissue and different disease grades ($p<0.05$) highlighted on chart using *. NEM = no evidence of malignancy, LSIL = low grade squamous intra-epithelial lesion, HSIL = high grade squamous intra-epithelial lesion, SCC = squamous cell carcinoma. n = number of samples

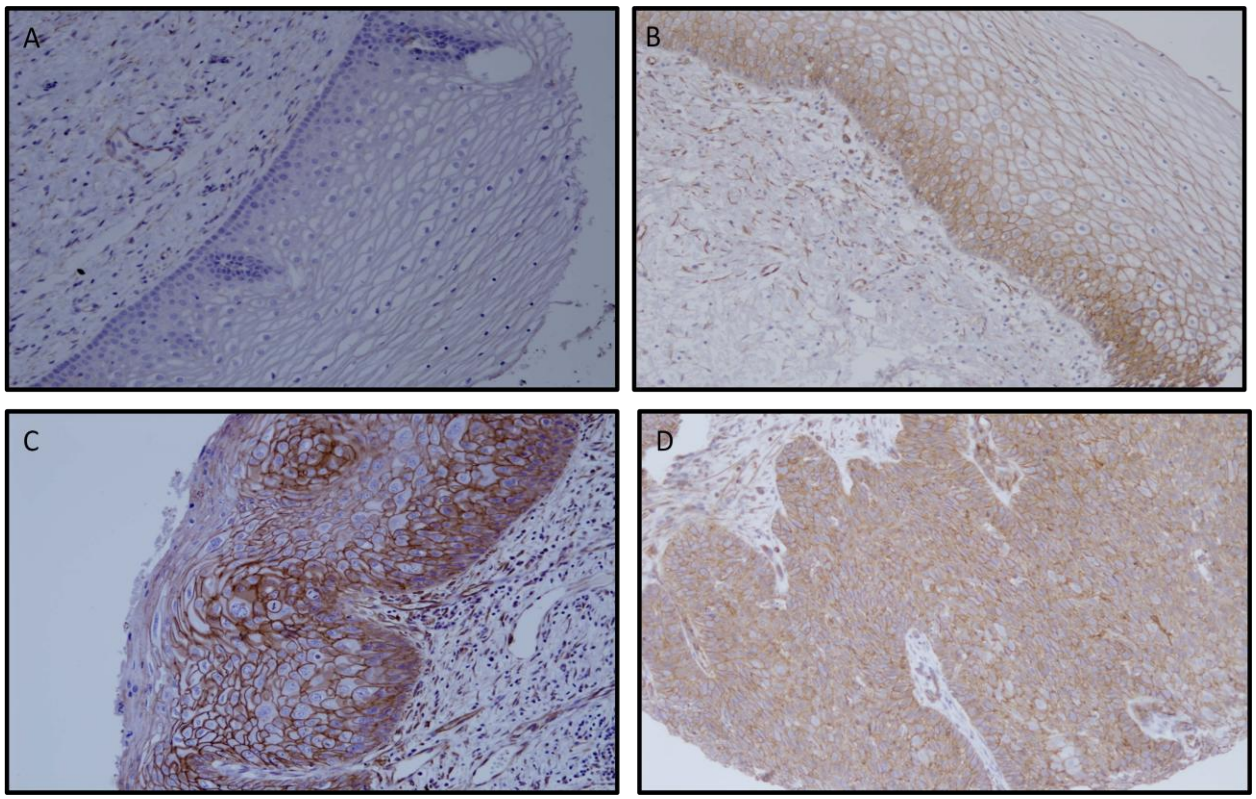

Figure 3.7 Expression of N-cadherin in cervical epithelium detected using immunohistochemistry

A = No evidence of malignancy (N.E.M), B = Low grade squamous epithelial lesion (LSIL), C = High grade squamous epithelial lesion (HSIL), D = Squamous cell carcinoma (SCC)

Table 3.5 Evaluation of N-cadherin staining intensity in normal cervical epithelium and neoplasia

	Staining Intensity			
Grade (n=sample no.)	**0**	**1+**	**2+**	**3+**
N.E.M (n=26)	8 (31%)	8 (31%)	8 (31%)	2 (7%)
LSIL (n=27)	1 (4%)	3 (11%)	15 (56%)	8 (29%)
HSIL (n=37)	3 (8%)	8 (22%)	9 (24%)	17 (46%)
SCC (n=10)	1 (10%)	3 (30%)	4 (40%)	2 (20%)

Table shows the scoring results for N-cadherin IHC staining of cervical TMAs. Staining intensity was assessed using a 0-3 scoring system as described in 3.5. As each cervical tissue specimen was sampled in triplicate, the results displayed in this table are the average of the three scores rounded to the nearest whole number.

Table 3.6 Statistical analysis of N-cadherin staining in normal cervical epithelium and neoplasia

Statistical analysis of N-cadherin staining results						
Groups	***Count***	***Sum***	***Average***	***Variance***	***SD***	**SE**
NEM	26	29.583	1.137808	0.890545	0.943687	0.185
LSIL	27	56.5	2.092593	0.577635	0.760023	0.1463
HSIL	37	77	2.081081	1.021021	1.010456	0.1562
SCC	10	17	1.7	0.9	0.948683	0.3
ANOVA	***SS***	***df***	***MS***	***F***	***P-value***	***F crit***
Between Groups	16.73562	3	5.57854	6.51993	<0.05	2.699393
Within Groups	82.1389	96	0.855614			
Total	98.87452	99				
SD = Standard Deviation, SE = Standard Error, SS = Sum of Squares, DF = Degrees of freedom, MS = Mean Square, F = F-Statistic, Fcrit = F-Critical value						

The IHC N-cadherin scoring data from table 3.5 was assessed using SPSS to determine the standard deviation and standard error within each group. A one way ANOVA analysis was performed to determine any statistically significant difference between the staining score of the different disease groups, with a p value of <0.05 considered significant.

3.5.3 Claudin 1

Claudin-1 displayed weak membranous staining in normal cervical epithelium, predominantly in the basal and intermediate layers. Low grade lesions showed moderate membranous staining in the dysplastic cells of the basal layers, with weaker staining in the differentiating cells of the intermediate and superficial layers. High grade lesions showed moderate to strong membranous staining throughout the epithelium. Squamous cell carcinoma cells showed strong membranous staining with some weak cytoplasmic activity (figure 3.9). The significance of changes in claudin-1 expression in normal tissue compared to different disease grades were determined using a one way analysis of variance (ANOVA) test (table 3.8) and a fisher least standard difference (LSD) post-hoc test, with a p value <0.05 deemed significant (figure 3.8).

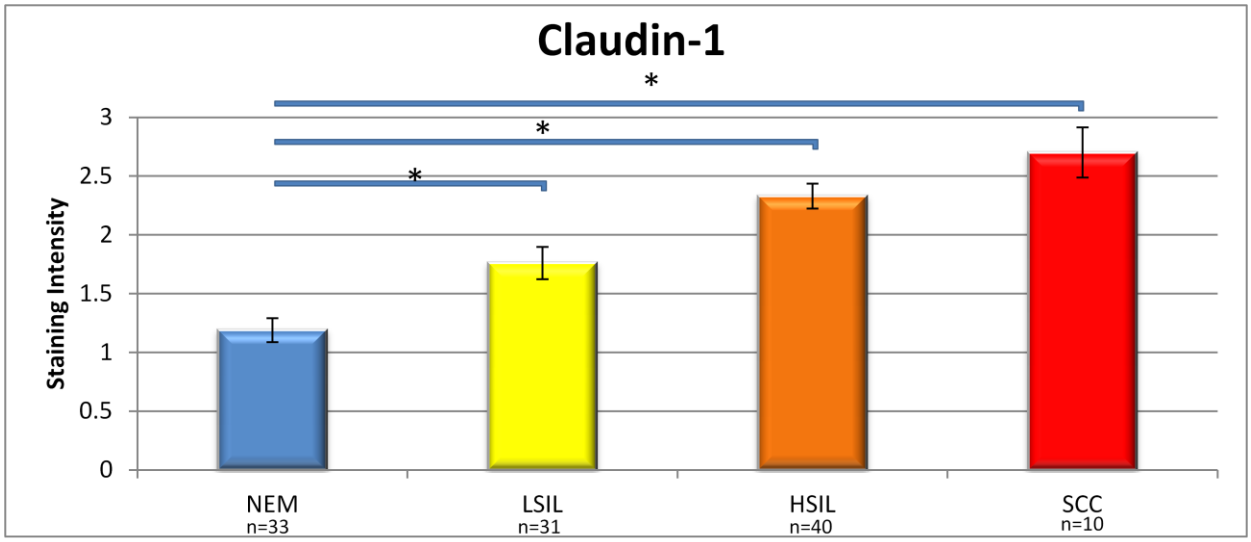

Figure 3.8 Bar chart showing the mean expression of claudin-1 according to pathological grade with error bars showing the standard error for each grade. Significant changes in expression between normal tissue and different disease grades ($p<0.05$) highlighted on chart using *. NEM = no evidence of malignancy, LSIL = low grade squamous intra-epithelial lesion, HSIL = high grade squamous intra-epithelial lesion, SCC = squamous cell carcinoma. n = number of samples

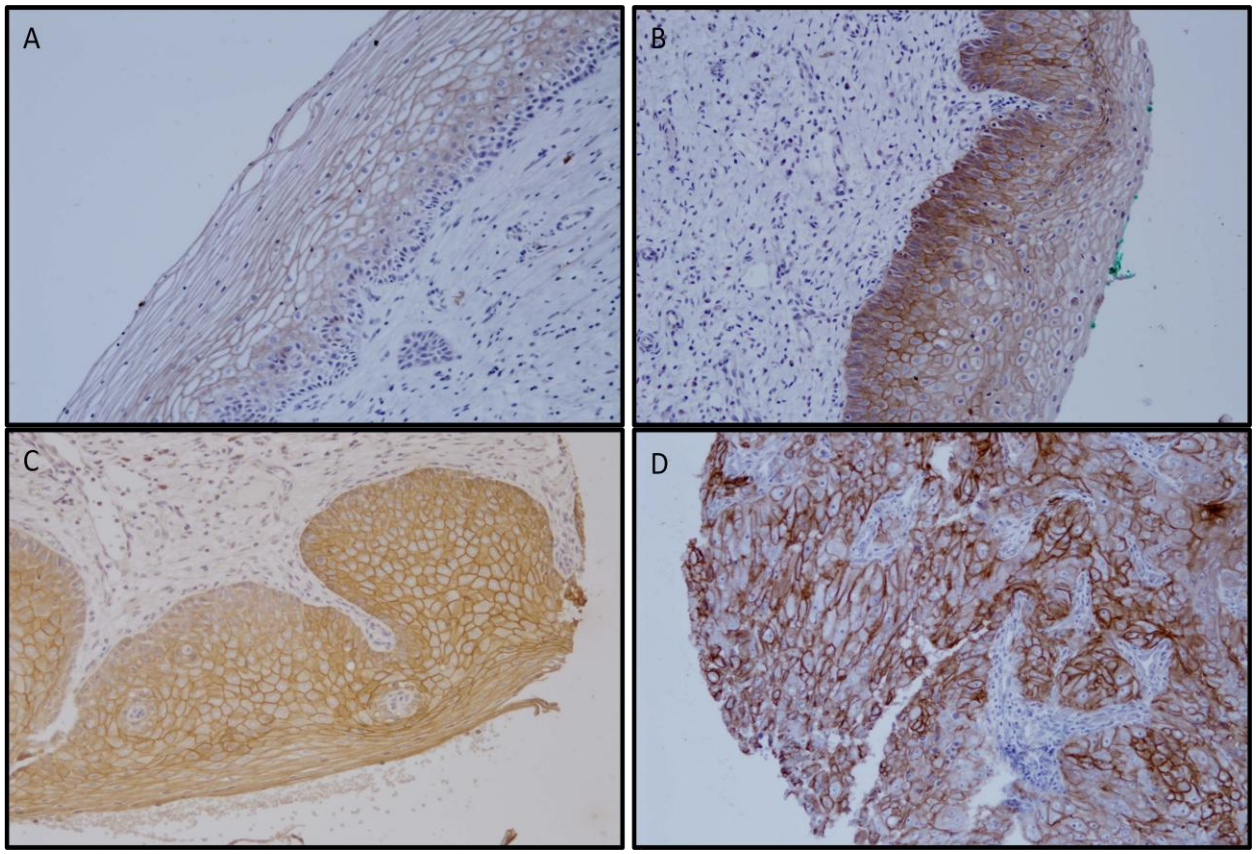

Figure 3.9 Expression of Claudin-1 in cervical epithelium detected using immunohistochemistry

A = No evidence of malignancy (N.E.M), B = Low grade squamous epithelial lesion (LSIL), C = High grade squamous epithelial lesion (HSIL), D = Squamous cell carcinoma (SCC)

Table 3.7 Evaluation of claudin-1 staining intensity in normal cervical epithelium and neoplasia

	Staining Intensity			
Grade (n= sample no)	**0**	**1+**	**2+**	**3+**
N.E.M (n=33)	3 (9%)	19 (53%)	11 (36%)	0 (0%)
LSIL (n=31)	0 (0%)	13 (42%)	12 (32%)	6 (26%)
HSIL (n=40)	0 (0%)	4 (10%)	17 (43%)	19 (47%)
SCC (n=10)	0 (0%)	1 (10%)	1 (10%)	8 (80%)

Table shows the scoring results for claudin-1 IHC staining of cervical TMAs. Staining intensity was assessed using a 0-3 scoring system as described in 3.5. As each cervical tissue specimen was sampled in triplicate, the results displayed in this table are the average of the three scores rounded to the nearest whole number

Table 3.8 Statistical analysis of claudin-1 staining in normal cervical epithelium and neoplasia

Statistical analysis of Claudin-1 staining results						
Groups	***Count***	***Sum***	***Average***	***Variance***	***SD***	**SE**
NEM	33	39.166	1.186848	0.345045	0.587406	0.1022
LSIL	31	54.5	1.758065	0.581183	0.762353	0.1369
HSIL	40	93	2.325	0.48141	0.693837	0.1067
SCC	10	27	2.7	0.455556	0.674949	0.2134
Source of Variation	***SS***	***df***	***MS***	***F***	***P-value***	***F crit***
Between Groups	30.95731	3	10.3191	22.10436	<0.05	2.687139
Within Groups	51.35193	110	0.466836			
Total	82.30924	113				
SD = Standard Deviation, SE = Standard Error, SS = Sum of Squares, DF = Degrees of freedom, MS = Mean Square, F = F-Statistic, Fcrit = F-Critical value						

The IHC claudin-1 scoring data from table 3.7 was assessed using SPSS to determine the standard deviation and standard error within each group. A one way ANOVA analysis was performed to determine any statistically significant difference between the staining score of the different disease groups, with a p value of <0.05 considered significant.

3.5.4 Claudin-7

Claudin-7 displayed weak membranous staining in normal cervical epithelium, predominantly in the basal and intermediate layers. Low grade lesions displayed weak to moderate membranous staining in the dysplastic cells of the basal layers, with less staining in the differentiating cells of the intermediate and superficial layers. High grade lesions displayed moderate to strong membranous staining throughout the epithelium. Squamous cell carcinoma cells displayed moderate membranous staining with some weak cytoplasmic positivity (figure 3.11). The significance of changes in claudin-7 expression in normal tissue compared to different disease grades were determined using a one way analysis of variance (ANOVA) test (table 3.10) and a fisher least standard difference (LSD) post-hoc test, with a p value <0.05 deemed significant (figure 3.10).

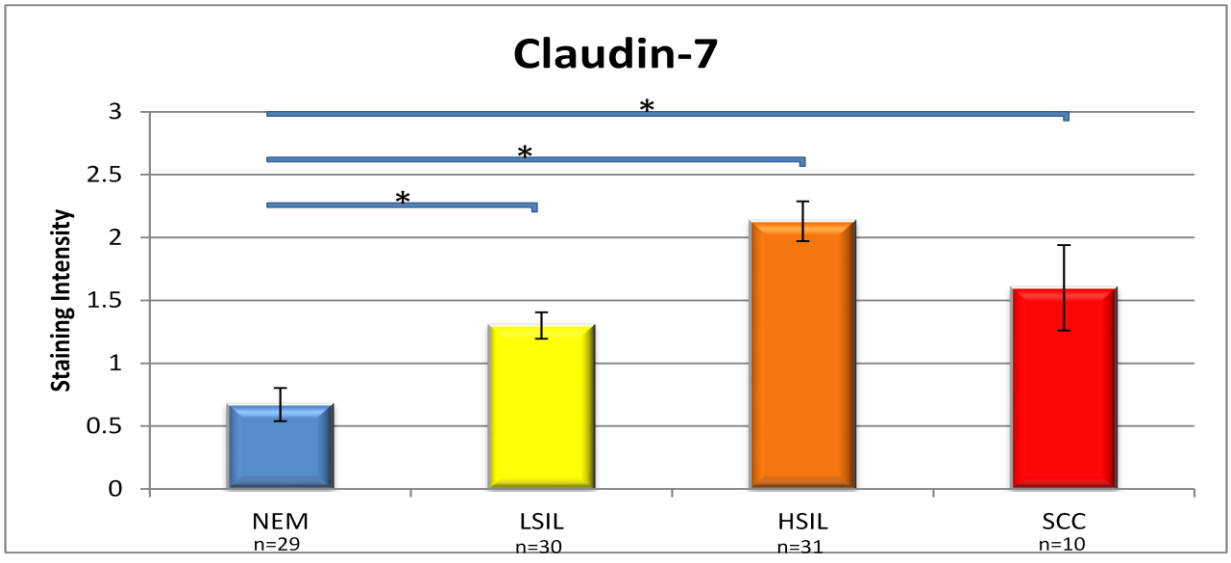

Figure 3.10 Bar chart showing the mean expression of claudin-7 according to pathological grade with error bars showing the standard error for each grade. Significant changes in expression between normal tissue and different disease grades ($p<0.05$) highlighted on chart using *. NEM = no evidence of malignancy, LSIL = low grade squamous intra-epithelial lesion, HSIL = high grade squamous intra-epithelial lesion, SCC = squamous cell carcinoma. n = number of samples

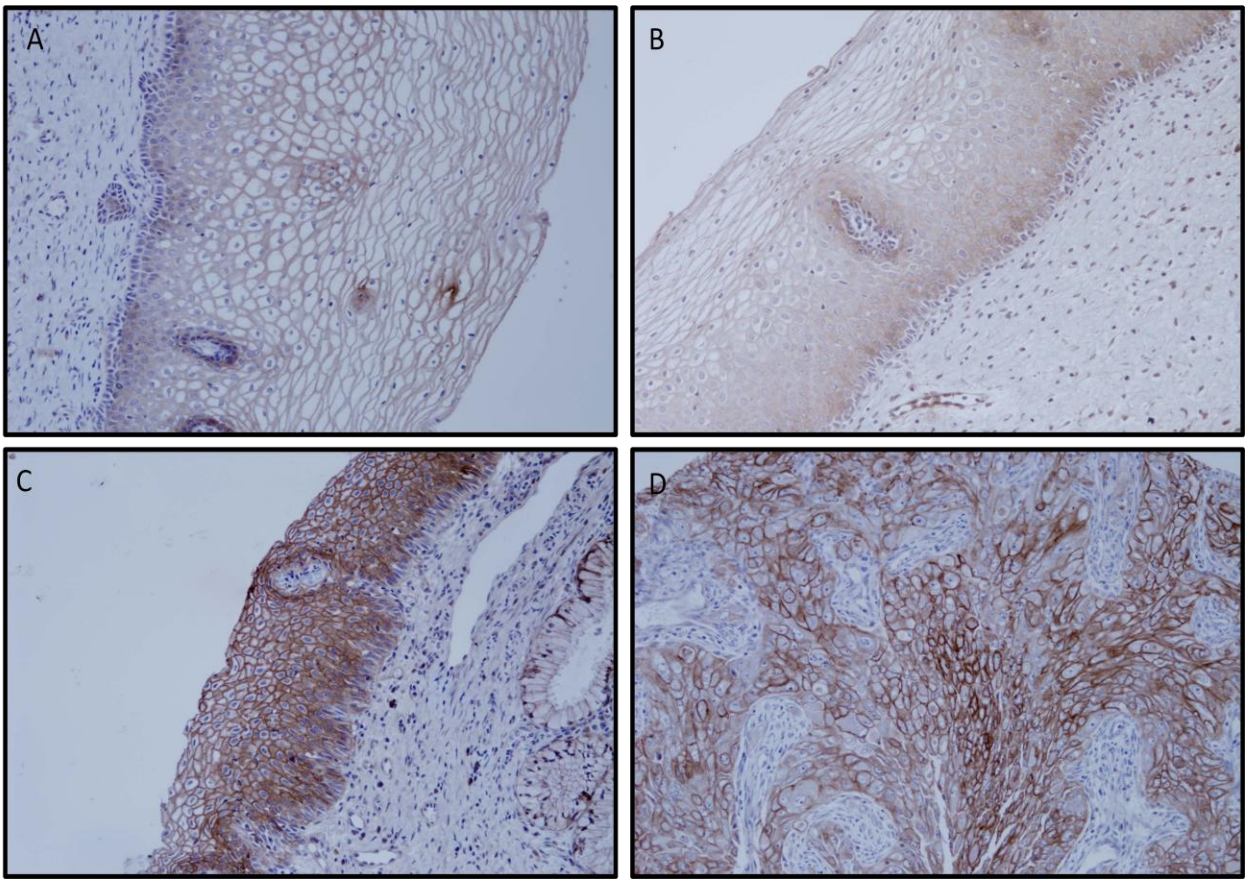

Figure 3.11 Expression of Claudin-7 in cervical epithelium detected using immunohistochemistry

A = No evidence of malignancy (N.E.M), B = Low grade squamous epithelial lesion (LSIL), C = High grade squamous epithelial lesion (HSIL), D = Squamous cell carcinoma (SCC)

Table 3.9 Evaluation of claudin-7 staining intensity in normal cervical epithelium and neoplasia

	Staining Intensity			
Grade (n=sample no.)	**0**	**1+**	**2+**	**3+**
N.E.M (n=29)	13 (45%)	12 (41%)	4 (14%)	0 (0%)
LSIL (n=30)	7 (21%)	13 (45%)	4 (14%)	6 (20%)
HSIL (n=31)	2 (7%)	5 (16%)	9 (29%)	15 (48%)
SCC (n=10)	1 (10%)	5 (50%)	1 (10%)	3 (30%)

Table shows the scoring results for claudin-7 IHC staining of cervical TMAs. Staining intensity was assessed using a 0-3 scoring system as described in 3.5. As each cervical tissue specimen was sampled in triplicate, the results displayed in this table are the average of the three scores rounded to the nearest whole number.

Table 3.10 Statistical analysis of claudin-7 staining in normal cervical epithelium and neoplasia

Statistical analysis of Claudin-7 staining results						
Groups	***Count***	***Sum***	***Average***	***Variance***	***SD***	**SE**
NEM	29	19.5	0.672414	0.504926	0.710582	0.132
LSIL	30	39	1.3	1.13793	1.055364	0.1055
HSIL	31	66	2.129032	0.882796	0.939572	0.1581
SCC	10	16	1.6	1.155556	1.074968	0.34
Source of Variation	***SS***	***df***	***MS***	***F***	***P-value***	***F crit***
Between Groups	34.09222	3	11.36407	16.10223	<0.05	2.698398
Within Groups	68.45729	97	0.705745			
Total	102.5495	100				
SD = Standard Deviation, SE = Standard Error, SS = Sum of Squares, DF = Degrees of freedom, MS = Mean Square, F = F-Statistic, Fcrit = F-Critical value						

The IHC claudin-7 scoring data from table 3.9 was assessed using SPSS to determine the standard deviation and standard error within each group. A one way ANOVA analysis was performed to determine any statistically significant difference between the staining score of the different disease groups, with a p value of <0.05 considered significant.

3.5.5 p120-catenin

p120-catenin showed weak membranous staining in normal cervical epithelium, predominantly in the basal and parabasal layers. Low grade lesions showed moderate membranous staining in the dysplastic cells of the basal layers, with less staining in the differentiating cells of the intermediate and superficial layers. High grade lesions showed strong membranous staining throughout the epithelium. Squamous cell carcinoma cells showed strong membranous and cytoplasmic staining (figure 3.13). The significance of changes in p120-catenin expression in normal tissue compared to different disease grades were determined using a one way analysis of variance (ANOVA) test (table 3.12) and a fisher least standard difference (LSD) post-hoc test, with a p value <0.05 deemed significant (figure 3.12).

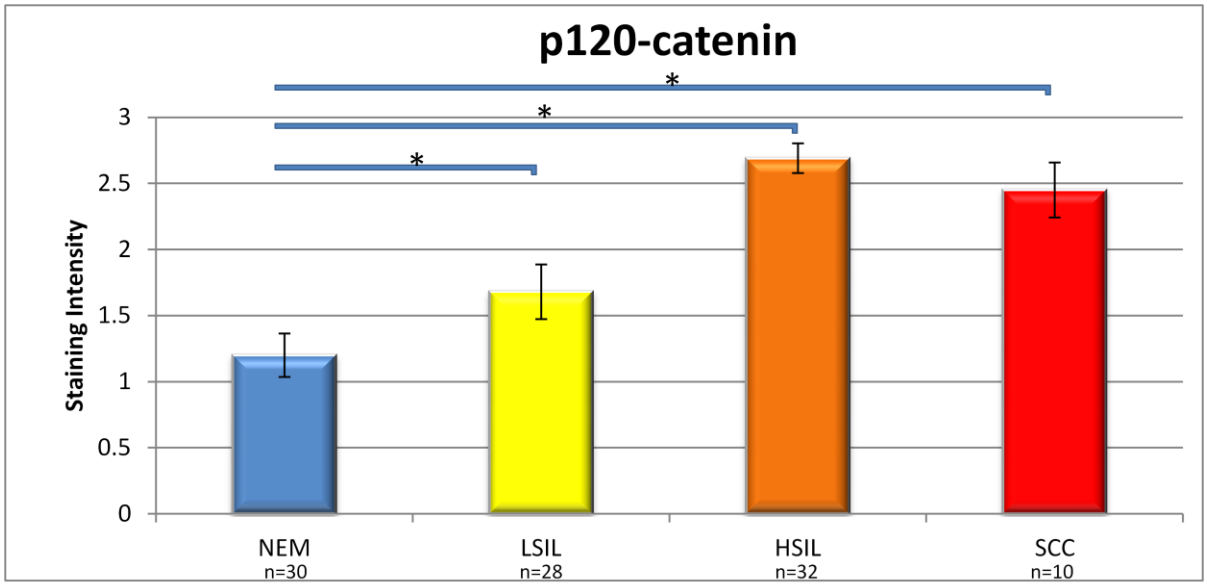

Figure 3.12 Bar chart showing the mean expression of p120-catenin according to pathological grade with error bars showing the standard error for each grade. Significant changes in expression between normal tissue and different disease grades ($p<0.05$) highlighted on chart using *. NEM = no evidence of malignancy, LSIL = low grade squamous intra-epithelial lesion, HSIL = high grade squamous intra-epithelial lesion, SCC = squamous cell carcinoma. n = number of samples

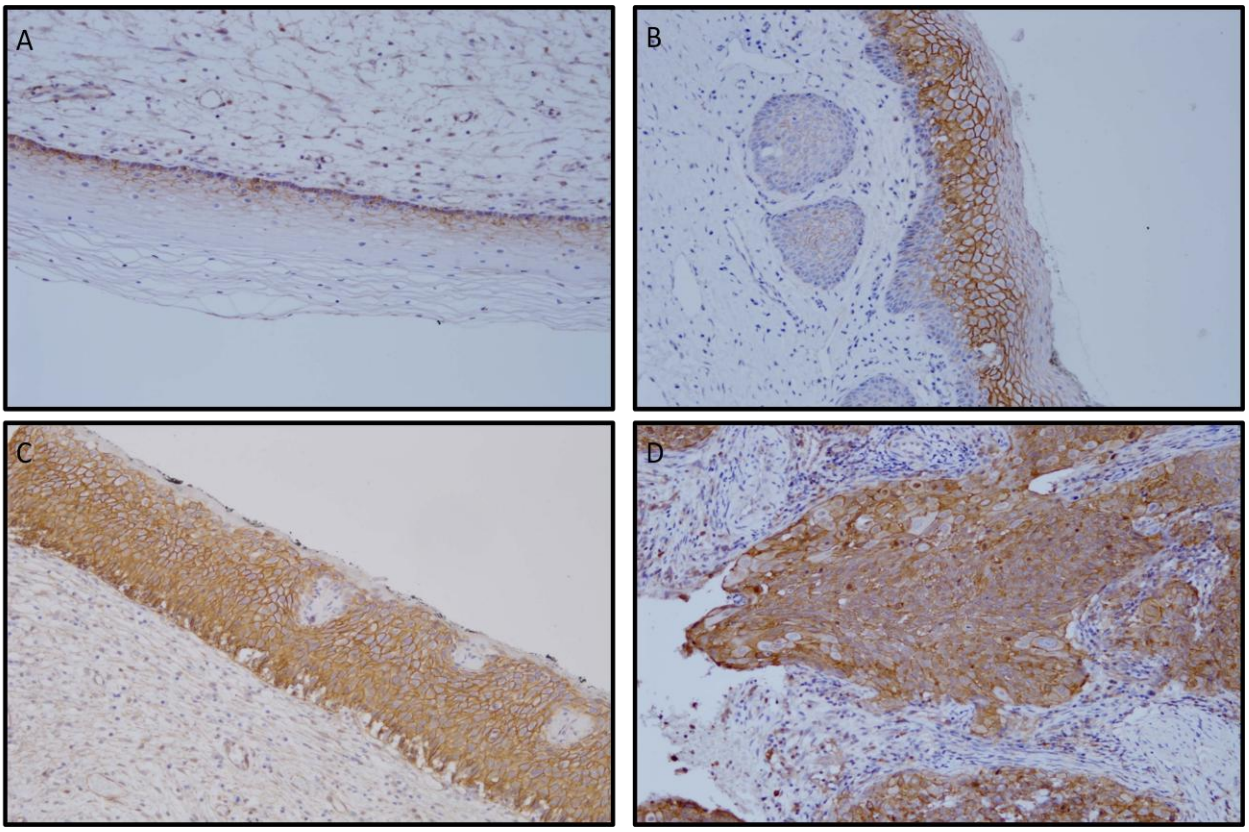

Figure 3.13 Expression of p120-catenin in cervical epithelium detected using immunohistochemistry

A = No evidence of malignancy (N.E.M), B = Low grade squamous epithelial lesion (LSIL), C = High grade squamous epithelial lesion (HSIL), D = Squamous cell carcinoma (SCC)

Table 3.11 Evaluation of p120-catenin staining intensity in normal cervical epithelium and neoplasia

	Staining Intensity			
Grade (n=sample no.)	**0**	**1+**	**2+**	**3+**
N.E.M (n=30)	7 (23%)	12 (40%)	8 (27%)	3 (10%)
LSIL (n=28)	7 (25%)	1 (4%)	14 (50%)	6 (21%)
HSIL (n=32)	0 (0%)	3 (9%)	4 (13%)	25 (78%)
SCC (n=10)	0 (0%)	1 (9%)	4 (36%)	6 (55%)

Table shows the scoring results for p120-catenin IHC staining of cervical TMAs. Staining intensity was assessed using a 0-3 scoring system as described in 3.5. As each cervical tissue specimen was sampled in triplicate, the results displayed in this table are the average of the three scores rounded to the nearest whole number

Table 3.12 Statistical analysis of p120-catenin staining in normal cervical epithelium and neoplasia

Statistical analysis of p120-catenin staining results						
Groups	***Count***	***Sum***	***Average***	***Variance***	***SD***	**SE**
NEM	30	36	1.2	0.803448	0.896353	0.1636
LSIL	28	47	1.678571	1.189153	1.090483	0.206
HSIL	32	86	2.6875	0.415323	0.644455	0.1127
SCC	10	27	2.454545	0.472727	0.687552	0.2073
Source of Variation	***SS***	***df***	***MS***	***F***	***P-value***	***F crit***
Between Groups	39.13415	3	13.04472	17.33115	<0.05	2.698398
Within Groups	73.00942	97	0.752674			
Total	112.1436	100				

SD = Standard Deviation, SE = Standard Error, SS = Sum of Squares, DF = Degrees of freedom, MS = Mean Square, F = F-Statistic, Fcrit = F-Critical value

The IHC p120-catenin scoring data from table 3.11 was assessed using SPSS to determine the standard deviation and standard error within each group. A one way ANOVA analysis was performed to determine any statistically significant difference between the staining score of the different disease groups, with a p value of <0.05 considered significant

3.5.6 Snail

In normal cervical epithelium an absence of staining was most often observed. In low grade lesions weak nuclear and cytoplasmic staining of dysplastic cells in the basal layer was observed with no staining of cells in the intermediate and superficial layers. In high grade lesions weak to moderate nuclear and cytoplasmic staining was observed of dysplastic cells in the basal and intermediate layers of the epithelium. In squamous cell carcinoma cases moderate nuclear and cytoplasmic staining of malignant cells was observed (figure 3.15). The significance of changes in SNAIL expression in normal tissue compared to different disease grades were determined using a one way analysis of variance (ANOVA) test (table 3.14) and a fisher least standard difference (LSD) post-hoc test, with a p value <0.05 deemed significant (figure 3.14).

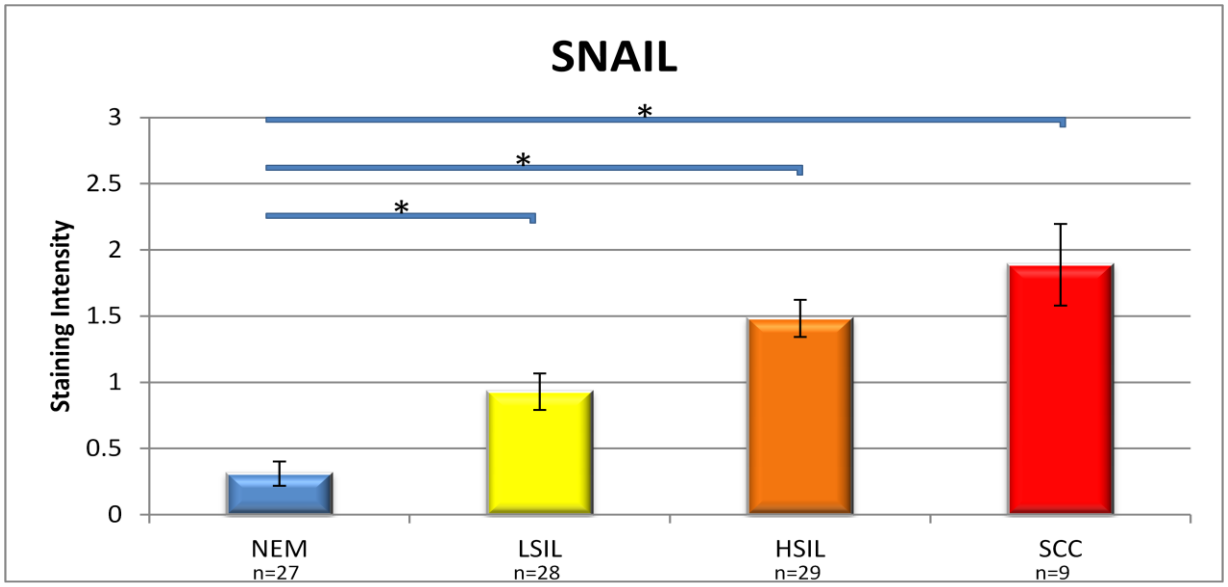

Figure 3.14 Bar chart showing the mean expression of SNAIL according to pathological grade with error bars showing the standard error for each grade. Significant changes in expression between normal tissue and different disease grades ($p<0.05$) highlighted on chart using *. NEM = no evidence of malignancy, LSIL = low grade squamous intra-epithelial lesion, HSIL = high grade squamous intra-epithelial lesion, SCC = squamous cell carcinoma. n = number of samples

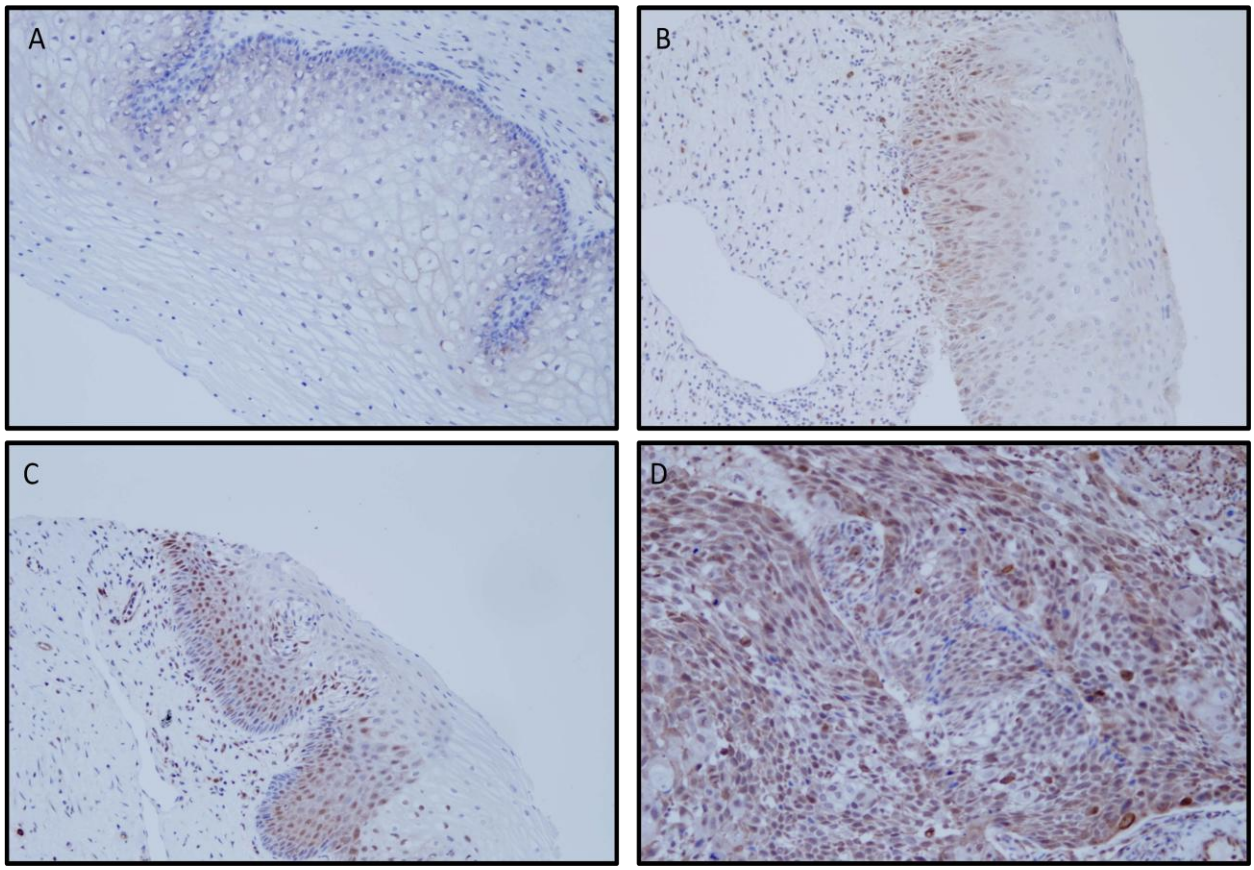

Figure 3.15 Expression of SNAIL in cervical epithelium detected using immunohistochemistry

(N.E.M) No evidence of malignancy, (LSIL) Low grade squamous epithelial lesion, (HSIL) High grade squamous epithelial lesion, (SCC) Squamous cell carcinoma

Table 3.13 Evaluation of Snail staining intensity in normal cervical epithelium and neoplasia

	Staining Intensity			
Grade (n=sample no.)	**0**	**1+**	**2+**	**3+**
N.E.M (n=27)	19 (70%)	7 (26%)	1 (4%)	0 (0%)
LSIL (n=28)	8 (29%)	13 (46%)	7 (25%)	0 (0%)
HSIL (n=29)	2 (7%)	13 (45%)	11 (38%)	3 (10%)
SCC (n=9)	0 (0%)	4 (40%)	2 (30%)	3 (30%)

Table shows the scoring results for SNAIL IHC staining of cervical TMAs. Staining intensity was assessed using a 0-3 scoring system as described in 3.5. As each cervical tissue specimen was sampled in triplicate, the results displayed in this table are the average of the three scores rounded to the nearest whole number.

Table 3.14 Statistical analysis of Snail staining in normal cervical epithelium and neoplasia

Statistical analysis of Snail staining results						
Groups	*Count*	*Sum*	*Average*	*Variance*	*SD*	SE
NEM	27	8.333	0.30863	0.232272	0.476968	0.0928
LSIL	28	26	0.928571	0.531746	0.729209	0.1378
HSIL	29	43	1.482759	0.597906	0.773244	0.14
SCC	9	17	1.888889	0.861111	0.927961	0.3093
Source of Variation	*SS*	*df*	*MS*	*F*	*P-value*	*F crit*
Between Groups	26.43769	3	8.812564	17.64647	<0.05	2.709402
Within Groups	43.44738	87	0.499395			
Total	69.88508	90				

SD = Standard Deviation, SE = Standard Error, SS = Sum of Squares, DF = Degrees of freedom, MS = Mean Square, F = F-Statistic, Fcrit = F-Critical value

The IHC SNAIL scoring data from table 3.13 was assessed using SPSS to determine the standard deviation and standard error within each group. A one way ANOVA analysis was performed to determine any statistically significant difference between the staining score of the different disease groups, with a p value of <0.05 considered significant.

3.6 Correlation between expression of different biomarkers

In order to assess any possible correlation between the expression of different biomarkers in cervical lesions, the mean expression for each biomarker in each disease grade was entered into microsoft excel and a correlation test was performed. The correlation co-efficient is expressed within a range of -1 to +1 inclusive, with -1 indicating a high inverse correlation and +1 indicating a high positive correlation between two biomarkers. E-cadherin was inversely correlated to all other biomarkers, as E-cadherin was the only biomarker with highest expression in NEM tissue and reduced expression in neoplastic lesions, with its strongest inverse correlation to N-cadherin (-0.85821). Apart from its strong inverse correlation to E-cadherin, N-cadherin also had a high positive correlation to Claudin-7 (0.784817). Claudin-1 expression was very highly correlated with both p120-catenin (0.92857) and SNAIL expression. (0.99966). Claudin-7 also displayed a strong correlation with SNAIL (0.820169) and p120-catenin (0.923247). Correlation coefficients for all biomarkers can be seen in table 3.15.

Table 3.15 Correlation coefficients between different biomarker staining results.

	ECAD	***NCAD***	***CLDN1***	***CLDN7***	***p120***	***SNAIL***
ECAD	1					
NCAD	-0.85821	1				
CLDN1	-0.62422	0.546993	1			
CLDN7	-0.56719	0.784817	0.822935	1		
p120	-0.50664	0.630428	0.92857	0.960345	1	
SNAIL	-0.64353	0.559515	0.99966	0.820169	0.923247	1

Coefficent of +1 indicates strong correlation. Coefficient of -1 indicates strong negative correlation

3.7 Summary & Key findings

A cohort of cervical tissue samples containing normal cervical tissue and all grades of cervical neoplasia were selected and retrieved from the Rotunda Maternity Hospital. Sections from all of the tissue blocks were cut and a H&E stain was performed to identify the area containing the lesion. Several tissue microarrays were then produced using the cervical tissue blocks, and these TMAs were imunohistochemically stained to examine the expression of several adherens and tight junction proteins in cervical tissue.

- The expression of several tight and adherens junction proteins is altered in pre-invasive and invasive cervical lesions
    - Reduction in the expression of E-cadherin in all grades of neoplasia compared to normal cervical epithelium
    - Increase in the expression of N-cadherin, claudin-1, claudin-7, p120-catenin, and SNAIL

- Change in expression for many proteins was observed even in low-grade lesions indicating some of these proteins may be of use as biomarkers for differentiating between borderline normal and LSIL lesions and also in identifying pre-invasive lesions more likely to progress to invasive cancers.

- Identified aberrant expression profile of AJ and TJ proteins in this study may offer further insight into the pathogenesis of cervical malignancies, potentially uncovering new targets for future therapies.

3.8 Discussion

This study aimed to examine the expression profiles of a range of adherens and tight junction proteins in normal cervical epithelium and in different grades of cervical neoplasia. To this end we utilised a cohort of cervical tissue samples from the Rotunda Maternity Hospital to create several tissue microarrays, each containing normal cervical tissue and all grades of neoplasia. We examined the expression of several adherens and tight junction proteins and a significant change in expression of these proteins was observed in both pre-invasive and invasive lesions. A change in expression of many adherens and tight junction proteins was observed in both low grade and high grade pre-cancer lesions and in invasive cancer. In particular, a reduction in the expression of E-cadherin and a reduction in the expression of N-Cadherin, claudin-1, claudin-7, p120-cateninand SNAIL was observed in all grades of neoplasia. This may indicate that some of these proteins could be of use as biomarkers for disease progression, potentially helping the identification of pre-cancerous lesions that are more likely to progress to invasive cancers, and also help to differentiate pre-cancerous lesions from other non-cancer related conditions in the cervical epithelium, such as metaplasia. To fully assess the usefulness of these proteins as markers of disease progression, it would be necessary to compare the expression of each protein to patient follow up information, such as patient outcomes. Unfortunately, due to ethical constraints, this information was not made available to this study. As a result of not having access to patient follow up information, this study was unable to assess if there is any relationship between changes in expression of a particular adherens or tight junction protein and aspects of patient outcome, such as prognosis. Further studies are therefore required to

determine if any of these proteins would be of use in a clinical setting as prognostic indicators or biomarkers for disease progression.

One limitation of this study, however, was the lower number of invasive cancer samples analysed compared to NEM, LSIL, and HSIL samples. Initially, during TMA design, it was intended to include 48 samples each of LSIL, HSIL and invasive cancer in the study. Unfortunately, inclusion of 48 invasive cancer samples was not possible as this study only had access to patient samples from the Rotunda Hospital that were treated between 2005-2007 and an insufficient number of invasive cancer samples were processed in the hospital during this period. Although in Ireland there are on average 180 cases of cervical cancer per year (WHO 2012), these cases are treated throughout all the maternity hospitals in the state, thus an individual hospital may only have a small number of patients presenting with cervical cancer per year. As a result, this study was limited to analysing 10 samples of invasive cancer. The sample number of this study was similar to the 12 SCC samples used by Wang et al., 2005 to assess p16 expression in cervical neoplasia, and was still sufficient to assess the expression profile of tight and adherens junction proteins in invasive cancer and to allow comparisons of expression of these proteins in normal cervical tissue and low and high grade lesions.

4. Detection and genotyping of HPV in cervical tissue samples

4.1 Introduction

The causal role of HPV in the development of cervical cancer had been well established and is highlighted by the fact that HPV DNA is detected in 99% of invasive cervical tumours [3]. Significant diversity exists within the HPV family, with over 120 HPV genotypes currently identified and 12 subgroups within the α-papillomvirus genus alone [14]. In a clinical setting HPV genotypes are classified into 'high-risk' and 'low-risk categories depending on their ability promote oncogenic changes within the cervical epithelium. HPV-16 and HPV-18 subtypes in particular are strongly associated with the development and persistence of pre-invasive cervical lesions, and subsequent development of invasive cervical cancer [207]. The viral proteins E6 and E7 are two of the main promoters of oncogenic change in cervical cells primarily though their interaction with p53 and pRb respectively, with HPV-16 E6 shown to have a higher affinity for p53 than other subtypes [31]. However, malignant transformation of cervical cells is a complex process involving more than interaction with p53 and pRb alone, and it is likely that the virus also possesses mechanisms for disrupting tight and adherens junctions and thus cell cohesion and polarity. It is possible that high risk HPV subtypes may also possess a more effective mechanism for disrupting cell cohesion and thus cervical lesions infected with a high risk HPV genotypes may display a different tight and adherens junction expression profile compared to lesions with a lower risk subtype.

4.2 Aims

- To investigate the prevalence of different HPV genotypes in the selected cohort of FFPE cervical tissue samples.
    - Extracting DNA from the samples and utilising a PCR based method to amplify any HPV DNA present in the samples.
    - HPV amplimers will then be sequenced and compared to known HPV sequences to discover the HPV genotype present in each sample.
- To investigate if there is a correlation between specific HPV genotypes and aberrant expression profiles of tight and adherens junction proteins, by comparing the detected genotypes to the results in chapter 3.

.

4.3 Optimisation of PCR

Optimization of PCR conditions for the amplification of the β-Globin gene (used as a control to assess DNA quality) and the HPV L1 gene using the PC03/04 and GP5+/6+ primer sets (table 4.1) respectively were performed using DNA extracted from cultured HPV-18+ HeLa cells. All PCR reactions were performed using the T Professional Basic thermocycler (Biometra). A series of PCR reactions were performed using different annealing temperatures and magnesium chloride concentrations to determine the conditions for optimum amplification of target genes. To aid in sequencing of the PCR products a M13 (uni -21) primer sequence was added to 5' end of the forward (GP5+) primer, producing a 168bp amplimer. This would allow sequencing of PCR products without having to send sample of primer and should aid in the successful sequencing of amplimers.

Table 4.1 Primers used for DNA quality assessment and HPV detection

Primer	Primer Sequence 5'-3'	Primer Concentration	Product Size
PC03	ACACAACTGTGTTCACTAGC	40nmol/µl	110bp
PC04	CAACTTCATCCACGTTCACC		
GP5+	TTTGTTACTGTGGTAGATACTAC	40nmol/µl	150bp
GP6+	GAAAAATAAACTGTAAATCAT		
GP5+ M13	TGTAAAACGACGGCCAGTTTTGTTACTGTG GTAGATACTAC	40nmol/µl	168bp

Primer sequences, primer concentration and product size for primers used in this chapter. GP5+/6+ sequence was retrieved from de Roda Husman et al. 1995 [208], PC03/04 sequence retrieved from de Roda Husman, Snijders, et al. 1995 [209]

4.3.1 PC03/04

The PC03/04 primer set amplifies a 110bp region of the β-Globin gene. Several PCR reactions were performed with this primer set using annealing temperatures from 58˚C to 60˚C and with $MgCl^{2+}$ concentration ranging from 1.5mM to 3.5mM. It was found that annealing temperature of 60°C and a magnesium concentration of 1.5mM $MgCl^{2+}$ was optimal and gave the strongest amplimer (Fig 4.1). DNA extracted from HeLa cells was used as the template for this optimisation reaction. Negative controls for optimisation reactions used H_2O instead of template DNA.

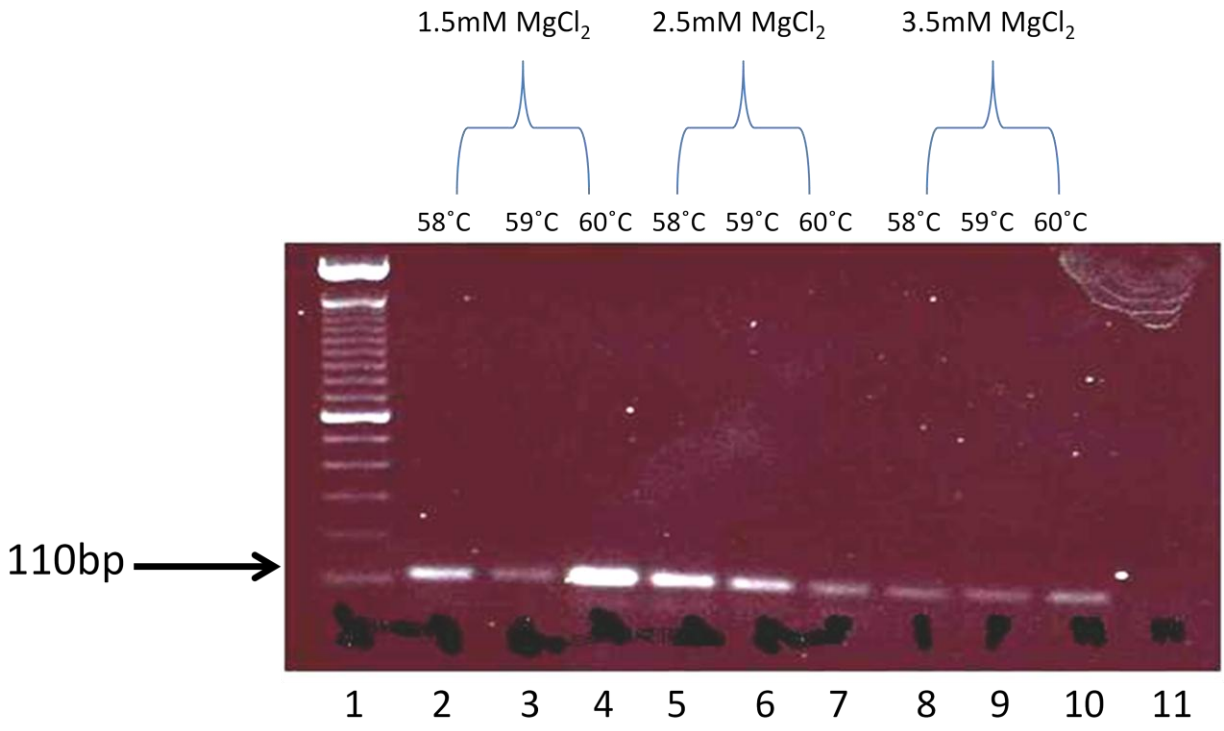

Figure 4.1 Optimisation of annealing temperature and $MgCl^{2+}$ concentration for PC03/04 primer set.

A range of temperatures from 58˚C to 60˚C and $MgCl^{2+}$ concentrations were examined with 60˚C and a $MgCl^{2+}$ concentration of 1.5mM determined to be optimum

4.3.2 GP5+/6+

HPV DNA was detected in cervical tissue samples using the GP5+/6+ primer set. This primer set amplifies a section of the L1 gene, producing a 150bp amplimer. Optimisation of this primer set was performed using magnesium chloride concentrations of 0 to 3.5mM (at 48°C) (Fig 4.2) and annealing temperature ranges of 48˚C to 55˚C (using 2.5mM $MgCl_2$) (Fig 4.3). It was found that an annealing temperature of 48°C and $MgCl^{2+}$ concentration of 2.5mM were optimum. DNA extracted from HeLa cells was used as the template for this optimisation reaction. Negative controls for optimisation reactions used H_2O instead of template DNA.

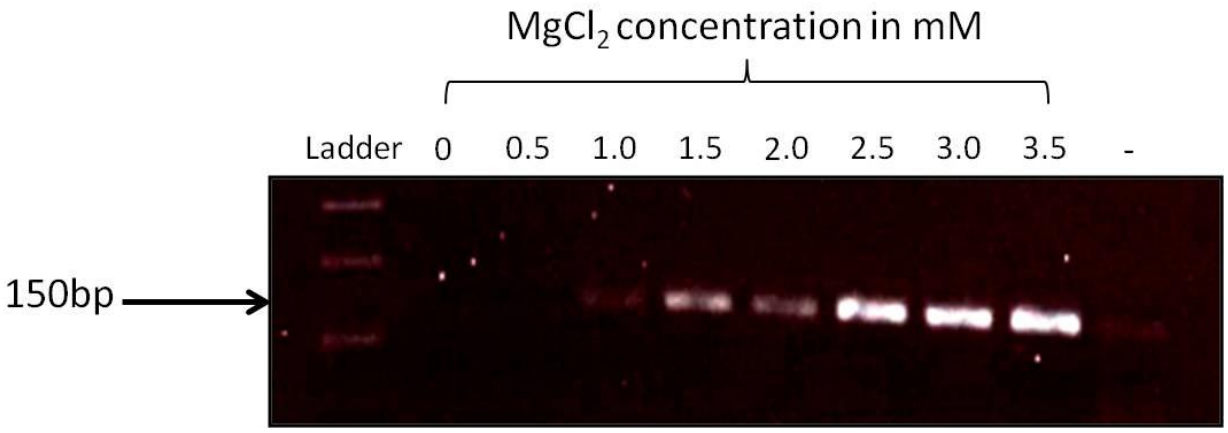

Figure 4.2 Optimisation of $MgCl^{2+}$ concentration for GP5+/6+ primer set.

Optimisation using a range of 0 to 3.5mM $MgCl^{2+}$ with 2.5mM determined to be the optimum concentration for this primer set.

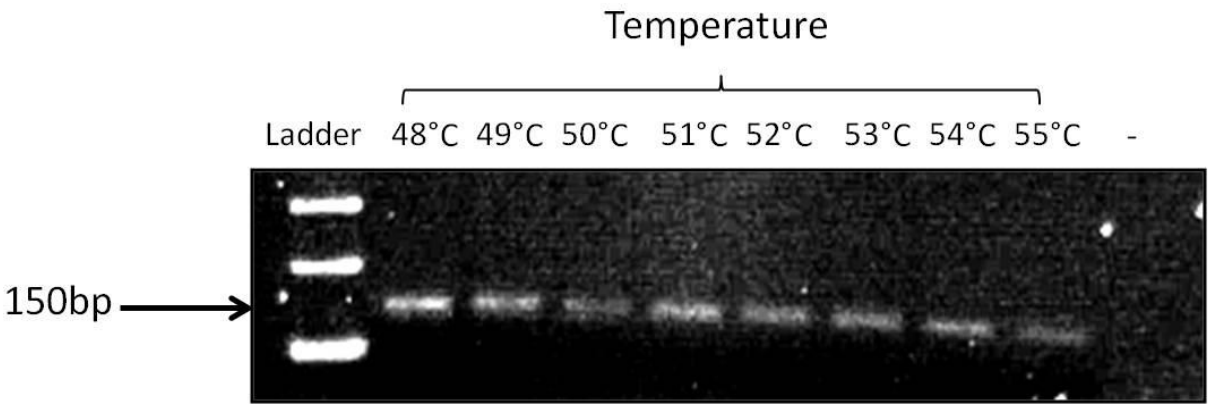

Figure 4.3 Optimisation of annealing temperature for GP5+/6+ primer set.

Optimisation of annealing temperature for GP5+/6+ primer set was performed using a temperature range of 48˚C to 55˚C. An annealing temperature of 48˚C was determined to be optimum.

4.4 Extraction of DNA from formalin fixed paraffin embedded cervical tissue.

From the 160 cases examined using the H&E stain DNA was extracted from 101 samples. During the sectioning of cervical tissue samples for DNA extraction the blade was changed after each sample and muscle tissue block was sectioned after every 10 cervical sections. Muscle tissue should not contain HPV DNA, as HPV is epitheliotropic [210] thus DNA extracted from muscle tissue ensured that no HPV DNA contamination was occurring during the DNA extraction process (Fig 4.4). With each reaction a positive control was carried out using DNA extracted from the HPV 18 positive cell line HeLa. A negative control reaction with water in place of template DNA was also included with each batch.

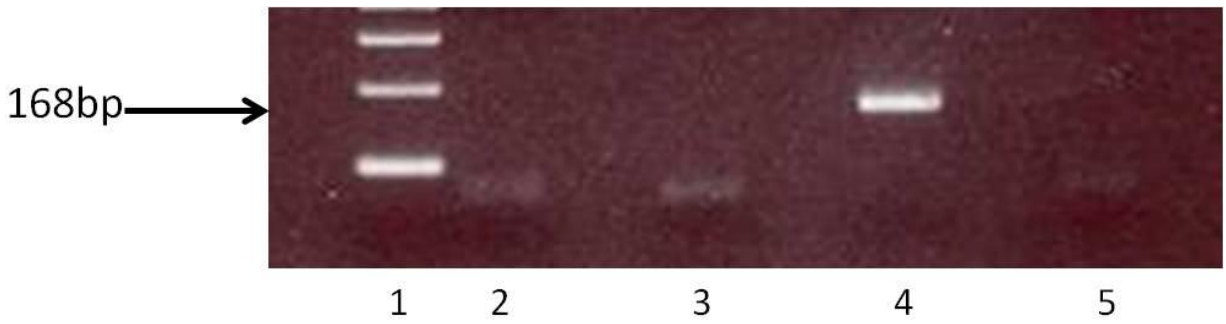

Figure 4.4 PCR amplification using GP5+/6+ primers on negative controls

Lane 1: 100bp ladder, Lane2: Muscle DNA 1, Lane 3: Muscle DNA 2, Lane 4: HeLa DNA (positive control), Lane 5: Negative Control (H_2O instead of template DNA)

In total DNA was extracted from 101 cervical samples. The presence of amplifiable DNA was detected using the PC03/04 primers, of which 85/101 (85%) samples were positive (Figure 4.5), while in the remaining 16 samples DNA of sufficient quality could not be extracted. Of the 85 samples in which amplifiable DNA was detected, HPV DNA was detected in 60 of these samples using the GP5+/6+ primer set (figure 4.6), while in the remaining 25 samples either no GP5+/6+ PCR product was detected, or the product was not of sufficient quality for sequencing. The HPV-genotypes detected in the 60 GP5+/6+ positive samples can be seen in table 4.3 and figure 4.9.

In N.E.M cervical samples DNA was extracted from 9 samples of which 8/9 samples produced amplifiable DNA. HPV DNA was detected in 5 of these samples (63%) while in 3 of the samples no HPV DNA could be detected. In 22/28 LSIL samples, DNA of sufficient quality for PCR was extracted, with HPV DNA detected in 12 of these 22 samples (55%). For HSIL samples DNA of sufficient quality for PCR was extracted from 45 of 54 samples. Of these 45 samples, HPV DNA was detected in 34/45 (73%) of samples. In all 10 SCC samples amplifiable DNA was extracted and HPV DNA was detected in 9/10 of these samples. For a summary of these results see (Table 4.2)

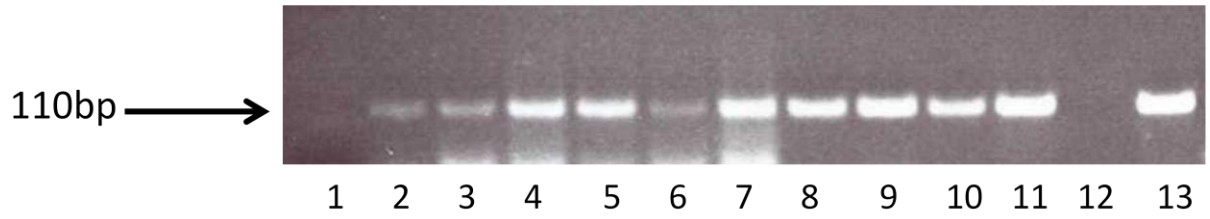

Figure 4.5 β-globin amplification of DNA extracted from cervical tissue

Lane 1: 100bp ladder, Lane 2-11: Cervical sample number 1-10, Lane 12: Negative Control, Lane 13: Positive Control

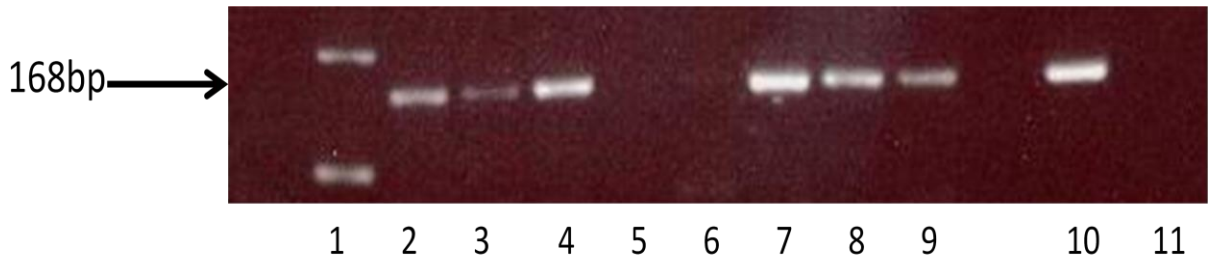

Figure 4.6 PCR detection of HPV DNA in cervical tissue samples using GP5+/6+ primer set.

Lane 1: 100bp ladder, Lane 2-9: Cervical sample number 1-8, Lane 10:, Positive Control, Lane 11: Negative Control.

Table 4.2 Detection of HPV DNA in cervical tissue samples using GP5+/6+ primers

Disease staus	No. of Samples tested	HPV+	HPV-	β-Globin Neg.
N.E.M	9	5 (63%)	3 (37%)	1
LSIL	28	12(55%)	10 (45%)	6
HSIL	54	34 (76%)	11 (24%)	9
SCC	10	9 (90%)	1 (10%)	0
Total	101	60 (71%)	25 (29%)	16

Summary of the results from PCR detection of HPV DNA in cervical tissues. SCC samples had the highest % positivity for HPV DNA.

N.E.M = No evidence of malignancy, LSIL = Low grade squamous intraepithelial lesion, HSIL = High grade squamous epithelial lesion, SCC = Squamous cell carcinoma**.**

4.5 HPV genotyping

Sequencing was performed by Eurofins DNA MWG Operon, Ebersberg, Germany. After PCR reactions were performed the products were purified by spin column, sequenced, and an electropherogram was produced (Figure 4.7). The electropherogram shows the absorbance peak of each nucleotide in the DNA strand and thus sequence of the strand. The sequenced PCR products were then matched for sequence homology with known L1 sequences of specific HPV genotypes using the Basic Local Alignment Search Tool (BLAST) (Figure 4.8). 60 samples were successfully sequenced, with HPV-16 the most common genotype detected (Figure 4.9)

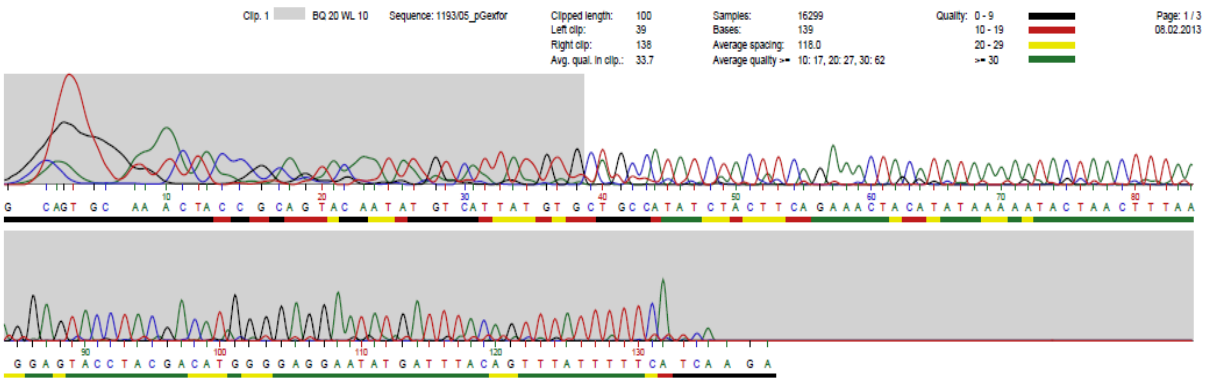

Figure 4.7 Example of an electropherogram produced from a GP5+/6+ amplimer.

Each nucleotide is tagged with a different fluorescent dye and detected simultaneously by a laser, allowing determination of base pair sequence in the DNA fragment.

Human papillomavirus type 16 strain ARG 1217-L1 L1 protein (L1) gene, partial cds

Sequence ID: gb|KC291277.1| **Length:** 396 **Number of Matches:** 1

Range 1: 53 to 146 GenBank Graphics ▼ Next Match ▲ Previous Match

Score	Expect	Identities	Gaps	Strand
174 bits(94)	9e-41	94/94(100%)	0/94(0%)	Plus/Plus

```
Query  1    CTGCCATATCTACTTCAGAAACTACATATAAAAATACTAACTTTAAGGAGTACCTACGAC  60
            ||||||||||||||||||||||||||||||||||||||||||||||||||||||||||||
Sbjct  53   CTGCCATATCTACTTCAGAAACTACATATAAAAATACTAACTTTAAGGAGTACCTACGAC  112

Query  61   ATGGGGAGGAATATGATTTACAGTTTATTTTTCA  94
            |||||||||||||||||||||||||||||||||
Sbjct  113  ATGGGGAGGAATATGATTTACAGTTTATTTTTCA  146
```

Figure 4.8 Example of results from BLAST analysis of sequenced HPV amplimers, showing level of sequence homology with known HPV sequences.

BLAST is an algorithm that allows comparison of an unknown DNA sequence with database of published sequences. In this case the query sequence matched published sequences from the HPV-16 L1 gene, indicating that the original sample contained HPV-16 DNA.

HPV DNA was successfully detected and genotyped in a total of 60 cervical tissue samples. HPV-16 was the most common genotype detected, with a total of 44/60 (73.3%) of successfully sequenced samples being HPV-16 positive. HPV-18 was the second most common genotype detected, with 11/60 (18.3%) of samples being HPV-18 positive. In total, 4 other HPV-

strains were detected with HPV-33 being present in 2/60 (3.3%) and HPV-6, HPV-58 and HPV-67 each detected in 1/60 (1.7%) of cases. HPV-16 and HPV-18 together were detected in 91.6% of overall cases and both genotypes were detected in cases of NEM and across all grades of neoplasia. Both HPV-33 genotypes detected were identified in HSIL lesions, as well as the only detected HPV-58 genotype. The low risk, HPV-6 genotype, was identified in a sample containing a LSIL lesion, as was the high risk HPV-67 genotype (Table 4.3)

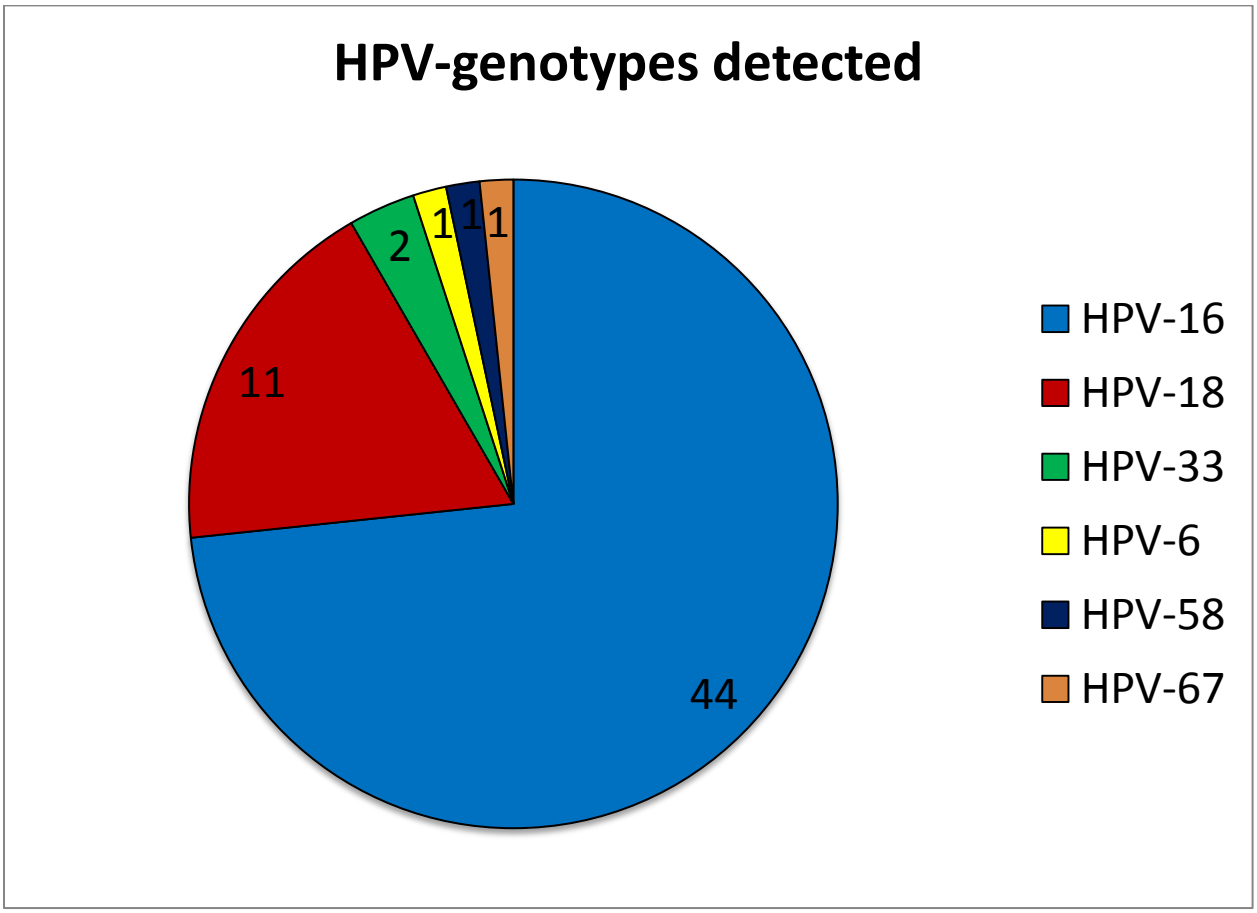

Figure 4.9 Pie chart displaying the prevalence of different HPV genotypes detected

HPV-16 was the most prevalent subtype detected with a 44 cervical samples testing positive for this genotype. HPV-18 DNA second most prevalent subtype, with 11 samples testing positive. A small number of samples tested positive for other genotypes including 2 for HPV-33 and 1 each for HPV-6, HPV-58 and HPV-67.

Table 4.3 Number of different HPV genotypes detected and their overall distribution per pathological grade

Pathological Grade	HPV-6	HPV-16	HPV-18	HPV-33	HPV-58	HPV-67
N.E.M (n=5)		3	2			
LSIL (n=12)	1	9	1			1
HSIL (n=34)		24	7	2	1	
SCC (n=9)		8	1			
Total (n=60)	1 (1.7%)	44 (73.3%)	11 (18.3%)	2 (3.3%)	1 (1.7%)	1(1.7%)

HPV-16 and HPV-18 were most frequently observed genotypes in all disease grades and the only subtypes detected in N.E.M tissue and invasive cancer samples. In low grade lesions HPV-6, HPV-18 and HPV-67 subtypes were also detected. In high grade lesions, HPV-33 was detected in 2 samples and HPV-58 in 1 sample in addition to 24 HPV-16 and 7 HPV-18 samples. (N.E.M) = No evidence of malignancy (LSIL) = Low grade squamous epithelial lesion, (HSIL) = High grade squamous epithelial lesion, (SCC) = Squamous cell carcinoma

4.6 Biomarker expression per HPV-genotype

Of the 60 cervical samples that were successfully genotyped, 31 of these had cores present on the tissue microarrays that could be graded. HPV-16 and HPV-33 positive samples had on average low expression of E-cadherin along with moderate to high expression of N-cadherin, claudin-1, claudin-7, p120-catenin and SNAIL (table 4.4). HPV-18 positive samples displayed on average moderate expression of E-cadherin, weak expression of N-cadherin, claudin-1, claudin-7 and SNAIL and high expression of p120-catenin. HPV-6 and HPV-67 positive samples both displayed high E-cadherin expression, moderate N-cadherin expression, weak claudin-1 expression and an absence of p120 catenin expression (table 4.4).

Table 4.4 Comparison of biomarker expression per HPV genotype

Genotype (number of samples, lesion grade)	**ECAD**	**NCAD**	**CLDN-1**	**CLDN-7**	**p120**	**SNAIL**
HPV-6 (1 LSIL)	3	2	1	3	0	N/A
HPV-16 (4 LSIL, 10 HSIL, 7 SCC)	0.824	2.316	2.425	1.75	2.526	1.7
HPV-18 (1 NEM, 4 HSIL, 1 SCC)	1.583	0.8666	1.3	1.1	2.6	0.7666
HPV-33 (2 HSIL)	0.5	2.5	2.5	1.5	3	1.5
HPV-67 (1 LSIL)	3	2	1	0	0	0

Mean IHC staining intensity for each biomarker per HPV genotype. Staining intensity was graded from 0-3 with 0 indicating no staining and 3 indicating strong staining intensity. HPV-16 and HPV-33 samples displayed on average the lowest expression of E-cadherin and highest expression of N-cadherin, claudin-1 and SNAIL compared to other HPV subtypes. HPV-6 and HPV-67 subtypes displayed the strongest E-cadherin expression and weakest claudin-1 and p120-catenin expression compared to other HPV subtypes.

4.7 Summary & Key Findings

DNA was extracted from the cohort of cervical tissue samples and the presence of HPV DNA in the samples was assessed using a PCR based method. A modified GP5+/6+ primer set producing an amplimer of 168bp was used, with the PC03/04 β-globin primer set used to assess the quality of the extracted DNA. For any samples that successfully produced an amplimer using the GP5+/6+set, this amplimer was sequenced and compared to known HPV sequences to determine the HPV genotype present in the sample.

- HPV DNA was detected in 60/101 (59%) of the cervical tissue samples
    - In 25/101 (25%) samples HPV DNA could not be detected, while in the remaining 16 samples (16%) no amplifiable DNA could be detected.
- The highest detection rate of HPV was in squamous cell carcinoma samples (90%), while the lowest detection rate was in LSIL samples, with HPV DNA detected in 12/22 (55%) of samples in which amplifiable DNA was detected.
- 6 different HPV genotypes were detected with HPV-16 being by far the most prevalent genotype, with 44/60 (73%) of samples containing HPV-16 DNA.

4.8 Discussion

This study aimed to examine the prevalence of HPV genotypes in the cohort of FFPE tissues used in the earlier study. A PCR based method using the GP5+/6+ consensus primer set was utilised in this study to detect HPV DNA in FFPE cervical tissue samples. Amplimers were sequenced and compared with published HPV sequenced using BLAST to assess the HPV genotype present in the sample. While this is a sensitive and reliable method for detecting HPV DNA, this method has some limitations. Infection with multiple HPV types is relatively common occurrence in normal cervical tissue and in cervical neoplasia with Huang et al., 2004 finding 28.9% of invasive cervical tumours co-infected with multiple HPV genotypes. Co-infection with multiple HPV types can have a significant effect on patient outcomes, with Munagala et al., 2009 finding that patients with multiple infections up to have a poorer response to treatment compared to patients with infected with a single HPV type. As the HPV detection method used in this study was unable to detect more than one HPV genotype in a sample, this study was unable to assess any relationship between HPV co-infection any expression of tight and adherens junction proteins. PCR systems using multiple primers such as PGMY09/11 and SPF-PCR are more robust in detecting multiple infections than systems using single consensus primers such as GP5+/6+. This may especially be true in cases of mixed infections where one type is present in a high viral load compared to the other genotype. Methods that use reverse line blot assays such as the commercial INNO-LiPA kit produced by Roche, instead of DNA sequencing are also more effective in determining the presence of multiple HPV genotypes in a single sample, however, for this study the cost of using such a kit was prohibitive.

One of the aims of this study was to assess if particular HPV genotypes are associated with a greater degree of aberrant AJ and TJ protein expression compared to other HPV gentoypes. This study was limited in its ability to compare and contrast the expression profile of AJ and TJ proteins across a large range of HPV genotypes, due to the predominance of HPV-16 and HPV-18 in the cohort of samples. In this study 73% of samples tested positive for HPV-16 and 18% tested positive for HPV-18. A small number or other HPV genotypes, such as HPV-6, HPV-33 and HPV-67 were detected although often only a single sample tested positive for these other genotypes, and overall only 9% of the sample tested positive for a non HPV-16 or HPV-18 genotype. With a small sample number of genotypes other than HPV-16 and -18 this study was limited in its ability to make meaningful or significant comparisons of AJ and TJ protein expression between different HPV genotypes. The high prevalence of HPV-16 and -18 in pre-cancerous and invasive cervical lesions has been well established with most studies identifying HPV-16 and -18 being responsible for around 70% of invasive cancers. This study detected and genotyped HPV from 60 cervical samples but higher number of samples would need to be analysed in order to have an adequate number of other HPV genotypes to offer a significant comparison between expression pattern of the different AJ and TJ proteins. This study was limited in the number of samples it could analyse due to ethical approval only granting access to retrospective cervical samples sent to the Rotunda hospital between 2005 and 2007.

5. The role of SNAIL in E-cadherin expression and investigation into the role of claudin-1 and claudin-7 on cervical cell tumourigenesis

5.1 Introduction

Changes in the expression of adherens and tight junction proteins are often observed in epithelial malignancies [116]. In chapter 3 of this study, an increase in expression of claudin-1, claudin-7 and SNAIL was observed in cases of cervical neoplasia. Claudin-1 and claudin-7 are both integral tight junction proteins and have both been implicated as having pro and anti tumourigenic properties depending on the tumour cell line [113], [124], [125], [211]. SNAIL is a zinc fingered transcriptional repressor protein and has been shown to be a potent repressor of E-cadherin expression when overexpressed in the epithelial MDCK cell line [212]. To the best of our knowledge, there is a lack of studies in the literature about the effect of claudin-1 and claudin-7 overexpression, or of the role SNAIL may play in the regulation E-cadherin expression, in cervical cell lines. In this chapter we will attempt to elucidate what role claudin-1, claudin-7 and SNAIL may play in cervical tumourigenesis.

5.2 Aims

- To determine the significance of the increased claudin-1, claudin-7 and snail expression observed in cervical neoplasia tissue samples in chapter 3 of this study.
- To elucidate the role these proteins may play in cervical tumourigenesis by performing a number of experiments in cervical cell lines.
    - To transfect two cervical cell lines that display high expression of SNAIL and no E-cadherin expression, HeLa and SiHa cells, with two siRNAs targeting SNAIL and the effect of SNAIL knockdown on E-cadherin expression would be examined.
    - To investigate the role of claudin-1 and claudin-7 overexpression by generating claudin-1 and claudin-7 overexpressing HeLa cell lines. The characteristics of these stable cell lines would then be assessed, in terms of cell proliferation/viability, permeability, invasion and migration.

5.3 siRNA mediated knockdown of SNAIL in HeLa cells

HeLa cells were transiently co-transfected two different siRNAs targeting SNAIL in order to establish knockdown of SNAIL expression in these cells. Two different siRNAs both targeting SNAIL were selected in order to maximise the level of gene knockdown. Endogenous expression of SNAIL in HeLa cells had previously been reported by Zhao et al., 2007 [213] and was confirmed by western blot before proceeding with siRNA experiments (data not shown) Cells were co-transfected with both siRNAs at concentrations of 100nM, 50nM, 20nM, 10nM, 5nM for 24 hours. A commercially purchased scrambled siRNA sequence (Ambion) that has no homology to any known mammalian gene was used as a negative control. The scrambled siRNA was validated by the manufacturer to ensure minimal non specific effects and to ensure that comparison of the gene-specific siRNA to the negative control gives a true picture of the effects of target-gene knockdown on gene expression and phenotype. No reduction of SNAIL protein expression was observed at all utilised siRNA concentrations, compared to the scrambled siRNA control (Figure 5.1). No detectable changes in cell morphology were observed at 24 hours post transfection, although cell viability was not assessed. The siRNAs used in this study were commercially purchased and were predesigned by the manufacturer, although not validated. One possibility for the lack of SNAIL knockdown was that siRNA sequences were not fully complementary to SNAIL mRNA sequences and therefore the mRNA was not efficiently targeted for degradation. The manufacturer offers several different siRNA variants that target SNAIL and offers to replace siRNAs that don't achieve significant knockdown with alternate siRNAs. To assess if the problem was with a lack of siRNA specificity or another factor, a similar

cervical cell line (SiHa) was transfected with the siRNA to see if knockdown could be achieved in this cell line.

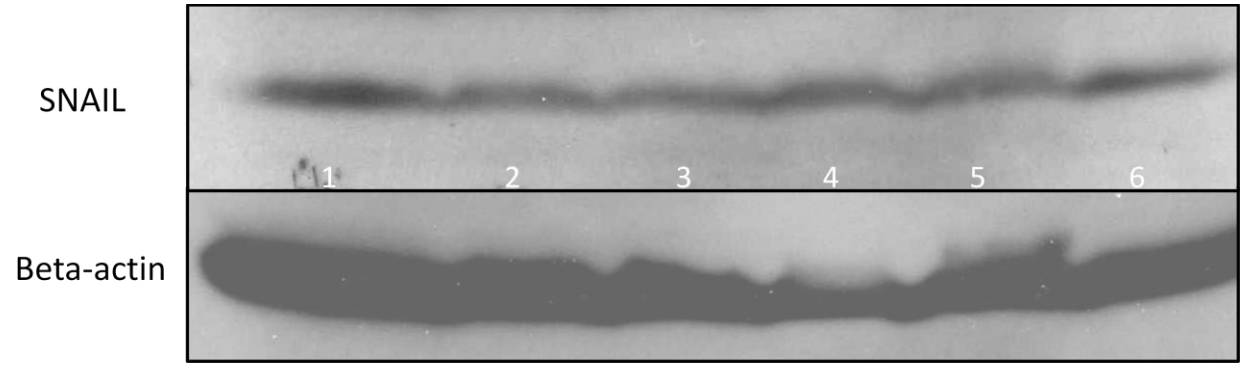

Figure 5.1 Western blot of HeLa cells transiently transfected with SNAIL siRNA

Lane 1: 100nM siRNA, Lane 2: 50nM siRNA, Lane 3: 25nM siRNA, Lane 4: 10nM siRNA, Lane 5: 5nM siRNA Lane 6: Scrambled siRNA

5.4 siRNA mediated knockdown of SNAIL in SiHa cells

After being unable to achieve significant knockdown of SNAIL expression in HeLa cells, another cervical cancer cell line, SiHa, was selected to evaluate the role SNAIL in the expression of E-cadherin. SiHa cells, like HeLa cells, do not express E-cadherin and display high SNAIL expression. Endogenous expression of SNAIL in SiHa cells was previously reported by Haaberg et al., 2008 [51] confirmed by western blot before proceeding with siRNA experiments (data not shown). SNAIL siRNAs were co-transfected at 100nM, 50nM, 5nM and also with a scrambled siRNA sequence as a negative control for 24 hours. No detectable changes in cell morphology were observed at 24 hours post transfection, although cell viability was not assessed. A reduction of SNAIL expression at the protein level was observed compared to the scrambled siRNA negative control, at all concentrations of siRNA (Figure 5.2).

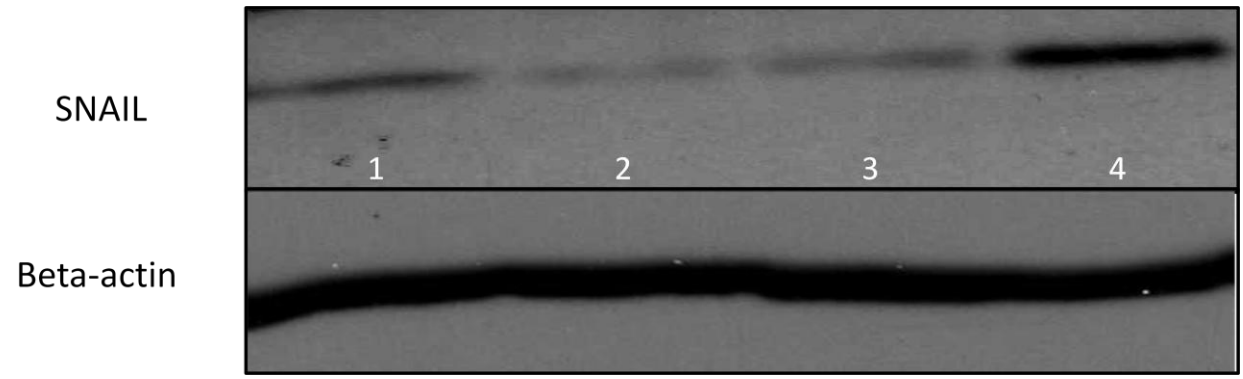

Figure 5.2 Western blot of SiHa cells transiently transfected with SNAIL siRNA.

Lane 1: 100nM siRNA, Lane 2: 50nm siRNA, Lane 3: 5nm siRNA, Lane 4: Scrambled siRNA

Although knockdown of SNAIL protein had already been confirmed by western blot, a preliminary real time PCR reaction was carried out on SiHa cDNA using SNAIL and GAPDH primers, to confirm knockdown of SNAIL mRNA. The CT value (cycle threshold) value is the cycle at which fluorescence achieves a certain threshold, and is inversely correlated to the amount of nucleic acid that was in the original sample. To account for any differences in overall cDNA concentration, the GAPDH housekeeping gene was used to normalise the SNAIL CT values and the relative expression was assessed using the $2^{-\Delta\Delta CT}$ method as described by Livak et al., 2001 [214]. An decrease in relative SNAIL expression was observed for all concentrations of siRNA , compared to the scrambled siRNA samples. The lowest observed relative expression was at the 100nM siRNA concentration, although both 50nM and 5nM concentrations were below the scrambled siRNA control (Figure 5.3).

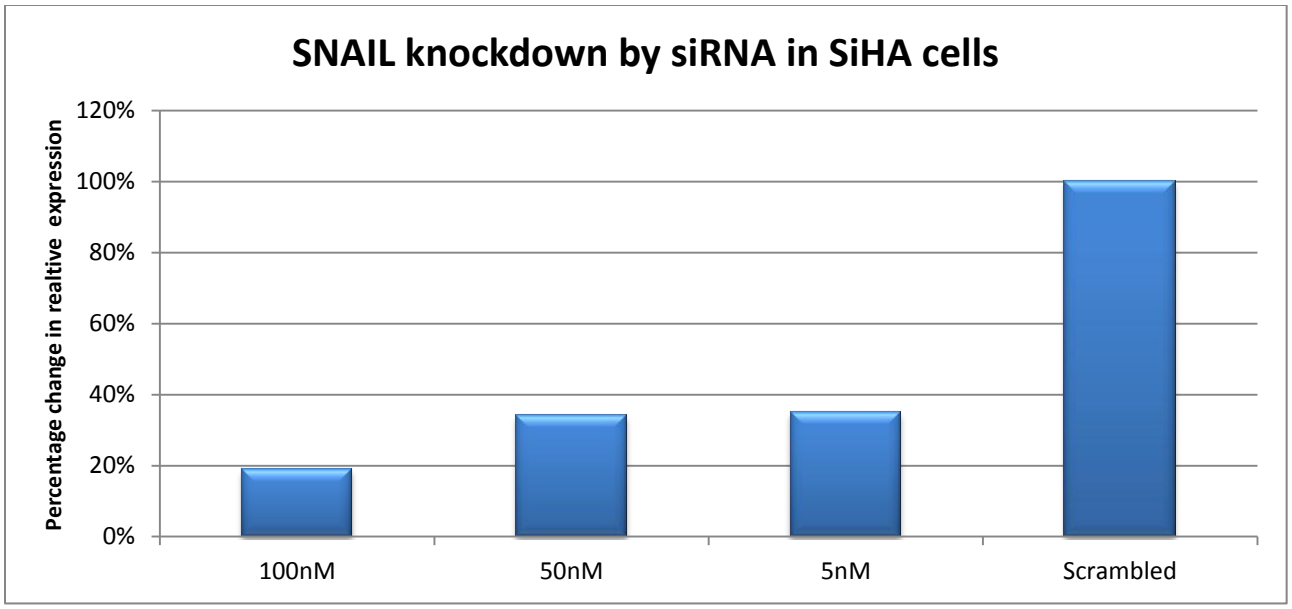

Figure 5.3 Bar chart of relative change in expression of SNAIL in SiHa cells transfected with different concentrations of siRNA. A reduction in relative SNAIL expression was observed at all concentration of siRNA compared to the scrambled siRNA control. The greatest reduction was observed at 100nm with just below 20% of relative expression observed.

5.5 Detection of E-cadherin in siRNA transfected SiHa

After determining that knockdown of SNAIL expression had been achieved at the mRNA and protein level, an investigation of the relationship between SNAIL and E-cadherin expression was performed. To assess if siRNA mediated knockdown of SNAIL affected E-cadherin protein expression, protein was extracted from transfected SiHa cells and a western blot was performed. As a positive control extracts from the CasKi cell line, that strongly expresses E-cadherin, were used.

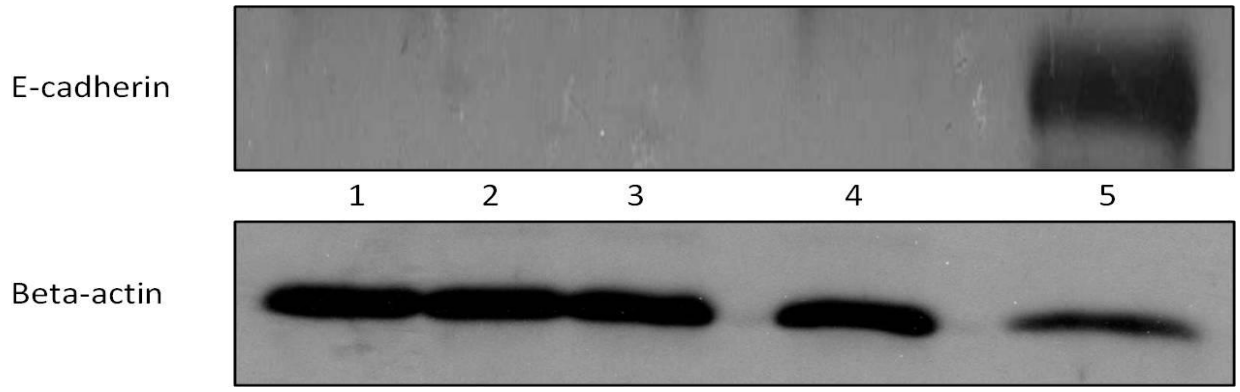

Figure 5.4 Western blot detection of E-cadherin protein in SNAIL siRNA transfected SiHa cells

Lane 1: 100nM SNAIL siRNA, Lane2: 50nM SNAIL siRNA, Lane3: 5nM SNAIL siRNA

Lane 4: Scrambled siRNA Lane 5: Positive Control (CasKi cell extracts)

No expression of E-cadherin was observed at any of the concentrations of transfected SNAIL siRNA or, as expected, in the scrambled siRNA negative control (Figure 5.4). CasKi cell extracts were used as a positive control for this experiment as they have high endogenous expression of E-cadherin. The lack of E-cadherin expression observed in SNAIL knockdown cells could be due to a number of reasons. It is possible that level of SNAIL knockdown achieved was not sufficient to nullify its effects in repressing E-cadherin expression. The highest concentration of siRNA used for transfection was 100nM, which is well above the range recommended by the manufacturer of 5-30nM. Another siRNA delivery method such as lentivirus particles may offer a greater level of SNAIL knockdown and perhaps have a greater effect on the level of E-cadherin expression. It is also possible that in SiHa cells there may be other factors, such as deletions in the E-cadherin gene itself that may negatively regulate E-cahderin and prevent its expression.

5.6 Transient transfection of HeLa cells with CLDN expression vectors.

An initial transient transfection of HeLa cells was carried out with the claudin-1 and claudin-7 expression vectors in order to establish whether claudin protein expression could be achieved in this cell line. Each vector contained a CMV promoter ahead of either a claudin-1 or claudin-7 ORF and a neomycin selection marker (Figure 5.7). Varying amounts of each plasmid were transfected, from 0.1µg to 2µg, to determine the optimum plasmid concentration.

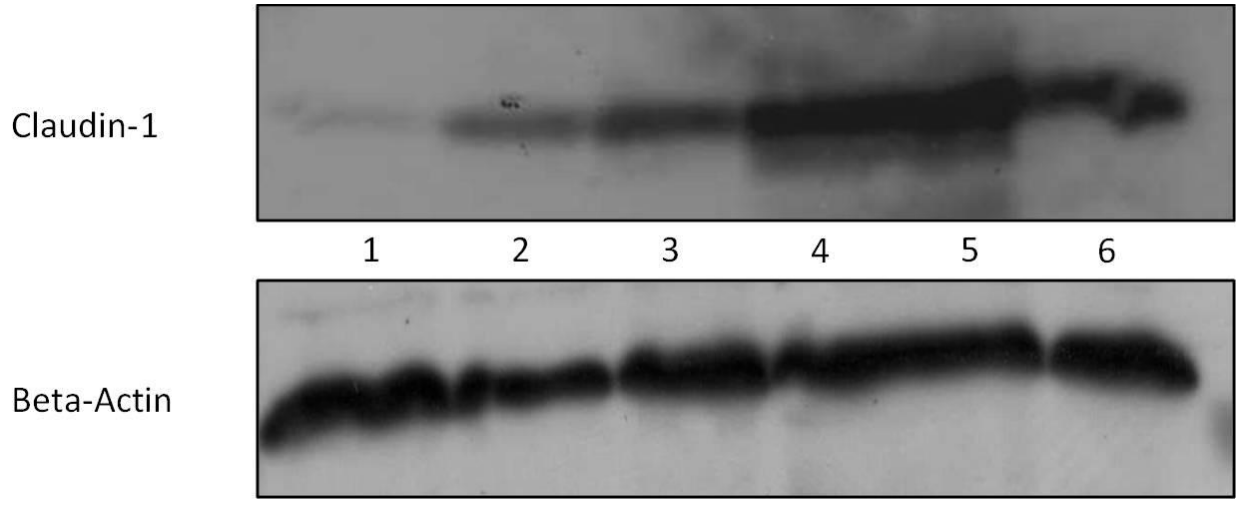

Figure 5.5 Western blot of HeLa cells transiently transfected with a range of Claudin-1 plasmid concentrations.

Lane 1: Untransfected HeLa, Lane 2: 0.1µg of plasmid, Lane 3: 0.25µg of plasmid, Lane 4: 0.5µg of plasmid, Lane 5: 1.0µg of plasmid, Lane 6: 2.0µg of plasmid.

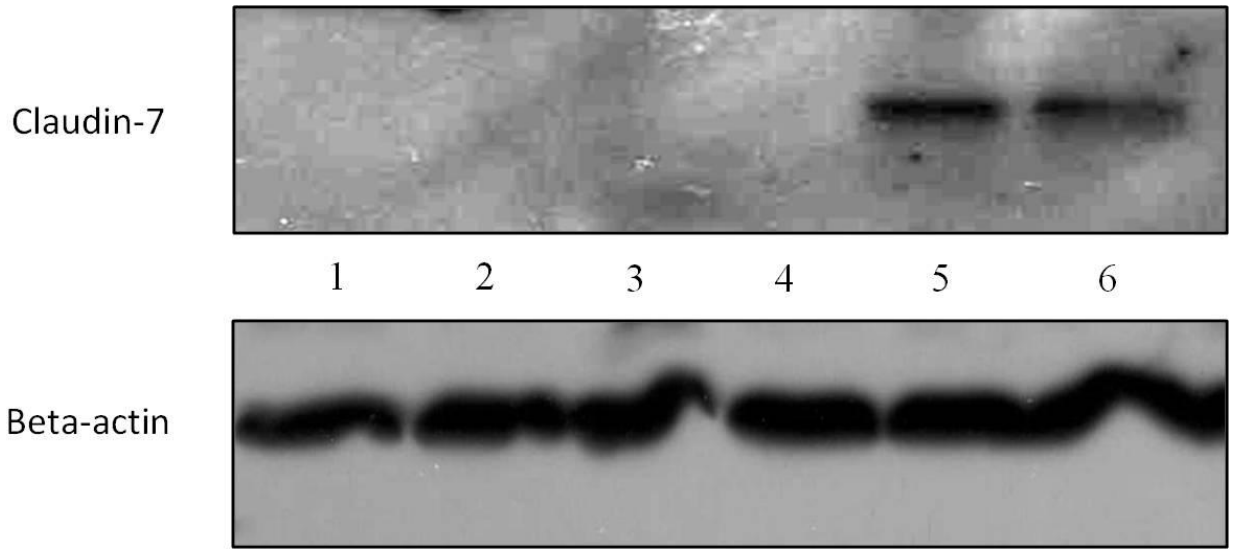

Figure 5.6 Western blot of HeLa cells transiently transfected with a range of Claudin-7 plasmid concentrations.

Lane 1: Untransfected HeLa, Lane 2: 0.1µg of plasmid, Lane 3: 0.25µg of plasmid, Lane 4: 0.5µg of plasmid, Lane 5: 1.0µg of plasmid, Lane 6: 2.0µg of plasmid.

HeLa cells transiently transfected with the Claudin-1 expression vector showed expression of Claudin-1 protein at all ranges of transfected plasmid, from (0.1µg to 2.0µg). Increased expression of Claudin-1 protein was observed with increasing plasmid concentration, with the highest expression observed with 0.5µg, 1.0µg and 2.0µg of plasmid (Figure 5.5). A very faint band was observed in the untransfected HeLa lane, likely as a result of an overflow of sample from an adjacent lane.

In HeLa cells transiently transfected with the claudin-7 expression vector, no expression of claudin-7 protein was observed in cells transfected with 0.1µg, 0.25µg, or 0.5µg of plasmid. Expression of claudin-7 protein was observed in HeLa cells transfected with 1.0µg and 2.0µg of

plasmid, with a similar level or protein expression observed for both plasmid concentrations (Figure 5.6).

5.7 PCR screening of claudin-1 stable clones

After transfection of HeLa cells with the claudin-1 expression vector, genticin selection was performed using G418 (Roche). Cells that survived genticin selection were cultured until isolated colonies of cells had formed. 50 colonies were picked, although only 42 successfully grew when subcultured, and DNA was extracted from each sample. To determine successful uptake of the expression vector and to ensure vector fidelity in each colony, a PCR was performed (figure 5.8) using primers listed in table 2.3. An outline of the area amplified by the claudin-1 primers within the expression vector can be seen in figure 5.7. For PCR reactions a sample of the expression vector was used as a positive control, and DNA extracted from untransfected HeLa was used as a negative control.

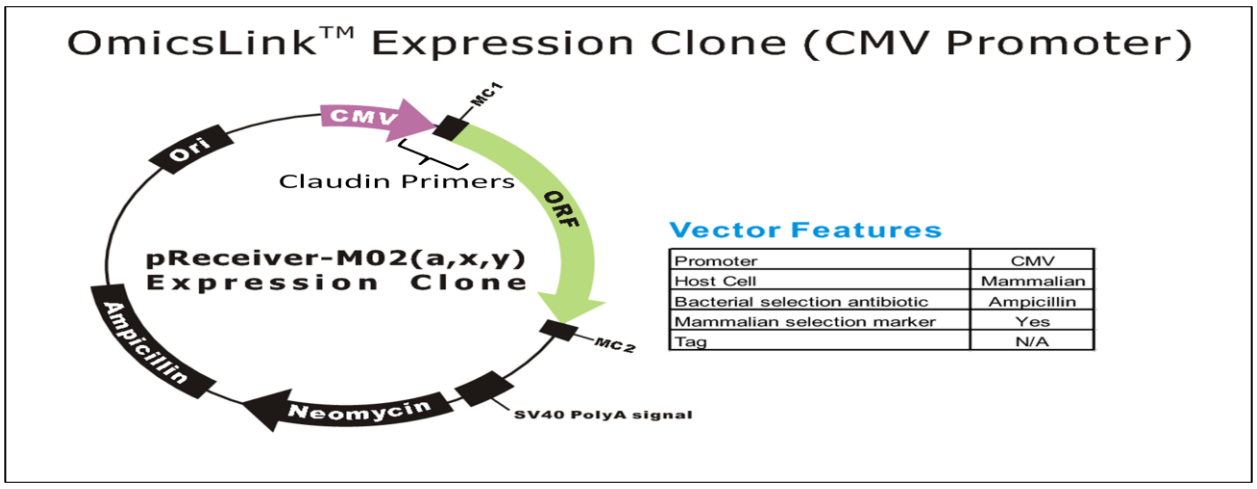

Figure 5.7 Outline of expression vector used for the production of stable cell lines.

Area of expression vector amplified by claudin primers is indicated, spanning from the CMV promoter to the claudin ORF.

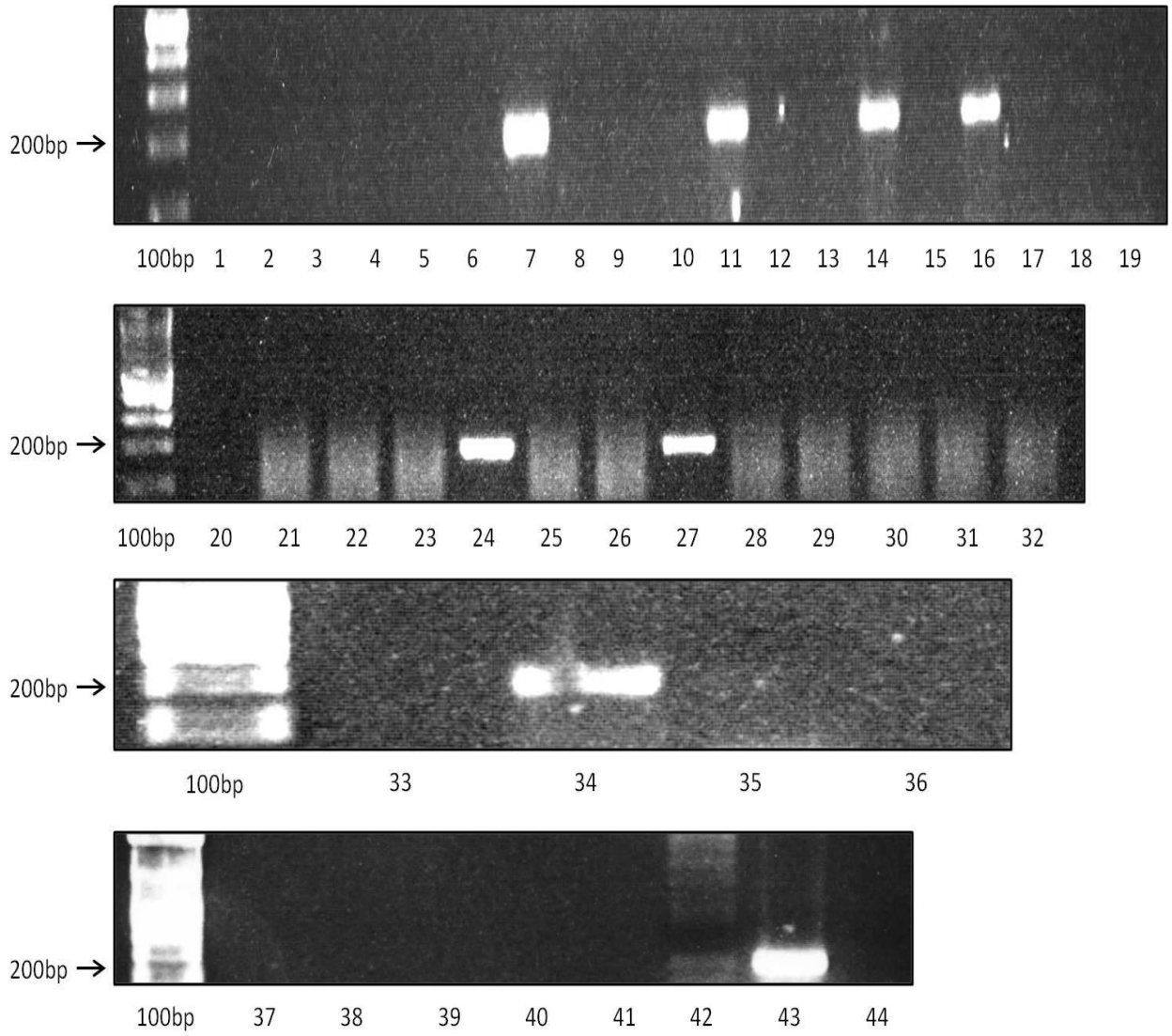

Figure 5.8 PCR screening of stably transfected claudin-1 colonies

100bp = 100 base pair DNA ladder, Lane 1-42: Colonies 1-42 respectively

Lane 43: Positive control (plasmid DNA) Lane 44: Negative control

After PCR screening the claudin-1 stable colonies, 8 different colonies were identified that successfully produced an amplimer : Colony#7, Colony#11, Colony#14, Colony#16, Colony#24, Colony#27, Colony#34, Colony#42 (figure 5.8), indicating that the expression vector had been successfully integrated and that the CMV-CLDN1 ORF area of the vector was intact. Amplimers were sequenced and compared to published CLDN1 ORF sequences using BLAST to ensure the area being amplified was homologous to the CLDN1 ORF (Figure 5.9). These colonies were then selected for western blotting analysis to assess if the claudin-1 was being expressed at the protein level. The overall length of the sequence analysed using BLAST was shorter than length of the amplicon as the sequencing method used 'clips' the sequence or automatically removes the low-quality sections at the start and end of the amplimer by using sequence quality scores.

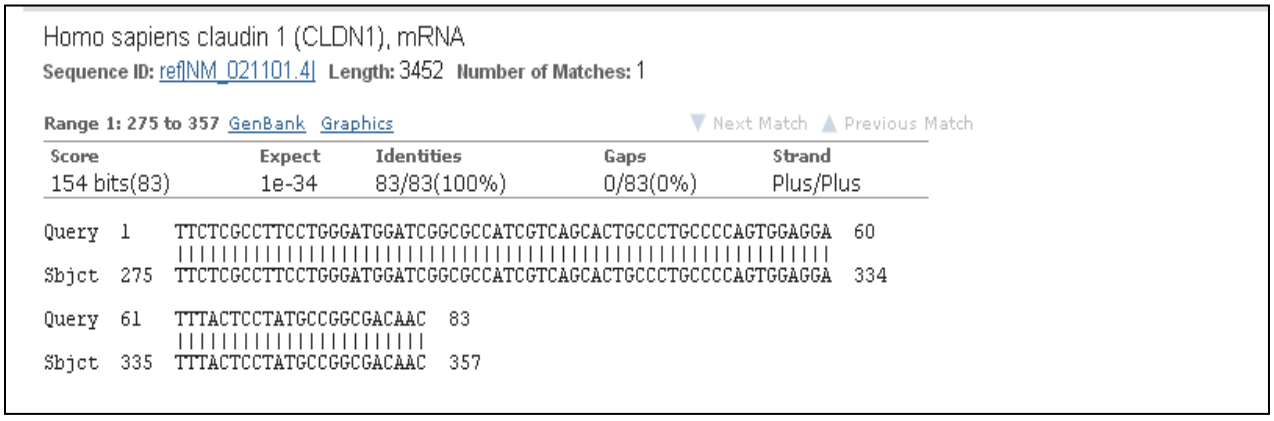
Homo sapiens claudin 1 (CLDN1), mRNA

Sequence ID: ref|NM_021101.4| **Length:** 3452 **Number of Matches:** 1

Range 1: 275 to 357 GenBank Graphics ▼ Next Match ▲ Previous Match

Score	Expect	Identities	Gaps	Strand
154 bits(83)	1e-34	83/83(100%)	0/83(0%)	Plus/Plus

```
Query  1    TTCTCGCCTTCCTGGGATGGATCGGCGCCATCGTCAGCACTGCCCTGCCCCAGTGGAGGA  60
            ||||||||||||||||||||||||||||||||||||||||||||||||||||||||||||
Sbjct  275  TTCTCGCCTTCCTGGGATGGATCGGCGCCATCGTCAGCACTGCCCTGCCCCAGTGGAGGA  334

Query  61   TTTACTCCTATGCCGGCGACAAC  83
            |||||||||||||||||||||||
Sbjct  335  TTTACTCCTATGCCGGCGACAAC  357
```

Figure 5.9 BLAST analysis of amplimer from claudin-1 stable colony showing sequence homology with published claudin-1 sequences

5.8 Western blot analysis of claudin-1 stable colonies

Following, the identification of colonies that had successful uptake of the expression vector, an assessment of the level of claudin-1 protein expression in each colony was carried out using western blotting.

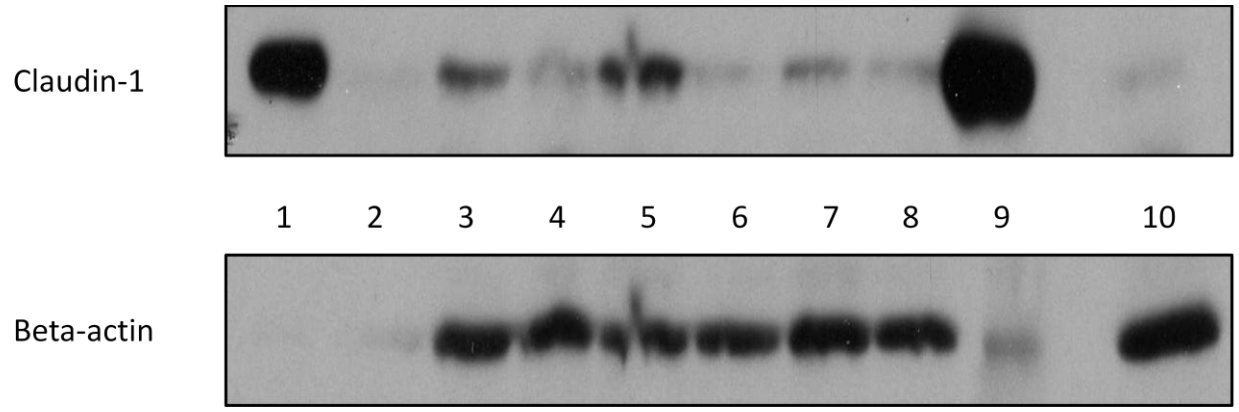

Figure 5.10 Western blot detection of claudin-1 in stable colonies

Lane 1: Colony #7 Lane 2: Colony#11 Lane3: Colony #14 Lane4: Colony#16

Lane 5: Colony #24 Lane 6: Colony#27 Lane7: Colony# 34 Lane8: Colony #42

Lane 9: Positive Control Lane 10: Untransfected HeLa

Western blot analysis showed varying levels claudin-1 expression in different colonies (figure 5.10). Colony #11 and #27 displayed very low expression, while moderate expression was observed in colonies #24 and #14. The highest observed expression was in colony#7 and therefore this colony was selected for use in further experiments and designated as C1-HeLa. Beta-actin bands in lanes 1 and 2 were slightly weak, likely as result of the chemluminescent substrate draining off the edge of the membrane. Equal loading of proteins was ensured however, by using a Bradford assay to match protein concentration before loading.

5.9 PCR screening of claudin-7 stable clones

After transfection of HeLa cells with the claudin-7 expression vector, genticin selection was performed using G418. Cells that survived genticin selection were cultured until isolated colonies of cells had formed. 50 colonies were selected, however only 42 colonies continued to grow when subcultured, and DNA was extracted from each of these colonies. To determine successful uptake of the expression vector and to ensure the vector fidelity in each colony, a PCR was performed (figure 5.11) using primers listed in table 2.3.

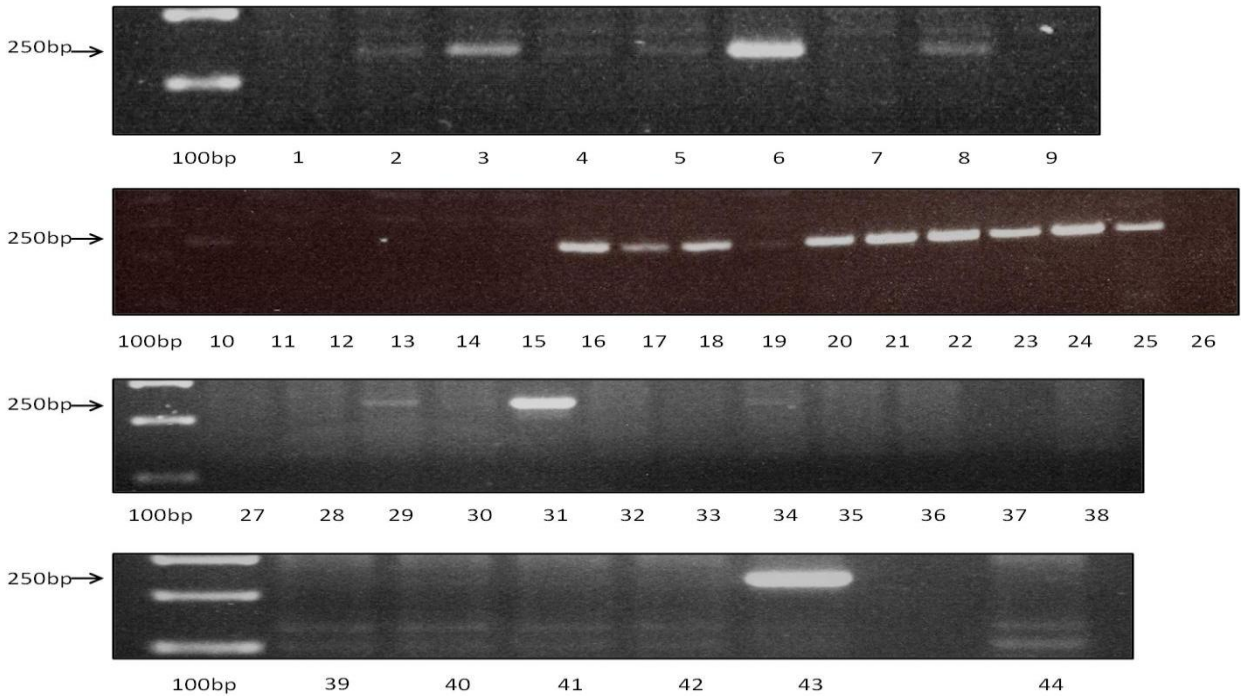

Figure 5.11 PCR screening of stably transfection claudin-7 colonies

100bp = 100 base pair DNA ladder

Lane1-42: Colonies 1-42 respectively

Lane 43: Positive control (plasmid DNA)

Lane 44: Negative control

After PCR screening the claudin-7 stable colonies, 8 different colonies were identified that successfully produced an amplimer : Colony#6, Colony#16, Colony#18, Colony#20, Colony#21, , Colony#23, Colony#24, Colony #31, indicating that the expression vector had been successfully integrated and that the CMV-claudin-7 ORF area of the vector was intact. Amplimers were sequenced and compared to published claudin-7 ORF sequences using BLAST to ensure the area being amplified was homologous to the claudin-7 ORF (figure 5.12). These colonies were then selected for western blotting analysis, to assess if the claudin-7 was being expressed at the protein level. The overall length of the sequence analysed using BLAST was shorter than length of the amplicon as the sequencing method used 'clips' the sequence or automatically removes the low-quality sections at the start and end of the amplimer by using sequence quality scores.

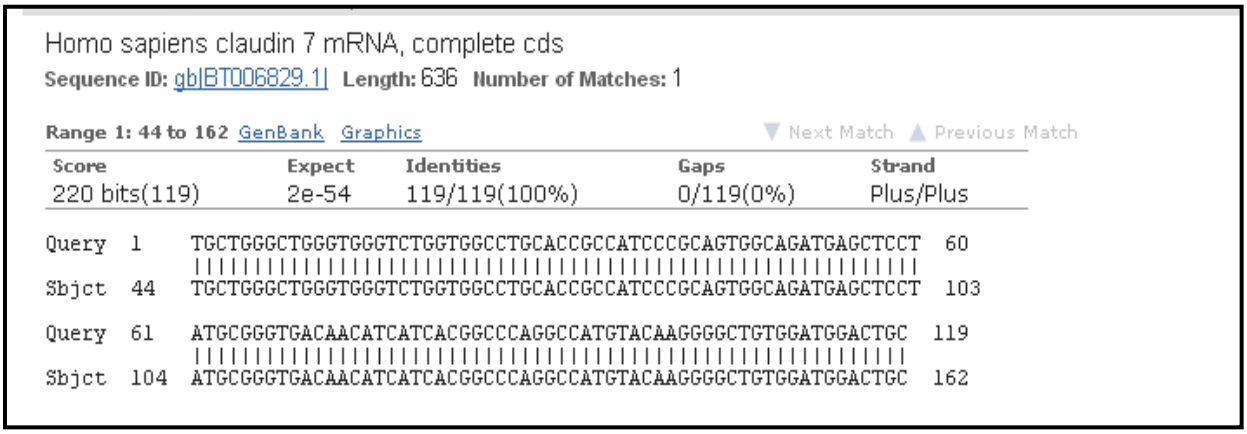

Figure 5.12 BLAST analysis of amplimer from claudin-7 stable colony showing sequence homology with published claudin-7 sequences.

5.10 Western blot analysis of claudin-7 stable colonies

Following, the identification of colonies that had successful uptake of the expression vector, an assessment of the level of claudin-7 protein expression in each colony was carried out using western blotting.

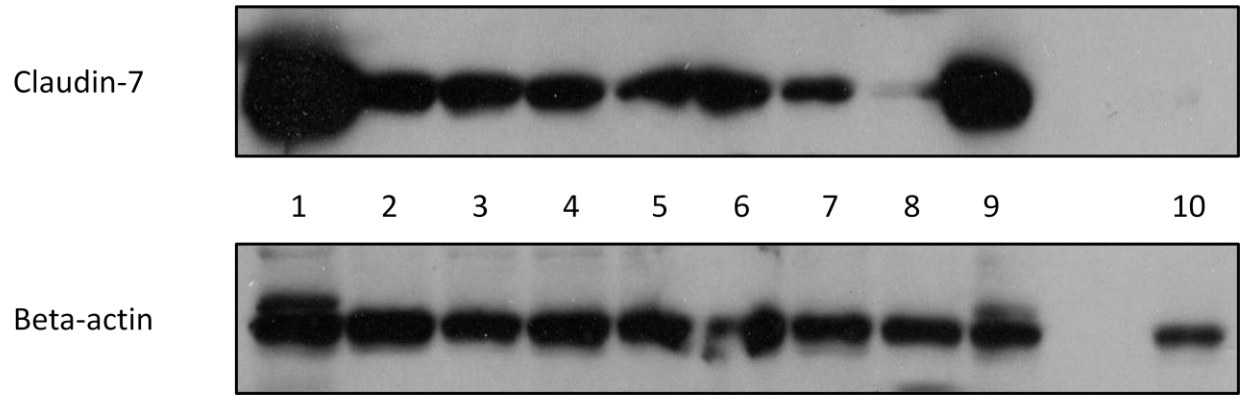

Figure 5.13 Western blot detection of claudin-1 in stable colonies

Lane 1: Colony #6 Lane 2: Colony#16 Lane3: Colony #18 Lane4: Colony#20

Lane 5: Colony #21 Lane 6: Colony#23 Lane7: Colony# 24 Lane8: Colony #31

Lane 9: Positive Control Lane 10: Untransfected HeLa

Western blot analysis showed varying levels claudin-7 expression in different colonies (figure 5.13). Colony #31 displayed very low expression, while moderate expression was observed in colonies #16, #18, #20, #21, #23, and #24. The highest observed expression was in colony#6 and therefore this colony was selected for use in further experiments and designated as C7-HeLa.

5.11 Assessment of the effect claudin-1 and claudin-7 expression on cell viability

The effect of claudin-1 and claudin-7 expression on the viability and proliferation of C1-HeLa and C7-HeLa stable cell lines was assessed using the MTT assay. Non-claudin transfected HeLa (Null HeLa) was used as a negative control to assess the endogenous level of viability in HeLa cells and to allow comparison with claudin transfected cell lines. Results indicate that Claudin-1 and Claudin-7 expression had no effect on the proliferative ability of Hela cells. Claudin-1 and Claudin-7 transfected cells showed a high level of proliferation at the 48hrs and 72 hrs timepoints of the assay, with absorbance values roughly doubling at each timepoint. The assay results from Claudin-1 and Claudin-7 stable cells lines closely matched those of non claudin expressing HeLa cells (Figure 5.14) indicating that Claudin-1 or 7 expression did not affect the viability or proliferation of the cells. In addition, no changes in cell morphology were observed. All experiments were carried out in triplicate on three separate occasions and one way ANOVA analysis indicated results were not statistically significant.

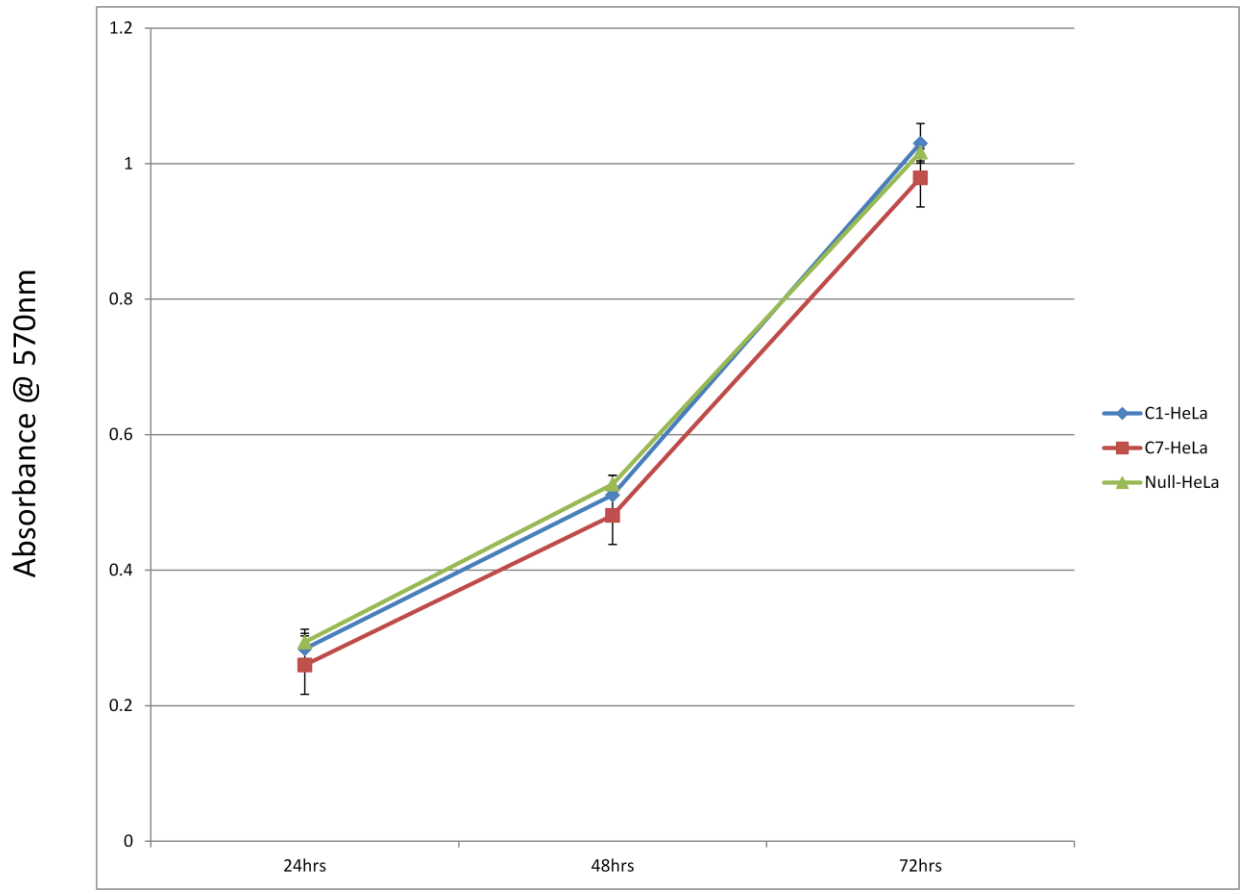

Figure 5.14 Graph showing proliferation of C1-Hela, C7-Hela and Hela-Null cell lines using MTT assay at 24hr, 48hr and 72 hr time points. Error bars show + or – one standard deviation.

5.12 The effect claudin-1 and claudin-7 expression on cell invasion

The effect of claudin-1 and claudin-7 expression on the invasive ability of HeLa cells was assessed using the C1-HeLa and C7-HeLa stable cell lines. The ability of cells to digest extracellular matrix components and permeate through a basement membrane was assessed using a boyden chamber assay. Non-claudin transfected HeLa (Null HeLa) was used as a negative control to assess the endogenous level of invasive ability in HeLa cells and to allow comparison with claudin transfected cell lines. C1-HeLa cells showed a very low invasive ability as evidenced by the low absorbance reading observed upon staining and lysis of invaded cells (Figure 5.15A). This result correlated with the observation of very few cells on the membrane when observed under a light microscope (Figure 5.15B). C7-Hela displayed a similar invasive ability to C1-Hela cells, with both a low number invaded cells observed when the membrane was observed under a light microscope (Figure 5.15C) and low absorbance reading observed when invaded cells stained and lysed (Figure 5.15A) Null-Hela, showed slightly higher invasive ability compared to C1-Hela and C7-Hela although overall the level of invasion was still very low (Figure 5.15A, 5.15D). A one way ANOVA test indicated results were not significant with a p value >0.05.

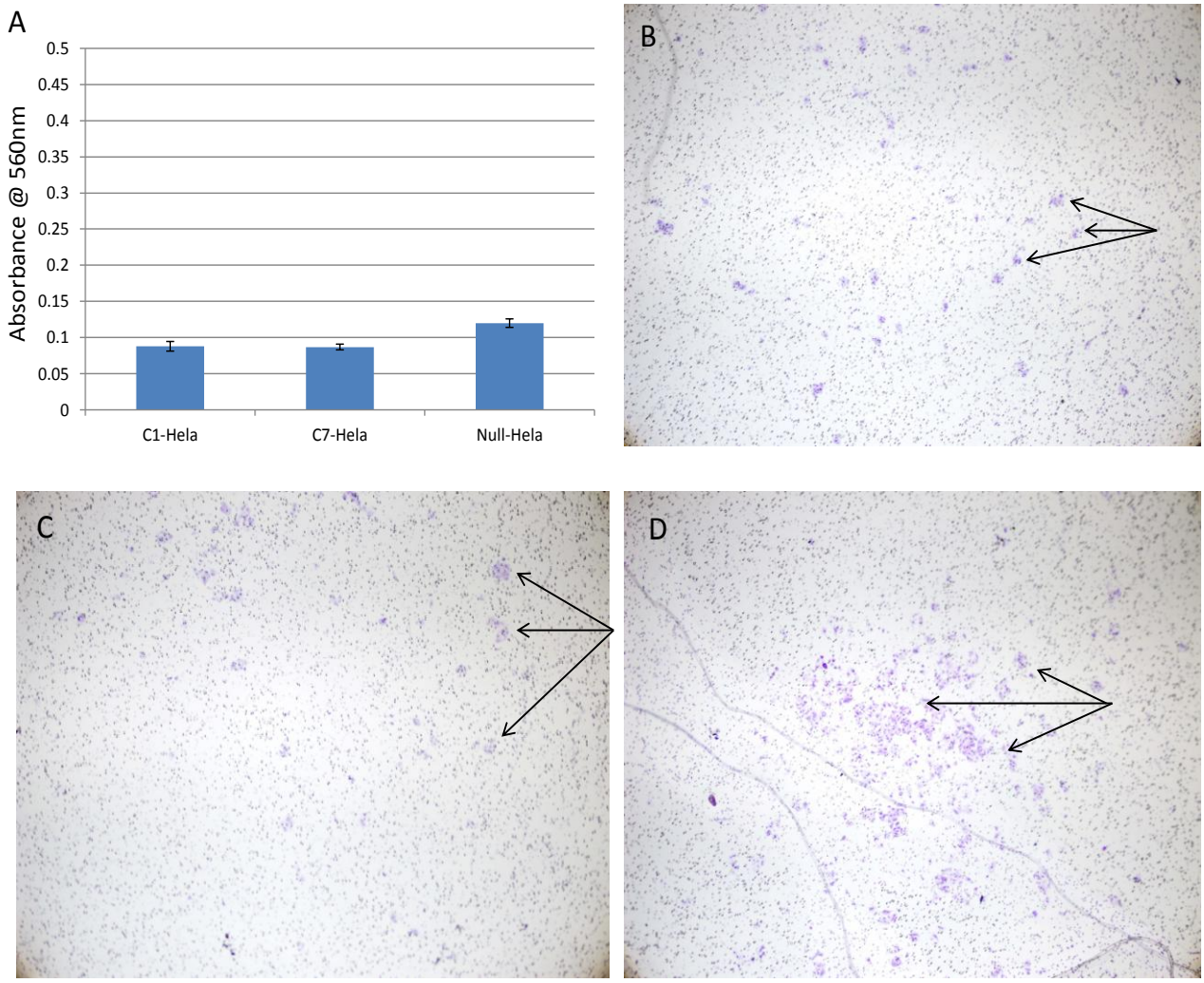

Figure 5.15 Cell invasion assay results for claudin-1 and claudin-7 stable cell lines

(**A)** Graph showing quantification of invaded Claudin-1, Claudin-7 transfected and untransfected Hela cells at 560nm following staining and extraction, error bars indicate + or – one standard deviation (**B)** Brightfield image of invaded claudin-1 transfected (**C)** claudin-7 transfected and (**D)** null-HeLa x40 magnification (arrows indicate invasive cells)

5.13 Effect of claudin-1 and claudin-7 expression on permeability

The effect of claudin-1 and claudin-7 expression on the permeability of HeLa cells was assessed using the C1-HeLa and C7-HeLa stable cell lines. Non-claudin transfected HeLa (Null HeLa) was used as a negative control to assess the endogenous level transepithlial electrical resistance in HeLa cells and to allow comparison with claudin transfected cell lines. To assess the permeability of stable cell lines, monolayers were cultured on transwell plates and the transepithelial electrical resistance was measured. Claudin-1 transfected cells displayed increased TEER values compared with non-transfected HeLa cells, with an average resistance of 27.55 Ω per cm^2 compared to 12.89 Ω per cm^2 for untransfected HeLa cells. Claudin-7 transfected cells had an average resistance of 28.26 Ω per cm^2 which is significant increase compared to the resistance of claudin null HeLa (Figure 5.16) and comparable to value observed for Claudin-1 transfected cells (Figure5.16). Results were analysed using a one way ANOVA test and were deemed to be statistically significant ($P<0.05$).

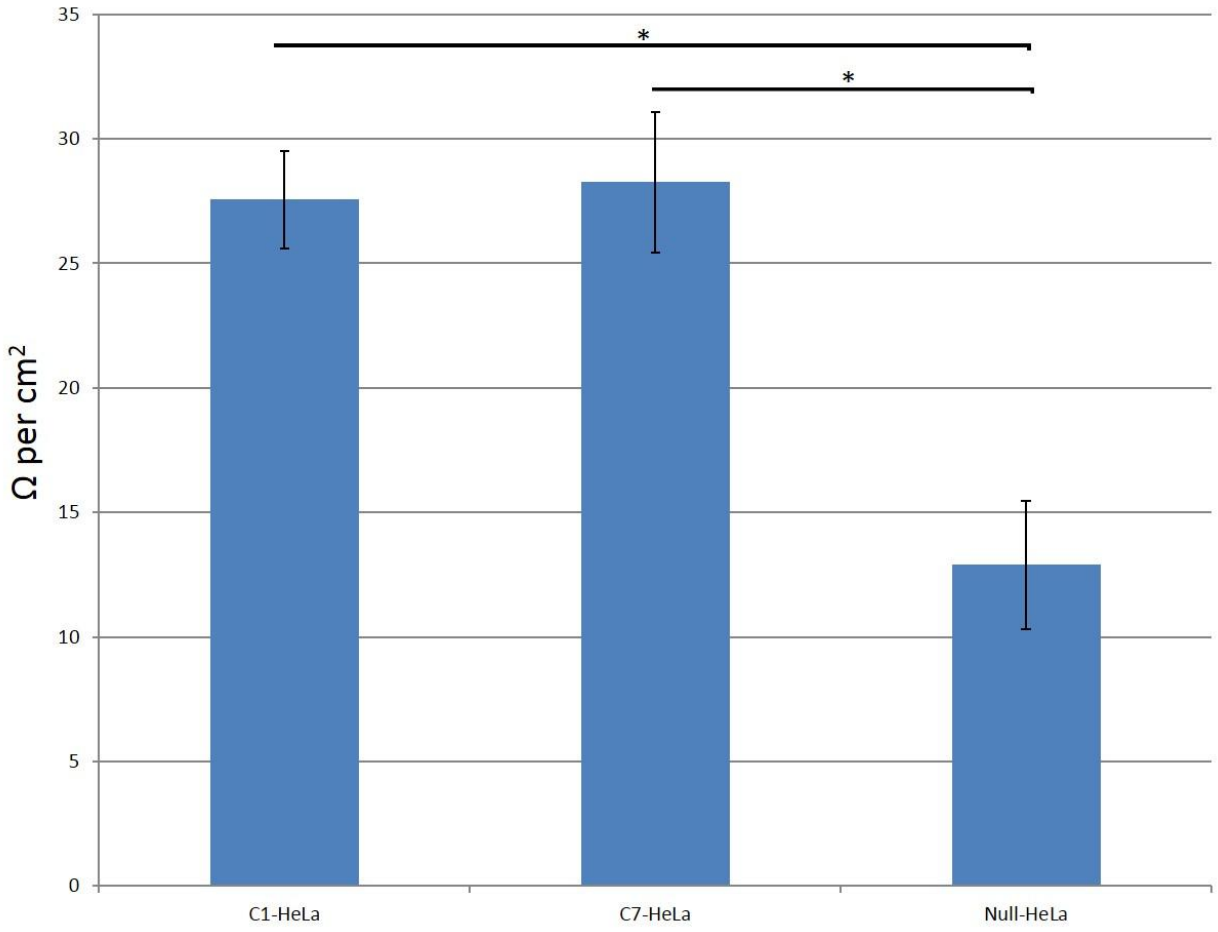

Figure 5.16 TEER reading for claudin-1, claudin-7 stable cell lines and null-HeLa

Graph showing average resistance per cm^2 in ohms for cultured monolayers of Claudin-1 transfected, Claudin-7 transfected and untransfected HeLa cells. Error bars indicate + or – one standard deviation. Significance ($p<0.05$) indicated using *.

5.14 Effect of claudin-1 and claudin-7 transfection on cell migration

The effect of Claudin-1 and Claudin-7 expression on the migratory ability of HeLa cells was assessed using a wound healing/gap closure assay. Non-claudin transfected HeLa (Null HeLa) was used as a negative control to assess the endogenous level of migratory ability in HeLa cells and to allow comparison with claudin transfected cell lines. After creating the gap in the cell monolayer, the size of the gap was measured using image j© software to ensure the gaps were close to equal size. The gap in the C1-HeLa, C7-HeLa and Null-HeLa were 840µm, 870µm, 850µm respectively at the beginning of the experiment (0 hours). Images of Null-HeLa show significant migration of cells into the gap after 24 hours and complete closure of the gap after 48 hours (Figure 5.17). The size of the gap had reduced after 24 hours for C1-HeLa although not to the same extent as the Null-HeLa at 24hours and the gap had not shown complete closure after 48 hours, in contrast to the Null-HeLa cells.

C7-HeLa showed a similar pattern to C1-HeLa with partial closure occurring after 24 hours but with gap closure still incomplete after 48 hours, unlike the HeLa-null cells which completely infiltrated and filled the gap after 48 hours (Figure 5.17). These results indicate that Claudin-1 and Claudin-7 transfection may have an effect on the migratory ability of HeLa cells, possibly impeding the motility of cells and their ability to detach from a group of cells and disperse.

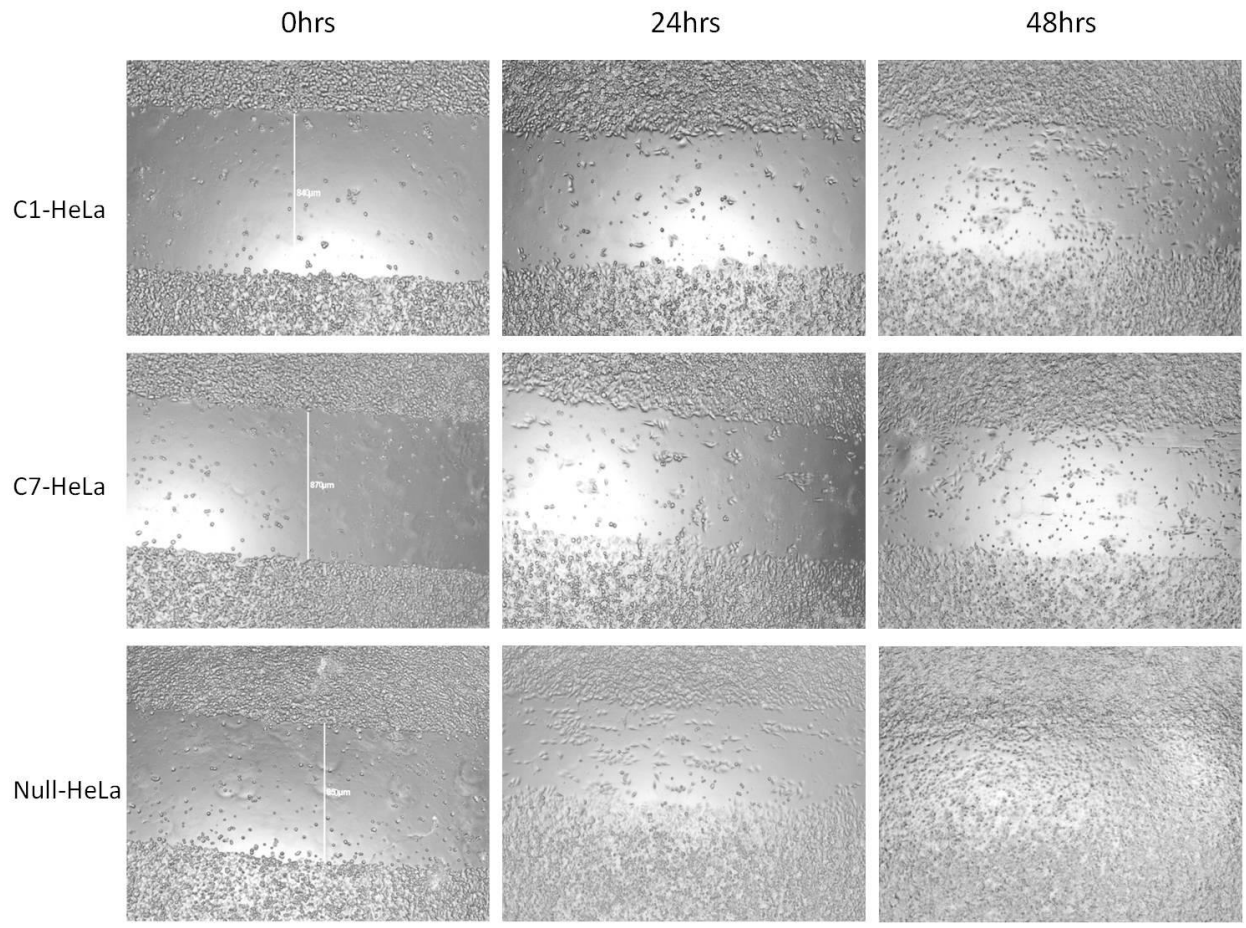

Figure 5.17 Cell migration assay images for claudin-1 and claudin-7 stable cell lines and untransfected HeLa

Gap closure assay showing migration of cells over 48hr time period. Initial width of gap was measured at 0 hour timepoint as being 840µm, 870µm and 850µm for C1-HeLa, C7-HeLa and Null-Hela respectively. Null-Hela showed partial migration of cells into the gap after 24 hours and complete gap closure at 48 hour timepoint. C1-HeLa showed partial gap closure at 24 hours and 48 hours but incomplete gap closure over 48 hour period. C7-HeLa showed a similar pattern to C1-HeLa with partial but incomplete gap closure after 48 hour time period.

5.15 Summary and Key findings

SNAIL has been shown to be a potent repressor of E-cadherin [141] and in this study an increase in SNAIL expression was observed in cases of cervical neoplasia. To assess what role SNAIL might have on E-cadherin expression in a cervical context, siRNA was purchased from Life Sciences and used to knockdown expression of SNAIL in two cervical cell lines, SiHa and HeLa. An increase in claudin-1 and claudin-7 expression in cases of cervical neoplasia was also observed in this study. To elucidate the role claudin overexpression may play in cervical neoplasia, HeLa cells were stably transfected with expression vectors containing the claudin-1 and claudin-7 genes to produce two separate stable cell lines expressing claudin-1 and claudin-7 respectively. The effect of claudin-1 and claudin-7 overexpresion on these cells, in terms of cell proliferation/viability, permeability, invasion and migration, was then assessed.

- Knockdown of SNAIL in SiHa cells had no effect on E-cadherin expression
- Claudin-1 and claudin-7 overexpression both had a similar effect on HeLa cells
    - Reduction in the migratory ability of transfected cells
    - Increase in trans-epithelial electrical resistance of cell monolayers, indicating decreased permeability.
    - No significant effect on cell invasion
    - No significant effect on cell proliferation/viability

5.16 Discussion

This study assessed the role SNAIL may play in the regulation of E-cadherin expression in two cervical cell lines, SiHa and HeLa. Both cell lines have high endogenous expression of SNAIL and do not express E-cadherin. As SNAIL has been shown to be a potent repressor of E-cadherin expression, this study used siRNAs targeting SNAIL to see if knockdown of SNAIL could be achieved and if it had an effect on E-cadherin expression in these cells lines. siRNA is widely used to tool in gene expression and silencing studies , however, the technique has limitations that must be considered. The transduction of siRNA into cells leads to only a transient knockdown of the gene of interest, with the duration of gene knockdown being determined by the rate of cell growth and the dilution of the siRNAs below a crucial threshold level that is necessary to maintain the inhibition of gene expression. As a result, the half-life of the target protein must be considered to ensure that protein does not outlast the duration of gene knockdown achieved by the siRNA. As SNAIL protein has a reported half-life of 20-45 minutes [215], cells were harvested after 24 hours in order to try and minimize dilution of the siRNA during cell growth and maximise knockdown of the SNAIL protein.

Another common limitation is of siRNA based techniques are the potential for off target effects. Off target effects occur through partial complementarity of the siRNA with unintended mRNA targets leading to down-regulation of non-target genes. The two siRNAs used in this study were purchased commercially and designed by Ambion using off-target effect prediction algorithms to ensure specificity for SNAIL mRNA only and to minimise any cross complementariness with other mRNA sequences.

Another limitation of siRNA based studies is the need for an effective delivery system, as siRNAs are naturally repelled by the negatively charged cell membrane. This study utilised a commercial lipofectamine, RNAi Max (Ambion), reagent to transfect siRNA into the target cells. This reagent had been specifically designed for transfection of siRNA and had been validated for use on HeLa cells by the manufacturer, which should have ensured effective transfection of siRNAs into target cells during the experiments performed in this study.

To investigate the effect of claudin-1 and claudin-7 transfection on HeLa cells a number of assays were used to assess cell behavior, such as migration, invasion, viability and permeability. To assess cell migration a wound-healing or gap closure assay was performed. This assay involves manually scraping a gap in a cultured monolayer and measuring the rate at which surrounding cells migrate into the space and fill the gap. The main limitation of this assay is the lack of precision associated with manually scratching the gap in the monolayer and the variability that can occur in the total area of the gap using this method. To minimise any variability in the size of the gap, the size of the gap was measured using image j software to ensure uniformity in the gap size and all assays were performed a minimum of 3 times. To assess the invasive ability of cells a boyden chamber assay was used. This assay measures the ability of cells to digest an extracellular matrix and pass through a semi-permeable membrane. A limitation of this method is that it lacks sensitivity when only a small number of cells invade through the membrane and thus with a weakly invasive cell line like HeLa, it is difficult to detect any statistically significant changes in invasive ability. It is therefore possible that if claudin transfection had only a minor effect on cell invasion, due to the low invasive ability of HeLa cells, this assay may lack the sensitivity to detect these changes. To measure the effect of

claudin transfection on cell monolayer permeability, TEER readings of cells cultured on a porous filter membrane were measured using a voltmeter. The ability of the voltmeter to accurately and reliably measure the resistance across the membrane is dependent on the correct and consistent positioning of the electrode in the transwell plate. TEER readings were measured 10 times and experiments performed in triplicate on 3 separate occasions, to ensure results were as accurate as possible any variability in resistance readings associated the positioning of the electrode was minimised.

6. Discussion

Adherens and tight junctions play a key role in maintaining the cohesive structure of epithelial tissue. Loss of cell-cell cohesion is a key mechanism in the development of epithelial malignancies, allowing cells to leave their site of origin and spread throughout the body, forming distant metastasis [216]. The significance of the process of metastasis is highlighted by the fact that 90% of cancer deaths are due to the formation of distant metastasis [203]. Since adherens and tight junctions in epithelial cells are important for maintaining tissue homeostasis by regulating epithelial barriers, and are important for cell adhesion and for cohesive structure, aberrant expression of the proteins that make up these structures is frequently observed in epithelial malignancies [116] [217] [218]. The aims of this study were to examine if various AJ and TJ proteins are aberrantly expressed in cases of cervical neoplasia, if these aberrant expression profiles are associated with any specific HPV subtype, and to analyse what effects aberrant AJ and TJ protein expression may have on dysplastic cervical cells.

To examine AJ and TJ protein expression several tissue microarrays were constructed containing normal cervical tissue and all grades of neoplasia. These tissue microarrays were stained using immunhistochemistry and assessed to see if there was any change in AJ and TJ protein expression in cases of cervical neoplasia. E-cadherin is an important part of adherens junctions being one of the main trans-membrane proteins in the junction and initiating cell-cell adhesion through trans-cadherin interactions between neighbouring cells. In this study normal cervical tissue displayed moderate E-cadherin staining in the basal and intermediate layers of the epithelium with weaker staining observed in the superficial layers of the epithelium, and

this is a staining pattern also observed by Vessey et al. 1995 [219] . E-cadherin expression is thought to be reduced in the superficial layers of the epithelium as the cells terminally differentiate, allowing these cells to be sloughed off and for new cells to move up through the epithelium [220]. Low grade lesions displayed significantly less staining than normal epithelium. Dysplastic cells in basal portion of the epithelium frequently displayed a lack of staining, while some weak staining was observed in the intermediate and superficial layers of the epithelium. High grade lesions often displayed a complete absence of staining with occasional weak staining observed in the superficial portion of the epithelium. The weak staining observed in the superficial sections of the epithelium most likely reflect the immature dysplastic cells beginning to mature further up the epithelium than in normal epithelium, where cells begin to mature in the basal and intermediate layers of the epithelium. Two different patterns were observed in squamous cell carcinoma samples with some samples displaying an absence of staining while others displayed weak staining. The dichotomy between weak and absent staining of sqaumous cell carcinomas most likely reflects the level of differentiation within the tumour, with Wu et al., 2000 showing that well differentiated squamous tumours often retain some level of E-cadherin expression while poorly differentiated tumours tend to lose all expression completely. The findings of this study are in agreement with other studies Munhoz, et al., 2009 [221] , Branca, et al., 2006 [222] that have observed a reduction of E-cadherin in cases of cervical intraepithelial neoplasia and squamous cell carcinomas compared to normal cervical epithelium., indicating that loss of E-cadherin expression may play an important role in cervical tumourigenesis.

This study found N-cadherin displayed predominantly weak membranous staining in normal cervical epithelium, mostly in the basal and intermediate layers. Low grade lesions displayed moderate membranous staining in the dysplatic cells of the basal layers, with weaker staining in the differentiating cells of the intermediate and superficial layers. High grade lesions showed moderate to strong membranous staining throughout the epithelium. Squamous cell carcinoma cells showed strong membranous staining with some weak cytoplasmic activity. Currently there are few studies of N-cadherin expression in cervical malignancies to directly compare the results of this study to. An immunohistochemistry based study by Fan et al. 2012 [223] found an increase in N-cadherin expression in LSIL, HSIL and invasive cancer compared to normal cervical epithelium, which is similar to the findings in this study. Another immunohistochemistry based study found increased expression of N-cadherin in oral squamous cell carcinoma samples, and that N-cadherin expression correlated with poor patient outcome [224]. The role of N-cahderin in tumourigenesis has been extensively studied in cell models which may offer insight into its potential role in cervical neoplasia. N-cadherin has been shown to promote motility and invasiveness in breast [132] and melanoma cells lines [225], which may indicate the increased expression observed in cases of cervical neoplasia in this study could be associated with cervical tumourigenesis.

This study observed an increase in staining of Claudin-1 and Claudin-7 in cervical neoplasia compared to normal cervical epithelium. A gradual increase in staining intensity for Claudin-1 was observed, with low grade lesions showing a slight increase, high grade lesions a more pronounced increase and squamous cell carcinoma samples showing the highest level of staining. Claudin-7 displayed a similar staining pattern to claudin-1 except the most intense

staining was observed in high grade lesions. The results of this study concur with other studies that have observed increased Claudin-1 and Claudin-7 expression in cervical neoplasia. Lee, et al., 2005 [226] observed gradually increased expressions of claudins-1 and -7 in accordance with progression from LSIL to HSIL and invasive carcinoma. Lee et al., 2005 [226] however, did not observe Claudin-1 or -7 expression in normal cervical epithelium and found the highest expression levels of Claudin-7 in invasive carcinoma samples, contrary to our findings. Sobel et al., 2005 [227] observed Claudin-1 and -7 expression in normal cervical epithelium with an increase in expression in low and high grade lesions and invasive carcinoma in concordance with our results. Sobel, et al., 2005 observed the highest level of expression for Claudin-7 in HSIL lesions, which concurs with this study, although they observed the highest expression of Claudin-1 in HSIL lesion whereas this study observed the greatest expression in invasive carcinoma samples. Claudins-1 and -7 are closely related TJ proteins [228], which may explain the similarities in staining patterns observed for both proteins in this study. Parallel up and down regulation of structurally similar claudin proteins has been observed in other cancer types such as prostatic adenocarcinomas [121]. Overexpression of Claudin-1 has been suggested to destabilise the tight junctions and lead to a loss of adhesion in oral squamous carcinoma cell lines [112], although in lung adenocarcinoma Claudin-1 has been observed to be a metastasis suppressor [115]

This study observed an increase in staining of p120 catenin in cervical neoplasia compared to normal cervical epithelium. HSIL lesions displayed the most intense staining pattern while both LSIL and squamous cell carcinoma displayed greater staining intensity than normal epithelium. p120 catenin is an integral part of adherens junctions with p120 binding

promoting the stabilisation of cadherin complexes on the plasma membrane and thus strengthens cell-cell adhesion [87]. The E-cadherin/p120-catenin complex is important for formation and maintenance of the adherens junctions, and Stairs, et al., 2011[229] found that in mouse models p120-catenin loss in the mouse oral cavity and esophagus leads to squamous cancers and suggested p120-catenin functions as a tumour suppressor gene.

p120 overexpression, however, can induce dramatic changes in cell morphology and increase cell motility [230]. These effects are apparently mediated by the ability of p120 to suppress RhoA activity and induce the activities of the related Rho GTPases, Rac1 and Cdc42 [230]. The dual role of p120, both promoting and inhibiting tumourigenesis, is thought to occur as a result of the interactions between p120 and E-cadherin. Endogenous p120 promotes the transformed growth of E-cadherin–deficient tumours by promoting Rac1 activation and inducing MAPK signaling. In contrast, p120 potently suppresses the growth of tumour cells expressing endogenous or exogenous E-cadherin [91]. In this study LSIL, HSIL and SCC samples frequently displayed a lack of positive staining for E-cadherin while strong positive staining for p120-catenin was observed for all grades of neoplasia. These findings suggest p120 may play a role in the pathogenesis of cervical neoplasia, although detection of the Rac1 and Cdc42 Rho GTPases in SIL and SCC samples would be needed to confirm this.

This study observed an increase in staining of SNAIL in cases of cervical neoplasia as compared to normal epithelium. Very few cases of normal cervical epithelium showed any staining with a gradual increase in staining observed in accordance with progression from LSIL to HSIL and invasive carcinoma. As yet, few studies have been published looking at SNAIL

expression in cervical neoplasia. Zhao et al., 2008 [231] analysed SNAIL expression at the transcriptional level finding SIL lesions and invasive carcinoma samples had much greater expression of SNAIL mRNA than normal cervical tissue. Increased expression of SNAIL in cervical neoplasia may be of significance, as SNAIL has been shown to a potent repressor of E-cadherin in epithelial cell lines [212]. This study attempted to gain further insight into the role that SNAIL might play in suppressing E-cadherin in cervical neoplasia, by performing siRNA mediated knockdown of SNAIL expression in two malignant cervical cell lines, HeLa and SiHa that lack E-cadherin expression. In HeLa cells we were unable to achieve significant knockdown of SNAIL expression, however, significant reduction in SNAIL was observed at the protein and mRNA level in SiHa cells. This reduction in SNAIL expression did not correspond to an increase in E-cadherin expression in transfected cells, for which there could be several explanations. It is possible that the potency of SNAIL is such that the level of knockdown we achieved in this study is insufficient to inhibit its repression of E-cadherin. It is also possible that there is another mechanism involved in repression of E-cadherin in the SiHa cell line and in cervical neoplasia. Loss of E-cadherin expression is observed in many different tumour types, and SNAIL mediated suppression is only one possible mechanism by which repression of E-cadherin may occur. E-cadherin promoter methylation [232] and the action of other transcriptional repressor proteins , Slug [233], SIP1 [234], and ZEB1 [235] may also play a role in suppressing E-cadherin expression. Further experiments are necessary to fully reveal the role that SNAIL may play in cervical tumorigenesis, however, the immunohistochemistry staining results in our cervical tissue samples indicate that its expression is associated with disease progression and thus it may be useful as a biomarker for disease progression. The role of HPV in promoting EMT is still

not fully understood although a number of studies are beginning to uncover interactions between HPV oncoproteins and key EMT pathways. Over expression of HPV16 E7 causes molecular changes indicative of a mesenchymal transition in normal human foreskin keratinocytes [236]. Expression of HPV16 E7 in normal human epithelial cells caused increased levels of vimentin and fibronectin and N-cadherin, all markers associated with a mesenchymal phenotype, whereas E-cadherin, a marker of the epithelial phenotype, was expressed at decreased levels [236]. In a similar study, many epithelial features were gradually eliminated and some mesenchymal traits were established in HPV16-transformed keratinocytes during HPV induced transformation [237]. These studies indicate that HPV proteins likely play a key role in driving EMT in cervical cancer.

After identifying aberrant expression of tight and adherens junction protein in cases of cervical neoplasia, the prevalence of different HPV genotypes in our samples was analysed. This would offer insights into the prevalence of HPV in the Irish population, and also allow comparisons between infection with certain HPV-genotypes and the expression profile of tight and adherens junction proteins. This study utilised a PCR based method to identify the presence of HPV DNA in FFPE cervical tissue samples. The GP5+/6+ consensus primer set was selected as it is capable of amplifying DNA from a broad spectrum of HPV types and produces a 150bp amplimer that can be subsequently sequenced to determine the HPV genotype of the sample. Other primer sets, such as SPF_{10} and MY09/11, can also be utilised in the detection and genotyping of HPV, however, they were not utilised for a number of reasons. The degradation of DNA in formalin-fixed samples hinders the PCR amplification of DNA fragments over 200bp [238]. As the MY09/11 primer set amplifies a 450bp part of the L1 genome it was not utilised in

this study. The SPF_{10} primer set is capable of detecting more HPV genotypes than the GP5+/6+ primer set and is more sensitive, however, as it uses multiple forward and reverse primer and amplifies a short 65bp sequence of the genome, that is unsuitable for sequencing, it was not utilised in this study.

This study detected HPV DNA in 60 of 101 samples examined (60%). HPV DNA was detected in 9 of 10 (90%) squamous cell carcinoma samples examined , in 12 of 28 (43%) of LSIL samples and 33 of 54 (61%) HSIL samples. For 16 of the 101 (16%) samples no beta-globin amplimers could be produced, indicating an absence of amplifiable DNA. It has previously been reported that HPV DNA is present in up to 99% of cervical cancers and 94% of CIN lesions [3]. This discrepancy in the levels of HPV DNA detection in this study and other studies may be due to a number of factors. Overall FFPE tissue is not ideal for PCR studies because of the damage done to DNA during the formalin fixation process, that causes fragmentation and cross linking of the DNA strands. The damage caused to DNA by formalin fixation is highlighted by the fact that in 16% of the analysed samples no amplifiable DNA could be detected at all using the beta-globin primers. For N.E.M samples that were beta-globin positive but GP5+/6+ negative it is possible that in these samples there was simply no HPV DNA present; in the vast majority of SIL samples however HPV DNA would be expected to be present. One factor that may explain why some SIL samples had amplifiable DNA present but still failed to produce an amplimer using the GP5+/6+ primers, is due to the relative lower level of HPV DNA compared to genomic DNA is the samples. In samples with SIL, the lesions may only cover a small area and overall only contain a few cells. While PCR amplification for β-globin may be successful in a given sample due to the fact that every cell within the tissue should contain a copy of the beta-globin gene,

the number of cells containing HPV DNA may be much lower, making detection of HPV more difficult. This effect is highlighted by the fact that the highest HPV detection rate was in invasive carcinoma samples, in which the majority of cells would be expected to contain HPV DNA.

A study by Steineau, et al., 2011 [239] using the same DNA extraction method as this study, was able to detect HPV DNA in 62.7% cases of formalin-fixed cervical neoplasia and other HPV induced carcinomas, which is comparable to the 60% detection rate of this study. Interestingly this study noted that by using an additional heating step during DNA extraction that HPV DNA detection was increased to 73.3% of samples. This study also found that they were unable to detect amplifiable DNA in 19% of their samples, which is comparable to the 16% of this study, and they also noted that with heat treatment this figure lowered to 5%. A study by Odida et al., 2010 [240] found a HPV DNA detection rate of 88.9% in formalin fixed paraffin embedded invasive cervical carcinoma samples , which contrasts with the 60% detection rate of this study. The study by Odida et al., 2010 utilised the SPF_{10} primer set which is capable of detecting a greater number of HPV types than the GP5+/6+ primer set utilised in this study, and also produces a shorter amplimer that is more effective in FFPE tissue, which may explain the greater detection rate compared to this study. Ideally all samples that were beta-globin negative or SIL lesions that were beta-globin positive but GP5+/6+ negative would have had the DNA extraction step repeated using more tissue, and possibly using the heating step described by Steineau et al., 2011 in order to try and increase the HPV DNA detection rate. Unfortunately this was not possible due to ethical constraints, as the tissue samples were only available for a limited time before they had to be returned to the hospital.

After detection of HPV DNA in samples, the amplified PCR products were sent for external sequencing by Eurofins MWG Operon, Ebersberg, Germany. Of the 60 samples successfully sequenced HPV-16 was by far the most common genotype detected with 77.3% of samples being HPV-16 positive. The second most common genotype detected was HPV-18 with 18.3% of samples, with HPV-16 and HPV-18 combined accounting for the vast majority, over 90%, of HPV genotypes detected. A large scale meta-study by Smith et al. 2007 [241] of HPV genotype global distribution in invasive cervical cancer and high-grade squamous intraepithelial lesions (HSIL) identified the highest prevalence of HPV16/18 in invasive carcinoma was in Europe, North America and Australia, with a prevalence 74-77% and global prevalence of 68%. All samples of invasive carcinoma in which HPV was detected in the study were HPV-16/18 positive; the discrepancy between the HPV-16/18 prevalence in this study is likely due to the relatively low sample number compared to the meta-study. The detection rate of HPV in HSIL lesions globally in the meta-study by Smith et al. 2007 was 84.9%, compared to the 61% detection rate of this study. One aspect that may explain the lower HPV detection rate in this study compared to the meta-study is the fact the meta-study compiled results from various different studies using a variety of tissue types, including FFPE tissue and fresh samples collected for cytological analysis, and a variety of HPV detection methods. This study examined FFPE tissue exclusively and, as has previously been discussed, it is likely that that this contributed to the lower detection rate compared to the meta-study. The prevalence of HPV-16/18 in the meta-study was 52% compared to 90% observed in this study. The higher prevalence observed in this study is likely due to the nature of samples utilised. Most tissues sample used in this study would have been referred for biopsy after several abnormal smear

tests, thus were likely cases with persistent lesions. HPV-16 infection in particular is strongly associated with persistent lesions [242], thus it is likely that our samples would be more inclined towards HPV-16 infected lesions. A significant number of samples in the meta-study (44%) were derived from thin-prep cytological preparations, which may not contain as many persistent lesions and therefore may contain a lower number of HPV-16 positive samples, compared to this study. Of the other subtypes detected HPV-6 was the only low risk genotype detected and was found in a LSIL sample. Low risk HPV subtypes are typically associated with benign condylomas and may also infrequently be associated with a LSIL lesion, with Clifford et al., 2005 [243] finding approximately 10% of HPV positive LSIL cases containing HPV-6 DNA. A small number of other high risk subtypes were detected, HPV-33 HPV-58 and HPV-67, with both HPV-33 samples associated with high grade lesions, HPV-58 positive sample didn't have a gradable core on the TMA and HPV-67 was associated with a LSIL sample. HPV-67 is a genotype from the same alpha-9 subgroup as many highly oncogenic HPV subtypes, such as HPV-16 and -33, however, it's association with cancer is less clear with only a few reports of HPV-67 being identified in cervical cancer cases [244] [245]. A combination of low frequency, lack of data on active transcription and it's transforming potential in model systems, has led HPV-67 to be classified as only probable/possible carcinogen [246]. A number of NEM samples also tested positive for HPV. HPV infection can often be asymptomatic, presenting with no discernable dysplasia. A study of 996 liquid cytology samples from Irish women aged between 16 and 72 by Keegan et al., 2007 found that 11.4% of samples with normal cytology tested positive for HPV, highlighting that infection with even high-risk HPV subtypes does not necessarily lead to the development of dysplasia.

One of the aims of this study was to examine if there was any association between an individual HPV genotype and aberrant expression of particular adherens and tight junction proteins. After successfully genotyping 60 samples, only 31 of these samples were available for comparison on the corresponding TMAs. The reasons for this discrepancy were twofold. Firstly, some samples were damaged during TMA construction process, meaning the cores were ungradable after IHC staining. Secondly, inaccurate punch sampling during TMA construction meant that in a number of cases the area containing the desired lesion was missed and an adjacent area of the epithelium was incorporated into the TMA instead. While this adjacent area of the epithelium was still graded by the pathologist and used for IHC staining, it could not be used for comparison with detected HPV genotypes, as it had been adjacent to another part of the epithelium containing a lesion with a different disease grade. Other methods that would have allowed detection of HPV directly in our TMA sections, such as chromatic in-situ hybridization (CISH), were explored however this method only distinguishes between high-risk low-risk subtypes and doesn't allow for comparison between specific subtypes of HPV.

After determining that several adherens and tight junction proteins were expressed aberrantly in cervical neoplasia, it was decided to examine further the role that claudin-1 and claudin-7 overexpression may play in cervical tumourigenesis. Claudin-1 and claudin-7 were selected for further analysis for a number of reasons. Firstly, the role of claudins in tumourigenesis is far from fully understood and is currently an area of significant research. The

difficulty in fully elucidating the role of claudins in cancer is highlighted by the fact that both up and downregulation of claudins is frequently observed in tumours. [116].

Secondly, while the results of this study and others [227],[247] have observed increased Claudin-1 and Claudin-7 in pre-invasive cervical lesions and in cases of cervical carcinoma, to the best of our knowledge, there have been no studies studying the effect of claudin-1 and claudin-7 overexpression in cervical cell lines. This study aimed to investigate the effect of Claudin-1 and 7 overexpression on the cervical carcinoma cell line HeLa, and to elucidate what role Claudin-1 and -7 overexpression may play in cervical carcinoma. To this end, stable cell lines expressing claudin-1 and claudin-7 were generated and their invasive, migratory, permeability and proliferative ability assessed.

This study found that Claudin-1 or Claudin-7 over expression had no significant effect on the invasive ability of HeLa cells. Studies have identified that Claudin-1 overexpression is associated with an increased invasiveness in oral carcinoma cells through upregulation of several matrix metalloproteases [112] [113]. Claudin-1 expressing colon carcinoma cells that underwent siRNA mediated knockdown of Claudin-1 displayed significantly decreased anchorage-independent growth and invasion with a significant decrease in MMP-9 activity. Conversely, claudin-1 overexpression suppresses metastasis and invasion in lung cancer cells [115]. The interaction between claudins and MMPs is likely to have a key influence on the invasive ability of malignant cells as the role of MMPs in digesting the extracellular matrix and promoting invasion has been well established [248] and claudins have previously been shown to promote activation of matrix metalloproteinase-2 in Human Embryonic Kidney cells [249]. Studies have previously reported that HeLa cells lack the alphavbeta3 integrin receptor [250]

which through its interaction with membrane type-1 metalloproteinase-2 (MT1-MMP), and tissue inhibitor of metalloproteinase-2 (TIMP-2) aids the activation of MMP-2 [251]. A lack of MMP-2 activation in HeLa cells may explain why they show low invasive ability and why the Claudin-1 and -7 overexpression in HeLa cells had no significant effect on the invasive ability of HeLa cells in this study.

The association between Claudin-1 and Claudin-7 expression and cell migration is also highly dependent on tumour type, with Claudin-1 expression associated with increased cell migration in breast cancer cells [252] and, conversely, associated with an inhibition of cell migration in lung cancer cells [211]. Claudin-7 expression is associated with increased migratory ability in ovarian carcinoma cells [125] but is associated with reduced migratory ability in lung carcinoma cells[124]. This study found that Claudin-1 and Claudin-7 overexpression reduced the migratory ability of HeLa cells. These results suggest there may be some establishment of homotypic claudin interaction between neighbouring cells leading to increased adhesion, or that claudin-1 and -7 transfection had a downstream effect on another motility related pathway. The exact mechanisms by which claudins contribute to cell migration and motility is still not fully understood. A recent study by Webb et al. 2013 [253] found that second extracellular loop of claudin-4 is able to interact with the extracellular environment to promote cell motility. Another mechanism through which claudins may influence cell motility and migration is through the N-WASP (neuronal Wiskott–Aldrich Syndrome protein) and ROCK (Rho-associated Coiled-coil Kinase) pathways. N-WASP is a key regulator of actin cytoskeleton remodeling which is an essential process for cell motility [254] [255], while ROCK is also involved in regulation of cell motility through modulation of the cytoskeleton [256] [257]. Loss

of claudin-5 in the breast cancer cell line MDA-MB-231 inhibited cell motility through involvement in signaling pathway of N-WASP and ROCK [258], while transfection of claudin-5 into a human endothelial cell line also reduced the motility of transfected cells through the same pathways [259]. Similar to claudin-5, it is possible that claudin-1 and claudin-7 may also interact with the N-WASP and ROCK signaling pathways to reduce cell motility, although further experiments would be needed to confirm this.

Aside from contributing to disruption in cellular cohesion, tight junction breakdown is thought to contribute to tumorigenesis through disorganised paracellular permeability allowing an unregulated flow of various potentially oncogenic molecules, such as growth factors and cytokines, through the epithelium [260]. This study found that claudin-1 and claudin-7 transfected cells showed increased TEER readings suggesting decreased permeability. Claudin-1 and claudin-7 are reported to increase TEER when transfected into cultured epithelial cells [109] although Claudin-1 transfected colon carcinoma cells showed reduced TEER readings [114]. The increased in TEER readings observed in claudin-1 and claudin-7 stable cell lines, along with the decreased migratory ability of these cells suggests that some level of claudin-claudin interaction may be re-established in these cell lines.

The role of claudins in tumourigenesis is still not fully understood, part of which relates to the fact that in certain tumours an increase in expression a particular claudin is associated with tumourigenesis, while in another tumour type a reduction of the same claudin is associated with tumourigenesis. Immunohistochemistry based studies of pre-invasive cervical lesions and cases of cervical carcinoma found an increase in expression of claudin-1 and claudin-7 compared to normal cervical epithelium[227],[247], which would suggest that in the

case of cervical malignancies claudin-1 and claudin-7 may be involved in oncogenic progression. The findings of this study, that claudin-1 and claudin-7 expression reduces HeLa cell migration, increases TEER and has no significant effect on cell invasion or proliferation, suggest that alteration in claudin-1 and claudin-7 expression alone are not responsible for tumourigenesis in cervical malignancies, but likely play a role as part of a larger process of tight junction disruption and cellular transformation. The process of tight junction dysregulation is a complex process likely involving the aberrant expression of several tight junction proteins. Claudin-1,-2,-4,-7 have been previously reported to be overexpressed in cervical pre-invasive lesions and cases of carcinoma[247]. Other non tight junction related proteins that are involved in cellular adhesion, such as E-cadherin and beta-catenin, are also reported to be aberrantly expressed in cervical malignancies [261]. The nature of any possible interactions between these proteins and how they contribute to tumourigenesis in cervical malignancies is yet to be fully understood, although experiments in other cell models may offer some insights. In colon carcinoma cell lines claudin-7 forms a complex with epithelial cell adhesion molecule (EpCAM), CD44v6 and CO-O29, that confers a higher degree of apoptosis resistance than lines devoid of any one of the four molecules [262]. A recent study also found that claudin-7 associates with claudin-1 and facilitates incorporation of claudin-1 into EpCAM-containing complexes, and that TJ formed readily after EpCAM knockdown; the acquisition of trans-epithelial electroresistance was enhanced, and TJ showed increased resistance to disruption by calcium chelation [263].

This study identified a change in expression of a number of key tight and adherens junction proteins in pre-invasive and invasive cervical lesions. The change in expression of a number of these proteins, often observed even in low grade lesions, suggest that disruption of

tight and adherens junction may be an early step in the oncogenic transformation of epithelial cervical cells. As such, many of these proteins may be of use as prognostic indications or biomarkers for disease progression. This study did not have access to patient follow up information, such as patient outcomes, and thus was unable to fully assess if there is any relationship between changes in expression of particular proteins and factors related to prognosis. Future studies with access to full patient follow up information, should seek to examine whether changes of tight and adherens protein expression in cases of cervical neoplasia are associated with any difference in various factors relating to prognosis, such as disease recurrence, resistance to treatment or survival rates. Further studies of this type would allow a more complete evaluation of the potential role that these proteins may play as biomarkers for disease progression or prognostic indicators. This may allow for the identification of pre-invasive lesions more likely to progress to invasive cancers or identify cancers more likely have poorer responses to treatment and thus give more information to physicians when assessing treatment options for patients.

This study detected and genotyped HPV DNA in number of cervical samples, with HPV 16 and 18 being by far the most prevalent subtypes detected, and aimed study aimed to assess whether infection with a particular HPV subtype was associated with an aberrant expression profile of adherens and tight junction proteins. Due to the predominance of HPV-16 in the sample cohort (73% of samples) and the low prevalence of other HPV genotypes, this study was limited in its ability to make significant comparisons of protein expression profiles between the different genotypes. Future studies with a larger cohort of non HPV-16 samples could offer greater insight into whether infection with different HPV genotypes is associated with differing

adherens and tight junction expression profiles. This may allow identification of HPV subtypes more associated with disruption of adherens and tight junction function and thus potentially with a greater risk of disease progression. If particular HPV genotypes are associated with a greater degree of aberrant protein expression, future studies may also aim to uncover the different mechanisms by which particular HPV genotype effect the expression of adherens and tight junction proteins in infected cervical cells.

Future studies may also examine the interactions between different tight and adherens junction proteins and explore if several proteins can act synergistically to promote tumourigenesis. The results of this study indicated that claudin-1 and claudin-7 expression alone in HeLa cells did not increase cell invasion and reduced the migratory ability of transfected cells. Other studies have begun to uncover the complex interactions between claudins and other proteins, within and outside of tight junctions, and how these interactions can promote invasion and other features associated with tumourigenesis. Studies by Kuhn et al., 2007 and Wu et al., 2013 have indicated claudins can interact with EpCam and other claudins to destabilise tight junctions and confer increased resistance to apoptosis in a synergistic mechanism that is reliant on co-expression of several proteins simultaneously. This study identified changes in expression of several adherens and tight junction protein in cervical tissue samples and future studies may focus on how co-expression of several of these proteins effects cell behaviour, such as invasion, migration and proliferation. By uncovering any potential mechanisms through which claudins can co-operate to promote invasion, it may identify new pathways that can be used for targeted therapies in cervical cancer treatment.

The future outlook for cervical cancer prevention is relatively positive due to a number of recent advancements. Early detection of pre-invasive lesions before they have a chance to progress to invasive cervical lesions has played a key role in the reduction of cervical cancer incidence. The introduction of cervical screening programmes in several countries, including Ireland, has helped greatly increase the detection rate of preinvasive lesions, which once detected can usually be removed without complication. Another recent development which should greatly reduce the incidence of cervical cancer is the introduction of vaccination programmes. Two vaccines are currently available, Cervarix which offers protection from HPV-16 and HPV-18, and Gardasil that offers protection from HPV-6,-11,-16 and -18. With HPV-16 and HPV-18 being responsible for approximately 70% of cervical cancer cases, a large reduction in the incidence of cervical cancer should be observed in countries with organised vaccination programmes. In Ireland the full benefits of the vaccination programme, in terms of lower cervical cancer incidence will not be seen immediately, but over a longer period of time. This is due to the fact vaccine is only effective in pre-sexually active women and is therefore currently mostly being administered to girls aged 12 to 14.

While the outlook for cervical cancer prevention is positive in most developed nations, the outlook for developing countries is less encouraging. Over 85% of cervical cancer deaths occur in developing countries (WHO 2012) and this is projected to rise to 90% by 2020 [264]. There are huge divergences in mortality rates between developing and developed nations. For example, in Malawi the mortaility rate is 38.3 per 100,000 people, compared to 1.8 per 100,000 in France (WHO 2012). The massive difference in mortality rates is principally down to a lack of funding for cervical screening and vaccination programmes in developing countries. There have,

however, been some encouraging signs recently that the burden of disease in developing countries may be eased. The Global Alliance for Vaccines and Immunisation (GAVI) is a public-private health charity that aims to increase access and availability of vaccines in developing countries. GAVI is currently trailing a HPV vaccination programme is in several developing countries with the aim of vaccinating 30 million girls by 2020. Although this programme will not completely address the overall burden of disease, it is hoped that it will pave the way for further implementation of vaccination programmes in developing countries and ultimately lead to significant reduction in cervical cancer incidence worldwide.

In summary, cervical cancer continues to be a significant cause of cancer deaths worldwide, although the successful implementation of screening and vaccination programmes should help reduce the burden of disease. Understanding the mechanisms by which HPV-induced cervical lesions acquire the ability to invade and metastasise and identifying biomarkers that may predict this process remains critically important. This study identified changes in expression of several adherens and tight junction proteins in cases of cervical neoplasia, and identified a possible association between aberrant adherens and tight junction expression and specific HPV genotypes. In order to elucidate how aberrant adherens and tight junction expression may promote cervical tumourigenesis, this study examined the overexpression of claudin-1 and claudin-7, and the knockdown of SNAIL, in cervical cell models. This study observed that SNAIL knockdown in cervical cancer cell lines is insufficient to induce E-caherin expression, which is a novel finding and indicates that another mechanism may be responsible for the repression of E-cadherin expression observed in cases of cervical neoplasia. Despite the increased expression of claudin-1 and claudin-7 observed in cases of cervical

neoplasia, claudin-1 or claudin-7 overexpression did not contribute to increased tumourigenesis in HeLa cells. On the contrary this study identified claudin-1 and claudin-7 overexpression reduces cell migration and decreases permeability in cervical cell models, which is a novel finding, and suggests that the development of invasive and metastatic characteristics in malignant cervical cells is likely reliant on the synergistic aberrant expression of several adhesion proteins.

7. References

1. Tjalma WAA, Van Waes TR, Van den Eeden LEM, Bogers JJPM. Role of human papillomavirus in the carcinogenesis of squamous cell carcinoma and adenocarcinoma of the cervix. Best Pract. Res. Clin. Obstet. Gynaecol. 2005;19:469–483. .

2. Kitchener HC, Castle PE, Cox JT. Chapter 7: Achievements and limitations of cervical cytology screening. Vaccine. 2006;24 Suppl 3:S3/63–70. .

3. Walboomers JM, Jacobs M V, Manos MM, Bosch FX, Kummer JA, Shah K V, Snijders PJ, Peto J, Meijer CJ, Muñoz N. Human papillomavirus is a necessary cause of invasive cervical cancer worldwide. J. Pathol. 1999;189:12–19. .

4. Burd EM. Human Papillomavirus and Cervical Cancer. Society. 2003;16:1–17..

5. Junqueria L, Carneiro J. The Female Reproductive System. Basic Histol. The Mc-Graw-Hill companies; 2005. p. 435–455. .

6. Stevens A, Lowe J. Female Reproductive System. Hum. Histol. New York: Elservier Mosby; 2005. p. 345–372. .

7. Jordan J, Singer A, Jones H, Shafi M. The functional anatomy of the cervix, the cervical epithlium and the stroma. Cervix 2nd Ed. Blackwell Publishing; 2006. p. 13–28. .

8. Castellsagué X. Natural history and epidemiology of HPV infection and cervical cancer. Gynecol. Oncol. 2008;110:S4–S7. .

9. Paavonen J, Naud P, Salmerón J, Wheeler CM, Chow S-N, Apter D, Kitchener H, Castellsague X, Teixeira JC, Skinner SR, Hedrick J, Jaisamrarn U, Limson G, Garland S, Szarewski A, Romanowski B, Aoki FY, Schwarz TF, Poppe WAJ, Bosch FX, Jenkins D, Hardt K, Zahaf T, Descamps D, Struyf F, Lehtinen M, Dubin G. Efficacy of human papillomavirus (HPV)-16/18 AS04-adjuvanted vaccine against cervical infection and precancer caused by oncogenic HPV types (PATRICIA): final analysis of a double-blind, randomised study in young women. Lancet. 2009. p. 301–314. .

10. Romanowski B. Long term protection against cervical infection with the human papillomavirus: Review of currently available vaccines. Hum. Vaccin. 2011. p. 161–169. .

11. Roden RB, Greenstone HL, Kirnbauer R, Booy FP, Jessie J, Lowy DR, Schiller JT. In vitro generation and type-specific neutralization of a human papillomavirus type 16 virion pseudotype. J. Virol. 1996;70:5875–5883. .

12. Syrjanen K, Syrjanen S. Papillomavirus infections in human pathology. 1st editio. Wiley; 2000. p. 11–53. .

13. De Villiers E-M, Fauquet C, Broker TR, Bernard H-U, zur Hausen H. Classification of papillomaviruses. Virology. 2004;324:17–27. .

14. Bernard H-U, Burk RD, Chen Z, van Doorslaer K, Hausen H zur, de Villiers E-M. Classification of papillomaviruses (PVs) based on 189 PV types and proposal of taxonomic amendments. Virology. 2010;401:70–79. .

15. Doorbar J. The papillomavirus life cycle. J. Clin. Virol. 2005;32 Suppl 1:S7–S15. .

16. Hebner CM, Laimins LA. Human papillomaviruses: basic mechanisms of pathogenesis and oncogenicity. Rev. Med. Virol. Wiley Online Library; 2006;16:83–97. .

17. Zheng Z-M, Baker CC. Papillomavirus genome structure, expression and post-transcriptional regulation. Front Biosci. 2006;11:2286–2302..

18. Woodman CBJ, Collins SI, Young LS. The natural history of cervical HPV infection: unresolved issues. Nat. Rev. Cancer. 2007;7:11–22. .

19. Lacey CJN, Lowndes CM, Shah K V. Chapter 4: Burden and management of non-cancerous HPV-related conditions: HPV-6/11 disease. Vaccine. 2006;24 Suppl 3:S3/35–41. .

20. Syrjänen KJ. Spontaneous evolution of intraepithelial lesions according to the grade and type of the implicated human papillomavirus (HPV). Eur. J. Obstet. Gynecol. Reprod. Biol. 1996;65:45–53. .

21. Arends MJ, Buckley CH, Wells M. Aetiology, pathogenesis, and pathology of cervical neoplasia. J. Clin. Pathol. 1998;51:96–103. .

22. Wright TC. CHAPTER 3 Pathology of HPV infection at the cytologic and histologic levels: Basis for a 2-tiered morphologic classification system. Int. J. Gynecol. Obstet. 2006. p. S22–S31. .

23. Flowers LC, McCall MA. Diagnosis and management of cervical intraepithelial neoplasia. Obstet. Gynecol. Clin. North Am. Elsevier; 2001;28:667–684. .

24. Apgar BS, Wright TC, Pfenninger JL. Loop electrosurgical excision procedure for CIN. Am. Fam. Physician. 1992;46:505–520. .

25. Kyrgiou M, Koliopoulos G, Martin-Hirsch P, Arbyn M, Prendiville W, Paraskevaidis E. Obstetric outcomes after conservative treatment for intraepithelial or early invasive cervical lesions: Systematic review and meta-analysis. Lancet. 2006;367:489–498. .

26. Turlington WT, Wright BD, Powell JL. Impact of the loop electrosurgical excision procedure on future fertility. J. Reprod. Med. 1996;41:815–818. .

27. Conner SN, Cahill AG, Tuuli MG, Stamilio DM, Odibo AO, Roehl KA, Macones GA. Interval From Loop Electrosurgical Excision Procedure to Pregnancy and Pregnancy Outcomes. Obstet. Gynecol. LWW; 2013;122:1154–1159. .

28. Johansson C, Schwartz S. Regulation of human papillomavirus gene expression by splicing and polyadenylation. Nat. Rev. Microbiol. 2013;11:239–251.

29. Longworth MS, Laimins LA. Pathogenesis of human papillomaviruses in differentiating epithelia. Microbiol. Mol. Biol. Rev. 2004;68:362–372. .

30. Cumming SA, McPhillips MG, Veerapraditsin T, Milligan SG, Graham S V. Activity of the human papillomavirus type 16 late negative regulatory element is partly due to four weak consensus 5′ splice sites that bind a U1 snRNP-like complex. J. Virol. Am Soc Microbiol; 2003;77:5167–5177. .

31. Ganguly N, Parihar SP. Human papillomavirus E6 and E7 oncoproteins as risk factors for tumorigenesis. J. Biosci. 2009;34:113–123. .

32. Muller M, Demeret C. The HPV E2-Host Protein-Protein Interactions: A Complex Hijacking of the Cellular Network. Open Virol. J. 2012;6:173–189..

33. Demeret C, Desaintes C, Yaniv M, Thierry F. Different mechanisms contribute to the E2-mediated transcriptional repression of human papillomavirus type 18 viral oncogenes. J. Virol. 1997;71:9343–9349. .

34. Doorbar J, Ely S, Sterling J, McLean C, Crawford L. Specific interaction between HPV-16 E1–E4 and cytokeratins results in collapse of the epithelial cell intermediate filament network. Nature Publishing Group; 1991; .

35. Tsai T-C, Chen S-L. The biochemical and biological functions of human papillomavirus type 16 E5 protein. Arch. Virol. 2003;148:1445–1453. .

36. Stöppler MC, Straight SW, Tsao G, Schlegel R, McCance DJ. The E5 gene of HPV-16 enhances keratinocyte immortalization by full-length DNA. Virology. 1996;223:251–254. .

37. Gao P, Zheng J. High-risk HPV E5-induced cell fusion: a critical initiating event in the early stage of HPV-associated cervical cancer. Virol. J. 2010;7:238. .

38. Münger K, Howley PM. Human papillomavirus immortalization and transformation functions. Virus Res. 2002;89:213–228. .

39. Scheffner M, Huibregtse JM, Vierstra RD, Howley PM. The HPV-16 E6 and E6-AP complex functions as a ubiquitin-protein ligase in the ubiquitination of p53. Cell. 1993;75:495–505. .

40. Garnett TO, Filippova M, Duerksen-Hughes PJ. Accelerated degradation of FADD and procaspase 8 in cells expressing human papilloma virus 16 E6 impairs TRAIL-mediated apoptosis. Cell Death Differ. 2006;13:1915–1926. .

41. Oh ST, Kyo S, Laimins LA. Telomerase activation by human papillomavirus type 16 E6 protein: induction of human telomerase reverse transcriptase expression through Myc and GC-rich Sp1 binding sites. J. Virol. 2001;75:5559–5566. .

42. Kirkpatrick KL, Mokbel K. The significance of human telomerase reverse transcriptase (hTERT) in cancer. Eur. J. Surg. Oncol. 2001;27:754–760. .

43. Narisawa-Saito M, Kiyono T. Basic mechanisms of high-risk human papillomavirus-induced carcinogenesis: roles of E6 and E7 proteins. Cancer Sci. 2007;98:1505–1511. .

44. Shin M-K, Balsitis S, Brake T, Lambert PF. Human papillomavirus E7 oncoprotein overrides the tumor suppressor activity of p21Cip1 in cervical carcinogenesis. Cancer Res. 2009;69:5656–5663. .

45. Zerfass-Thome K, Zwerschke W, Mannhardt B, Tindle R, Botz JW, Jansen-Dürr P. Inactivation of the cdk inhibitor p27KIP1 by the human papillomavirus type 16 E7 oncoprotein. Oncogene. 1996;13:2323–2330. .

46. Gartel AL, Radhakrishnan SK. Lost in transcription: p21 repression, mechanisms, and consequences. Cancer Res. 2005;65:3980–3985. .

47. Brehm A, Nielsen SJ, Miska EA, McCance DJ, Reid JL, Bannister AJ, Kouzarides T. The E7 oncoprotein associates with Mi2 and histone deacetylase activity to promote cell growth. EMBO J. 1999;18:2449–2458. .

48. Merad M, Ginhoux F, Collin M. Origin, homeostasis and function of Langerhans cells and other langerin-expressing dendritic cells. Nat. Rev. Immunol. 2008;8:935–947. .

49. Connor JP, Ferrer K, Kane JP, Goldberg JM. Evaluation of Langerhans' cells in the cervical epithelium of women with cervical intraepithelial neoplasia. Gynecol. Oncol. 1999;75:130–135. .

50. Hubert P, Caberg J-H, Gilles C, Bousarghin L, Franzen-Detrooz E, Boniver J, Delvenne P. E-cadherin-dependent adhesion of dendritic and Langerhans cells to keratinocytes is defective in cervical human papillomavirus-associated (pre)neoplastic lesions. J. Pathol. 2005;206:346–355. .

51. Caberg J-HD, Hubert PM, Begon DY, Herfs MF, Roncarati PJ, Boniver JJ, Delvenne PO. Silencing of E7 oncogene restores functional E-cadherin expression in human papillomavirus 16-transformed keratinocytes. Carcinogenesis. 2008;29:1441–1447. .

52. Laurson J, Khan S, Chung R, Cross K, Raj K. Epigenetic repression of E-cadherin by human papillomavirus 16 E7 protein. Carcinogenesis. 2010;31:918–926. .

53. Kim YT, Zhao M. Aberrant cell cycle regulation in cervical carcinoma. Yonsei Med. J. 2005;46:597–613. .

54. Carter JJ, Wipf GC, Madeleine MM, Schwartz SM, Koutsky LA, Galloway DA. Identification of human papillomavirus type 16 L1 surface loops required for neutralization by human sera. J. Virol. 2006;80:4664–4672. .

55. Giroglou T, Florin L, Schäfer F, Streeck RE, Sapp M. Human papillomavirus infection requires cell surface heparan sulfate. J. Virol. 2001;75:1565–1570. .

56. Kieback E, Müller M. Factors influencing subcellular localization of the human papillomavirus L2 minor structural protein. Virology. 2006;345:199–208. .

57. Pereira R, Hitzeroth II, Rybicki EP. Insights into the role and function of L2, the minor capsid protein of papillomaviruses. Arch. Virol. 2009;154:187–197. .

58. Brink AATP, Snijders PJF, Meijer CJLM. HPV detection methods. Dis. Markers. 2007;23:273–281. .

59. Villa LL, Denny L. CHAPTER 7 Methods for detection of HPV infection and its clinical utility. Int. J. Gynecol. Obstet. 2006. p. S71–S80. .

60. Mullis K. Process for amplifying nucleic acid sequences. US Pat. 4,683,202 [Internet]. 1987.

61. Snijders PJF, Heideman DAM, Meijer CJLM. Methods for HPV detection in exfoliated cell and tissue specimens. APMIS. 2010;118:520–528. .

62. Kleter B, van Doorn LJ, ter Schegget J, Schrauwen L, van Krimpen K, Burger M, ter Harmsel B, Quint W. Novel short-fragment PCR assay for highly sensitive broad-spectrum detection of anogenital human papillomaviruses. Am. J. Pathol. 1998;153:1731–1739. .

63. Zaravinos A, Mammas IN, Sourvinos G, Spandidos DA. Molecular detection methods of human papillomavirus (HPV). Int. J. Biol. Markers. Wichtig; 2009;24:215–222. .

64. Fristrom D. The cellular basis of epithelial morphogenesis. A review. Tissue Cell. Elsevier; 1988;20:645–690. .

65. Meng W, Takeichi M. Adherens junction: molecular architecture and regulation. Cold Spring Harb. Perspect. Biol. 2009;1:a002899. .

66. Baum B, Georgiou M. Dynamics of adherens junctions in epithelial establishment, maintenance, and remodeling. J. Cell Biol. 2011;192:907–917. .

67. Ehrlich JS, Hansen MDH, Nelson WJ. Spatio-temporal regulation of Rac1 localization and lamellipodia dynamics during epithelial cell-cell adhesion. Dev. Cell. 2002;3:259–270. .

68. Ridley AJ. Rho GTPases and actin dynamics in membrane protrusions and vesicle trafficking. Trends Cell Biol. Elsevier; 2006;16:522–529. .

69. Vasioukhin V, Bauer C, Yin M, Fuchs E. Directed actin polymerization is the driving force for epithelial cell-cell adhesion. Cell. 2000;100:209–219. .

70. Yamanaka T, Horikoshi Y, Suzuki A, Sugiyama Y, Kitamura K, Maniwa R, Nagai Y, Yamashita A, Hirose T, Ishikawa H, Ohno S. PAR-6 regulates aPKC activity in a novel way and mediates cell-cell contact-induced formation of the epithelial junctional complex. Genes Cells. 2001;6:721–731. .

71. González-Mariscal L, Betanzos A, Nava P, Jaramillo BE. Tight junction proteins. Prog. Biophys. Mol. Biol. 2003;81:1–44.

72. Hartsock A, Nelson WJ. Adherens and tight junctions: structure, function and connections to the actin cytoskeleton. Biochim. Biophys. Acta (BBA)-Biomembranes. Elsevier; 2008;1778:660–669. .

73. Steed E, Balda MS, Matter K. Dynamics and functions of tight junctions. Trends Cell Biol. 2010;20:142–149. .

74. Balda MS, Matter K. Tight junctions at a glance. J. Cell Sci. The Company of Biologists Ltd; 2008;121:3677–3682. .

75. Furuse M, Sasaki H, Tsukita S. Manner of interaction of heterogeneous claudin species within and between tight junction strands. J. Cell Biol. 1999;147:891–903. .

76. Balda MS, Flores-Maldonado C, Cereijido M, Matter K. Multiple domains of occludin are involved in the regulation of paracellular permeability. J. Cell. Biochem. 2000;78:85–96. .

77. Bazzoni G. The JAM family of junctional adhesion molecules. Curr. Opin. Cell Biol. 2003;15:525–530. .

78. Guillemot L, Paschoud S, Pulimeno P, Foglia A, Citi S. The cytoplasmic plaque of tight junctions: a scaffolding and signalling center. Biochim. Biophys. Acta. 2008;1778:601–613. .

79. Stelwagen K, McFadden HA, Demmer J. Prolactin, alone or in combination with glucocorticoids, enhances tight junction formation and expression of the tight junction protein occludin in mammary cells. Mol. Cell. Endocrinol. 1999;156:55–61. .

80. Jiang WG, Bryce RP, Horrobin DF, Mansel RE. Regulation of tight junction permeability and occludin expression by polyunsaturated fatty acids. Biochem. Biophys. Res. Commun. 1998;244:414–420. .

81. Harhaj NS, Antonetti DA. Regulation of tight junctions and loss of barrier function in pathophysiology. Int. J. Biochem. Cell Biol. 2004;36:1206–1237. .

82. Holgate ST. Epithelium dysfunction in asthma. J. Allergy Clin. Immunol. 2007;120:1233–1244; quiz 1245–1246. .

83. Coyne CB, Vanhook MK, Gambling TM, Carson JL, Boucher RC, Johnson LG. Regulation of airway tight junctions by proinflammatory cytokines. Mol. Biol. Cell. 2002;13:3218–3234. .

84. Persidsky Y, Ramirez SH, Haorah J, Kanmogne GD. Blood-brain barrier: structural components and function under physiologic and pathologic conditions. J. Neuroimmune Pharmacol. 2006;1:223–236. .

85. Huntsman DG, Caldas C. Assignment1 of the E-cadherin gene (CDH1) to chromosome 16q22. 1 by radiation hybrid mapping. Cytogenet. Genome Res. Karger Publishers; 1999;83:82–83. .

86. Halbleib JM, Nelson WJ. Cadherins in development: cell adhesion, sorting, and tissue morphogenesis. Genes Dev. 2006;20:3199–3214. .

87. Gooding JM, Yap KL, Ikura M. The cadherin-catenin complex as a focal point of cell adhesion and signalling: new insights from three-dimensional structures. Bioessays. 2004;26:497–511. .

88. Pećina-Slaus N. Tumor suppressor gene E-cadherin and its role in normal and malignant cells. Cancer Cell Int. 2003;3:17.

89. Yeatman TJ. A renaissance for SRC. Nat. Rev. Cancer. 2004;4:470–480. .

90. Reynolds AB, Roczniak-Ferguson A. Emerging roles for p120-catenin in cell adhesion and cancer. Oncogene. 2004;23:7947–7956. .

91. Soto E, Yanagisawa M, Marlow LA, Copland JA, Perez EA, Anastasiadis PZ. p120 catenin induces opposing effects on tumor cell growth depending on E-cadherin expression. J. Cell Biol. 2008;183:737–749. .

92. Ishiyama N, Lee SH, Liu S, Li GY, Smith MJ, Reichardt LF, Ikura M. Dynamic and Static Interactions between p120 Catenin and E-Cadherin Regulate the Stability of Cell-Cell Adhesion. Cell. 2010;141:117–128. .

93. Skoudy A, Gomez S, Fabre M, Garcia de Herreros A. p120-catenin expression in human colorectal cancer. Int J Cancer. 1996;68:14–20.

94. Liu Y, Wang Y, Zhang Y, Miao Y, Zhao Y, Zhang PX, Jiang GY, Zhang JY, Han Y, Lin XY, Yang LH, Li QC, Zhao C, Wang EH. Abnormal expression of p120-catenin, E-cadherin, and small GTPases is significantly associated with malignant phenotype of human lung cancer. Lung Cancer. 2009;63:375–382. .

95. Lal-Nag M, Morin PJ. The claudins. Genome Biol. 2009;10:235. .

96. Shin K, Fogg VC, Margolis B. Tight junctions and cell polarity. Annu. Rev. Cell Dev. Biol. 2006;22:207–235. .

97. Krause G, Winkler L, Mueller SL, Haseloff RF, Piontek J, Blasig IE. Structure and function of claudins. Biochim. Biophys. Acta. 2008;1778:631–645. .

98. Krause G, Winkler L, Mueller SL, Haseloff RF, Piontek J, Blasig IE. Structure and function of claudins. Biochim. Biophys. Acta. 2008;1778:631–645. .

99. Findley MK, Koval M. Regulation and roles for claudin-family tight junction proteins. IUBMB Life. 2009;61:431–437. .

100. Rangel LBA, Agarwal R, D'Souza T, Pizer ES, Alò PL, Lancaster WD, Gregoire L, Schwartz DR, Cho KR, Morin PJ. Tight junction proteins claudin-3 and claudin-4 are frequently overexpressed in ovarian cancer but not in ovarian cystadenomas. Clin. Cancer Res. 2003;9:2567–2575. .

101. Dhawan P, Singh AB, Deane NG, No Y, Shiou S-R, Schmidt C, Neff J, Washington MK, Beauchamp RD. Claudin-1 regulates cellular transformation and metastatic behavior in colon cancer. J. Clin. Invest. 2005;115:1765–1776. .

102. Tokés A-M, Kulka J, Paku S, Szik A, Páska C, Novák PK, Szilák L, Kiss A, Bögi K, Schaff Z. Claudin-1, -3 and -4 proteins and mRNA expression in benign and malignant breast lesions: a research study. Breast Cancer Res. 2005;7:R296–R305. .

103. Morita K, Miyachi Y. Tight junctions in the skin. J. Dermatol. Sci. 2003;31:81–89. .

104. Reyes JL, Lamas M, Martin D, del Carmen Namorado M, Islas S, Luna J, Tauc M, González-Mariscal L. The renal segmental distribution of claudins changes with development. Kidney Int. 2002;62:476–487. .

105. Zhu Y, Brännström M, Janson P-O, Sundfeldt K. Differences in expression patterns of the tight junction proteins,claudin 1, 3, 4 and 5, in human ovarian surface epithelium as compared to epithelia in inclusion cysts and epithelial ovarian tumours. Int. J. Cancer. Wiley Subscription Services, Inc., A Wiley Company; 2006;118:1884–1891.

106. Turksen K, Troy T-C. Barriers built on claudins. J. Cell Sci. 2004;117:2435–2447. .

107. Furuse M, Hata M, Furuse K, Yoshida Y, Haratake A, Sugitani Y, Noda T, Kubo A, Tsukita S. Claudin-based tight junctions are crucial for the mammalian epidermal barrier: a lesson from claudin-1-deficient mice. J. Cell Biol. 2002;156:1099–1111. .

108. Coyne CB, Gambling TM, Boucher RC, Carson JL, Johnson LG. Role of claudin interactions in airway tight junctional permeability. Am. J. Physiol. Lung Cell. Mol. Physiol. 2003;285:L1166–L1178. .

109. Tsukita S, Yamazaki Y, Katsuno T, Tamura A. Tight junction-based epithelial microenvironment and cell proliferation. Oncogene. 2008;27:6930–6938. .

110. Angelow S, Ahlstrom R, Yu ASL. Biology of claudins. Am. J. Physiol. Renal Physiol. 2008;295:F867–F876. .

111. Evans MJ, von Hahn T, Tscherne DM, Syder AJ, Panis M, Wölk B, Hatziioannou T, McKeating JA, Bieniasz PD, Rice CM. Claudin-1 is a hepatitis C virus co-receptor required for a late step in entry. Nature. 2007;446:801–805. .

112. Dos Reis PP, Bharadwaj RR, Machado J, Macmillan C, Pintilie M, Sukhai MA, Perez-Ordonez B, Gullane P, Irish J, Kamel-Reid S. Claudin 1 overexpression increases invasion and is associated with aggressive histological features in oral squamous cell carcinoma. Cancer. 2008;113:3169–3180. .

113. Oku N, Sasabe E, Ueta E, Yamamoto T, Osaki T. Tight junction protein claudin-1 enhances the invasive activity of oral squamous cell carcinoma cells by promoting cleavage of laminin-5 gamma2 chain via matrix metalloproteinase (MMP)-2 and membrane-type MMP-1. Cancer Res. 2006;66:5251–5257. .

114. Huo Q, Kinugasa T, Wang L, Huang J, Zhao J, Shibaguchi H, Kuroki M, Tanaka T, Yamashita Y, Nabeshima K, Iwasaki H, Kuroki M. Claudin-1 protein is a major factor involved in the tumorigenesis of colorectal cancer. Anticancer Res. 2009;29:851–857. .

115. Chao Y-C, Pan S-H, Yang S-C, Yu S-L, Che T-F, Lin C-W, Tsai M-S, Chang G-C, Wu C-H, Wu Y-Y, Lee Y-C, Hong T-M, Yang P-C. Claudin-1 is a metastasis suppressor and correlates with clinical outcome in lung adenocarcinoma. Am. J. Respir. Crit. Care Med. 2009;179:123–133. .

116. Kwon MJ. Emerging roles of claudins in human cancer. Int. J. Mol. Sci. 2013;14:18148–18180.

117. Tatum R, Zhang Y, Salleng K, Lu Z, Lin J-J, Lu Q, Jeansonne BG, Ding L, Chen Y-H. Renal salt wasting and chronic dehydration in claudin-7-deficient mice. Am. J. Physiol. Renal Physiol. 2010;298:F24–F34. .

118. Alexandre MD, Lu Q, Chen Y-H. Overexpression of claudin-7 decreases the paracellular Cl- conductance and increases the paracellular Na+ conductance in LLC-PK1 cells. J. Cell Sci. 2005;118:2683–2693. .

119. Johnson AH, Frierson HF, Zaika A, Powell SM, Roche J, Crowe S, Moskaluk CA, El-Rifai W. Expression of tight-junction protein claudin-7 is an early event in gastric tumorigenesis. Am. J. Pathol. 2005;167:577–584. .

120. Tassi RA, Bignotti E, Falchetti M, Ravanini M, Calza S, Ravaggi A, Bandiera E, Facchetti F, Pecorelli S, Santin AD. Claudin-7 expression in human epithelial ovarian cancer. Int. J. Gynecol. Cancer. 2008;18:1262–1271.

121. Sheehan GM, Kallakury BVS, Sheehan CE, Fisher HAG, Kaufman RP, Ross JS. Loss of claudins-1 and -7 and expression of claudins-3 and -4 correlate with prognostic variables in prostatic adenocarcinomas. Hum. Pathol. 2007;38:564–569. .

122. Usami Y, Chiba H, Nakayama F, Ueda J, Matsuda Y, Sawada N, Komori T, Ito A, Yokozaki H. Reduced expression of claudin-7 correlates with invasion and metastasis in squamous cell carcinoma of the esophagus. Hum. Pathol. 2006;37:569–577. .

123. Lioni M, Brafford P, Andl C, Rustgi A, El-Deiry W, Herlyn M, Smalley KSM. Dysregulation of claudin-7 leads to loss of E-cadherin expression and the increased invasion of esophageal squamous cell carcinoma cells. Am. J. Pathol. 2007;170:709–721. .

124. Lu Z, Ding L, Hong H, Hoggard J, Lu Q, Chen Y-H. Claudin-7 inhibits human lung cancer cell migration and invasion through ERK/MAPK signaling pathway. Exp. Cell Res. 2011;317:1935–1946. .

125. Dahiya N, Becker KG, Wood WH, Zhang Y, Morin PJ. Claudin-7 is frequently overexpressed in ovarian cancer and promotes invasion. PLoS One. 2011;6:e22119. .

126. Darido C, Buchert M, Pannequin J, Bastide P, Zalzali H, Mantamadiotis T, Bourgaux J-F, Garambois V, Jay P, Blache P, Joubert D, Hollande F. Defective claudin-7 regulation by Tcf-4 and Sox-9 disrupts the polarity and increases the tumorigenicity of colorectal cancer cells. Cancer Res. 2008;68:4258–4268. .

127. Derycke LDM, Bracke ME. N-cadherin in the spotlight of cell-cell adhesion, differentiation, embryogenesis, invasion and signalling. Int. J. Dev. Biol. 2004;48:463–476. .

128. Derycke LDM, Bracke ME. N-cadherin in the spotlight of cell-cell adhesion, differentiation, embryogenesis, invasion and signalling. Int. J. Dev. Biol. Univeristy of the Basque Country Press; 1999; 2004;48:463–476. .

129. Arikkath J, Reichardt LF. Cadherins and catenins at synapses: roles in synaptogenesis and synaptic plasticity. Trends Neurosci. 2008;31:487–494. .

130. Hazan RB, Qiao R, Keren R, Badano I, Suyama K. Cadherin switch in tumor progression. Ann. N. Y. Acad. Sci. 2004;1014:155–163. .

131. Wheelock MJ, Shintani Y, Maeda M, Fukumoto Y, Johnson KR. Cadherin switching. J. Cell Sci. 2008;121:727–735. .

132. Hazan RB, Phillips GR, Qiao RF, Norton L, Aaronson SA. Exogenous expression of N-cadherin in breast cancer cells induces cell migration, invasion, and metastasis. J. Cell Biol. 2000;148:779–790. .

133. De Wever O, Westbroek W, Verloes A, Bloemen N, Bracke M, Gespach C, Bruyneel E, Mareel M. Critical role of N-cadherin in myofibroblast invasion and migration in vitro stimulated by colon-cancer-cell-derived TGF-beta or wounding. J. Cell Sci. 2004;117:4691–4703. .

134. Suyama K, Shapiro I, Guttman M, Hazan RB. A signaling pathway leading to metastasis is controlled by N-cadherin and the FGF receptor. Cancer Cell. Elsevier; 2002;2:301–314. .

135. Navarro P, Ruco L, Dejana E. Differential localization of VE- and N-cadherins in human endothelial cells: VE-cadherin competes with N-cadherin for junctional localization. J. Cell Biol. 1998;140:1475–1484. .

136. Mariotti A, Perotti A, Sessa C, Rüegg C. N-cadherin as a therapeutic target in cancer. Expert Opin. Investig. Drugs. 2007;16:451–465. .

137. Erez N, Zamir E, Gour BJ, Blaschuk OW, Geiger B. Induction of apoptosis in cultured endothelial cells by a cadherin antagonist peptide: involvement of fibroblast growth factor receptor-mediated signalling. Exp. Cell Res. 2004;294:366–378. .

138. Twigg SR, Wilkie AO. Characterisation of the human snail (SNAI1) gene and exclusion as a major disease gene in craniosynostosis. Hum. Genet. 1999;105:320–326. .

139. Pérez-Mancera PA, Pérez-Caro M, González-Herrero I, Flores T, Orfao A, de Herreros AG, Gutiérrez-Adán A, Pintado B, Sagrera A, Sánchez-Martín M, Sánchez-García I. Cancer development induced by graded expression of Snail in mice. Hum. Mol. Genet. 2005;14:3449–3461. .

140. Nieto MA. The snail superfamily of zinc-finger transcription factors. Nat. Rev. Mol. Cell Biol. 2002;3:155–166. .

141. Peinado H, Ballestar E, Esteller M, Cano A. Snail mediates E-cadherin repression by the recruitment of the Sin3A/histone deacetylase 1 (HDAC1)/HDAC2 complex. Mol. Cell. Biol. 2004;24:306–319. .

142. Martínez-Estrada OM, Cullerés A, Soriano FX, Peinado H, Bolós V, Martínez FO, Reina M, Cano A, Fabre M, Vilaró S. The transcription factors Slug and Snail act as repressors of Claudin-1 expression in epithelial cells. Biochem. J. 2006;394:449–457. .

143. Emadi Baygi M, Soheili ZS, Schmitz I, Sameie S, Schulz WA. Snail regulates cell survival and inhibits cellular senescence in human metastatic prostate cancer cell lines. Cell Biol Toxicol. 2010;26:553–567.

144. Kierszenbaum A, Tres L. Essential concepts Epithelium. Histol. Cell Biol. 3rd Editio. Elsevier; 2012. .

145. Ross M, Wojciech P. Embryonic Connective Tissue. Histol. A Text Atlas. Lippincott Williams & Wilkins; 2010. .

146. Acloque H, Thiery JP, Nieto MA. The physiology and pathology of the EMT. EMBO Rep. Wiley Online Library; 2008;9:322–326. .

147. Vićovac L, Aplin JD. Epithelial-mesenchymal transition during trophoblast differentiation. Acta Anat. (Basel). 1996;156:202–216. .

148. Sauka-Spengler T, Bronner-Fraser M. A gene regulatory network orchestrates neural crest formation. Nat. Rev. Mol. Cell Biol. 2008;9:557–568. .

149. Strutz F, Zeisberg M, Ziyadeh FN, Yang C-Q, Kalluri R, Müller GA, Neilson EG. Role of basic fibroblast growth factor-2 in epithelial-mesenchymal transformation. Kidney Int. 2002;61:1714–1728. .

150. Kalluri R, Weinberg RA. The basics of epithelial-mesenchymal transition. J. Clin. Invest. 2009;119:1420–1428. .

151. Thiery JP. Epithelial-mesenchymal transitions in tumour progression. Nat. Rev. Cancer. 2002;2:442–454. .

152. Yang J, Weinberg RA. Epithelial-mesenchymal transition: at the crossroads of development and tumor metastasis. Dev. Cell. 2008;14:818–829. .

153. Iwatsuki M, Mimori K, Yokobori T, Ishi H, Beppu T, Nakamori S, Baba H, Mori M. Epithelial-mesenchymal transition in cancer development and its clinical significance. Cancer Sci. 2010;101:293–299. .

154. Sabbah M, Emami S, Redeuilh G, Julien S, Prévost G, Zimber A, Ouelaa R, Bracke M, De Wever O, Gespach C. Molecular signature and therapeutic perspective of the epithelial-to-mesenchymal transitions in epithelial cancers. Drug Resist. Updat. 2008;11:123–151. .

155. Miettinen PJ, Ebner R, Lopez AR, Derynck R. TGF-beta induced transdifferentiation of mammary epithelial cells to mesenchymal cells: involvement of type I receptors. J. Cell Biol. 1994;127:2021–2036. .

156. Peinado H, Olmeda D, Cano A. Snail, Zeb and bHLH factors in tumour progression: an alliance against the epithelial phenotype? Nat. Rev. Cancer. 2007;7:415–428. .

157. Thiery JP, Acloque H, Huang RYJ, Nieto MA. Epithelial-mesenchymal transitions in development and disease. Cell. 2009;139:871–890. .

158. Moreno-Bueno G, Portillo F, Cano A. Transcriptional regulation of cell polarity in EMT and cancer. Oncogene. 2008;27:6958–6969. .

159. Whiteman EL, Liu CJ, Fearon ER, Margolis B. The transcription factor snail represses Crumbs3 expression and disrupts apico-basal polarity complexes. Oncogene. Nature Publishing Group; 2008;27:3875–3879. .

160. Spaderna S, Schmalhofer O, Wahlbuhl M, Dimmler A, Bauer K, Sultan A, Hlubek F, Jung A, Strand D, Eger A, Kirchner T, Behrens J, Brabletz T. The transcriptional repressor ZEB1 promotes metastasis and loss of cell polarity in cancer. Cancer Res. 2008;68:537–544. .

161. Wang X, Nie J, Zhou Q, Liu W, Zhu F, Chen W, Mao H, Luo N, Dong X, Yu X. Downregulation of Par-3 expression and disruption of Par complex integrity by TGF-β during the process of epithelial to mesenchymal transition in rat proximal epithelial cells. Biochim. Biophys. Acta - Mol. Basis Dis. 2008;1782:51–59. .

162. Ozdamar B, Bose R, Barrios-Rodiles M, Wang H-R, Zhang Y, Wrana JL. Regulation of the polarity protein Par6 by TGFbeta receptors controls epithelial cell plasticity. Science. 2005;307:1603–1609. .

163. Korpal M, Lee ES, Hu G, Kang Y. The miR-200 family inhibits epithelial-mesenchymal transition and cancer cell migration by direct targeting of E-cadherin transcriptional repressors ZEB1 and ZEB2. J. Biol. Chem. 2008;283:14910–14914. .

164. Zhang J-P, Zeng C, Xu L, Gong J, Fang J-H, Zhuang S-M. MicroRNA-148a suppresses the epithelial-mesenchymal transition and metastasis of hepatoma cells by targeting Met/Snail signaling. Oncogene. 2013;1–8.

165. Ma L, Young J, Prabhala H, Pan E, Mestdagh P, Muth D, Teruya-Feldstein J, Reinhardt F, Onder TT, Valastyan S, Westermann F, Speleman F, Vandesompele J, Weinberg RA. miR-9, a MYC/MYCN-activated microRNA, regulates E-cadherin and cancer metastasis. Nat. Cell Biol. 2010;12:247–256. .

166. Chandler I, Houlston R, Landberg G. A practical guide to constructing and using tissue microarrays. Methods in Biobanking. Springer; 2011. p. 363–373. .

167. Battifora H. The multitumor (sausage) tissue block: novel method for immunohistochemical antibody testing. Lab. Invest. 1986;55:244–248. .

168. Kononen J, Bubendorf L, Kallioniemi A, Bärlund M, Schraml P, Leighton S, Torhorst J, Mihatsch MJ, Sauter G, Kallioniemi OP. Tissue microarrays for high-throughput molecular profiling of tumor specimens. Nat. Med. 1998;4:844–847. .

169. Giltnane JM, Rimm DL. Technology insight: Identification of biomarkers with tissue microarray technology. Nat. Clin. Pract. Oncol. 2004;1:104–111. .

170. Coons AH, Creech HJ, Jones RN. Immunological properties of an antibody containing a fluorescent group. Proc. Soc. Exp. Biol. Med. Soc. Exp. Biol. Med. (New York, NY). Royal Society of Medicine; 1941. p. 200–202. .

171. Ramos-Vara JA. Technical aspects of immunohistochemistry. Vet. Pathol. 2005;42:405–426. .

172. C.R T. Chapter 1: Techniques of Immunohiustochemistry: Principles, Pitfalls and Standardization. In: D.Dabbs, editor. Diagnostic Immunohistochem. Churchill Livingstone Elsevier; 2006. p. 1–42. .

173. Huang SN, Minassian H, More JD. Application of immunofluorescent staining on paraffin sections improved by trypsin digestion. Lab. Invest. 1976;35:383–390. .

174. Shi SR, Key ME, Kalra KL. Antigen retrieval in formalin-fixed, paraffin-embedded tissues: an enhancement method for immunohistochemical staining based on microwave oven heating of tissue sections. J. Histochem. Cytochem. 1991;39:741–748. .

175. Hsu SM, Raine L, Fanger H. Use of avidin-biotin-peroxidase complex (ABC) in immunoperoxidase techniques: a comparison between ABC and unlabeled antibody (PAP) procedures. J. Histochem. Cytochem. 1981;29:577–580. .

176. Bratthauer GL. The avidin-biotin complex (ABC) method and other avidin-biotin binding methods. Methods Mol. Biol. 2010;588:257–270. .

177. Kim TK, Eberwine JH. Mammalian cell transfection: the present and the future. Anal. Bioanal. Chem. 2010;397:3173–3178. .

178. Pfeifer A, Verma IM. Gene therapy: promises and problems. Annu. Rev. Genomics Hum. Genet. 2001;2:177–211. .

179. Graham FL, van der Eb AJ. A new technique for the assay of infectivity of human adenovirus 5 DNA. Virology. 1973;52:456–467. .

180. Hawley-Nelson P, Ciccarone V. Transfection of cultured eukaryotic cells using cationic lipid reagents. Curr. Protoc. Neurosci. 2001;Appendix 1:Appendix 1F. .

181. Mehier-Humbert S, Guy RH. Physical methods for gene transfer: improving the kinetics of gene delivery into cells. Adv. Drug Deliv. Rev. 2005;57:733–753. .

182. Neumann E, Schaefer-Ridder M, Wang Y, Hofschneider PH. Gene transfer into mouse lyoma cells by electroporation in high electric fields. EMBO J. 1982;1:841–845. .

183. Murnane JP, Yezzi MJ, Young BR. Recombination events during integration of transfected DNA into normal human cells. Nucleic Acids Res. 1990;18:2733–2738. .

184. Wurm FM. Production of recombinant protein therapeutics in cultivated mammalian cells. Nat. Biotechnol. 2004;22:1393–1398. .

185. Van Steensel B. Chromatin: constructing the big picture. EMBO J. 2011;30:1885–1895. .

186. Covarrubias L, Nishida Y, Terao M, d'Eustachio P, Mintz B. Cellular DNA rearrangements and early developmental arrest caused by DNA insertion in transgenic mouse embryos. Mol. Cell. Biol. Am Soc Microbiol; 1987;7:2243–2247. .

187. Hamada T, Sasaki H, Seki R, Sakaki Y. Mechanism of chromosomal integration of transgenes in microinjected mouse eggs: sequence analysis of genome-transgene and transgene-transgene junctions at two loci. Gene. Elsevier; 1993;128:197–202. .

188. Mark WH, Signorelli K, Blum M, Kwee L, Lacy E. Genomic structure of the locus associated with an insertional mutation in line 4 transgenic mice. Genomics. Elsevier; 1992;13:159–166. .

189. Rijkers T, Peetz A, Rüther U. Insertional mutagenesis in transgenic mice. Transgenic Res. Springer; 1994;3:203–215. .

190. Fire A, Xu S, Montgomery MK, Kostas SA, Driver SE, Mello CC. Potent and specific genetic interference by double-stranded RNA in Caenorhabditis elegans. Nature. 1998;391:806–811. .

191. Hamilton AJ, Baulcombe DC. A species of small antisense RNA in posttranscriptional gene silencing in plants. Science (80-.). 1999;286:950–2. .

192. Bartel DP. MicroRNAs: Genomics, Biogenesis, Mechanism, and Function. Cell. 2004. p. 281–297. .

193. Ryther RCC, Flynt AS, Phillips JA, Patton JG. siRNA therapeutics: big potential from small RNAs. Gene Ther. 2005;12:5–11. .

194. Bernstein E, Caudy AA, Hammond SM, Hannon GJ. Role for a bidentate ribonuclease in the initiation step of RNA interference. Nature. 2001;409:363–366. .

195. Vermeulen A, Behlen L, Reynolds A, Wolfson A, Marshall WS, Karpilow J, Khvorova A. The contributions of dsRNA structure to Dicer specificity and efficiency. RNA. 2005;11:674–682. .

196. Matranga C, Tomari Y, Shin C, Bartel DP, Zamore PD. Passenger-strand cleavage facilitates assembly of siRNA into Ago2-containing RNAi enzyme complexes. Cell. Elsevier; 2005;123:607–620. .

197. Rand TA, Petersen S, Du F, Wang X. Argonaute2 cleaves the anti-guide strand of siRNA during RISC activation. Cell. Elsevier; 2005;123:621–629. .

198. Eamens AL, Smith NA, Curtin SJ, Wang M-B, Waterhouse PM. The Arabidopsis thaliana double-stranded RNA binding protein DRB1 directs guide strand selection from microRNA duplexes. RNA. 2009;15:2219–2235. .

199. Agrawal N, Dasaradhi PVN, Mohmmed A, Malhotra P, Bhatnagar RK, Mukherjee SK. RNA interference: biology, mechanism, and applications. Microbiol. Mol. Biol. Rev. 2003;67:657–685. .

200. Sioud M. Therapeutic potential of small interfering RNAs. Drugs Future. 2004;29:741–750. .

201. Medici D, Hay ED, Olsen BR. Snail and Slug Promote Epithelial-Mesenchymal Transition through ^{N_L} -Catenin – T-Cell Factor-4-dependent Expression of Transforming Growth Factor- ^{N_L} 3. Mol. Biol. Cell. 2008;19:4875–4887. .

202. Paulukat J, Bosmann M, Nold M, Garkisch S, Kämpfer H, Frank S, Raedle J, Zeuzem S, Pfeilschifter J, Mühl H. Expression and release of IL-18 binding protein in response to IFN-gamma. J. Immunol. 2001;167:7038–7043. .

203. Mehlen P, Puisieux A. Metastasis: a question of life or death. Nat. Rev. Cancer. 2006;6:449–458. .

204. Pummi K, Malminen M, Aho H, Karvonen SL, Peltonen J, Peltonen S. Epidermal tight junctions: ZO-1 and occludin are expressed in mature, developing, and affected skin and in vitro differentiating keratinocytes. J. Invest. Dermatol. 2001;117:1050–1058. .

205. Hofmann M, Stoss O, Shi D, Büttner R, Van De Vijver M, Kim W, Ochiai A, Rüschoff J, Henkel T. Assessment of a HER2 scoring system for gastric cancer: Results from a validation study. Histopathology. 2008;52:797–805. .

206. Wang J-L, Zheng B-Y, Li X-D, Nokelainen K, Angström T, Lindström MS, Wallin K-L. p16INK4A and p14ARF expression pattern by immunohistochemistry in human papillomavirus-related cervical neoplasia. Mod. Pathol. 2005;18:629–637. .

207. Schiffman M, Castle PE, Jeronimo J, Rodriguez AC, Wacholder S. Human papillomavirus and cervical cancer. Lancet. 2007. p. 890–907. .

208. De Roda Husman AM, Walboomers JM, van den Brule AJ, Meijer CJ, Snijders PJ. The use of general primers GP5 and GP6 elongated at their 3’ ends with adjacent highly conserved sequences improves human papillomavirus detection by PCR. J. Gen. Virol. 1995;76 (Pt 4):1057–1062. .

209. De Roda Husman AM, Snijders PJ, Stel H V, van den Brule AJ, Meijer CJ, Walboomers JM. Processing of long-stored archival cervical smears for human papillomavirus detection by the polymerase chain reaction. Br. J. Cancer. 1995;72:412–417. .

210. Wood NH, Khammissa RAG, Chikte UME, Meyerov R, Lemmer J, Feller L. The pathobiology and mechanisms of infection of HPV. SADJ. 2010;65:124–126. .

211. Chao YC, Pan SH, Yang SC, Yu SL, Che TF, Lin CW, Tsai MS, Chang GC, Wu CH, Wu YY, Lee YC, Hong TM, Yang PC. Claudin-1 is a metastasis suppressor and correlates with clinical outcome in lung adenocarcinoma. Am J Respir Crit Care Med. 2009;179:123–133.

212. Peinado H, Ballestar E, Esteller M, Cano A. Snail mediates E-cadherin repression by the recruitment of the Sin3A/histone deacetylase 1 (HDAC1)/HDAC2 complex. Mol. Cell. Biol. 2004;24:306–319. .

213. Zhao L, Chen W, Taylor KM, Cai B, Li X. LIV-1 suppression inhibits HeLa cell invasion by targeting ERK1/2-Snail/Slug pathway. Biochem. Biophys. Res. Commun. 2007;363:82–88. .

214. Livak KJ, Schmittgen TD. Analysis of relative gene expression data using real-time quantitative PCR and the 2(-Delta Delta C(T)) Method. Methods . 2001;25:402–408.

215. De Herreros AG, Peiró S, Nassour M, Savagner P. Snail family regulation and epithelial mesenchymal transitions in breast cancer progression. J. Mammary Gland Biol. Neoplasia. 2010. p. 135–147. .

216. Zetter BR. Adhesion molecules in tumor metastasis. Semin. Cancer Biol. 1993;4:219–229. .

217. Martin TA, Jiang WG. Loss of tight junction barrier function and its role in cancer metastasis. Biochim. Biophys. Acta. 2009;1788:872–891. .

218. Vasioukhin V. Adherens junctions and cancer. Subcell. Biochem. 2012;60:379–414.

219. Vessey CJ, Wilding J, Folarin N, Hirano S, Takeichi M, Soutter P, Stamp GW, Pignatelli M. Altered expression and function of E-cadherin in cervical intraepithelial neoplasia and invasive squamous cell carcinoma. J Pathol. 1995;176:151–159. .

220. Felix JC, Lonky NM, Tamura K, Yu KJ, Naidu Y, Lai CR, Lonky SA. Aberrant expression of E-cadherin in cervical intraepithelial neoplasia correlates with a false-negative Papanicolaou smear. Am. J. Obstet. Gynecol. 2002. p. 1308–1314. .

221. Munhoz NG, Rodrigues DA, Pedregosa JF, Rodrigues JO, Junqueira MSG, Yonamine PTK, Pereira SF, Uezato S, Pandossio T, Martins EKL. The Use of Molecular Markers (p16, Ki-67 and E-Cadherin) in Uterine Cervical Biopsies. Open Pathol. J. 2009;3. .

222. Branca M, Giorgi C, Ciotti M, Santini D, Di Bonito L, Costa S, Benedetto A, Bonifacio D, Di Bonito P, Paba P, Accardi L, Mariani L, Syrjänen S, Favalli C, Syrjänen K. Down-regulation of E-cadherin is closely associated with progression of cervical intraepithelial neoplasia (CIN), but not with high-risk human papillomavirus (HPV) or disease outcome in cervical cancer. Eur. J. Gynaecol. Oncol. 2006;27:215–223. .

223. FAN Qiong, BAO Wei, YANG Ting-ting, LIU Xiao-yi WD. Expression and clinical significance of Twist, E-cadherin and N-cadherin in cervical squamous cell carcinoma. J. Shanghai Jiaotong Univ. (Medical Sci. 2012;32. .

224. DI Domenico M, Pierantoni GM, Feola A, Esposito F, Laino L, DE Rosa A, Rullo R, Mazzotta M, Martano M, Sanguedolce F, Perillo L, D'Angelo L, Papagerakis S, Tortorella S, Bufo P,

Lo Muzio L, Pannone G, Santoro A. Prognostic significance of N-Cadherin expression in oral squamous cell carcinoma. Anticancer Res.. 2011;31:4211–4218.

225. Maret D, Gruzglin E, Sadr MS, Siu V, Shan W, Koch AW, Seidah NG, Del Maestro RF, Colman DR. Surface expression of precursor N-cadherin promotes tumor cell invasion. Neoplasia. 2010;12:1066–1080. .

226. Lee JW, Lee SJ, Seo J, Song SY, Ahn G, Park CS, Lee JH, Kim BG, Bae DS. Increased expressions of claudin-1 and claudin-7 during the progression of cervical neoplasia. Gynecol. Oncol. 2005;97:53–59. .

227. Sobel G, Páska C, Szabó I, Kiss A, Kádár A, Schaff Z. Increased expression of claudins in cervical squamous intraepithelial neoplasia and invasive carcinoma. Hum. Pathol. 2005;36:162–169. .

228. Hewitt KJ, Agarwal R, Morin PJ. The claudin gene family: expression in normal and neoplastic tissues. BMC Cancer. 2006;6:186. .

229. Stairs DB, Bayne LJ, Rhoades B, Vega ME, Waldron TJ, Kalabis J, Klein-Szanto A, Lee J-S, Katz JP, Diehl JA, Reynolds AB, Vonderheide RH, Rustgi AK. Deletion of p120-catenin results in a tumor microenvironment with inflammation and cancer that establishes it as a tumor suppressor gene. Cancer Cell. 2011;19:470–483. .

230. Grosheva I, Shtutman M, Elbaum M, Bershadsky AD. p120 catenin affects cell motility via modulation of activity of Rho-family GTPases: a link between cell-cell contact formation and regulation of cell locomotion. J. Cell Sci. 2001;114:695–707. .

231. Zhao L, Chen W, Li X. [Expression of SNAIL mRNA in uterine cervical cancer is detected by real-time PCR]. Sichuan da xue xue bao. Yi xue ban= J. Sichuan Univ. Med. Sci. Ed. 2008;39:414–417. .

232. Nojima D, Nakajima K, Li LC, Franks J, Ribeiro-Filho L, Ishii N, Dahiya R. CpG methylation of promoter region inactivates E-cadherin gene in renal cell carcinoma. Mol. Carcinog. 2001;32:19–27. .

233. Bolós V, Peinado H, Pérez-Moreno MA, Fraga MF, Esteller M, Cano A. The transcription factor Slug represses E-cadherin expression and induces epithelial to mesenchymal transitions: a comparison with Snail and E47 repressors. J. Cell Sci. 2003;116:499–511. .

234. Comijn J, Berx G, Vermassen P, Verschueren K, Van Grunsven L, Bruyneel E, Mareel M, Huylebroeck D, Van Roy F. The two-handed E box binding zinc finger protein SIP1 downregulates E-cadherin and induces invasion. Mol. Cell. 2001;7:1267–1278. .

235. Sánchez-Tilló E, Lázaro A, Torrent R, Cuatrecasas M, Vaquero EC, Castells A, Engel P, Postigo A. ZEB1 represses E-cadherin and induces an EMT by recruiting the SWI/SNF chromatin-remodeling protein BRG1. Oncogene. 2010;29:3490–3500. .

236. Hellner K, Mar J, Fang F, Quackenbush J, Münger K. HPV16 E7 oncogene expression in normal human epithelial cells causes molecular changes indicative of an epithelial to mesenchymal transition. Virology. 2009;391:57–63. .

237. Geiger T, Sabanay H, Kravchenko-Balasha N, Geiger B, Levitzki A. Anomalous features of EMT during keratinocyte transformation. PLoS One. 2008;3. .

238. Inoue T, Nabeshima K, Kataoka H, Koono M. Feasibility of archival non-buffered formalin-fixed and paraffin-embedded tissues for PCR amplification: an analysis of resected gastric carcinoma. Pathol. Int. 1996;46:997–1004. .

239. Steinau M, Patel SS, Unger ER. Efficient DNA extraction for HPV genotyping in formalin-fixed, paraffin-embedded tissues. J. Mol. Diagn. 2011;13:377–381. .

240. Odida M, de Sanjose S, Sandin S, Quiros B, Alemany L, Lloveras B, Quint W, Kleter B, Alejo M, van Doorn L-J, Weiderpass E. Comparison of human papillomavirus detection between freshly frozen tissue and paraffin embedded tissue of invasive cervical cancer. Infect. Agent. Cancer. 2010;5:15. .

241. Smith JS, Lindsay L, Hoots B, Keys J, Franceschi S, Winer R, Clifford GM. Human papillomavirus type distribution in invasive cervical cancer and high-grade cervical lesions: a meta-analysis update. Int. J. Cancer. 2007;121:621–632. .

242. Londesborough P, Ho L, Terry G, Cuzick J, Wheeler C, Singer A. Human papillomavirus genotype as a predictor of persistence and development of high-grade lesions in women with minor cervical abnormalities. Int. J. Cancer. 1996;69:364–368. .

243. Clifford GM, Rana RK, Franceschi S, Smith JS, Gough G, Pimenta JM. Human papillomavirus genotype distribution in low-grade cervical lesions: comparison by geographic region and with cervical cancer. Cancer Epidemiol. Biomarkers Prev. 2005;14:1157–1164. .

244. Andersson S, Mints M, Sällström J, Wilander E. The relative distribution of oncogenic types of human papillomavirus in benign, pre-malignant and malignant cervical biopsies: A study with human papillomavirus deoxyribonucleic acid sequence analysis. Cancer Detect. Prev. 2005;29:37–41. .

245. Schiffman M, Clifford G, Buonaguro FM. Classification of weakly carcinogenic human papillomavirus types: addressing the limits of epidemiology at the borderline. Infect. Agent. Cancer. 2009;4:8. .

246. Halec G, Schmitt M, Dondog B, Sharkhuu E, Wentzensen N, Gheit T, Tommasino M, Kommoss F, Bosch FX, Franceschi S, Clifford G, Gissmann L, Pawlita M. Biological activity of probable/possible high-risk human papillomavirus types in cervical cancer. Int. J. Cancer. 2013;132:63–71.

247. Szabó I, Kiss A, Schaff Z, Sobel G. Claudins as diagnostic and prognostic markers in gynecological cancer. Histol. Histopathol. 2009;24:1607–1615. .

248. Egeblad M, Werb Z. New functions for the matrix metalloproteinases in cancer progression. Nat. Rev. Cancer. 2002;2:161–174. .

249. Miyamori H, Takino T, Kobayashi Y, Tokai H, Itoh Y, Seiki M, Sato H. Claudin promotes activation of pro-matrix metalloproteinase-2 mediated by membrane-type matrix metalloproteinases. J. Biol. Chem. 2001;276:28204–28211. .

250. Chatterjee N, Chatterjee A. Role of alphavbeta3 integrin receptor in the invasive potential of human cervical cancer (SiHa) cells. J. Environ. Pathol. Toxicol. Oncol. 2001;20:211–221. .

251. Mitra A, Chakrabarti J, Chattopadhyay N, Chatterjee A. Membrane-associated MMP-2 in human cervical cancer. J. Environ. Pathol. Toxicol. Oncol. 2003;22:93–100. .

252. Blanchard A a, Ma X, Dueck KJ, Penner C, Cooper SC, Mulhall D, Murphy LC, Leygue E, Myal Y. Claudin 1 expression in basal-like breast cancer is related to patient age. BMC Cancer. 2013;13:268.

253. Webb PG, Spillman M a, Baumgartner HK. Claudins play a role in normal and tumor cell motility. BMC Cell Biol. [Internet]. 2013;14:19.

254. Takenawa T, Suetsugu S. The WASP-WAVE protein network: connecting the membrane to the cytoskeleton. Nat. Rev. Mol. Cell Biol. 2007;8:37–48. .

255. Derivery E, Gautreau A. Generation of branched actin networks: assembly and regulation of the N-WASP and WAVE molecular machines. Bioessays. 2010;32:119–131. .

256. Riento K, Ridley AJ. Rocks: multifunctional kinases in cell behaviour. Nat. Rev. Mol. Cell Biol. 2003;4:446–456. .

257. Schofield A V, Steel R, Bernard O. Rho-associated coiled-coil kinase (ROCK) protein controls microtubule dynamics in a novel signaling pathway that regulates cell migration. J. Biol. Chem. 2012;287:43620–43629.

258. Escudero-Esparza A, Jiang WG, Martin TA. Claudin-5 is involved in breast cancer cell motility through the N-WASP and ROCK signalling pathways. J Exp Clin Cancer Res. 2012;31:43. .

259. Escudero-Esparza A, Jiang WG, Martin TA. Claudin-5 participates in the regulation of endothelial cell motility. Mol. Cell. Biochem. 2012. p. 71–85. .

260. Singh AB, Sharma A, Dhawan P. Claudin family of proteins and cancer: an overview. J. Oncol. 2010;2010:541957. .

261. Fadare O, Reddy H, Wang J, Hileeto D, Schwartz PE, Zheng W. E-cadherin and β-catenin expression in early stage cervical carcinoma: a tissue microarray study of 147 cases. World J. Surg. Oncol. 2005;3:38. .

262. Kuhn S, Koch M, Nübel T, Ladwein M, Antolovic D, Klingbeil P, Hildebrand D, Moldenhauer G, Langbein L, Franke WW, Weitz J, Zöller M. A complex of EpCAM, claudin-7, CD44 variant isoforms, and tetraspanins promotes colorectal cancer progression. Mol. Cancer Res. 2007;5:553–567. .

263. Wu C-J, Mannan P, Lu M, Udey MC. Epithelial cell adhesion molecule (EpCAM) regulates claudin dynamics and tight junctions. J. Biol. Chem. 2013;288:12253–12268.

264. Parkin DM, Bray F. Chapter 2: The burden of HPV-related cancers. Vaccine. 2006;24. .

Appendix

Mayer's Haematoxylin

2g haematoxylin (Merck)

100g aluminium sulphate (BDH)

0.4g Sodium Iodate (EMD Chemicals)

Make up to 2 litres with distilled water and leave overnight

2g citric acid (BDH)

Mix and Boil for 5 minutes

Allow to Cool and filter before use

1% Eosin

1g eosin powder (Merck) dissolved in 100ml water

Spirit (96%)

960ml absolute alcohol (Merck) made up to 1 litre with distilled water

70% Alcohol

700ml absolute ethanol (Merck) made up to 1 litre with distilled water

2% agarose gel

2g agarose powder (Invitrogen)

100ml of TBE (invitrogen)

Boil in microwave until dissolved

Cool to 60˚C

Add 0.5µg/ml Ethidium Bromide (Fluka)

Mix and gently poor into template

6x DNA loading buffer (50ml)

0.25% bromophenol blue (BDH)

0.25% xylene cyanol (BDH)

30% glycerol (BDH)

0.01mol/l citrate buffer (pH6)

2.1g citric acid (BDH)

Add approximately 800ml distilled water

Adjust to pH 6 using 2M NaOH

Make solution up to 1 litre

0.01mol/l EDTA buffer (pH8)

3.7g EDTA (BDH)

Add approximately 800ml distilled water

Adjust pH to pH 8 using 2M NaOH

Phosphate Buffered Saline (PBS)

Add 1 PBS tablet (Sigma) to 100ml distilled water.

0.1% protease

0.1g protease type 24 (Sigma) in 100ml PBS

3% Hydrogen Peroxide in methanol

1ml 30% hydrogen peroxide (BDH)

9ml Methanol (Fluka)

0.06% 2,4 diaminobenzidine (DAB)

16ml PBS injected into 1 container of DAB (Sigma)

1XTBS (Tris-buffered saline)

1.21g Tris + 4.38g NaCl in 500ml dH_2O

T-TBS 1X

To 1 liter of TBS 1X, add 1 mL of Tween 20.

1X Running Buffer

1.5g Tris + 7.2g glycine + 0.5g SDS in 500ml H2O

1X Transfer Buffer

0.6g Tris

2.882g glycine

adjust to pH 8.3 in 200ml H_2O

APS 10%

0.1 g Ammonium Persulfate

1 mL distilled H_2O

LB Broth

5g Tryptone (Lab M)

5g NaCl (Merck)

2.5g Yeast extract (Lab M)

Mix with 500ml distilled water and autoclave

0.1M $CaCl_2$

5.5g $CaCl_2$ (Fisher Scientific)

Mix with 250ml distilled water

Publications

Cunniffe, C., Ryan, F., Lambkin, H., & Brankin, B. (2011). Expression of tight and adherens junction proteins in cervical neoplasia. *British journal of biomedical science*, 69(4), 147-153. 2011

Cunniffe C, Brankin B, Ryan F, Lambkin H, "Expression of E-cadherin in cervical neoplasia" Beatson International Cancer Conference: Cancer Models and Novel Therapies Jul 3-6 2011

Cunniffe C, Brankin B, Ryan F, Lambkin H, "Expression of tight and adherens junctions in cervical neoplasia", 27th International Papillomavirus Conference Berlin Sep 17-22th 2011

Orrù, B, Cunniffe C, Ryan F, Schwartz S. "Development and validation of a novel reporter assay for human papillomavirus type 16 late gene expression." *Journal of virological methods* 183, no. 2 (2012): 106-116.

Cunniffe C, Brankin B, Lambkin H, Ryan F. "The role of claudin-1 and claudin-7 in cervical neoplasia" Anticancer Res 2014 34 (6). In print